TNO Built Environment and Geosciences

Princetonlaan 6
P.O. Box 80015
3508 TA Utrecht
The Netherlands

www.tno.nl

T +31 30 256 46 19
F +31 30 256 46 05
info@nitg.tno.nl

TNO report

2006-U-R0037/B

VELMOD-1
Joint Industry Project

Date	March 1, 2006
Author(s)	Dhr. Drs. W. van Dalfsen Dhr. Drs. J.C. Doornenbal Mevr. Drs. S. Dortland Dhr. Drs. J.L. Gunnink
Assignor	EBN, PetroCanada, NAM, Total, Wintershall
Project number	005.45062
Classification report Title Abstract Report text Appendices	B - Vertrouwelijk
Number of pages	67 (incl. appendices)
Number of appendices	5

Contents

Table of figures

Tables

1 Introduction

TNO and exploration and production (E&P) companies in the Netherlands have started a Joint Industry Project, called VELMOD. In this project, a seismic velocity model is developed for the entire Netherlands region, both onshore and offshore. The VELMOD results will serve two purposes. First: to perform time-depth conversion of seismic horizons in regional mapping projects and in studies on hydrocarbon fields and prospects, where a fully fledged model is lacking. Second: to facilitate depth migration of 3D seismic data.

Specifically, VELMOD applies to seismic horizons that are time domain representations of the bases of the following lithostratigraphic layers (Van Adrichem Boogaert and Kouwe, 1997):

1. North Sea Supergroup (N)
2. Chalk Group (CK)
3. Rijnland Group (KN)
4. Niedersachsen, Schieland and Scruff Groups (S)
5. Altena Group (AT)
6. Upper and Lower Germanic Trias Groups (R)
7. Zechstein Group (ZE)
8. Upper Rotliegend Group (RO)
9. Limburg Group (DC).

Per layer and on an areal grid of 1 km x 1 km, VELMOD provides parameter values for conversion of seismic traveltime into depth.

Previous to the VELMOD project, TNO conducted two velocity modelling studies for the onshore area. Their results facilitated the seismic mapping process for fifteen onshore map sheets (at a scale of 1:250,000) published in the period 1985-2004.The first study included 61 onshore boreholes. When it became clear that the resulting velocity model did not perform well, particularly on map sheets with inversion areas, a second study was initiated, including more boreholes than the first study. The resulting onshore velocity model is specified in the Geological Atlas of the Subsurface of the Netherlands – onshore (2004).

The onshore velocity studies were extended to the offshore in the SNET project of TNO. Offshore boreholes were added to the database of the onshore boreholes, resulting in a database of some 630 SNET boreholes. Doornenbal (2001) used these boreholes to point a way to a velocity model in which the Netherlands region is subdivided in areas with constant velocity parameters per layer.

The VELMOD project builds upon the SNET project, and was broken down as follows:

VELMOD-1 Phase 1 (May – September 2005): The SNET database is extended by boreholes with digital calibrated sonic (DCS) logs, which can be retrieved from the Dutch data repository DINO. A velocity modelling method based on instantaneous sonic velocities is developed and its performance is evaluated in comparison with the more common method based on interval velocities and mid depths. The most promising method of velocity modelling is selected.

VELMOD-1 Phase 2 (September 2005 – February 2006): The selected method of velocity modelling is used to construct the VELMOD-1 velocity model, based on data from the DINO data repository.

VELMOD-2 (March 2006 – November 2006): Construction of the VELMOD-2 velocity model based on data from the DINO data repository in conjunction with data from participating companies.

Phases 1 and 2 of VELMOD-1 are reported in this document.

2 Available data

The VELMOD-1 project had at its disposal borehole data from the Dutch data repository DINO. The values of the base depths of the various layers at the boreholes in this dataset are a result of TNO interpretation of the borehole data. There are two types of velocity data.

2.1 Interval velocities of the SNET project

First are interval velocities V_{int} for the selected lithostratigraphic layers at borehole locations. These data stem from TNO's SNET project that resulted in velocity models used in previous regional mapping projects. The available interval velocity data are presented per borehole in Appendix A. The corresponding borehole locations are shown in Figure 2.1.

Not all interval velocity data of Appendix A were used in VELMOD. Rejected were interval velocities of boreholes, where layer thickness is less than 5 ms (one-way-traveltime). These interval velocities tend to present themselves as outliers in graphical results (V_{int}-z_{mid} plots, variograms) of intermediate processing steps. Also rejected were a number of other outliers, whose interval velocities are at odds with the values at surrounding boreholes, or are questionable from a geophysical point of view. Rejected interval velocities are marked in Appendix A.

Also marked in Appendix A are SNET boreholes with DCS data, where the interval velocity assigned in the SNET project is disregarded in favour of the DCS based interval velocity given in Appendix C. The status of the disregarded interval velocities in Appendix A is marked as SNET>DCS.

It is noted that the North Sea Supergroup offers a relatively low number of interval velocities (307) compared with the numbers (498 and 478) for respectively the Chalk Group and the Rijnland Group. This is due to the fact that sonic logging practically never starts at ground surface. At a borehole where many hundreds of meters of the North Sea Supergroup were not logged, for example borehole BTL-01 (Figure 2.2), it is not possible to calculate a value for this interval velocity, unless the sonic data can be calibrated with other data (well shoot or seismic). As calibration data for many SNET boreholes are not available in the DINO data repository, the number of interval velocities for the North Sea Supergroup is relatively small.

Incompleteness of sonic data for the North Sea Supergroup affects not only the number, but also the accuracy of its interval velocities. Contrary to layers which are logged completely from top to base, interval velocities for the North Sea Supergroup cannot be evaluated by only integrating slowness. It is necessary to account by some other way for the traveltime across the shallow depth range without sonic data. Eventual available well shoot data, however, mostly fall short in quantity and in accuracy to assure an unambiguous value of the interval velocity. Therefore, the accuracy of interval velocities of the North Sea Supergroup is affected badly by procedural difficulties and inconsistencies, in comparison with the accuracy of interval velocities of deeper layers.

2.2 Calibrated instantaneous velocities

Digital calibrated logs of instantaneous velocity v_{sl} (z) are the second type of data available in the VELMOD project. These logs are the result of calibration of digital sonic (DCS) logs. They were mostly obtained as so called TIMC-curves from E&P companies and deposited in the DINO data repository.

The VOLONZ software of TNO was applied to approximate the instantaneous velocities per layer with a linear velocity function $v_{lin}(z)$ whose parameters are denoted as v_0 and k: $v_{lin}(z) = v_0 + kz$. The function $v_{lin}(z)$ meets the condition that its corresponding layer traveltime equals the traveltime according to the instantaneous velocities v_{sl} (z) of the digital calibrated sonic log. It is noted that the following relation holds: $V_{int} = v_{lin}(z_{mid}) = v_0 + ½k(z_t + z_b)$, where z_t and z_b represent depth to top, respectively base of the layer.

A graph of the calibrated instantaneous velocities, and their linearisation, of the DCS borehole (BTL-01) is presented in Figure 2.3. Note that the calibrated instantaneous velocities vary in discrete steps, not continuously as expected. This is due to insufficient precision of the traveltime (T) data from which the calibrated instantaneous velocities were derived. It may be noted that the non-calibrated instantaneous velocities of borehole BTL-01 (Figure 2.2) differ from the calibrated ones (Figure 2.3).

Appendix B contains the graphs of calibrated instantaneous velocities for the whole set of DCS boreholes. According to these graphs, the layer of the Zechstein Groups was also addressed by VOLONZ, but its v_0- and k-values for the Zechstein Group are to be ignored. The v_0- and k-values of the DCS boreholes, together with interval velocities, are listed per layer in Appendix C. As in Appendix A, rejected interval velocities are marked in Appendix C, as are the DCS based interval interval velocities which were ignored in favour of SNET interval velocities (DCS>SNET). Locations of the DCS boreholes are shown, together with those of the SNET boreholes, in Figure 2.1.

2.3 Seismic traveltime isochores of the Zechstein Group

Apart from the borehole data, the project had at its disposal a compilation of preliminary two-way seismic traveltimes across the ZE-layer, taken from TNO interpreted 2D and 3D seismic reflection surveys in the Netherlands region. A map of these data is presented in Figure 2.4. On this map, areas are distinguished of type A, B and C. Area A is characterised by thick halite deposits and salt flow. In the B-areas, there are relatively thick proportions of non-halite salts, whereas clastic deposits tend to dominate the layer of the Zechstein Group in area C.

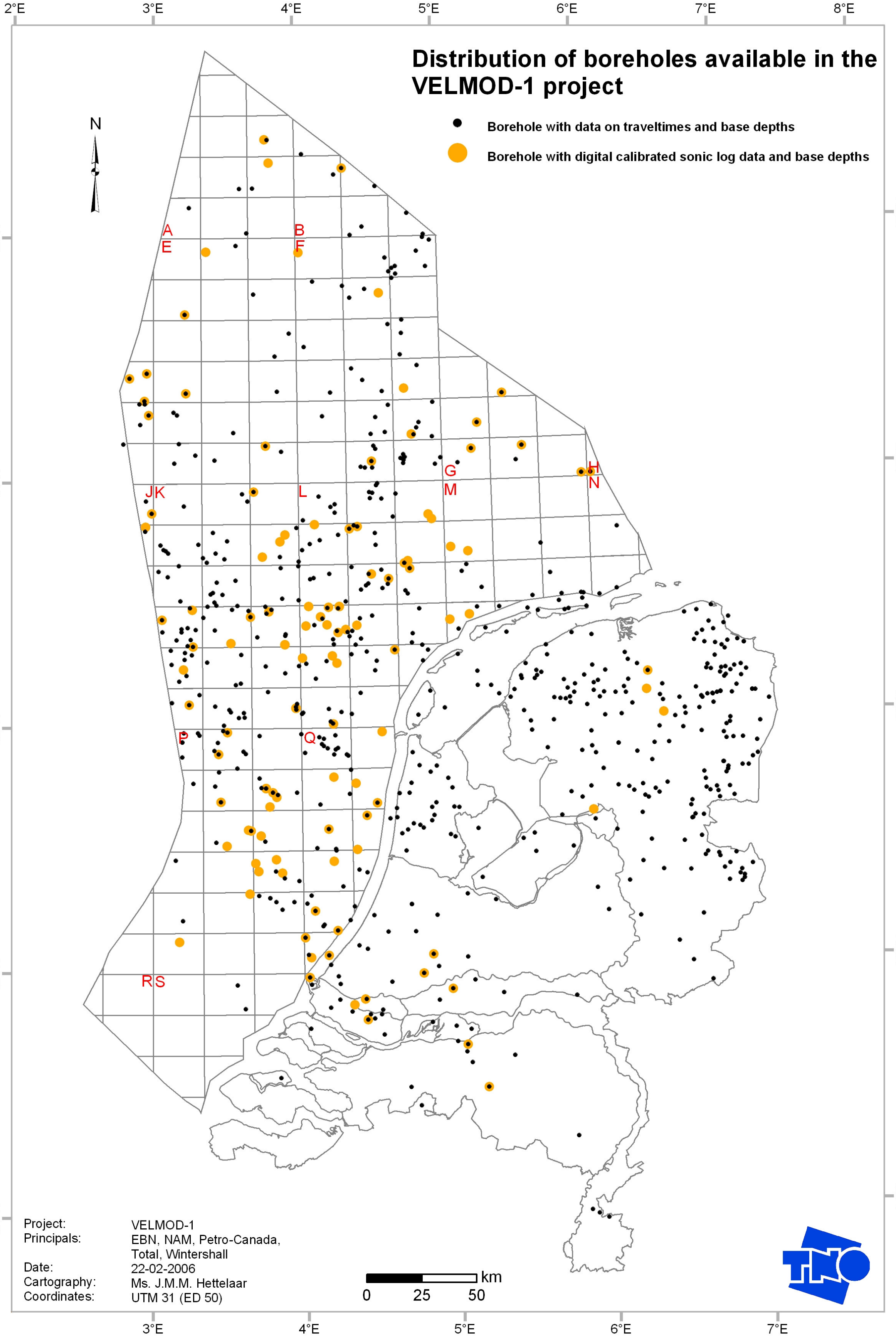

Figure 2.1: Distribution of boreholes available in the VELMOD-1 project

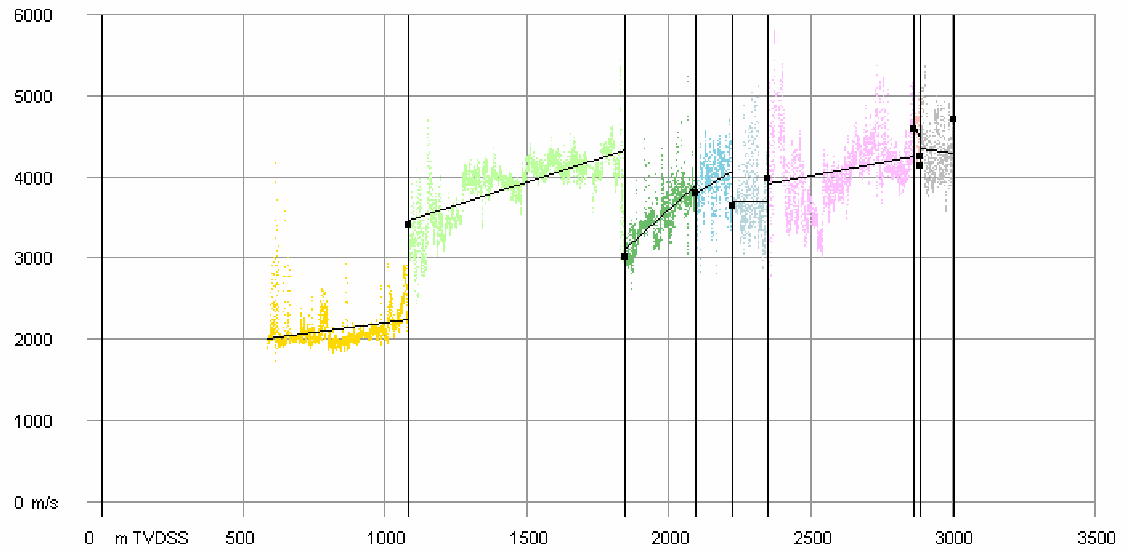

Figure 2.2: Instantaneous velocities (not calibrated) in borehole BTL-01

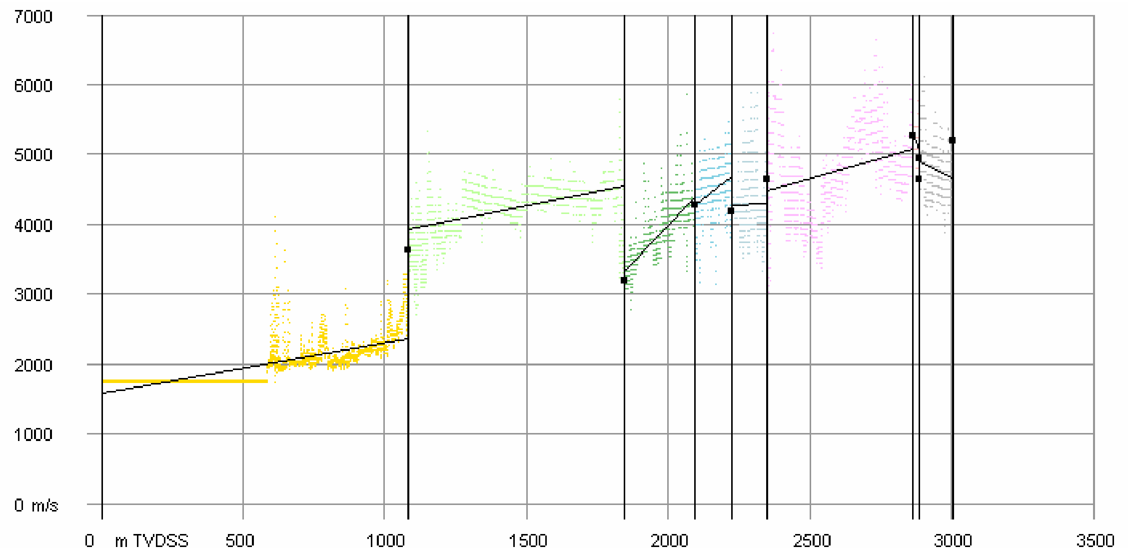

Figure 2.3: Linearisation of calibrated instantaneous velocities in borehole BTL-01

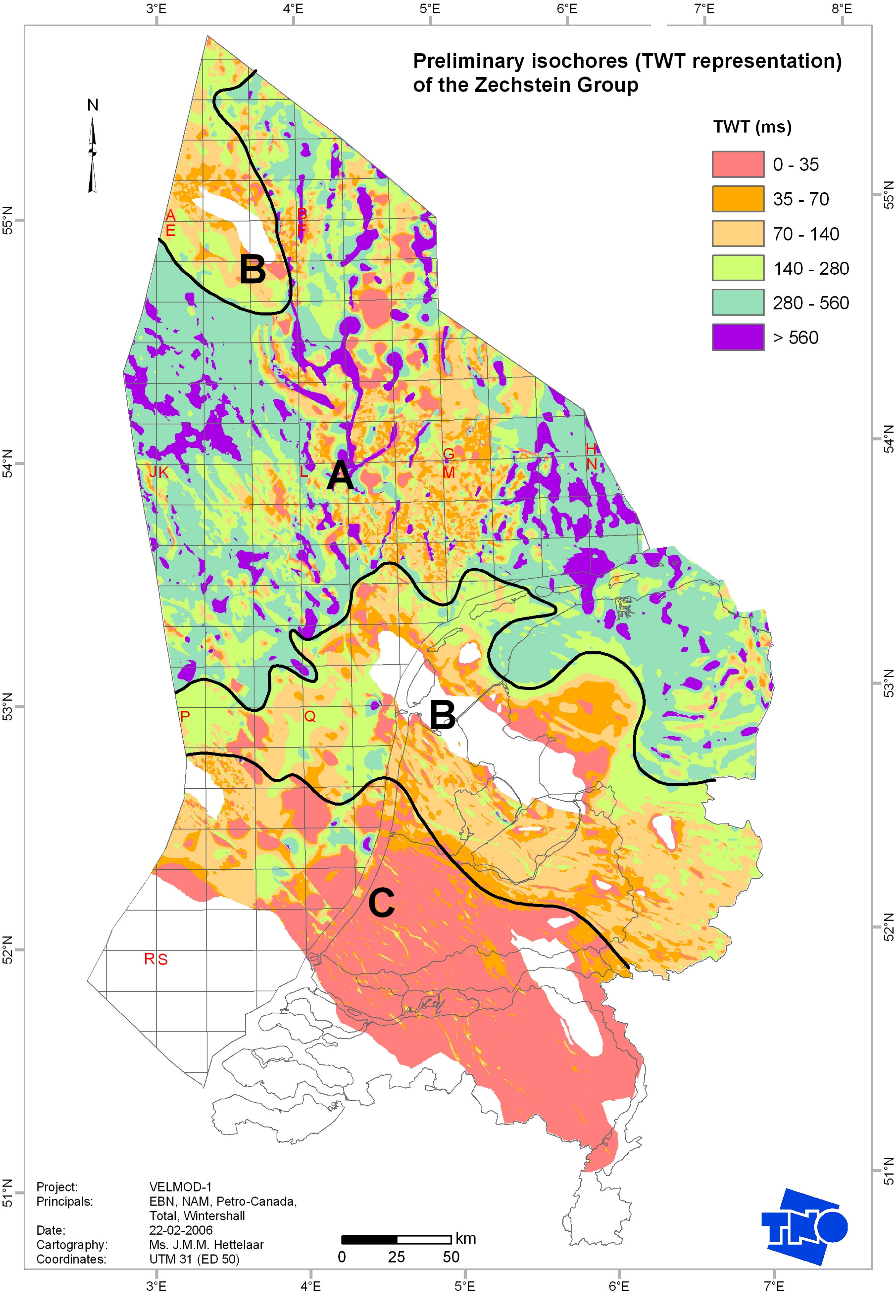

Figure 2.4: Preliminary isochores (TWT representation) of the Zechstein Group

3 The velocity model: characteristics and approaches

The velocity model is characterised by the following features:

- For layers other than the Zechstein Group, seismic velocity at a grid cell is modelled to vary linearly with depth z: $V(z) = V_0 + Kz$. The layer-specific parameters V_0 and K are allowed to vary laterally.
- Velocity in the layer of the Zechstein Group is modelled on the basis of inferences about the type (halite, anhydrite, clastics) of the Zechstein deposits.
- At borehole locations, the model effectuates tie-in of depth-converted seismic horizons with depths known from borehole data, provided that seismic horizons and borehole data are correct.
- The more boreholes available with calibrated sonic data, the less the uncertainty in the velocity model.
- A Sequential Gaussian Simulation (SGS) approach of determining the velocity parameters of a layer implies measures to quantify uncertainty in the velocity parameters.

In the first phase of the project, two approaches were taken to construct a preliminary velocity model of the Chalk Group. One approach is through analysis of the V_{int}-z_{mid} pairs of boreholes (Appendix A), and the other is through analysis of v_0-k pairs of boreholes with DCS logs (Appendix C). These approaches are described below.

The velocity model for the Zechstein Group is specified by means of a grid of V_{int} values. For the determination of these values, use was made of seismic traveltime data as described in Section 3.3.

In reading this report, one must keep in mind the difference between the upper case parameters V_0, K and the lower case parameters v_0, k. The latter pair of parameters refers explicitly to a VOLONZ linearisation of instantaneous velocities as shown in Figure 2.3 and Appendix B. Contrary, the upper case parameters do not necessarily mimic the instantaneous velocities through the relation $V(z) = V_0 + Kz$. Their values have to be such that they define seismic traveltimes ($\Delta T = T_b - T_t$) through a layer that are equal to the true traveltimes at borehole locations, and are approximately correct traveltimes at other locations.

3.1 Vint-zmid approach

Interval velocities (V_{int}) plotted against mid-depths (z_{mid}) are much in use to establish a global velocity function

$$V_{global}(z) = V_{0,global} + K_{global} z \quad (1)$$

to be used in the construction of a velocity model for time-depth conversion of the time-domain base horizon of a subsurface layer. The linear least squares fit to a set of V_{int}-z_{mid} pairs defines the parameters $V_{0,gobal}$ and K_{global} of the global velocity function. Figure 3.1 presents the linear least squares fit to V_{int}-z_{mid} pairs of the Chalk Group.

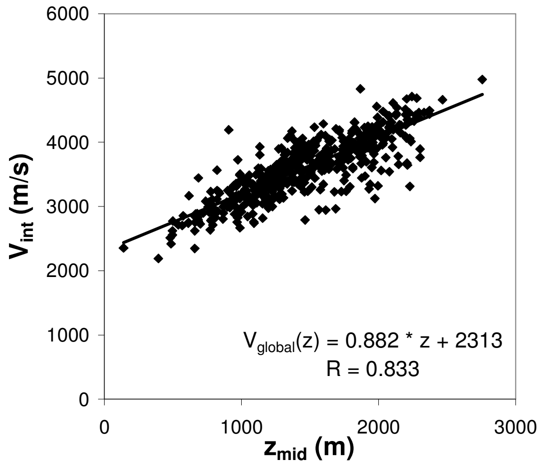

Figure 3.1: $V_{int} - z_{mid}$ plot of the Chalk Group (CK)

The global velocity function does not necessarily represent normal compaction of the Chalk Group with depth. This means that $V_{0,global}$ and K_{global} actually are fitting parameters not describing any single, well-defined physical phenomenon. Rather, the scatter of points testifies that V_{int} is controlled by several factors. These are lateral lithological variations in the Chalk Group, uplift with respect to maximum burial depth and under-compaction due to overpressure. Moreover, V_{int}- and z_{mid}-values are affected by measurement errors.

In view of the poorly defined physical meaning of the parameters $V_{0,\ global}$ and K_{global}, it is clear that they have to be dealt with as convenient ad hoc parameters. In velocity modelling, we prefer to assign constant $K = K_{global}$ values to the grid cells, whereas V_0 is allowed to deviate from $V_{0,global}$. Deviations from the trendline are evaluated at borehole locations by drawing a line with its slope set to K_{global} through the V_{int}-z_{mid} point. The intercept of the line with the y-axis is the V_0 value for that borehole. This can be represented by the formula:

$$V_0 - V_{0,global} = V_{\text{int}} - V_{global}(z_{mid}) \qquad (2)$$

or

$$V_0 = V_{\text{int}} - K_{global} * z_{mid} \qquad (3)$$

Geostatistical modelling of the V_0-values results in a V_0-grid for time-depth conversion.

The parameters V_0 and K ensure tie-in of the layer base depth at a borehole with the time-depth converted layer base from the seismic horizon, provided that seismic horizons and borehole data are correct.

3.2 Instantaneous velocity based v0-k approach

In the first phase of the project it was investigated whether it is useful to construct a velocity model on the basis of the parameters v_0 and k resulting from layerwise linearization of instantaneous velocities. These parameters are defined by the relation $v_{lin}(z) = v_0 + kz$, as illustrated in Figure 2.2.

In Figure 3.2 v_0-values of the Chalk Group are plotted against their corresponding k-values. In view of this figure, it is tempting to assume that v_0 is related linearly to k, written as $v_0 = a – bk$. This relation offers a method to arrive at V_0- and K-values of a velocity model. The main points of this method are described below.

We note that the seismic traveltime through a layer (ΔT) can be written as (Japsen, 1993):

$$\Delta T = \frac{1}{k} \ln\left[1 + \frac{k(z_b - z_t)}{v(z_t)}\right] \qquad (4)$$

Assuming $v_0 = a – bk$ with values of a and b fixed, then the above relation can be rewritten as:

$$\Delta T = \frac{1}{k} \ln\left[1 + \frac{k(z_b - z_t)}{a + k(z_t - b)}\right] \qquad (5)$$

Now, k can be solved from the above equation, given a borehole with known depths z_t and z_b to top and base of a layer, and known seismic traveltime ΔT through that layer. Then this k-value is assigned to the parameter K of the velocity model, and the corresponding parameter V_0 is calculated according to $V_0 = V_{int} – kz_{mid}$.

With the above method, k has to be solved numerically. A more simple way to calculate a k-value is found when a Taylor series expansion is applied to the equation for ΔT, followed by truncation of this series. With a first order Taylor series expansion, K can be written as:

$$K = \frac{V_{\text{int}} - a}{z_{mid} - b} \qquad (6)$$

In this case, the corresponding parameter V_0 is calculated according to $V_0 = a – bK$.

A note has to be made with respect to Figure 3.2. It shows that most k-values are in the range of 0-5 s^{-1}, but there are also excessively high and low values. These excessive values are mostly related to small layer thicknesses. Instantaneous velocities across these thin layers vary more under the influence of changes in lithology than under the influence of compaction. This results in k-values that are not realistic from a compaction point of view. For example the negative k-value of nearly -125 in Figure 3.2 is related to borehole P06-A-04, where the thickness of the Chalk Group is only 2.4 ms (Appendix C).

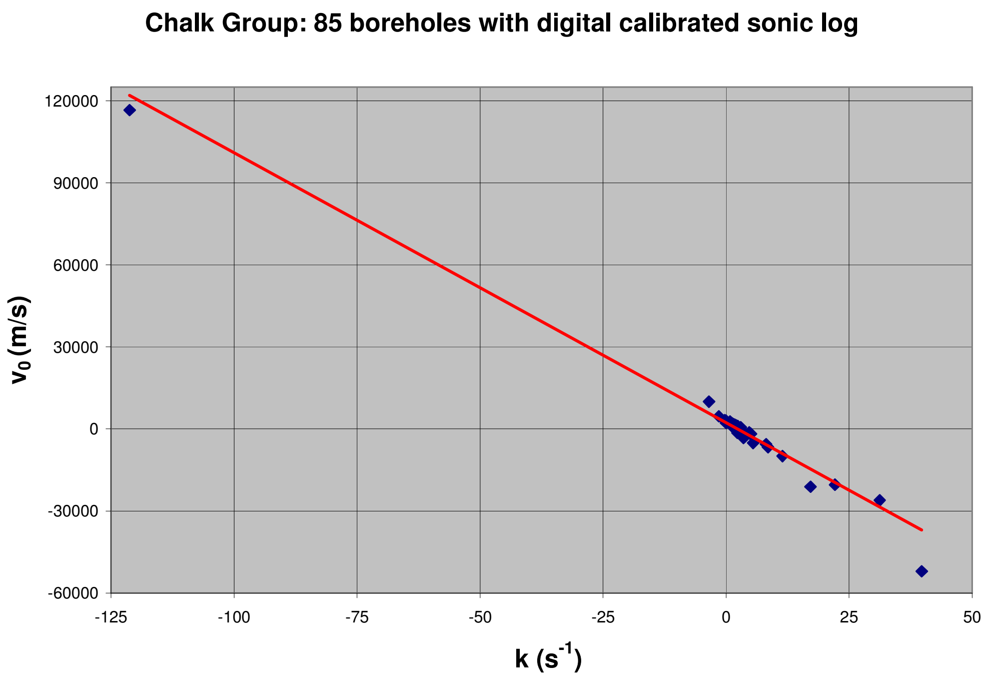

Figure 3.2: Linear relation between v_0 and k according to digital calibrated sonics of the Chalk Group

3.3 Velocity model of the Zechstein Group

The interval velocity for the Zechstein Group depends mainly on the proportion of halite in the layer, rather than on its depth. Therefore this layer is modelled with interval velocities that are related in a simple way to the relative proportion of halite in the layer.

It is assumed that the interval velocity of the Zechstein Group approximates the acoustic velocity (roughly 4500 m/s) of halite, where the Zechstein layer has a considerable thickness. At locations where the thickness is relatively small, non-halites may cause deviations from the halite velocity. Two cases may be distinguished. First, the occurrence of anhydrites and carbonates that result in relatively high interval velocities. Second, the occurrence of a large proportion of clastics whose influence on the interval velocity is less clear. The above cases are expressed in Figure 3.3, showing V_{int} as a function of two-way traveltime TWT according to sonic log data.

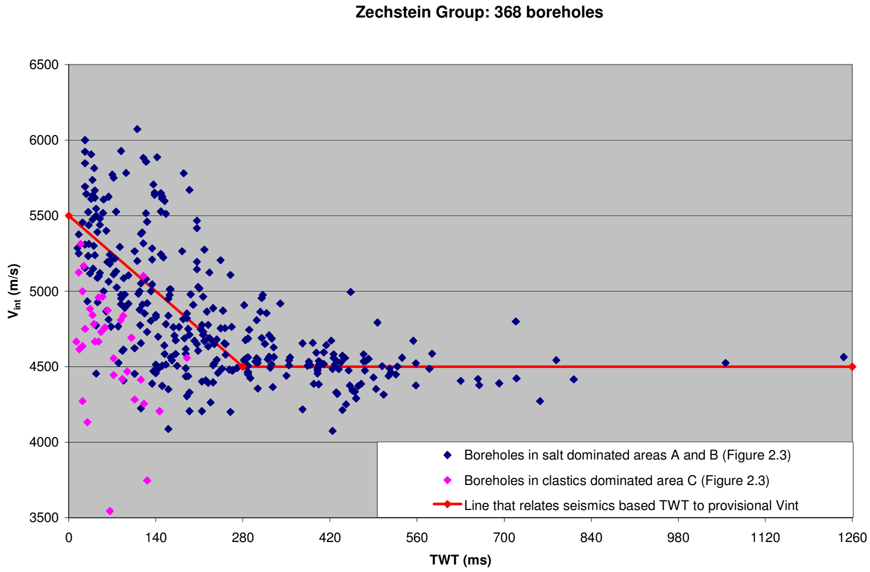

Figure 3.3: Schematic relation between interval velocity and two-way-traveltime in the Zechstein Group

Figure 3.3 is used to model Zechstein layer interval velocities. Where the seismic based two-way traveltime (Figure 2.4) is more than 280 ms, the interval velocity is provisionally set at 4500 m/s. Where two-way traveltime is less than 280 ms, interval velocity is provisionally set at the value according to sloping line segment in the figure. This can be expressed in the next equation:

$$V_{\text{int}} = 4500 \qquad \text{for } TWT \geq 280\ ms$$
$$V_{\text{int}} = 5500 - 3.57 * TWT \qquad \text{for } TWT < 280\ ms \qquad (7)$$

These provisional interval velocities can deviate from the known sonics based interval velocities. Therefore, in the next step, the provisional interval velocities at borehole locations are subtracted from the known sonics based interval velocities. After geostatistical modelling of these differences the ‘deviation map’ is added to the provisional interval velocity map, resulting in the final velocity model for the Zechstein Group.

4 The two different approaches of model building: comparison and selection

4.1 Vint-zmid approach

Starting from the global parameters $V_{0,global}$ and K_{global} for the Chalk Group, the velocity model parameter V_0 was determined at the borehole locations. Then a geostatistical modelling procedure, as described in Chapter 6, was applied to obtain a grid of V_0-values.

4.2 Instantaneous velocity based v0-k approach

In Figure 4.1 are presented v_0-k pairs of the Chalk Group at 66 boreholes, together with a segment of the line $v_0 = a – bk$. The parameter values of the line are: a = 3919 m/s and b = 1709 m. Both end points of the line segment in Figure 4.1 stem from a normal velocity-depth trend in Japsen (1998), that was somewhat improved upon later (Japsen, 2000).

This normal velocity-depth trend, consisting of a number of red line segments in Figure 4.2, models the increase of compressional wave velocity in sediments of the North Sea Chalk Group at monotonous burial (no uplift phases) under hydrostatic conditions (no undercompaction due to overpressure). The various segments imply that the increase velocity, that is due to compaction, changes with burial depth. This is to be expected as compaction approaches a limiting value towards great burial depth.

Also plotted in Figure 4.2 (dots) are V_{int}-values against z_{mid}-values at boreholes in the Netherlands territory. The scatter of dots around the normal velocity-depth trend may be interpreted as the result of uplift, exhumation and undercompaction (Van Dalfsen et al., 2005).

Figure 4.3 shows the population of various k-intervals for the Chalk Group. It is noted that the various slopes in the velocity-depth trend (Figure 4.2) agree with the two intervals (1.25-1.75 s^{-1} and 1.75-2.25 s^{-1}) mostly populated with k-values (Figure 4.3).

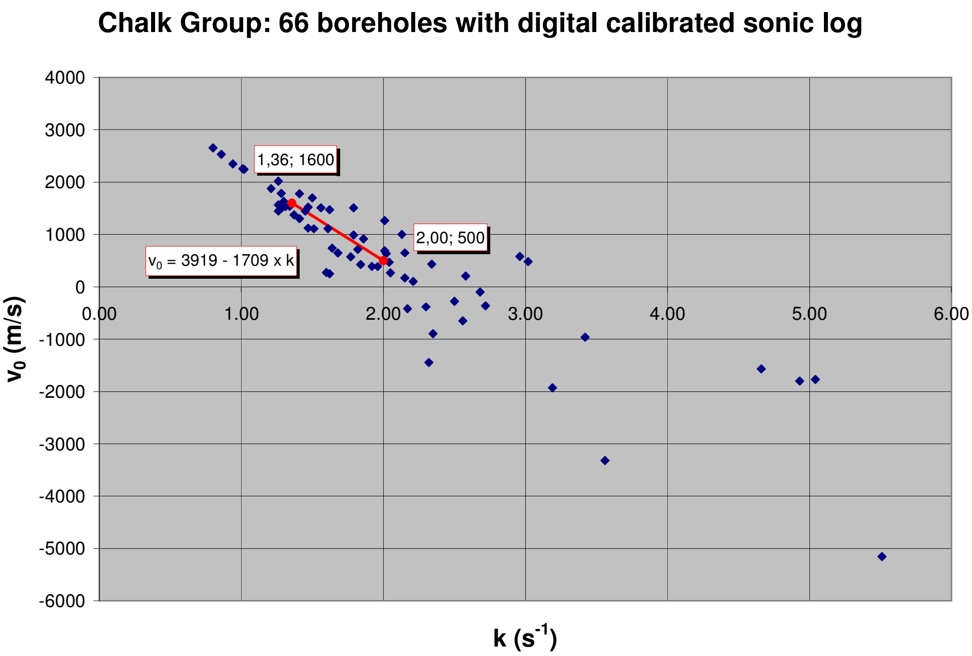

Figure 4.1: Linear trend between v_0 and k as inferred from a normal velocity-depth trend (Japsen, 1998)

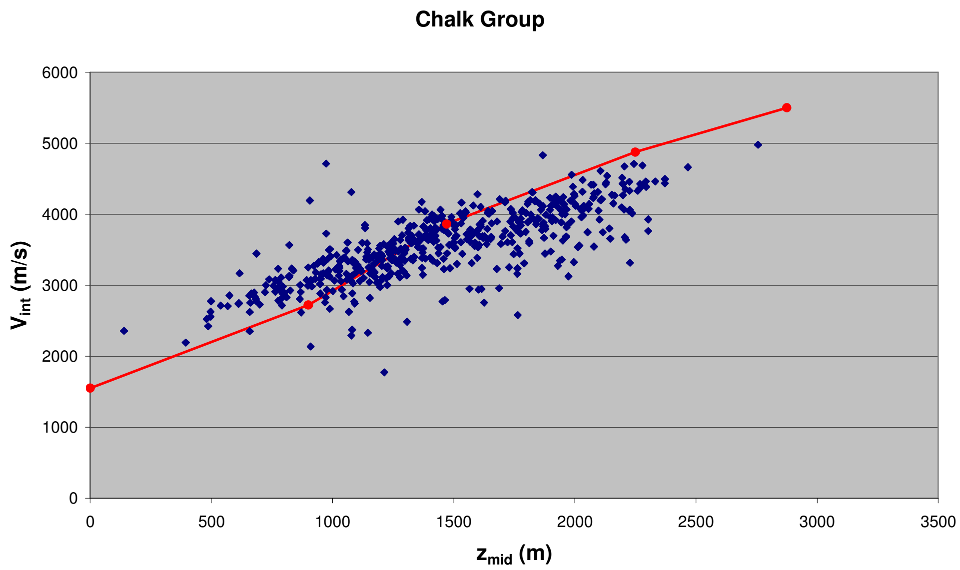

Figure 4.2: Normal velocity-depth trend of Japsen (2000) with (V_{int},z_{mid})-points of the Chalk Group in the Netherlands region

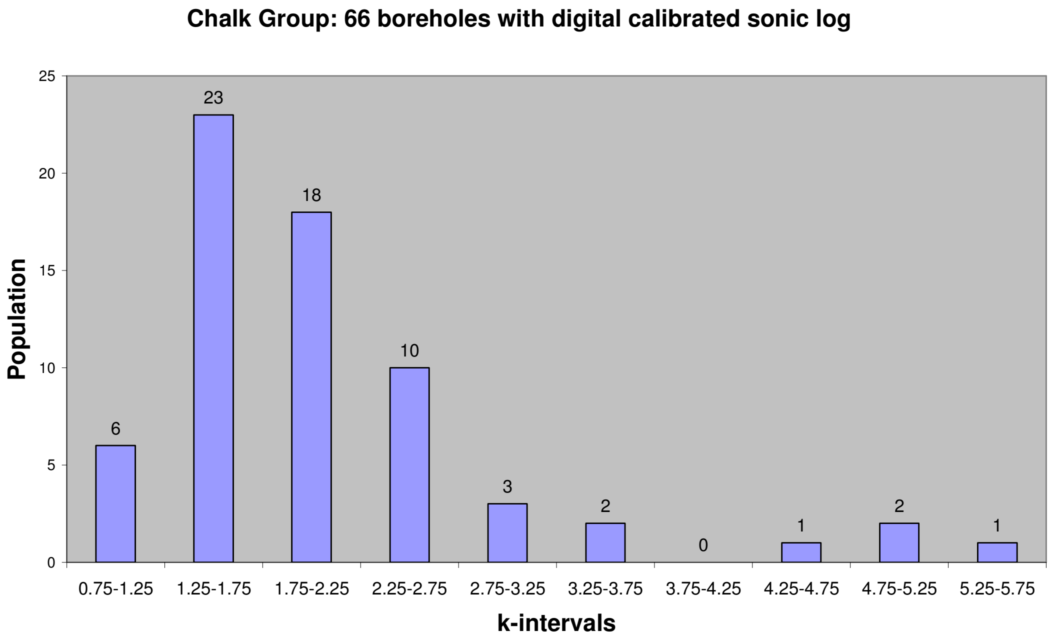

Figure 4.3: Population of k-intervals for the Chalk Group

To the parameter a in equation 3 was added a perturbation Δa, meant to account for non-normal velocity-depth trends due to uplift and overpressure. This perturbation is borehole dependent and is calculated according to $\Delta a = V_{int} - v_{Nlin}(z_{mid})$. The function $v_{Nlin}(z)$ is a linear approximation of the normal velocity-depth trend.

The calculation of K and V_0 is straightforward, as described in section 3.2, with the parameter a in equation 3 replaced by a + Δa. This resulted in geostatistically modelled maps of K and V_0.

4.3 Comparison and selection

The performance of the approaches was evaluated with a cross validation procedure. In cross validation, each data point is successively left out and predicted from the rest of the data. This was done for the two approaches. With the values of the predicted parameters the travel times through the Chalk Group were calculated (Appendix D) and compared with the known travel times. The difference between calculated and known travel times was smaller in the V_{int}-z_{mid} approach then in the v_0-k approach.

The results of the two approaches were presented to the VELMOD-1 participants at the meeting on September 9, 2005. It was shown that the difference between calculated and known travel times was smaller in the V_{int}-z_{mid} approach then in the v_0-k approach. It was then decided to proceed with the V_{int}-z_{mid} method.

5 Subdivision into regions based on tectonic history

Throughout the years TNO geologists and geophysicists have gained extensive knowledge about the subsurface of the Dutch territory. By regional mapping projects TNO has produced thickness and depth maps of the lithostratigraphic layers (Geological Atlas of the Subsurface of the Netherlands – onshore , 2004).
From seismic, log and biostratigraphic analysis, it is known that (groups of) structural elements have experienced significantly different tectonic histories. Based on this knowledge we have made a subdivision into tectonic regions for each lithostratigraphic layer. Figure 5.1 shows the main Mesozoic structural elements in the on- and offshore Dutch territory. Especially areas that have experienced inversion show a significantly different velocity structure compared to stable areas. These areas are for example the West Netherlands Basin (WNB), the Roer Valley Graben (RVG), Central Graben (CGB) and Broad Fourteens Basin (BFB). These areas experienced uplift during the Late Cretaceous. In Figure 5.1 are shown in green the basins that have also experienced uplift during the middle Jurassic. Due to this inversion, the Lower Jurassic deposits (Altena Group) have been eroded.

Taking into account the distribution, depth, and thickness of the different lithostratigraphic layers and the tectonic history of the structural elements, it is possible to make a first subdivision into two regions (Figure 5.2):

1) inverted Mesozoic basins
2) less- or non-inverted areas.

The Niedersachsen, Schieland and Scruff Groups (S) are only present in the inverted Mesozoic basins. However, due to differences in (timing and amount of) uplift, it is desirable to discriminate between the structural elements. Consequently, for the Niedersachsen, Schieland and Scruff Groups we have made an extra subdivision into three regions (Figure 5.2):

1a) Central Graben
1b) Broad Fourteens Basin, Central Netherlands Basin, West Netherlands Basin, Roer Valley Graben and Lower Saxony Basin
1c) Terschelling Basin, Vlieland Basin and Step Graben

The Altena Group (AT) has been subdivided into the same regions. However, since the Altena Group is mainly present in the first two regions, region 1c does not contribute in the modelling.

For the other layers, no subdivision into regions has been made in the final geostatistical modelling. For the North Sea Supergroup a subdivision into tectonic regions is of less relevance, since its velocity structure has been less influenced by tectonic movements. For the Chalk Group, at first a subdivision into regions 1 and 2 had been made. However, the results showed that the V_0 distribution was better predicted without this subdivision into regions (lower standard deviations). In addition, the correlation coefficient of the interval velocities (V_{int}) plotted against middle depths (z_{mid}), did not show a significant improvement when the data was subdivided into regions. Moreover, the resulting discontinuities in the V_0 distribution at the region boundaries were undesirable. Therefore, in the final geostatistical modelling no subdivision into regions was made for the Chalk Group.

For the Rijnland Group, the subdivision into regions has been tested as well, but has been rejected for the same reasons. Moreover, the parameters of the trendline in the V_{int}-z_{mid} plots (K_{global} and $V_{0,global}$) were roughly the same for the regions as well as for the data set as a whole. A subdivision of the Rijnland Group into two separate units, the Holland Formation and Vlieland Formation, would be more preferable, since it is known from borehole logs that these two formations have a different velocity distribution.

For the Upper and Lower Germanic Trias Groups (R) another approach would be preferable. From borehole logs it is known that the Lower Germanic Trias Group is more homogeneous than the Upper Germanic Trias Group. Interval velocities are influenced by this difference. Furthermore, the Upper Germanic Trias Group is not present everywhere. Therefore, TNO intends to divide the Germanic Trias Groups into two lithostratigraphic units; the Upper Germanic Trias Group (RN) and the Lower Germanic Trias Group (RB). Until then, we will carry out the geostatistical modelling on the Trias Groups as a whole.

Finally, for the Upper Rotliegend Group (RO) and Limburg Group (DC) no subdivision was introduced for the geostatistical modelling.

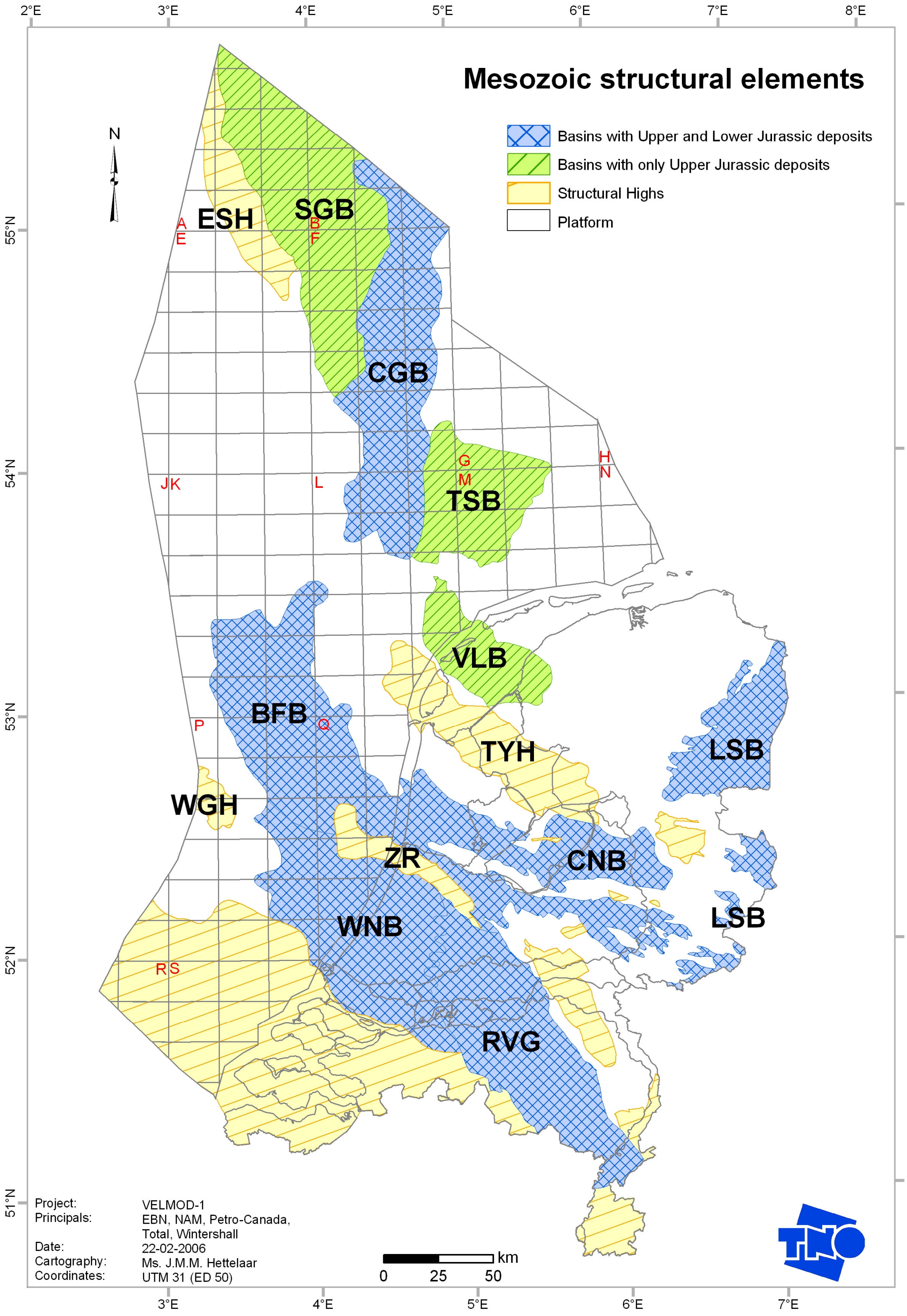

Figure 5.1: Main Mesozoic structural elements.

Abbreviations: BFB= Broad Fourteens Basin, CGB= Central Graben, CNB= Central Netherlands Basin, ESH = Elbow Spit High, LBM= London-Brabant Massif, LSB= Lower Saxony Basin, RVG= Roer Valley Graben, SGB= Step Graben, TSB= Terschelling Basin, TYH= Texel IJsselmeer High, VLB= Vlieland Basin, WGH= Winterton-Gulf High, WNB= West Netherlands Basin, ZR = Zandvoort Ridge.

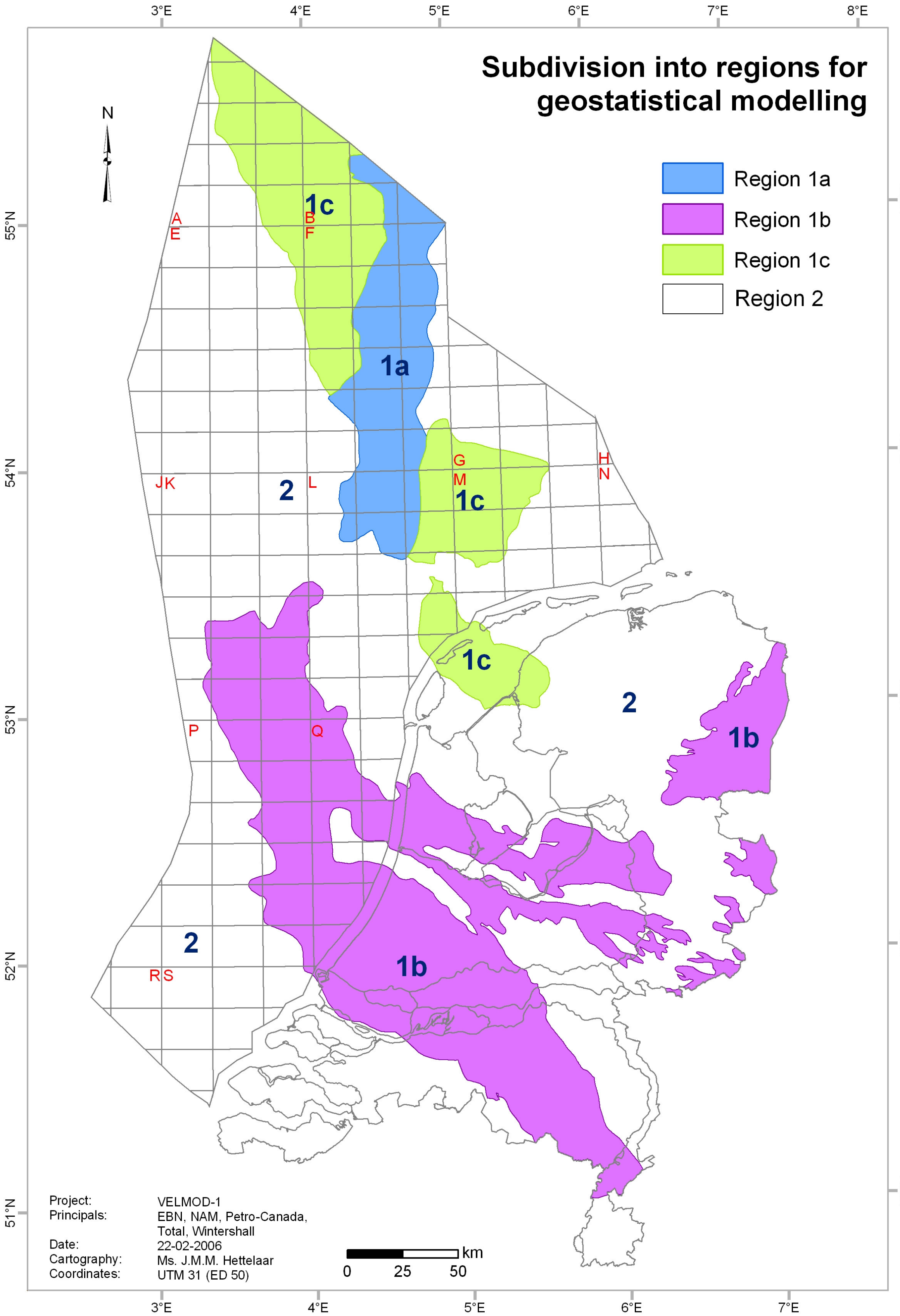

Figure 5.2: Subdivision into regions for geostatistical modelling

6 Geostatistical modelling

Within the range of geostatistical methods one can distinguish between estimation methods and simulation methods. The first group includes the Kriging method, the second group includes for example Sequential Gaussian Simulation and Sequential Indicator Simulation.

With estimation methods the estimated value at a given location is the “best” estimate in a least-squares fit sense, with the local variance being minimized. However, the map with these “best” local estimates is not necessarily the best estimate for the area as a whole. Interpolation algorithms tend to smooth local details of the spatial variation; low values are being overestimated, high values underestimated. Another disadvantage of interpolation methods is the fact that the smoothing is not uniform but dependent on local data configuration. The smoothing is minimal close to data locations and increases with distance from the data locations. This results in a higher variation in predicted values in areas with a high data density than in areas with a low data density, while in reality the variation of the parameter might be the same in both areas. Another disadvantage of the smoothing of the kriging estimation is the fact that the kriging results do not confirm with the input data; the histogram and the variogram of the kriging results do not have the same properties as the input data. Furthermore, the kriging standard deviation is not dependent on the local data values, but only on the data configuration. Therefore, the kriging standard deviation can not be used as a measure of local uncertainty.

Instead of a map with “best” local estimates and their standard deviation – as provided with the kriging estimation - simulation methods provide so-called realizations; these realizations have the same statistical properties as the input data (histogram and variogram) and honor the data at their location. Also, the realizations provide a measure of joint uncertainty of the results; in realizations all the estimation locations (grid-cells) are considered simultaneously rather than one at a time, as is done in traditional kriging. Because of these considerations we choose to use a simulation method to obtain a correct way to quantify the uncertainty in the results, together with a best estimate of the expected value.

After generating multiple realizations a mean estimated map and measure of uncertainty can be derived from the ensemble of realizations. We have chosen for the Sequential Gaussian Simulation method, because of its rather simple implementation. Because of the Gaussian distribution that is required by this method, the mean and the variance are sufficient to characterize the uncertainty in the results.

6.1 Sequential Gaussian Simulation

To be able to perform Sequential Gaussian Simulation (SGS) it is necessary to transform all data to Gaussian space (Figure 6.1). After transformation, a variogram is produced from the transformed data and Simple Kriging is performed to obtain a mean

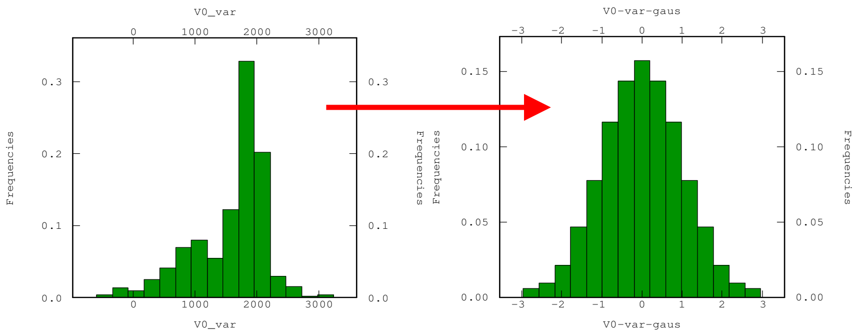

Figure 6.1: Example of transforming the data into Gaussian space

and variance for a prediction location (Figure 6.2). The weights used in this Kriging procedure are obtained from the variogram model fitted to the data. The mean and variance at the prediction location together form a distribution, from which a value is randomly drawn (Figure 6.3). This value will be the simulated value for the grid cell.

This value is added to the dataset and will be used as data point when Simple Kriging is performed to obtain a mean and variance for the next prediction location. This procedure is repeated until all grid cells have been visited. We now have one realization. This realization is back transformed into normal space. The whole procedure is repeated to obtain multiple realizations. Each realization has approximately the same statistical properties (histogram and variogram) as the original data. Furthermore, each realization satisfies the original data at the data locations. From the ensemble of realizations a mean and measure of uncertainty (standard deviation) is derived.

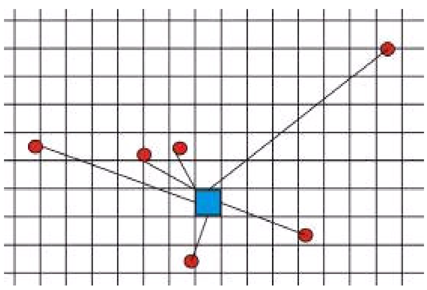

Figure 6.2: Prediction location (blue grid cell) and data locations (red dots)

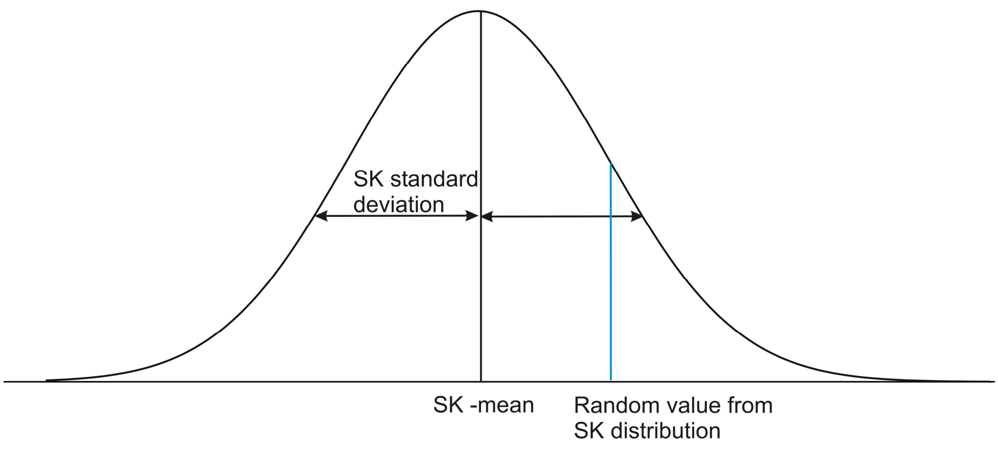

Figure 6.3: Simple Kriging distribution at a prediction location based on the SK mean and standard deviation

6.2 The variogram

An important tool in the estimation procedure is the variogram. The variogram is a so-called “two-point” statistic measure, showing the average squared difference for pairs of points separated by a certain distance. As the distance increases, the average difference will normally increase, until a certain distance at which the average difference is levelling off, see Figure 6.4. At this distance, called the range, there is no spatial correlation between the data points anymore; in Figure 6.4, the range is about 120000 meter. The nugget is the spatial correlation occurring at very small distances, together with the spatial uncorrelated measurements error. The sill is the variance that occurs at the specific distance. At the range, the sill is about the variance of the dataset, which equals to 1.0 in the case of Gaussian transformed variables.

The experimental variogram gives, at a specified distance interval, the average variance. To use the variogram in estimation, a variogram model is fitted through the experimental variogram. Not every model is allowed to be used through the experimental variogram, only so called positive-definite models. For more detail see Goovaerts (1997) and Deutsch and Journel (1998).

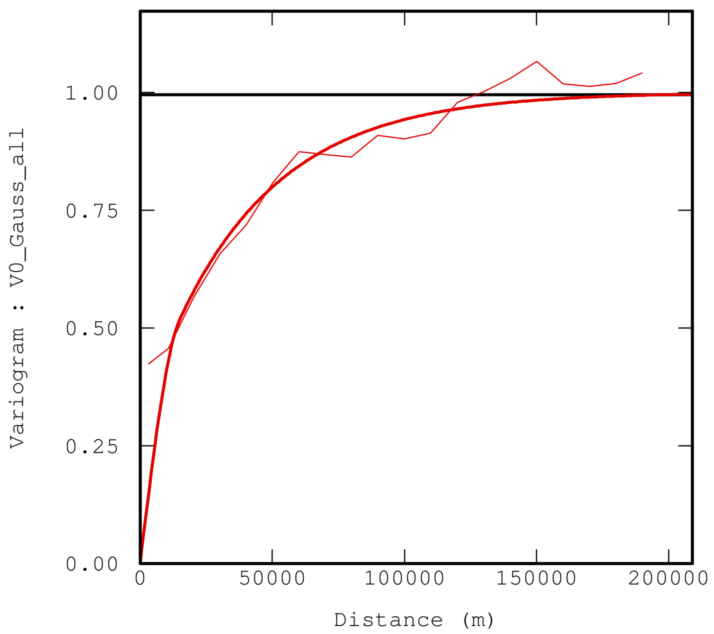

Figure 6.4: Variogram model Chalk Group

Sometimes there are two or more spatial structures superimposed in the experimental variogram. Variogram models can be added, so in the modelling of the variogram different spatial structures can be accounted for.

Increasing the nugget effect causes the estimates to become more like simple averaging of the available data. It reduces the spatial correlation effect in the data and causes the estimates to take values close to the regional average. Therefore we choose to set the nugget effect to 0, thereby implying that the short distance correlation and the measurements error are less important in a regional study.

The range is used in the SGS procedure to determine how “close” the sample are, in a statistical way. Increasing the range makes the sample look more closer, more correlated. A very small range causes the estimates to become like the simple average of the data.

7 Results

7.1 Global interval velocities and K-values

As a first step interval velocities (V_{int}) are plotted against mid-depths (z_{mid}) for each layer, taking into account the regions as described in section 5. To obtain estimates for the global interval velocity described by equation 1 in section 3.1:

$$V_{global}(z) = V_{0,global} + K_{global} z \quad \text{(1, repeated)}$$

a trendline is determined by using multilinear regression. The coefficients are obtained by minimizing the squared error between the true and the estimated value, summed over all the active data:

$$\sum_a \left(Z_a - a_0 + \sum_i a_i Y_a^i \right)^2 \quad (8)$$

with Z the target variable as a function of a set of N explanatory variables Y^i. For each layer the trendline is plotted, together with its correlation coefficient R and global velocity equation (Figure 7.1 to Figure 7.11). The correlation coefficients and parameters K_{global} and $V_{0\ global}$ are summarized in Table 7.1.

Table 7.1: K_{global} and $V_{0,global}$ values per region for each of the individual lithostratigraphic layers, according to the VELMOD-1 project

Layer	Region	# SNET	# DCS	K_{global}	$V_{0,global}$	R
N	**No subdivision**	**269**	**78**	**0.288**	**1777**	**0.781**
CK	**No subdivision**	**445**	**74**	**0.882**	**2313**	**0.833**
KN	**No subdivision**	**432**	**95**	**0.492**	**2132**	**0.718**
S	**No subdivision**	**109**	**31**	**0.247**	**2748**	**0.305**
S	Region 1a	39		0.626	1466	0.628
S	Region 1b	69		0.658	2309	0.729
S	Region 1c	26		0.959	994	0.873
AT	**No subdivision**	**134**	**26**	**0.340**	**2438**	**0.552**
AT	Region 1a	28		0.404	1946	0.598
AT	Region 1b	131		0.528	2182	0.731
R	**No subdivision**	**332**	**58**	**0.362**	**3112**	**0.549**
RO	**No subdivision**	**227**	**47**	**0.335**	**3084**	**0.504**
DC	**No subdivision**	**86**	**44**	**0.217**	**3533**	**0.596**

For comparison, for the groups with subdivision into regions the parameters are also given for the whole dataset. It can be seen that for the Niedersachsen, Schieland and Scruff Groups (S) the correlation coefficient for the dataset as a whole was 0.305, which is significantly lower than the correlation between V_{int} and z_{mid} for the boreholes grouped into regions (R=0.628, 0.729 and 0.873). Moreover, the parameter K increases significantly when a subdivision into regions is applied. The same can be observed in the Altena Group. It thus emphasizes the importance of the subdivision into regions for these layers.

The above results compare well with results of the SNET project, compiled in Table 7.2. The values that can be compared are highlighted in blue in both Table 7.1 and Table 7.2.

Table 7.2: K_{global} and $V_{0,global}$ values per region for each of the individual lithostratigraphic layers, according to the SNET project

Layer	Region	# Boreholes	K_{global}	$V_{0,global}$	R
N	**No subdivision**	**304**	**0.287**	**1776**	**0.779**
N	North	184	0.289	1767	0.782
N	East and South	40	0.417	1760	0.807
N	South-West	80	0.465	1696	0.767
CK	**No subdivision**	**466**	**0.875**	**2321**	**0.836**
CK	Central Graben	18	0.910	1597	0.848
CK	North	45	1.049	1781	0.855
CK	South	403	1.031	2156	0.918
KN	**No subdivision**	**480**	**0.504**	**2099**	**0.740**
KN	Central Graben	57	1.064	621	0.873
KN	North	198	0.584	1899	0.876
KN	North-East	29	0.819	1310	0.892
KN	East	115	0.615	2027	0.756
KN	West	29	0.776	1598	0.784
KN	South-West	52	0.728	2026	0.834
S	**No subdivision**	**128**	**0.247**	**2687**	**0.319**
S	Central Graben	37	0.372	1889	0.607
S	North	24	0.619	1849	0.762
S	East	21	0.566	2285	0.750
S	West	4	0.734	1881	0.760
S	South-West1	29	0.534	2770	0.779
S	South-West2	13	0.750	2038	0.797
AT	**No subdivision**	**154**	**0.328**	**2459**	**0.587**
AT	Central Graben	7	0.521	1500	0.875
AT	North	23	0.645	1424	0.783
AT	East	35	0.483	2093	0.847
AT	West	10	0.363	2361	0.628
AT	South-West1	63	0.435	2451	0.699
AT	South-West2	16	0.322	2490	0.696
R	**No subdivision**	**376**	**0.366**	**3095**	**0.553**
R	North	136	0.466	2575	0.773
R	East	103	0.409	3098	0.741
R	South-West	137	0.474	3097	0.635
RO/RV	**No subdivision**	**275**	**0.374**	**3019**	**0.507**
DC	**No subdivision**	**97**	**0.254**	**3443**	**0.686**

The regionalization in the SNET project was based on a clustering algorithm, which did not take into account structural elements. For this reason, the regional boundaries tend to be rather capricious from a geological point of view. As the clustering was performed layerwise, the subdivision for one layer may differ from that for another layer. The above aspects of subdivision of the various layers make the use of its corresponding velocity model less attractive.

Table 7.1 and Table 7.2 highlight an important aspect of downscaling constant V_0, K velocity models to smaller regions. They show that the K-value tends to increase, when an adequate subdivision in regions is made. In thought, this process of shrinking a certain region into a smaller region may be carried on until only a very small region is left around a certain borehole. Obviously, then one ends up with the parameters k and v_0 of that borehole.

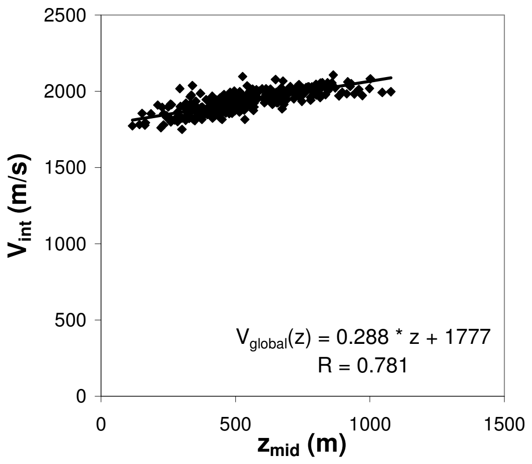

Figure 7.1: V_{int} – z_{mid} plot of the North Sea Supergroup (N)

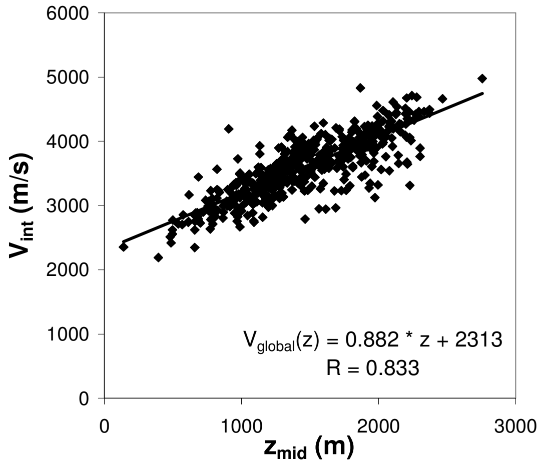

Figure 7.2: V_{int} – z_{mid} plot of the Chalk Group (CK)

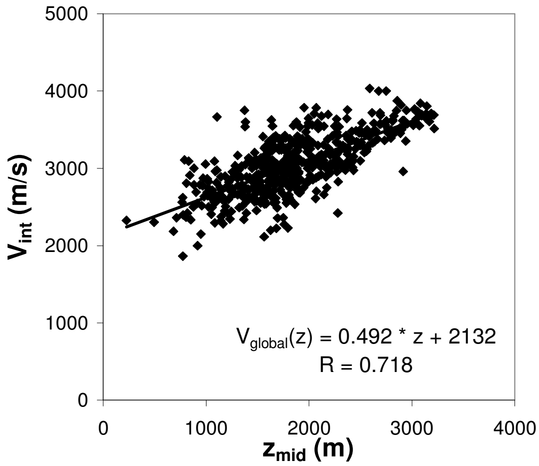

Figure 7.3: $V_{int} - z_{mid}$ plot of the Rijnland Group (KN)

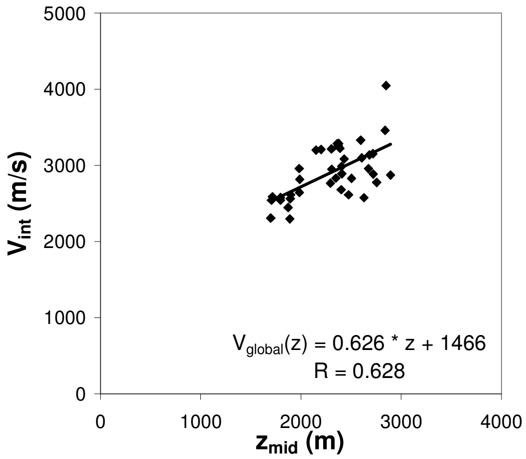

Figure 7.4: $V_{int} - z_{mid}$ plot of the Niedersachsen, Schieland and Scruff Groups (S), region 1a

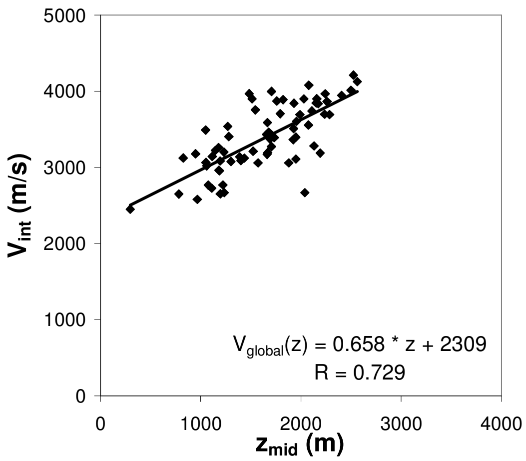

Figure 7.5: $V_{int} - z_{mid}$ plot of the Niedersachsen, Schieland and Scruff Groups (S), region 1b

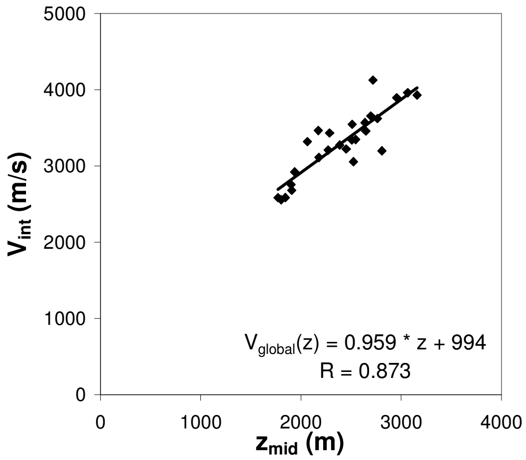

Figure 7.6: $V_{int} - z_{mid}$ plot of the Niedersachsen, Schieland and Scruff Groups (S), region 1c

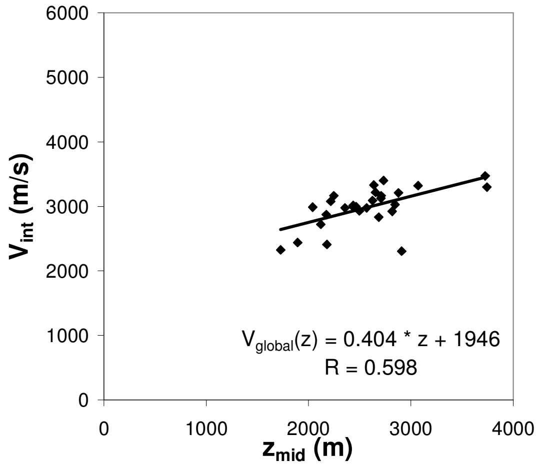

Figure 7.7: $V_{int} - z_{mid}$ plot of the Altena Group (AT), region 1a

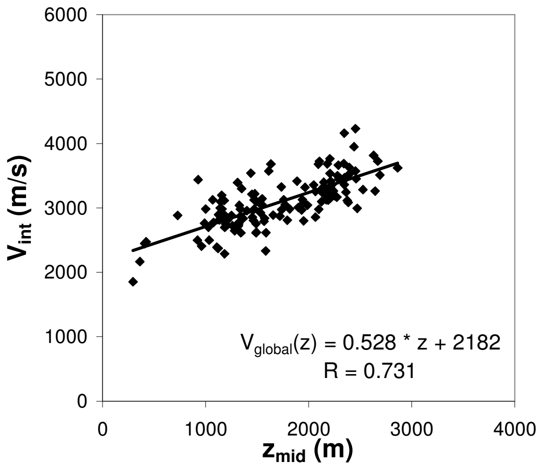

Figure 7.8: $V_{int} - z_{mid}$ plot of the Altena Group (AT), region 1b

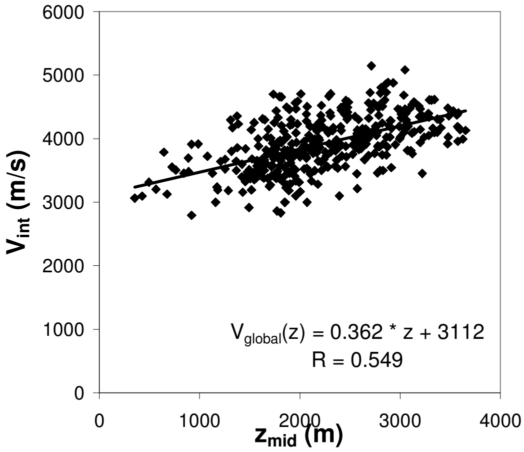

Figure 7.9: $V_{int} - z_{mid}$ plot of the Upper and Lower Germanic Trias Groups (R)

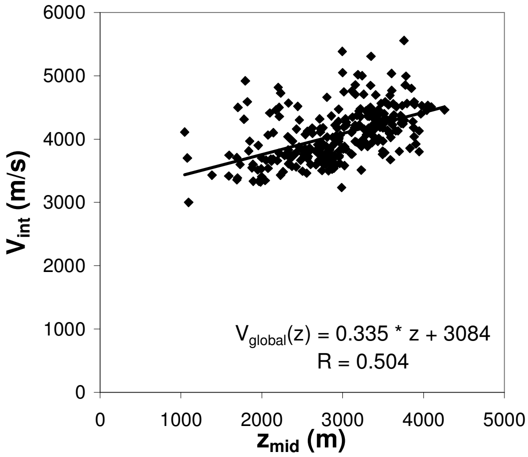

Figure 7.10: $V_{int} - z_{mid}$ plot of the Rotliegend Group (RO)

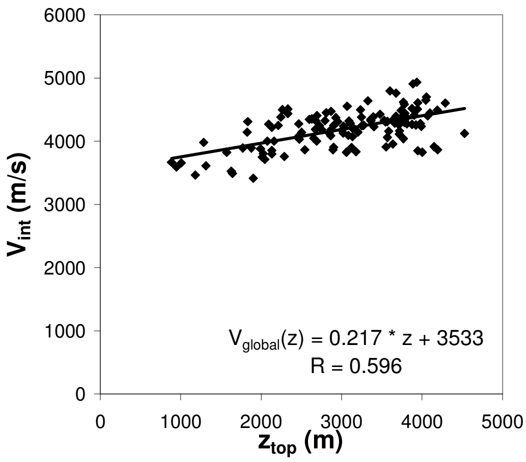

Figure 7.11: $V_{int} - z_{top}$ plot of the Limburg Group (DC)

7.2 Variogram modelling

The Simple Kriging algorithm in the Sequential Gaussian procedure uses a variogram model to determine the weights for the data points within the search radius. For each layer a variogram model is fitted to the experimental variogram of the (to Gaussian space transformed) data belonging to each region, or to the whole dataset when no subdivision into regions is used for that specific layer. For all models the sill is set to 1, which is, per definition, the variance of the Gaussian dataset, and the nugget to 0. A non-zero nugget indicates that repeated measurements at the same point yield different values. By choosing a zero nugget, we disregard errors in the V_{int} data.

In the next figures the variogram models are shown, that have been used for the geostatistical modelling of the parameter V_0 for the various layers. The variogram for the difference between V_{int}-values from borehole data and the ZE isochore map (Figure 2.4) based V_{int}-values at the locations of those boreholes is also shown. All V_0- and V_{int}-values, except for the Limburg Group, are assigned to the coordinates E_{mid} en N_{mid} (UTM31, ED50) that locate where the borehole is at the mid-depth z_{mid} of the layer. E_{mid}, N_{mid} and z_{mid} are listed in Appendices A and C. For the Limburg Group the V_0-value is assigned to the top of the layer.

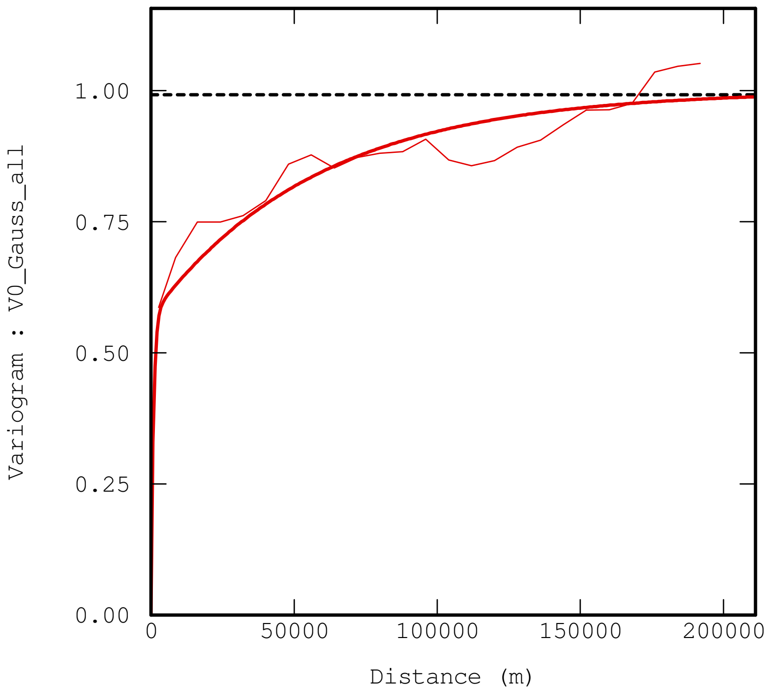

Figure 7.12: Variogram model for the North Sea Supergroup

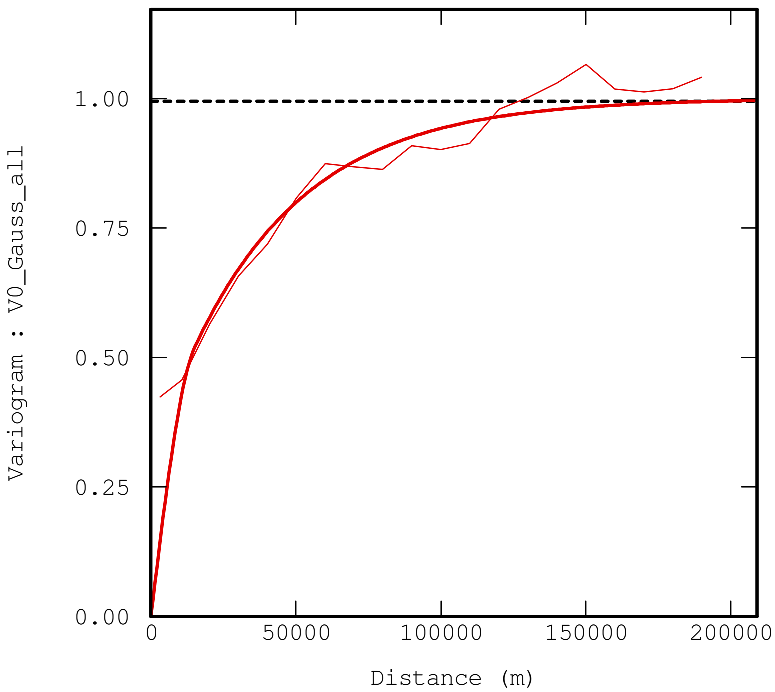

Figure 7.13: Variogram model for the Chalk Group

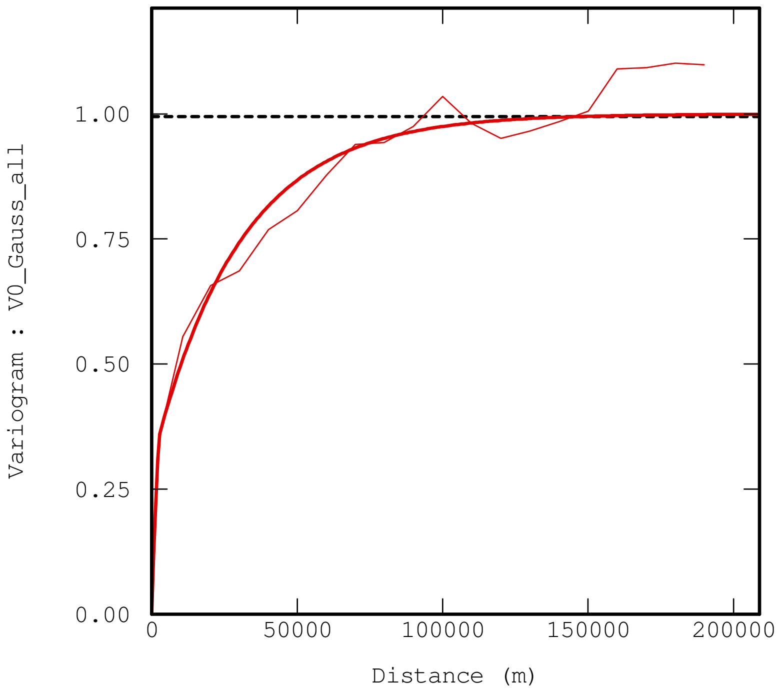

Figure 7.14: Variogram model for the Rijnland Group

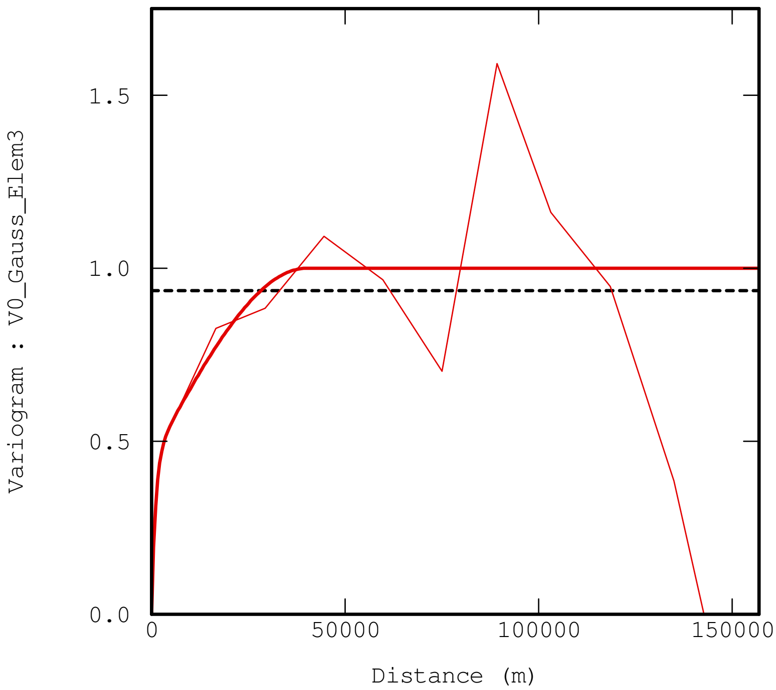

Figure 7.15: Variogram model for the Niedersachsen, Schieland and Scruff Groups, region 1a

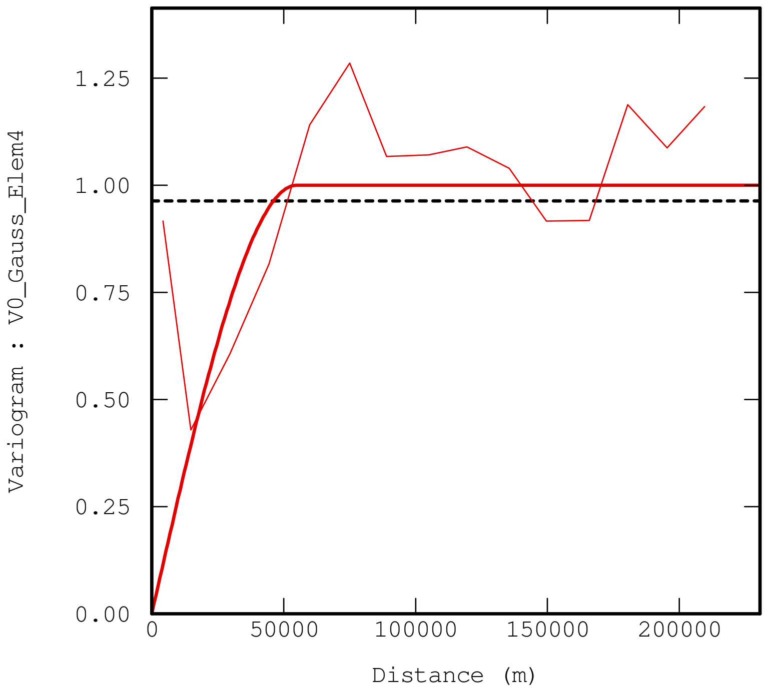

Figure 7.16: Variogram model for the Niedersachsen, Schieland and Scruff Groups, region 1b

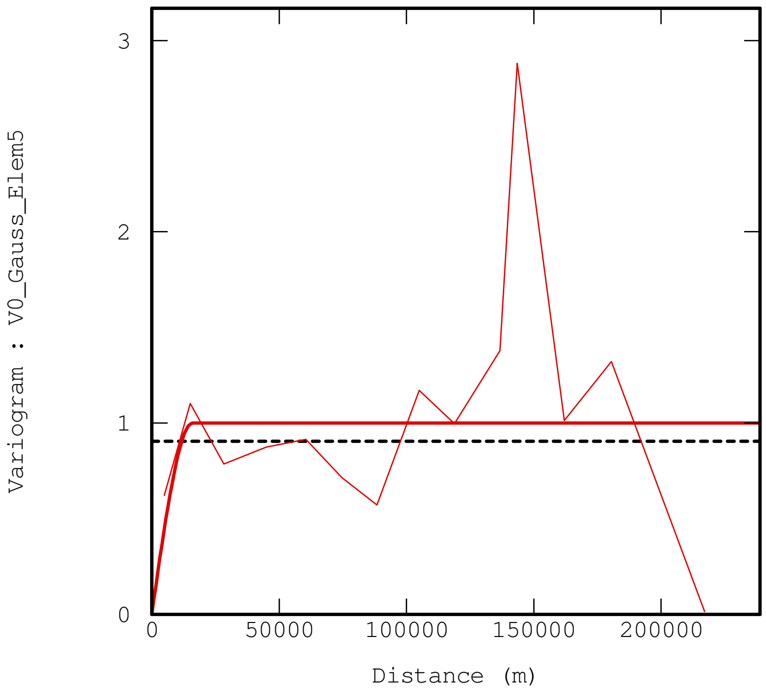

Figure 7.17: Variogram model for the Niedersachsen, Schieland and Scruff Groups, region 1c

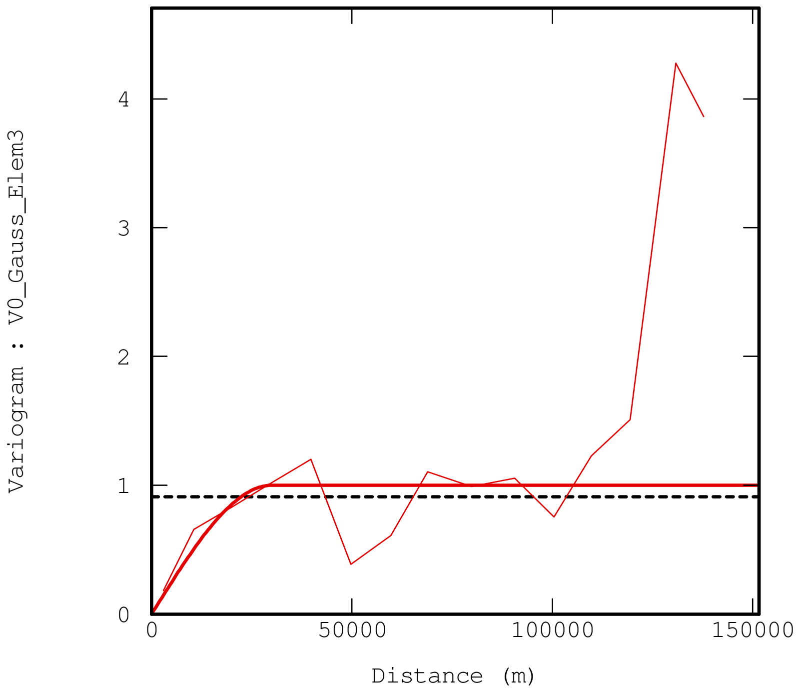

Figure 7.18: Variogram model for the Altena Group, region 1a

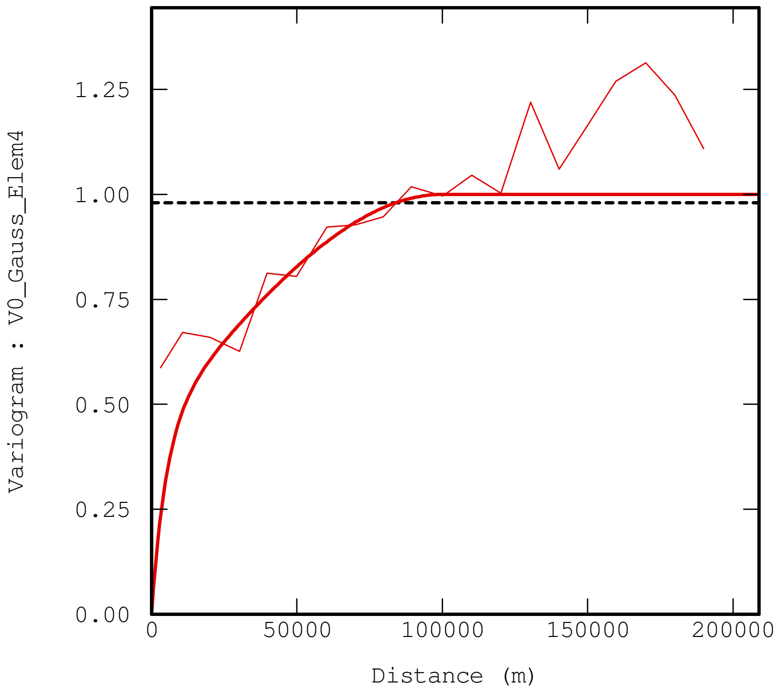

Figure 7.19: Variogram model for the Altena Group, region 1b

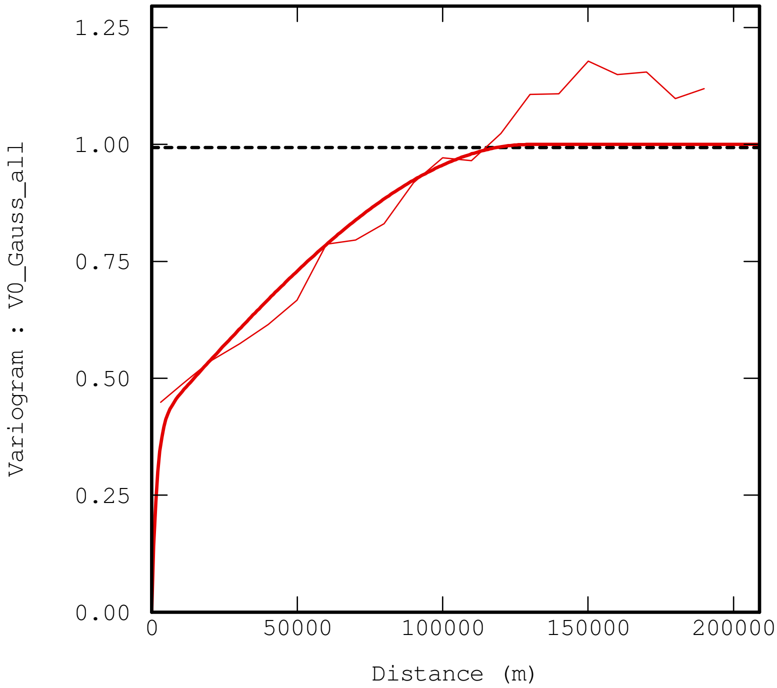

Figure 7.20: Variogram model for the Upper and Lower Germanic Trias Groups

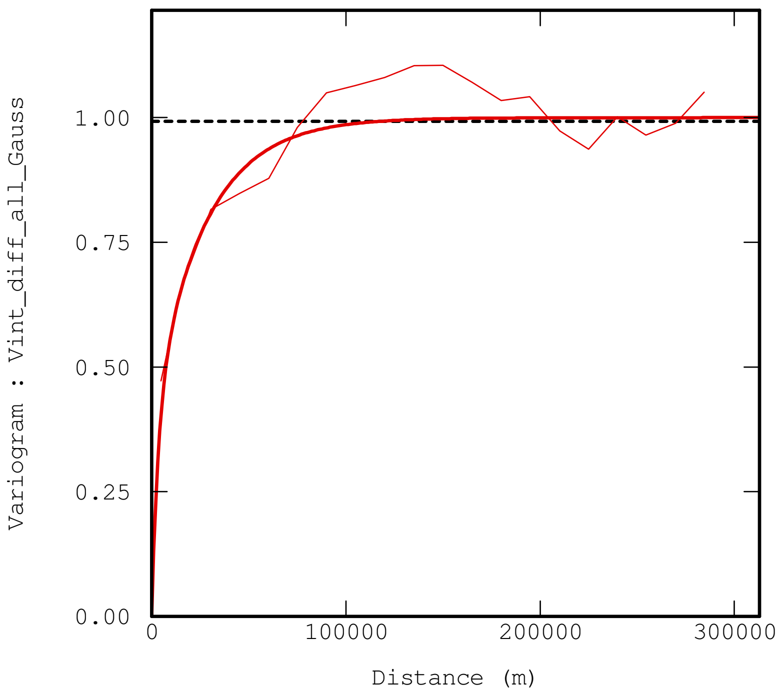

Figure 7.21: Variogram model for the the Zechstein Group for the difference between V_{int} from boreholes and V_{int} based on TWT

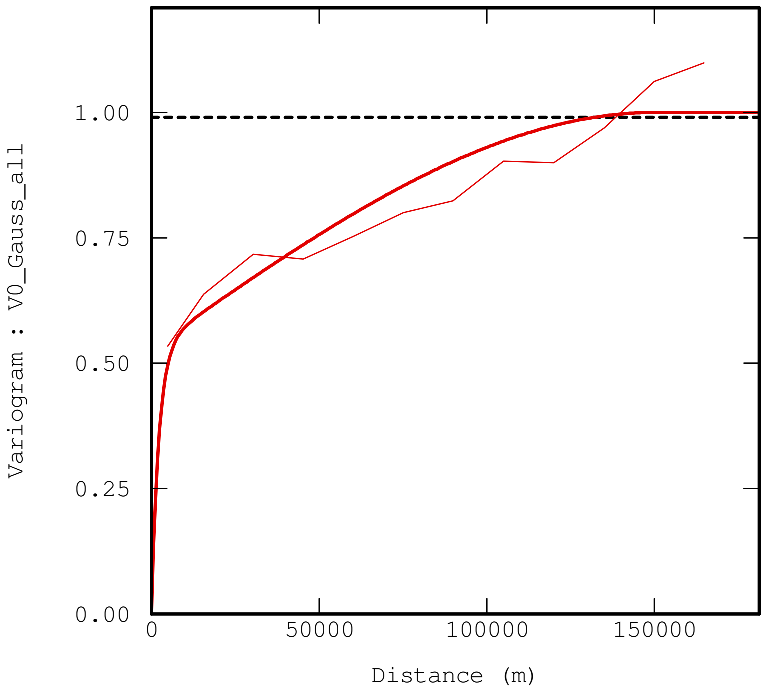

Figure 7.22: Variogram model for the Upper Rotliegend Group

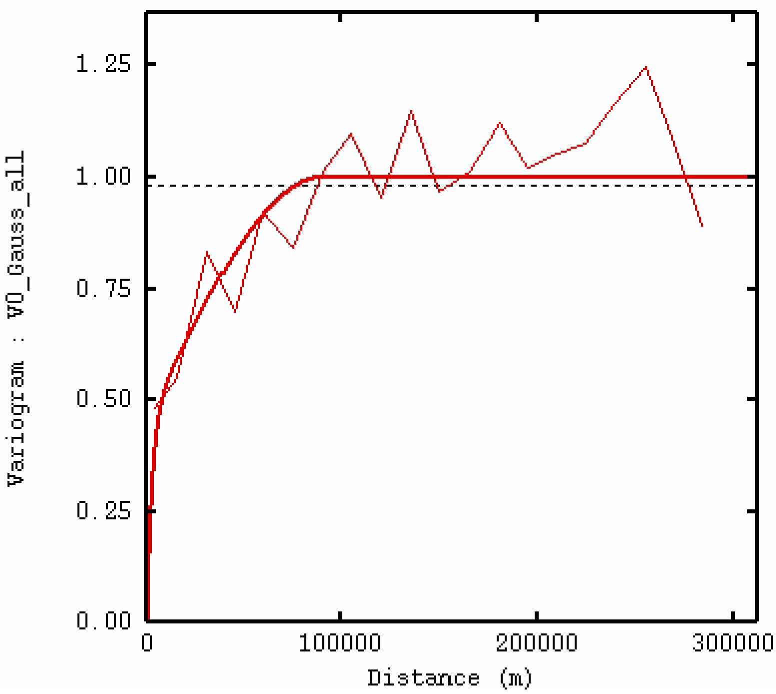

Figure 7.23: Variogram model for the Limburg Group

7.3 Velocity modelling

Within the Sequential Gaussian Simulation 50 realizations of the V_0 distribution have been generated for the various layers and regions. The final V_0 distribution map is the mean of these 50 realizations, its corresponding uncertainty map the standard deviation of the 50 realizations. For layers that have been subdivided into regions, the realizations have been generated per region, after which the resulting mean and standard deviation of the different regions have been merged into one final V_0-distribution map and one uncertainty map for the whole area.

The V_0 distributions and their uncertainty (standard deviation) for the various lithostratigraphic layers, when applicable, are shown starting at Figure 7.24. Results of the geostatistical modelling for the Zechstein Group are shown in Figure 7.36 (deviation map), Figure 7.37 (V_{int} distribution) and Figure 7.38 (standard deviation). For interpretation of the results, isochore maps and time maps of the bases of the lithostratigraphic layers are given in Appendix E.

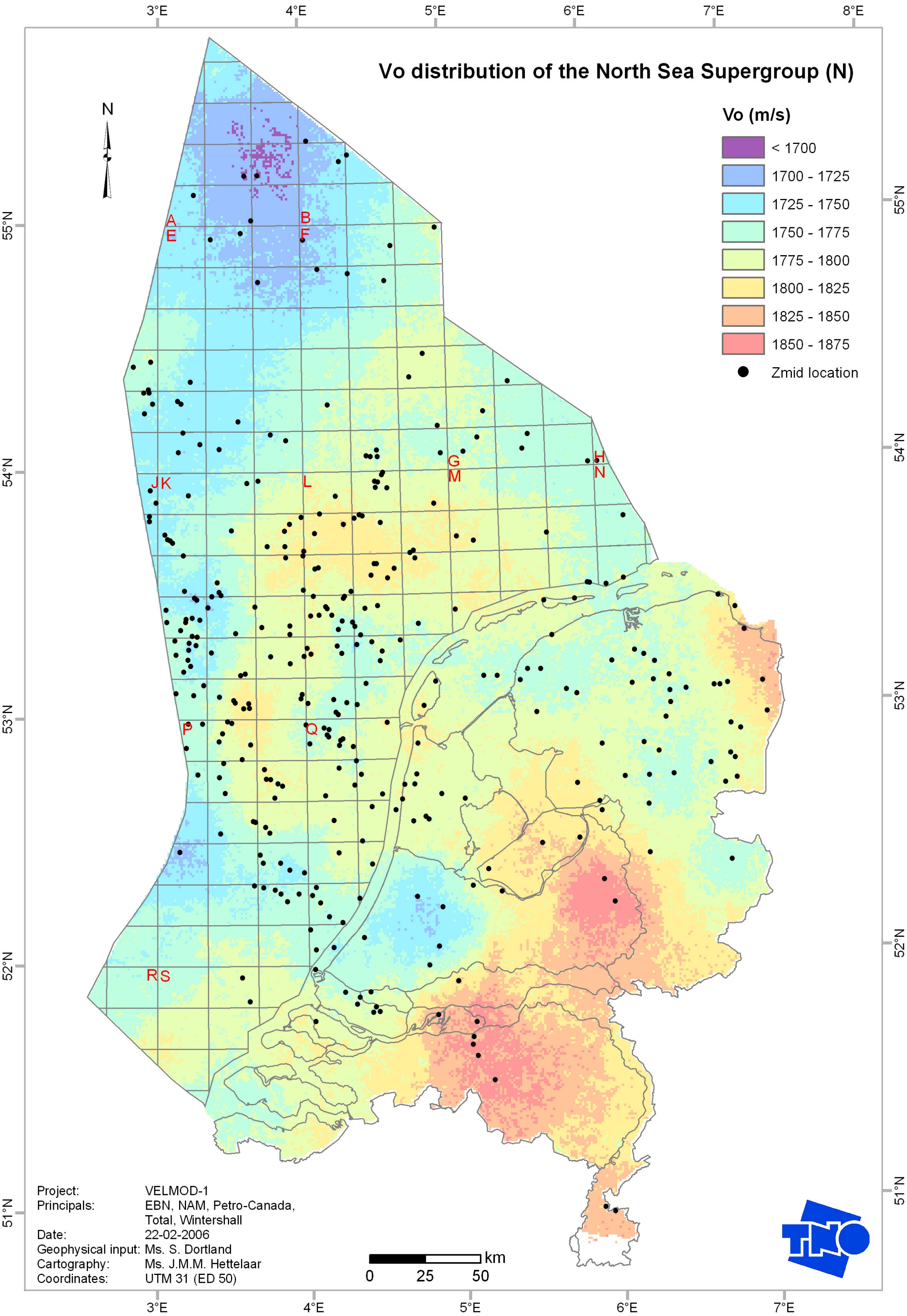

Figure 7.24: V_0 distribution of the North Sea Supergroup (N)

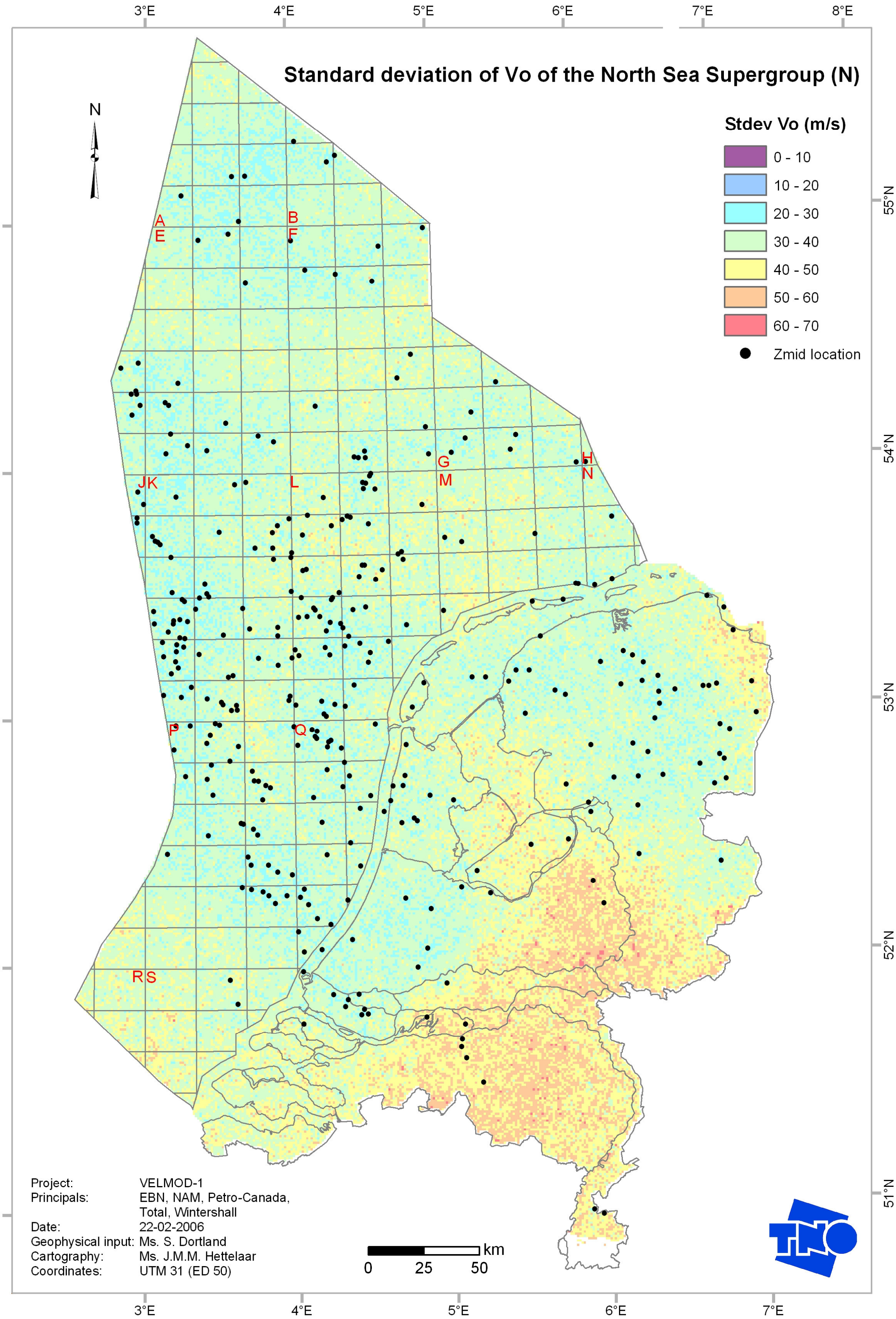

Figure 7.25: Uncertainty (standard deviation) of the V_0 distribution of the North Sea Supergroup (N)

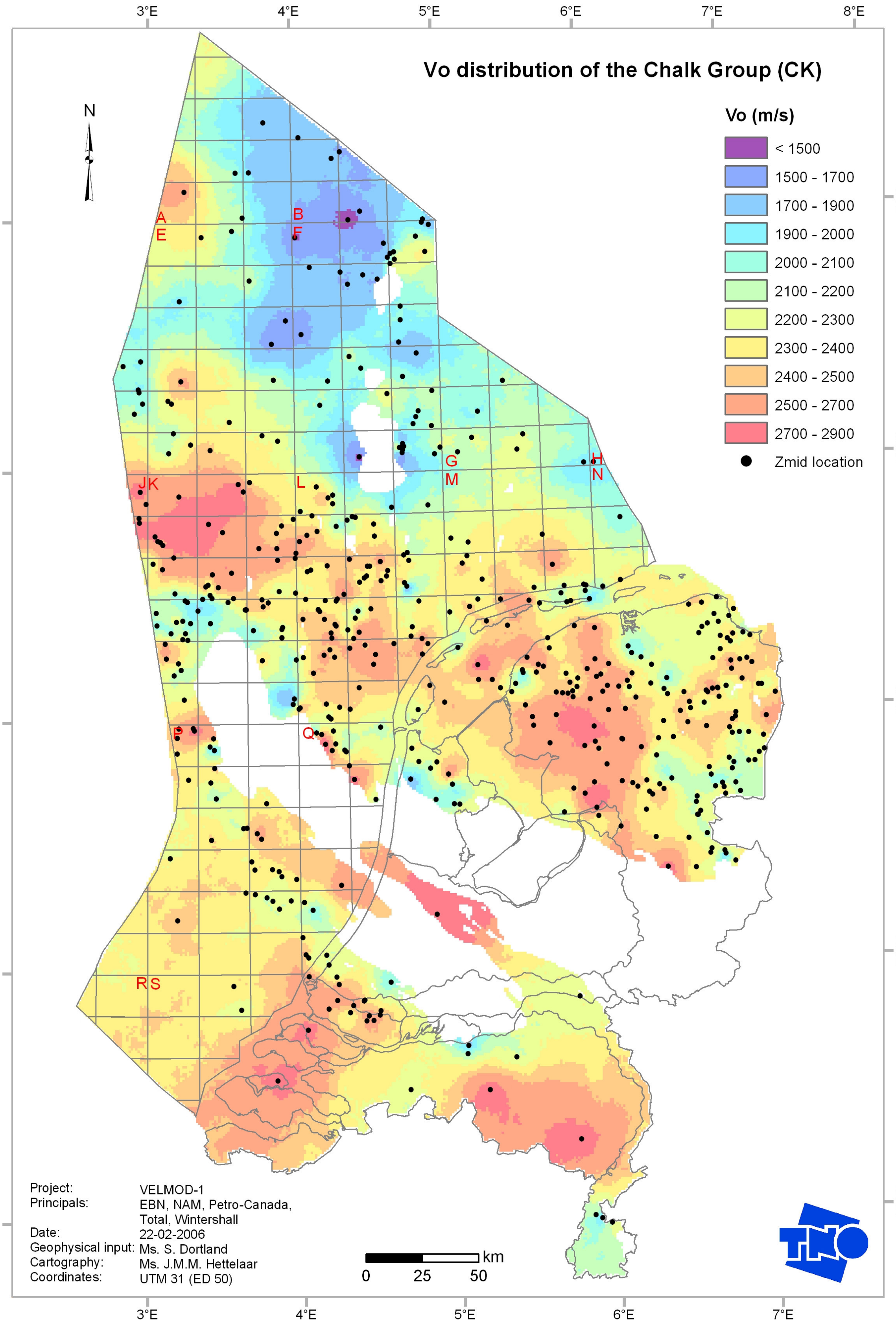

Figure 7.26: V_0 distribution of the Chalk Group (CK)

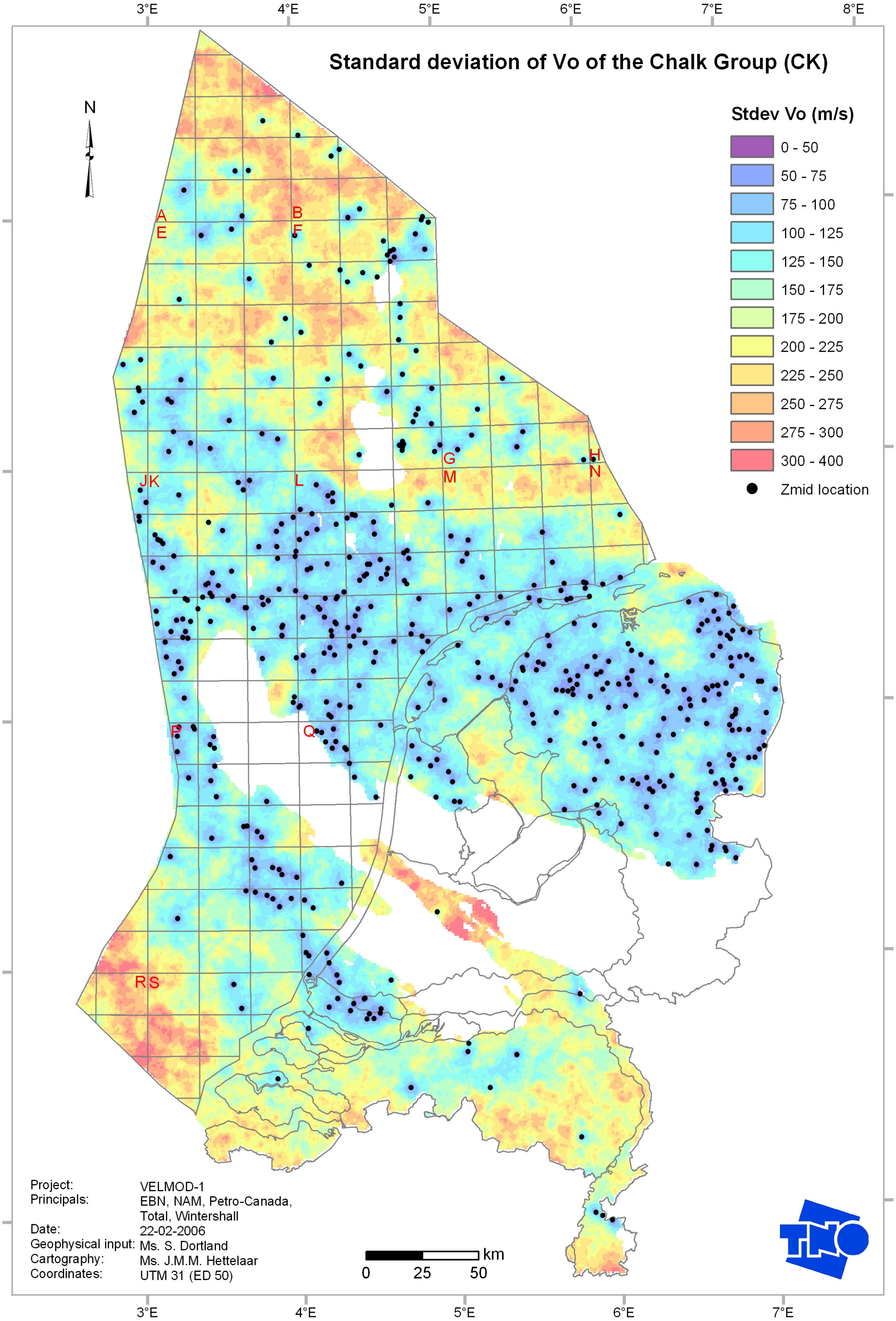

Figure 7.27: Uncertainty (standard deviation) of the V_0 distribution of the Chalk Group (CK)

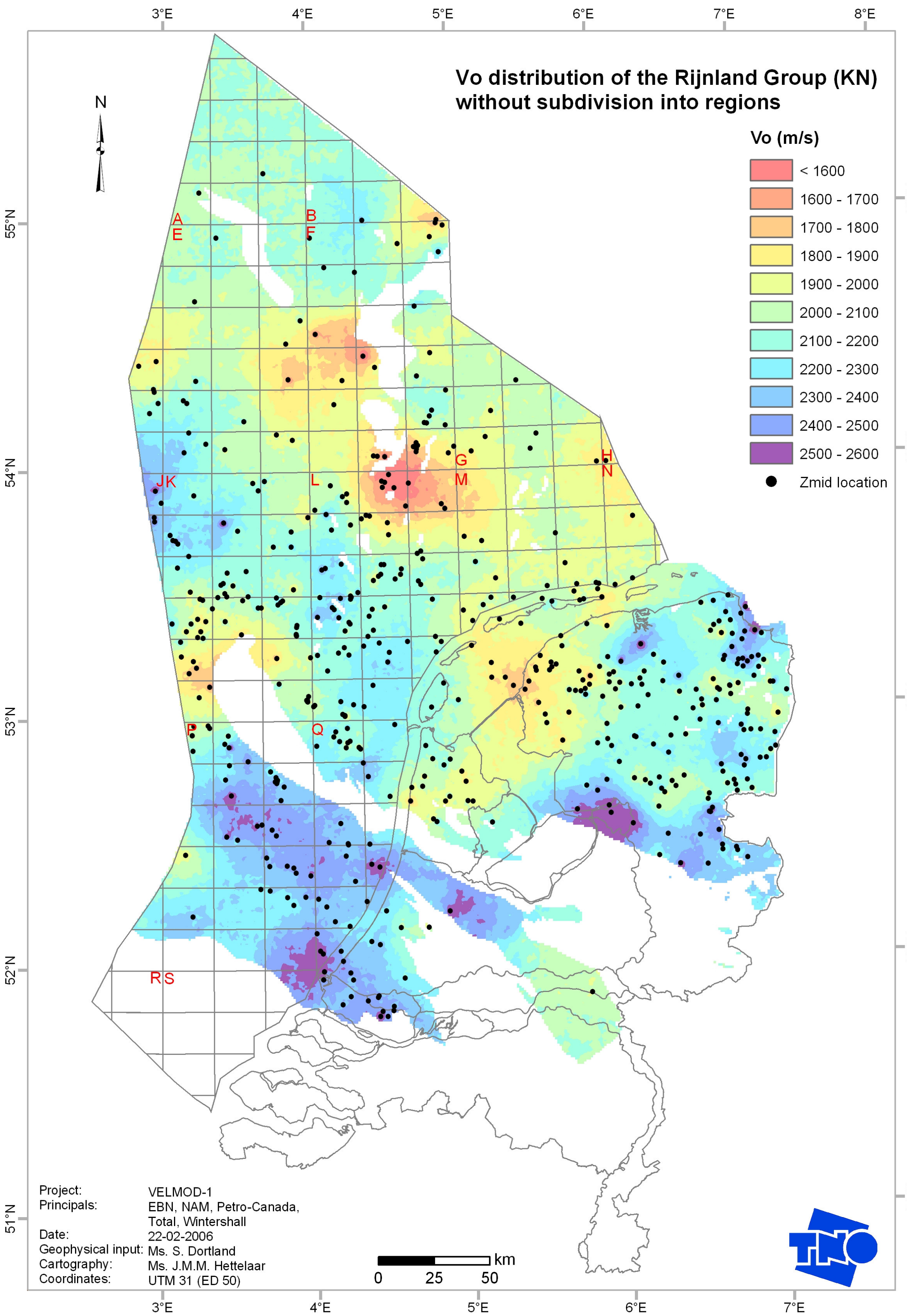

Figure 7.28: V_0 distribution of the Rijnland Group (KN)

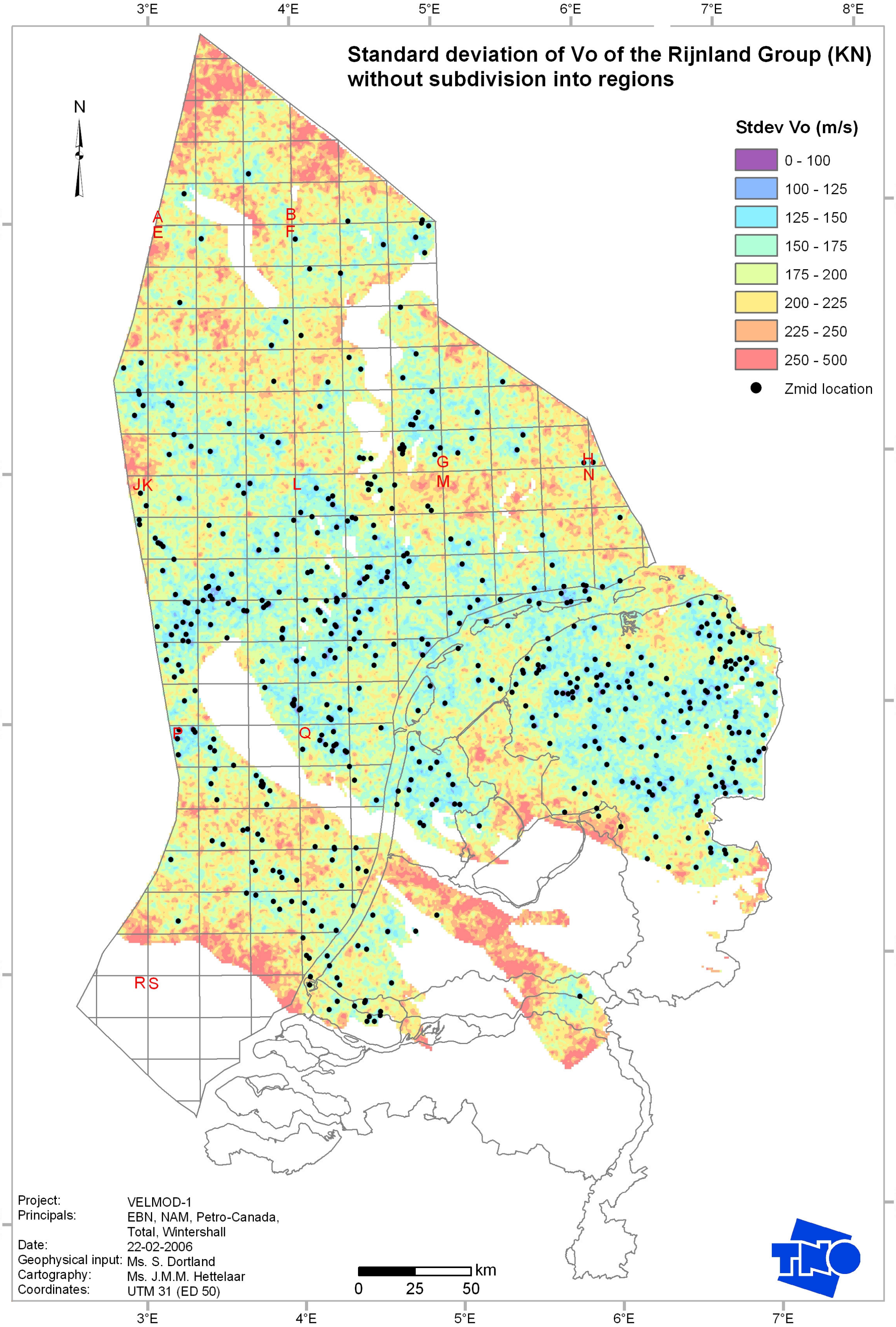

Figure 7.29: Uncertainty (standard deviation) of the V_0 distribution of the Rijnland Group (KN)

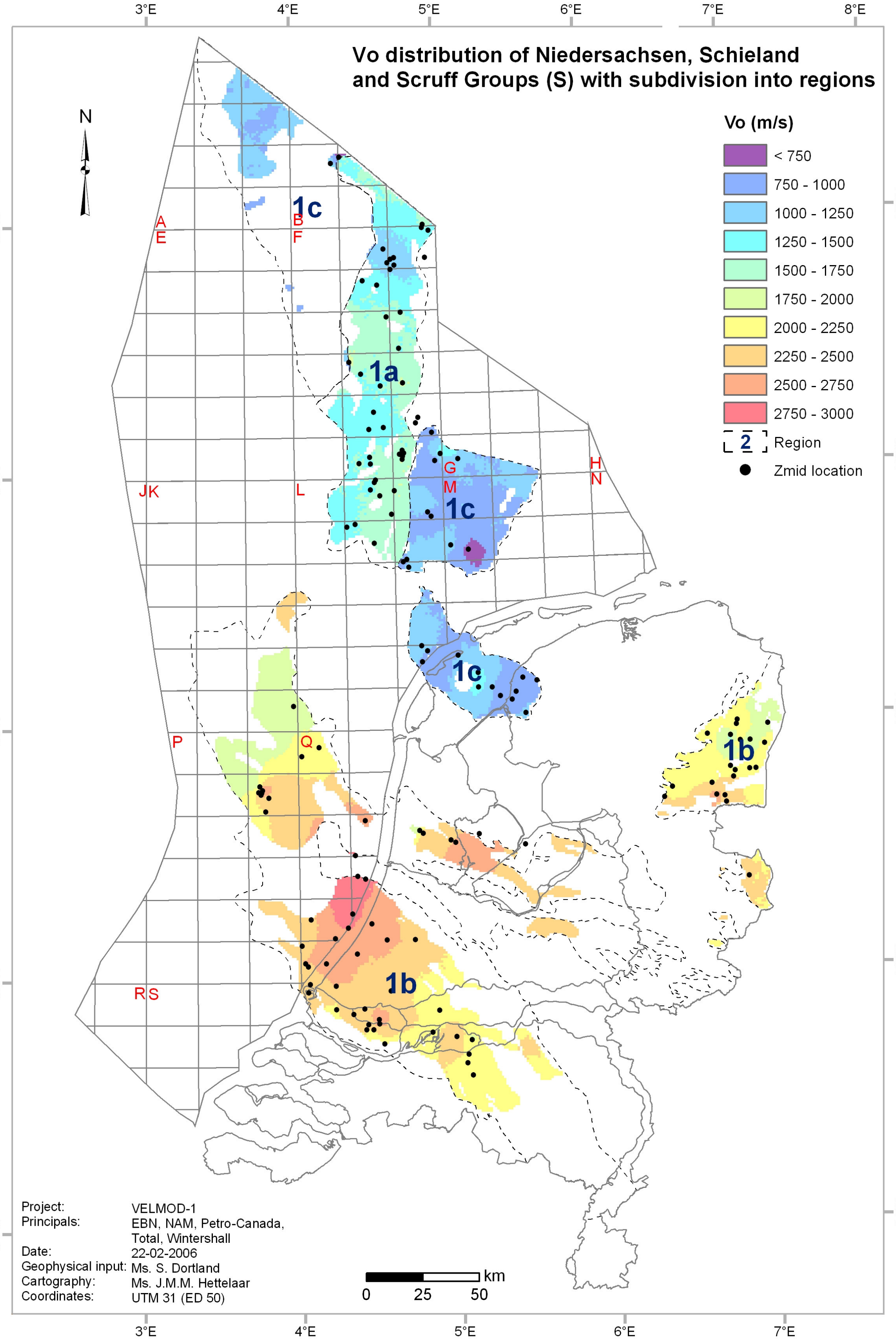

Figure 7.30: V_0 distribution of the Niedersachsen, Schieland and Scruff Groups (S) with subdivision into regions

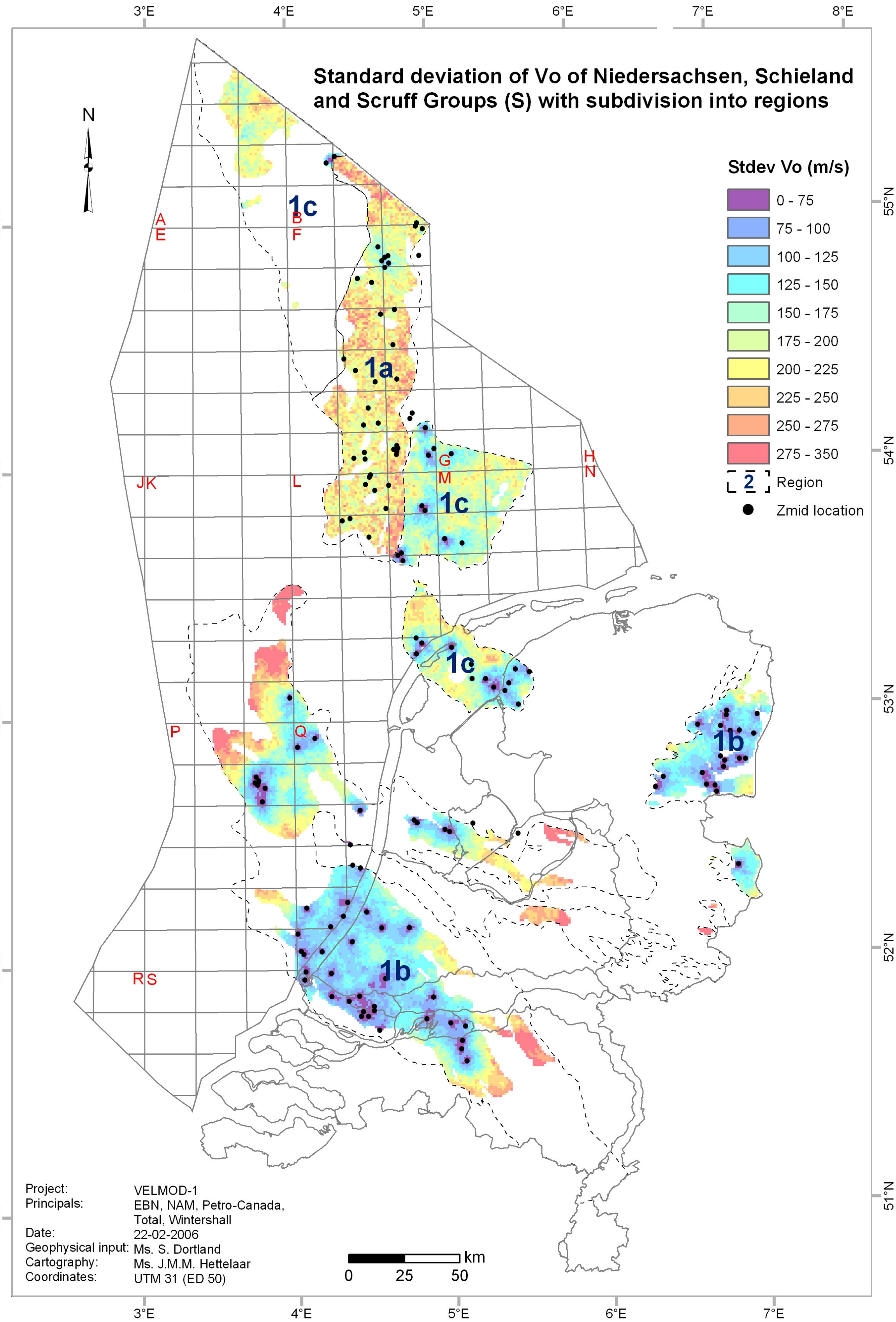

Figure 7.31: Uncertainty (standard deviation) of the V_0 distribution of the Niedersachsen, Schieland and Scruff Groups (S) with subdivision into regions

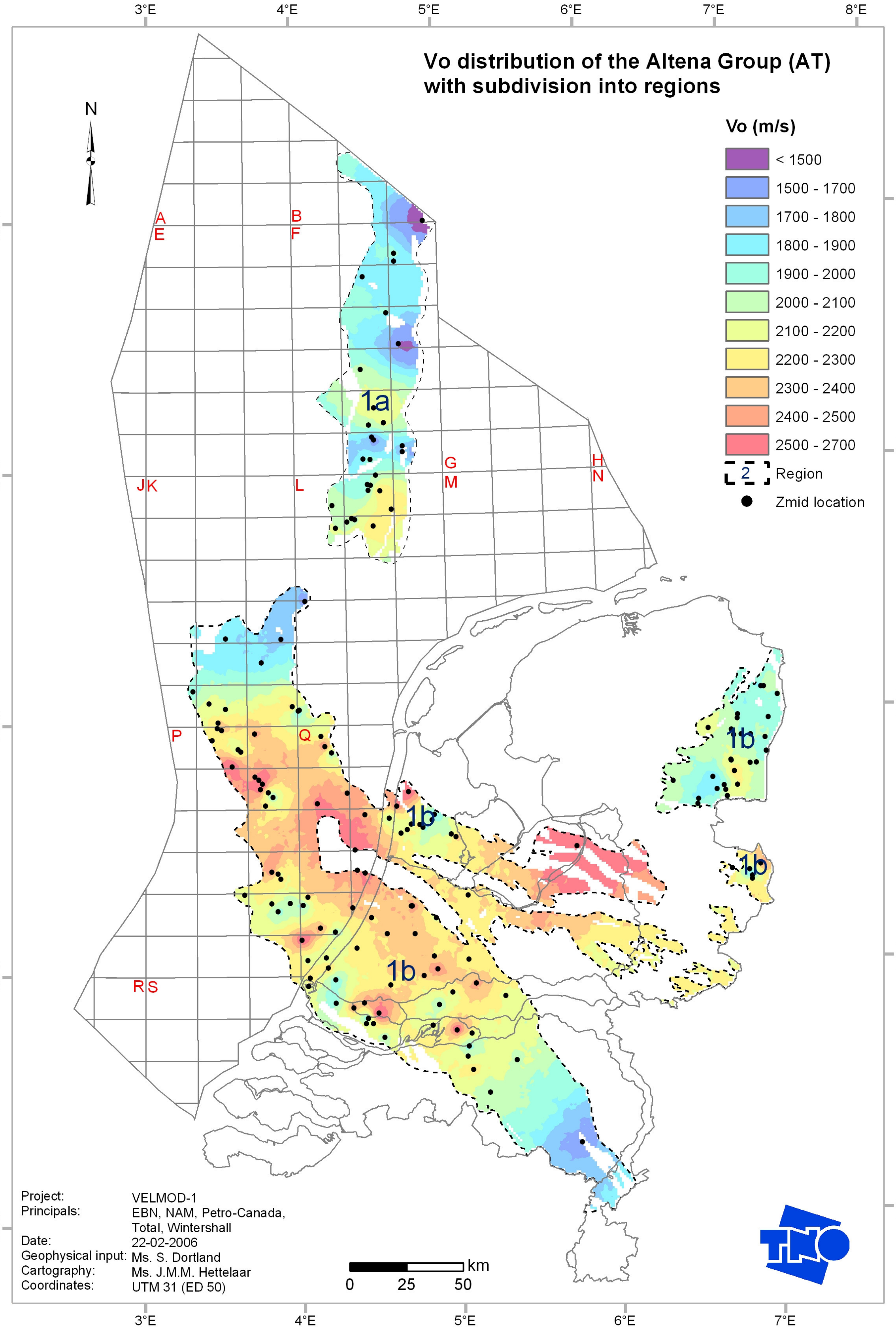

Figure 7.32: V_0 distribution of the Altena Group (AT) with subdivision into regions

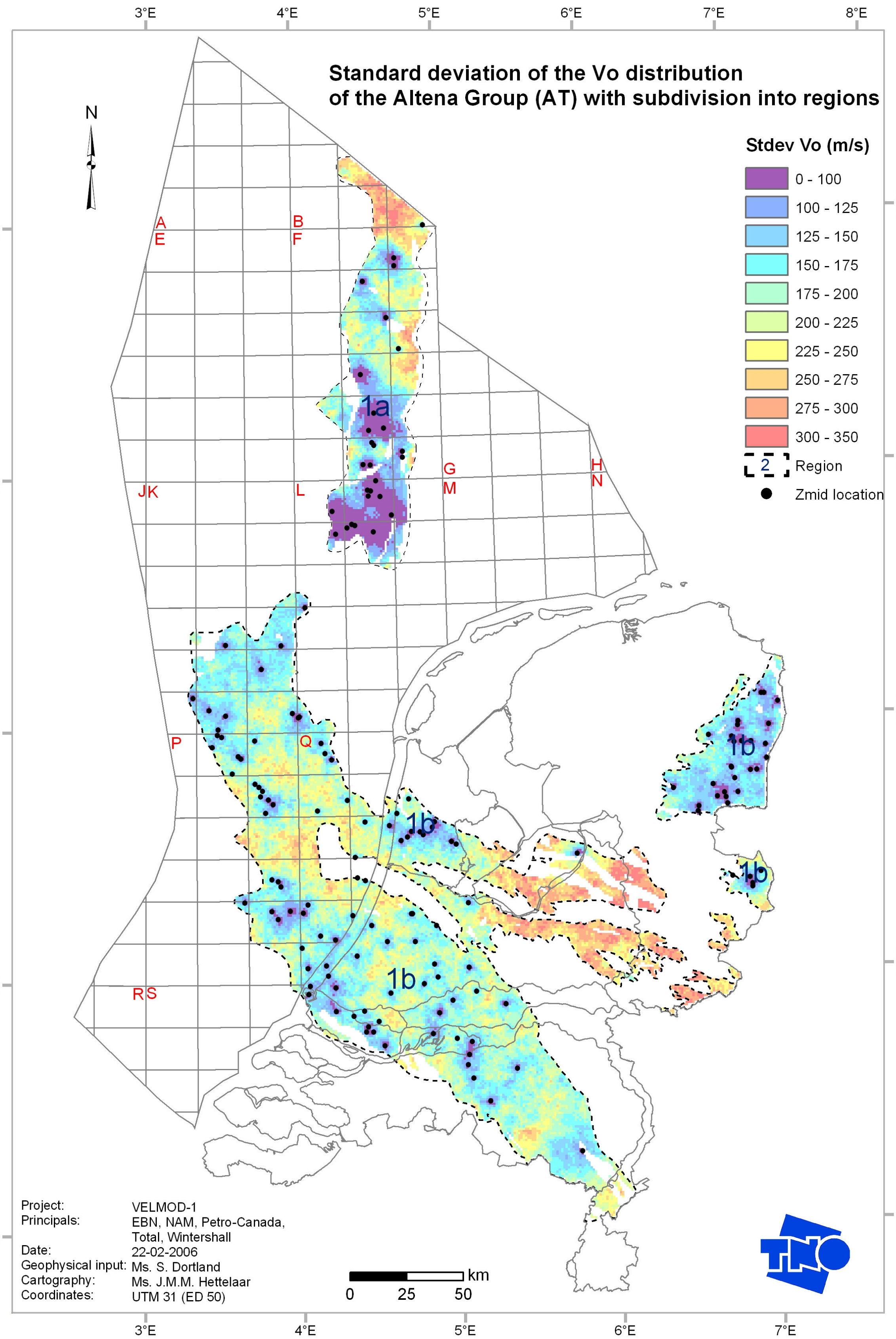

Figure 7.33: Uncertainty (standard deviation) of the V_0 distribution of the Altena Group (AT) with subdivision into regions

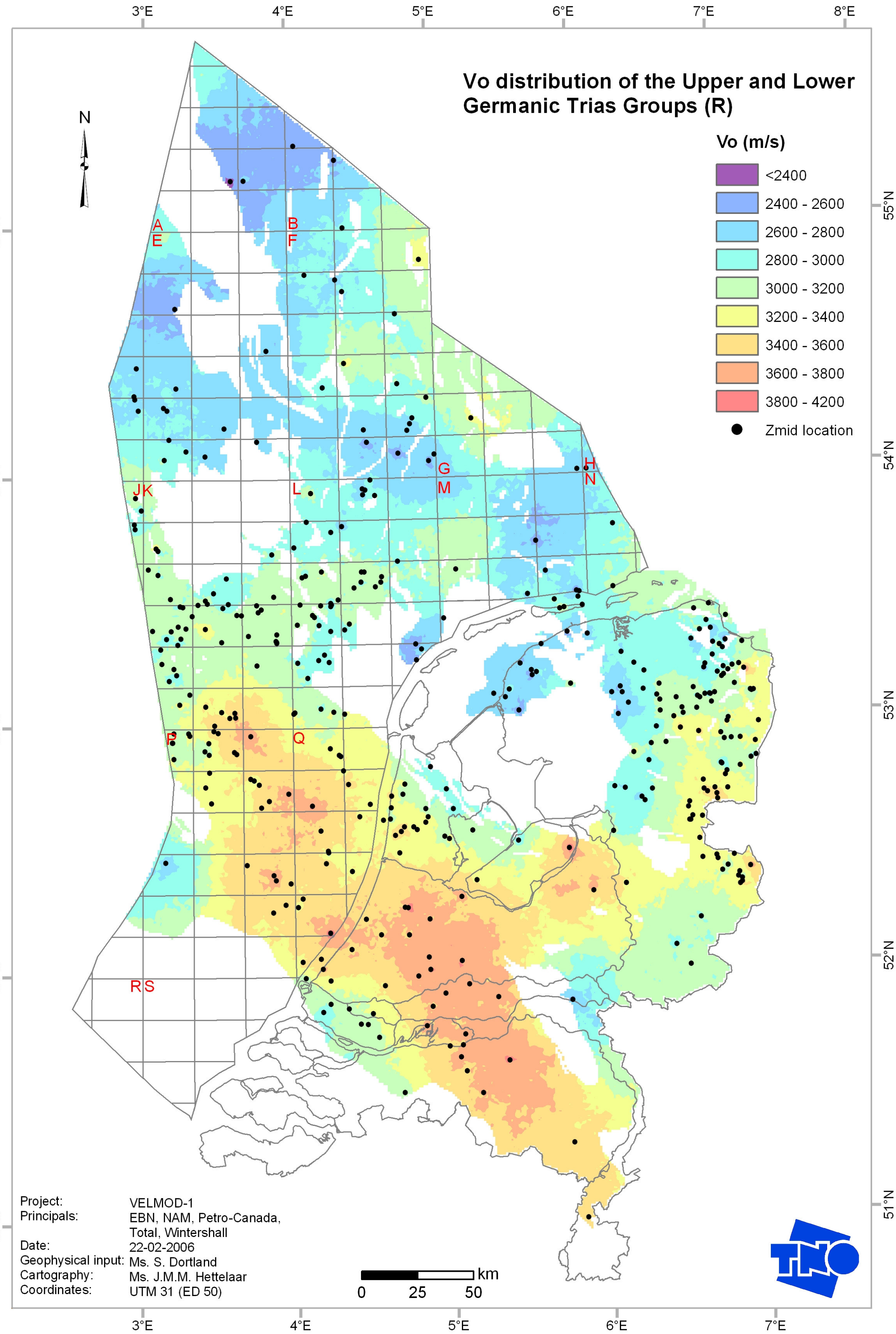

Figure 7.34: V_0 distribution of the Upper and Lower Germanic Trias Groups (R)

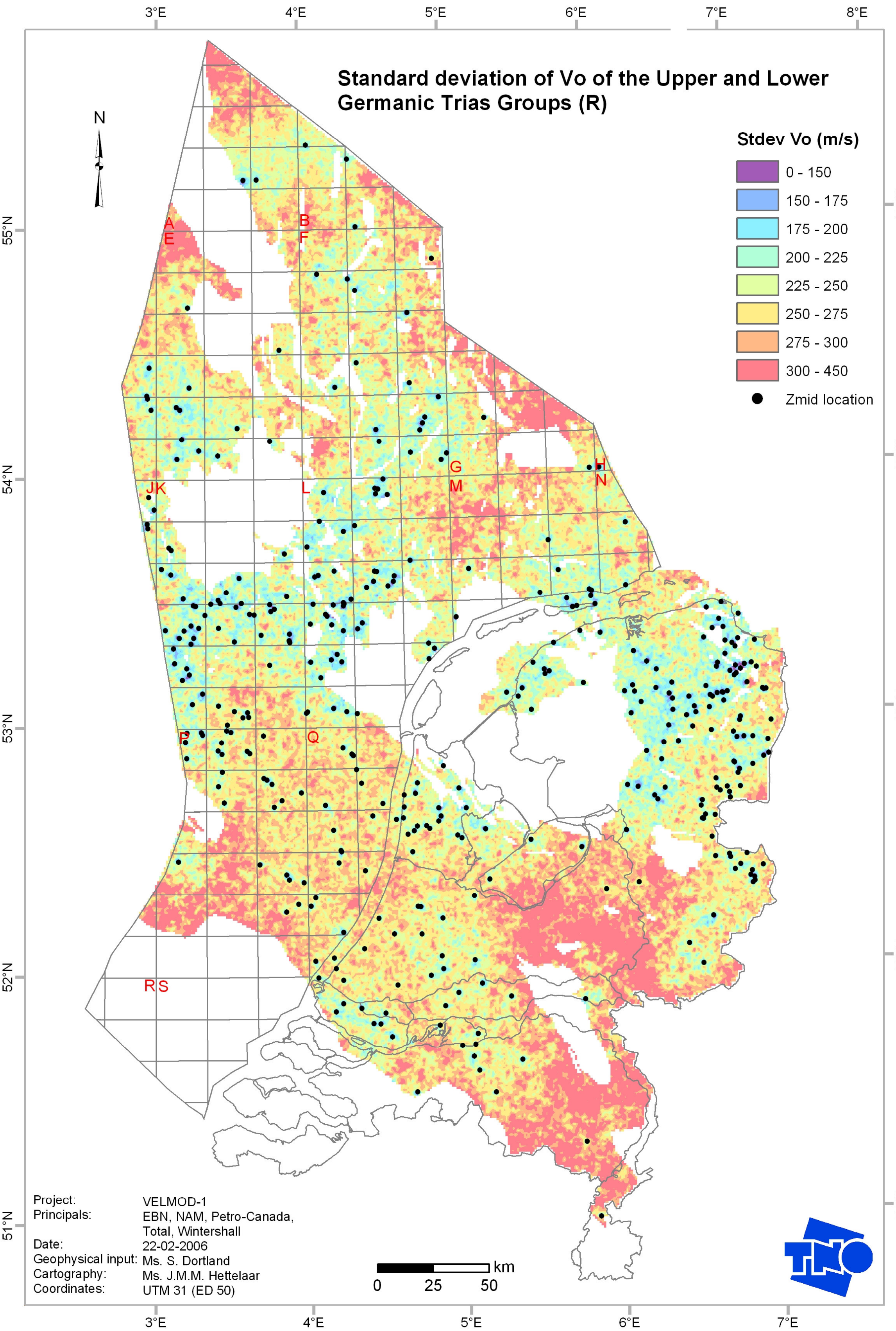

Figure 7.35: Uncertainty (standard deviation) of the V_0 distribution of the Upper and Lower Germanic Trias Groups (R)

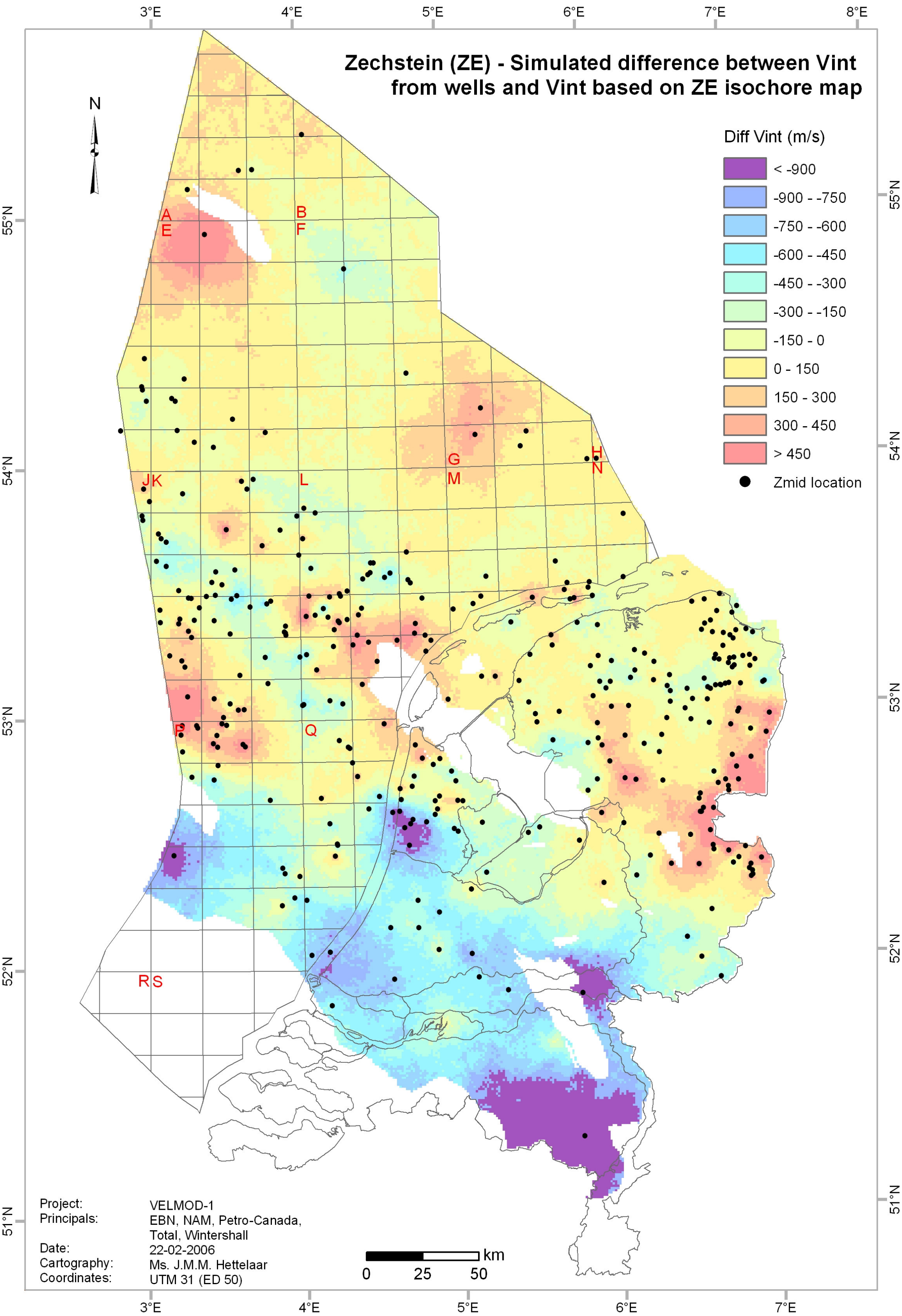

Figure 7.36: Deviation map of the Zechstein Group showing the simulated difference between V_{int} from boreholes and V_{int} based on the ZE isochore map

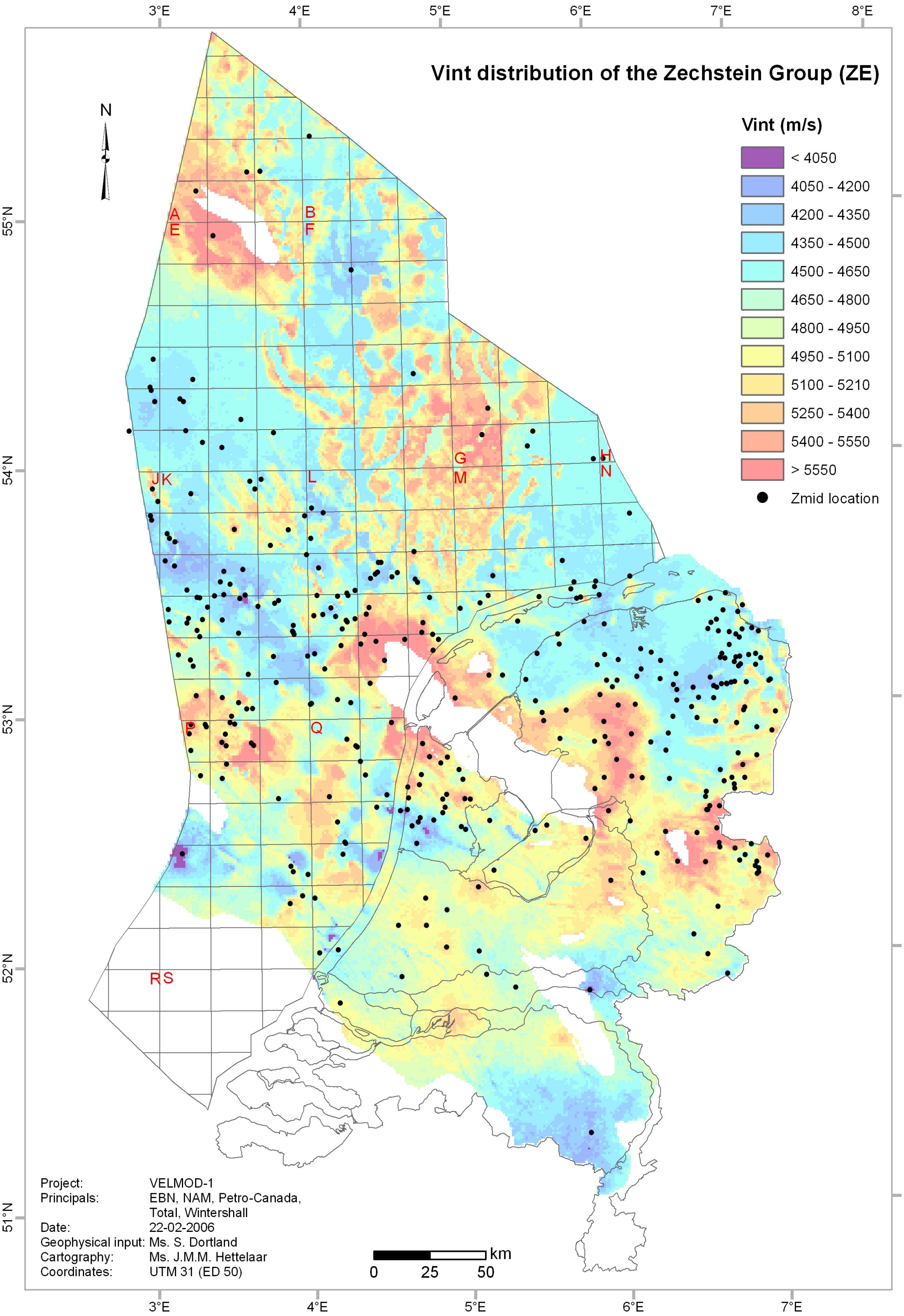

Figure 7.37: V_{int} distribution of the Zechstein Group (ZE)

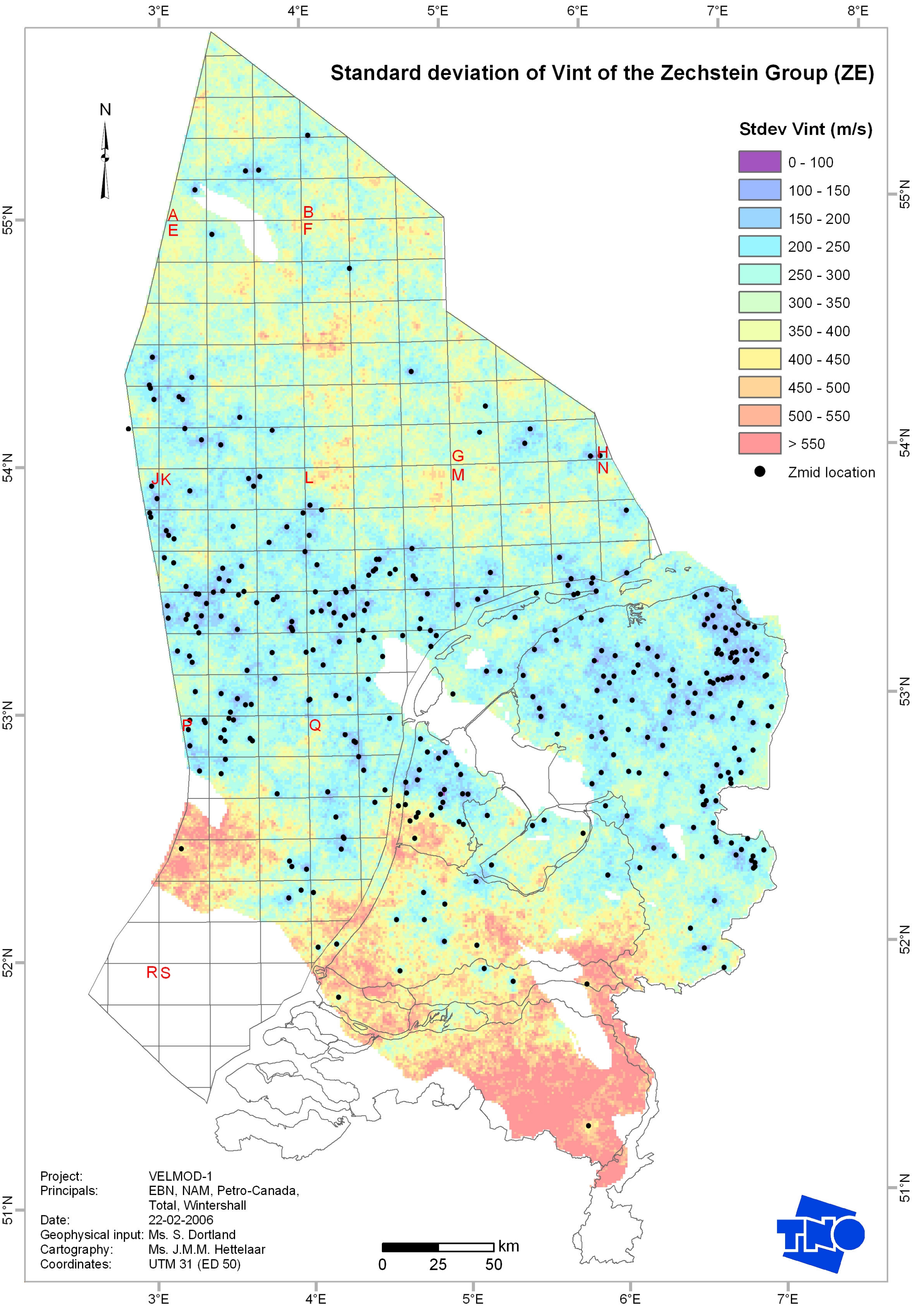

Figure 7.38: Uncertainty (standard deviation) of the V_{int} distribution of the Zechstein Group (ZE)

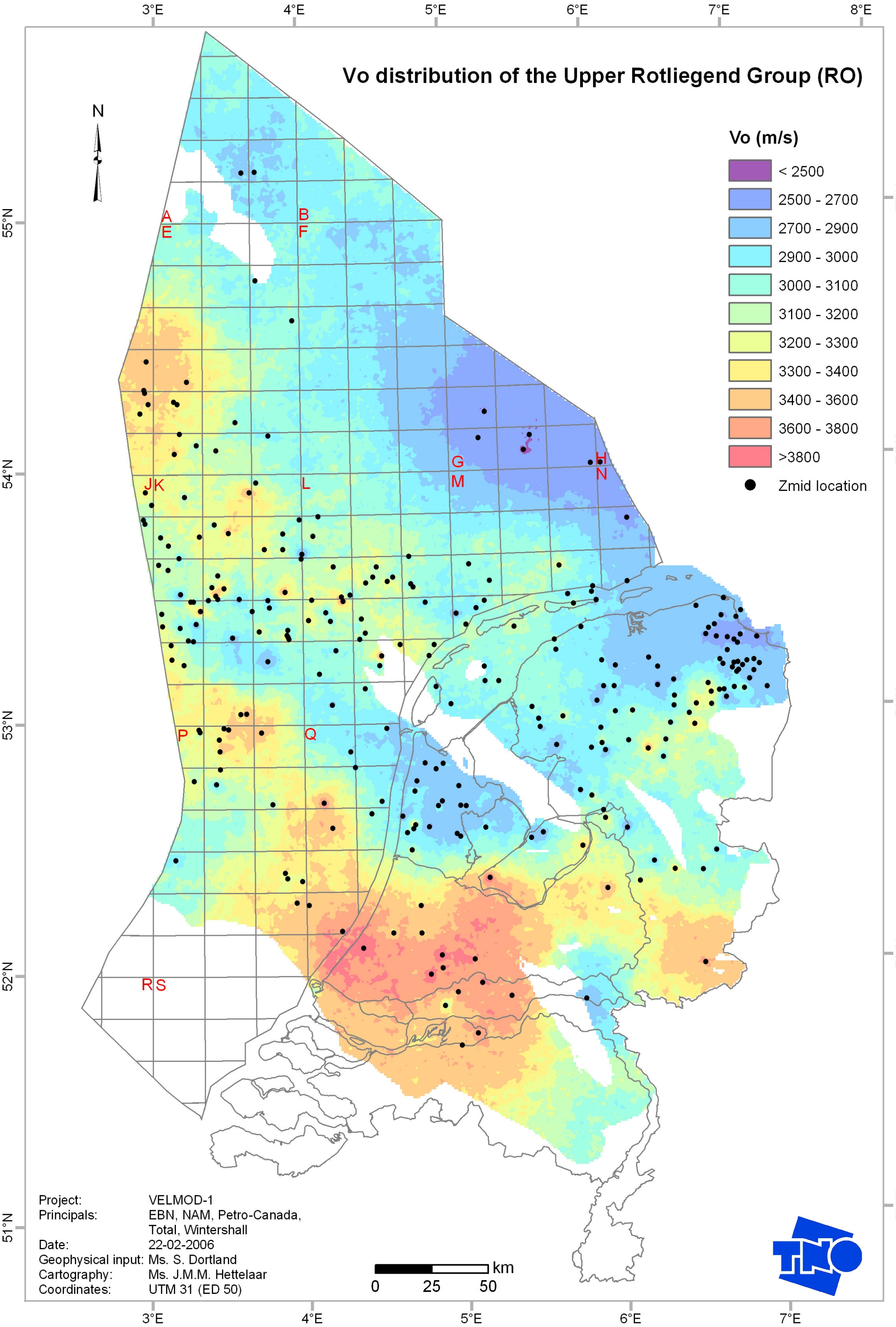

Figure 7.39: V_0 distribution of the Upper Rotliegend Group (RO)

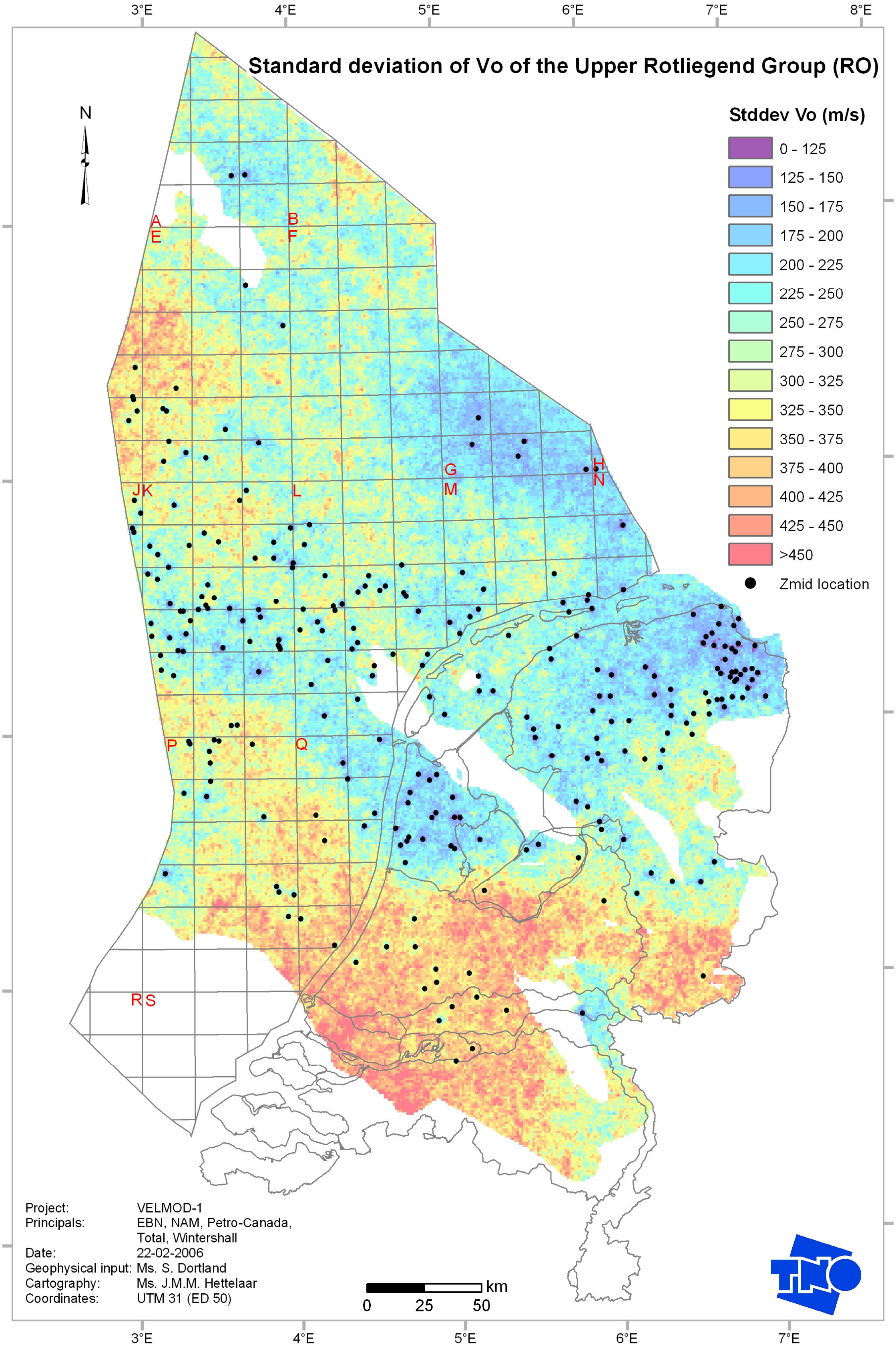

Figure 7.40: Uncertainty (standard deviation) of the V_0 distribution of the Upper Rotliegend Group (RO)

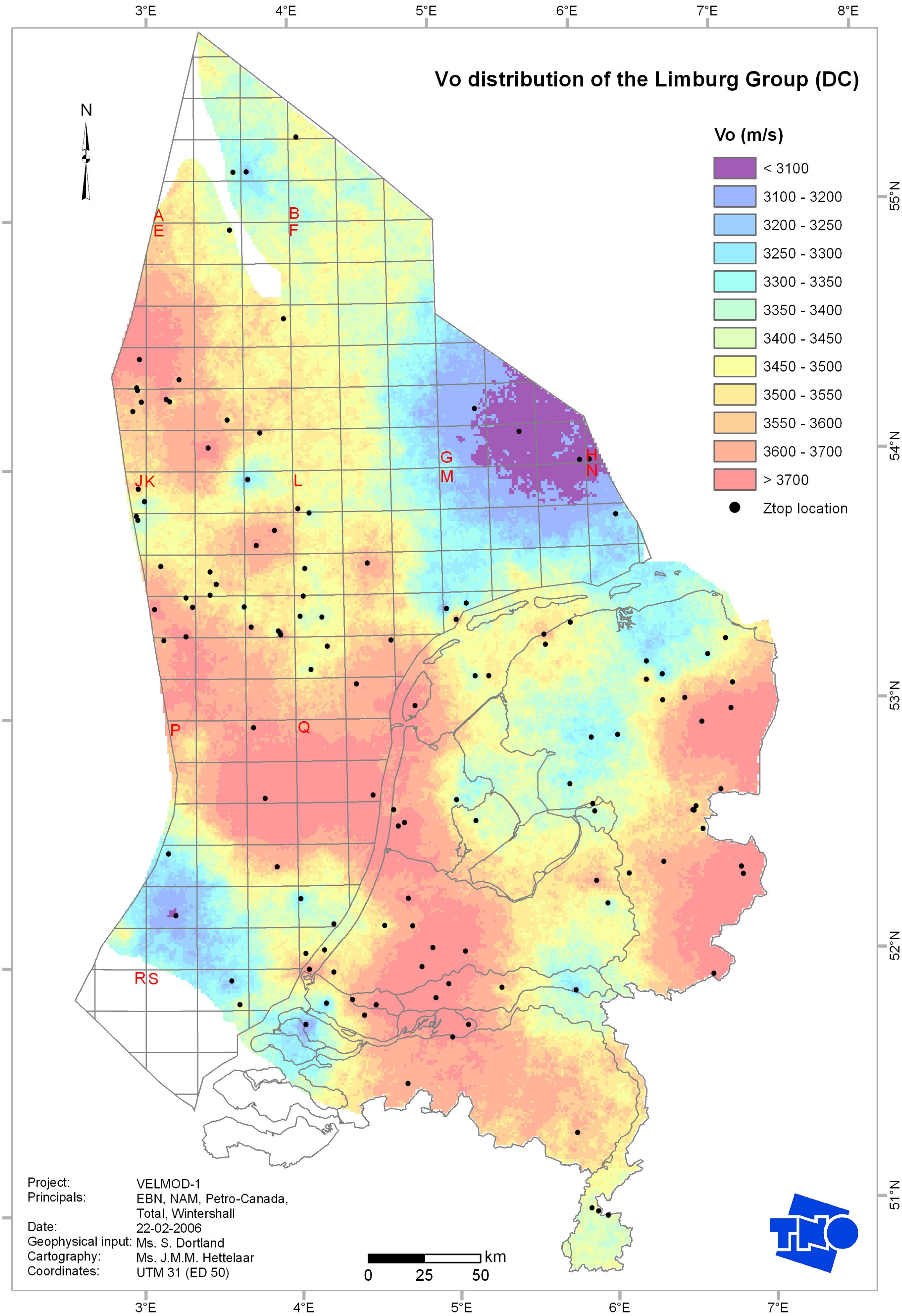

Figure 7.41: V_0 distribution of the Limburg Group (DC)

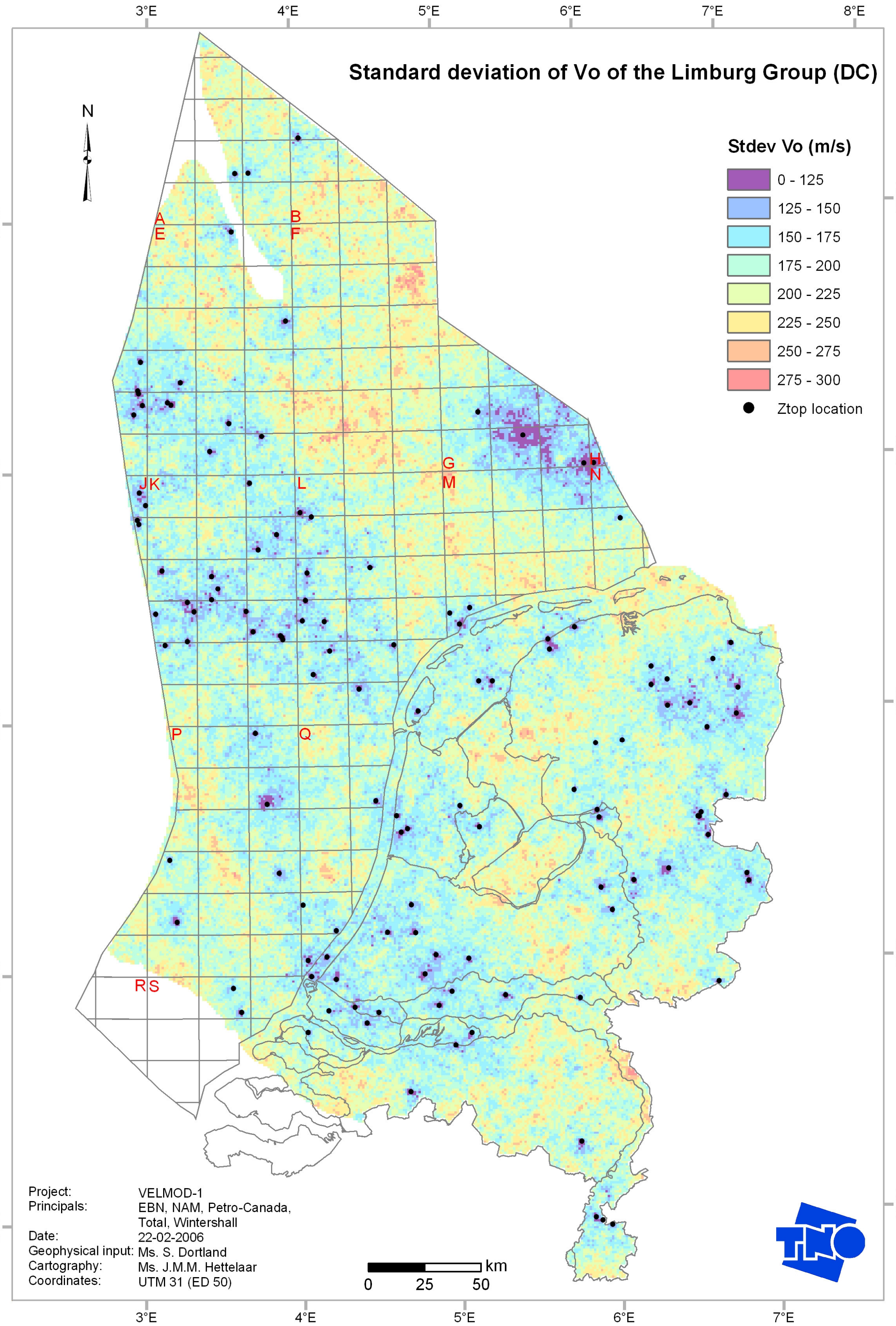

Figure 7.42: Uncertainty (standard deviation) of the V_0 distribution of the Limburg Group (DC)

8 Conclusions and recommendations

Conclusions

1. The instantaneous velocity based v_0-k method of velocity modelling is more complicated and less accurate than the V_{int}-z_{mid} method.
2. The V_{int}-z_{mid} method is particularly suited to model seismic velocities in clastic layers.
3. In modelling seismic velocities for the layer of the Zechstein Group, advantage can be taken of seismics derived isochore map of two-way-traveltime data.
4. A 9-layer seismic velocity model, based on data from the TNO DINO data repository, is constructed for the Netherlands on- and offshore areas.

Recommendations

1. The seismic velocity model constructed under VELMOD-1 may be improved with principal's digital calibrated sonic log data, not present in the TNO DINO data repository.
2. The present velocity model for the Trias layer and also for the Rijnland Group may be replaced. It should be investigated to check the feasibility and added value of a subdivision of these layers into the following layers:
    - Subdivision of the Trias layer into the Upper Germanic Trias Group (RN) and the Lower Germanic Trias Group (RB)
    - Subdivision of the Rijnland Group in the Holland and Vlieland formations

9 References

Deutsch, C.V. and A.G. Journel, 1998, GSLIB, Geostatistical Software, Library and User's guide, Oxford University Press

Doornenbal, J.C., 2001, Regional velocity models of the Netherlands territory, 63rd EAGE Conference Expanded Abstracts, Paper A08

Van Adrichem Boogaert, H.A. and Kouwe, W.F.P., 1997, Stratigraphic nomenclature of the Netherlands, revision and update by RGD and NOGEPA. Mededelingen Rijks Geologische Dienst, Nr. 50

Goovaerts, P., 1997, Geostatistics for Natural Resources Evaluation, Oxford University Press

Japsen, P., 1993, Influence of Lithology and Neogene Uplift on Seismic Velocities in Denmark: Implications for Depth Conversion of Maps, AAPG Bulletin, V. 77, No. 2, P. 194-211

Japsen, P., 1998, Regional Velocity-Depth Anomalies, North Sea Chalk: A Record of Overpressure and Neogene Uplift and Erosion, AAPG Bulletin, V. 82, No. 11, P 2031-2074

Japsen, P., 2000, Investigation of multi-phase erosion using reconstructed shale trends based on sonic data. Sole Pit axis, North Sea, Global and Planetary Change 24 (2000) 189-210

TNO – National Geological Survey, 2004, Geological Atlas of the Subsurface of the Netherlands - onshore

Van Dalfsen, W., Mijnlieff, H.F. and Simmelink, H.J., 2005, Interval velocities of a Triassic claystone : key to burial history and velocity modelling, 67th EAGE Conference Expanded Abstracts, Poster P178

A Data of the SNET project

The data is available on CD.

Table A. 1: Explanation of abbreviations used in Appendix A

Abbreviation	**Description**
Status	V_{int} is accepted or rejected for V_{int}-z_{mid} analysis and geostatistical modelling. SNET>DCS: DCS data is used in stead of SNET data
UWI	Borehole identifier
Borehole	Name of the borehole
Layer	Lithostratigraphic layer
E_t	Location (Easting) of the borehole at the top of the layer
N_t	Location (Northing) of the borehole at the top of the layer
z_t	Depth of the top of the layer [m]
z_b	Depth of the base of the layer [m]
TWT_t	Two way traveltime to the top of the layer
TWT_b	Two way traveltime to the base of the layer
ΔT	One way traveltime vertical through layer
T_b	One way traveltime to the base of the layer
E_b	Location (Easting) of the borehole at the bottom of the layer
N_b	Location (Northing) of the borehole at the bottom of the layer
E_0	Location (Easting) of the borehole at reference surface
N_0	Location (Northing) of the borehole at reference surface
E_b-E_0	Deviation (Easting)
N_b-N_0	Deviation (Northing)
Δz	True vertical thickness [m]
E_{mid}	Location (Easting) of the borehole at the mid-depth of the layer
N_{mid}	Location (Northing) of the borehole at the mid-depth of the layer
z_{mid}	Mid-depth of the layer [m]
V_{int}	Interval velocity [m/s]

B Graphs of instantaneous velocities of DCS logs and their linearisation with VOLONZ

On the next pages the graphs of instantaneous velocities of DCS logs and their linearisation with VOLONZ are shown. The graphs are also available on CD.

Table B. 1: Color legend of the VOLONZ graphs

No.	**Layer**	**Abbr.**	**VOLONZ color**
1	North Sea Supergroup	N	yellow
2	Chalk Group	CK	light green
3	Rijnland Group	KN	dark green
4	Niedersachsen, Schieland and Scruff Groups	S	dark blue
5	Altena Group	AT	light blue
6	Upper and Lower Germanic Trias Groups	R	purple
7	Zechstein Group	ZE	pink
8	Upper Rotliegend Group	RO	brown
9	Limburg Group	DC	grey

UWI	Borehole
7825	A12-03
8108	A15-02
7534	B14-02
3697	BKZ-01
2497	BRA-01
2474	BTL-01
7018	D12-01
7657	D12-03
7704	D12-04
7682	D15-02
8009	E02-02
7737	E04-01
7513	E10-01
7028	E18-02
7970	F01-01
7770	F05-03
8037	F12-03
7915	F15-07
7559	F17-06
7823	G11-02
7523	G16-01
7590	G17-02
7079	G18-01
7080	H16-01
2667	HST-02-S1
7722	J03-02
7936	J06-A-01
7738	K03-01
7980	K06-06
8025	K06-08
8114	K06-N-01
7133	K10-11
7566	K10-12
8142	K10-V-02
7666	K11-09
7926	K11-11
7561	K12-A-04
7683	K12-B-03
7758	K12-B-05
8059	K12-B-06
8053	K13-14
7235	K16-04
7580	K18-KOTTER-05
7622	K18-KOTTER-07-10
7632	K18-KOTTER-08-01
7639	K18-KOTTER-09-12
2653	KDZ-02
1097	KGB-01
8062	L03-03
8126	L03-04
8173	L04-06
7617	L05-04
7824	L05-05
7952	L06-01
7519	L08-04
7969	L08-11
7542	L09-02
7828	L09-04
7301	L10-22

UWI	Borehole
7303	L10-24
7721	L10-27
7806	L10-29
7348	L10-F-01
7302	L10-G-01
7602	L10-K-01-S1
7712	L10-K-01-S2
7662	L10-K-02
7811	L10-L-02
7357	L11-08
7368	L13-05
7369	L13-06
7608	L13-FD-101
7594	L14-05
7677	L16-LOGGER-04-S2
7978	M04-01
8128	M04-02
7724	M10-03
7836	M10-04
3730	MRK-01
3721	MSG-01
2442	NRZ-01
3751	OBLZ-01
8494	P02-04
7596	P02-07
7552	P05-05
8495	P06-A-01
8630	P06-A-02
8497	P06-A-03
7427	P06-A-04
7598	P06-A-06
7619	P06-B-01
8531	P06-C-01
7997	P06-S-01
7431	P08-02
7557	P08-04
7527	P08-05-S1
7434	P09-02
7764	P12-07
8049	P12-12
7749	P12-C-06
7935	P14-A-01
8070	P16-01
2659	PKP-01
3713	PRN-01
8096	Q02-04
7530	Q04-04
7656	Q05-01
8054	Q05-05
7495	Q07-04
7837	Q08-06
7499	Q08-B-01
7739	Q10-03
7650	Q13-04
7702	Q13-05
7524	Q16-03
7925	Q16-FA-101
3799	WWN-02
2344	ZVH-01

Calibrated instantaneous velocities and linearisation per layer at borehole: A12-03

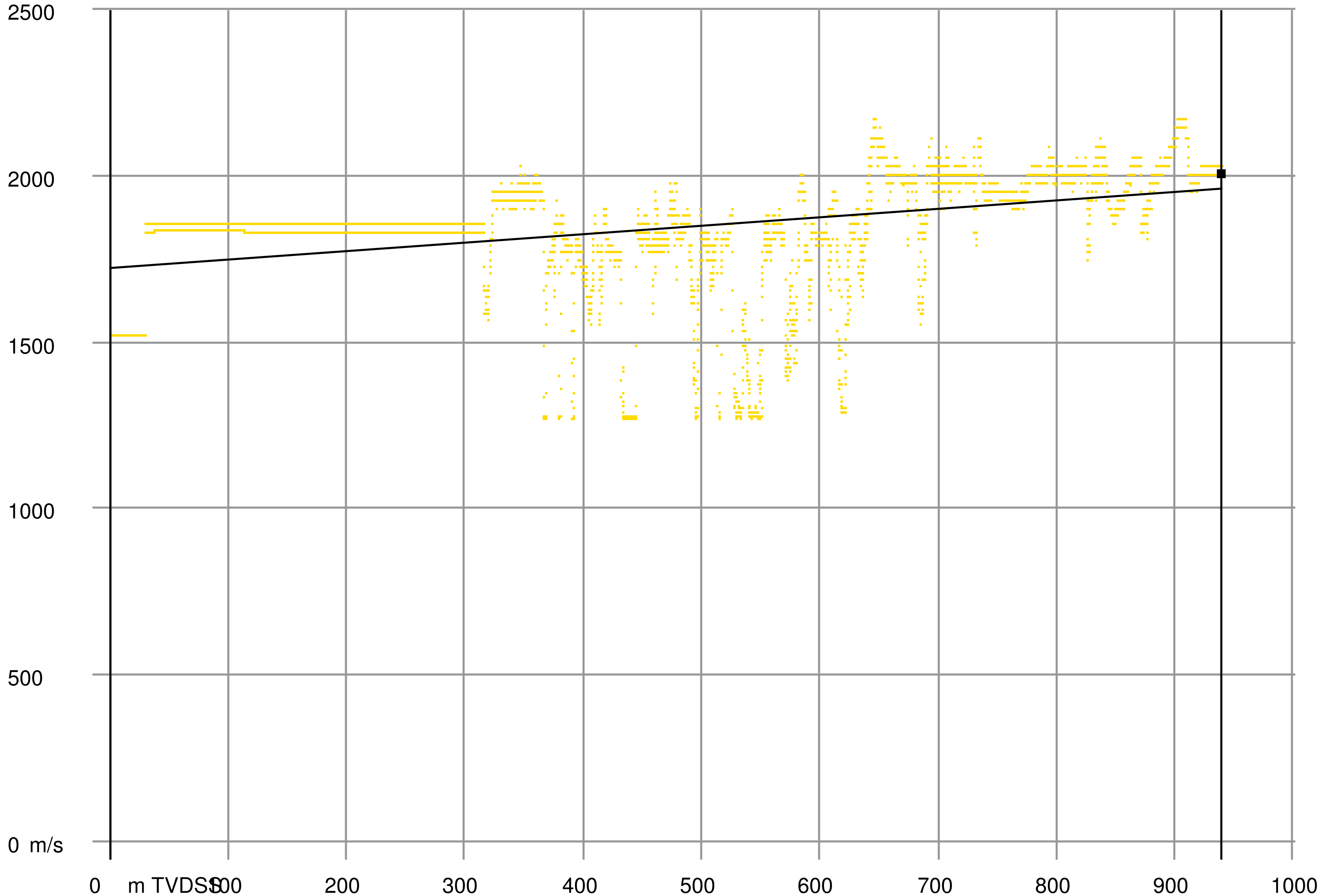

Calibrated instantaneous velocities and linearisation per layer at borehole: A15-02

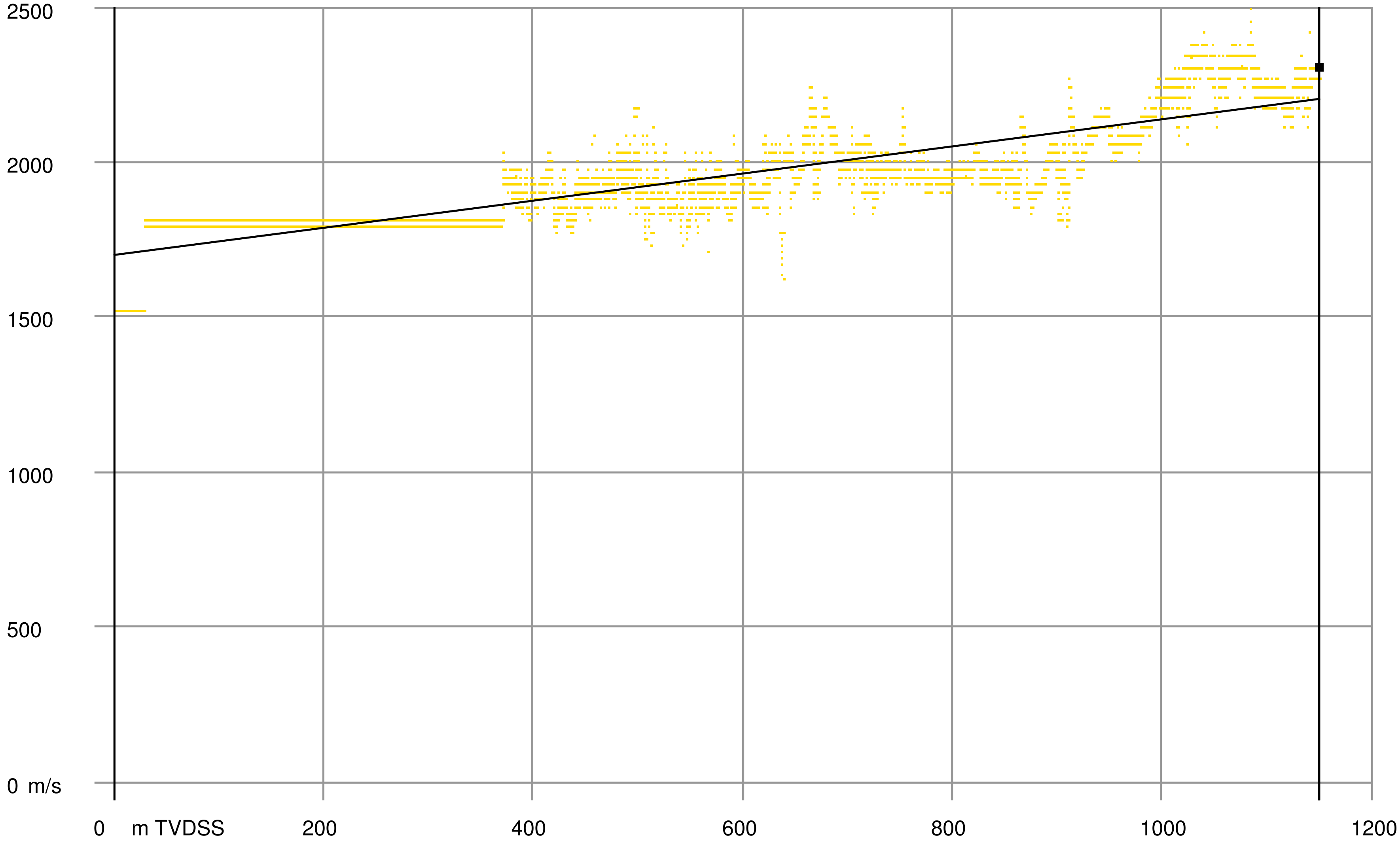

Calibrated instantaneous velocities and linearisation per layer at borehole: B14-02

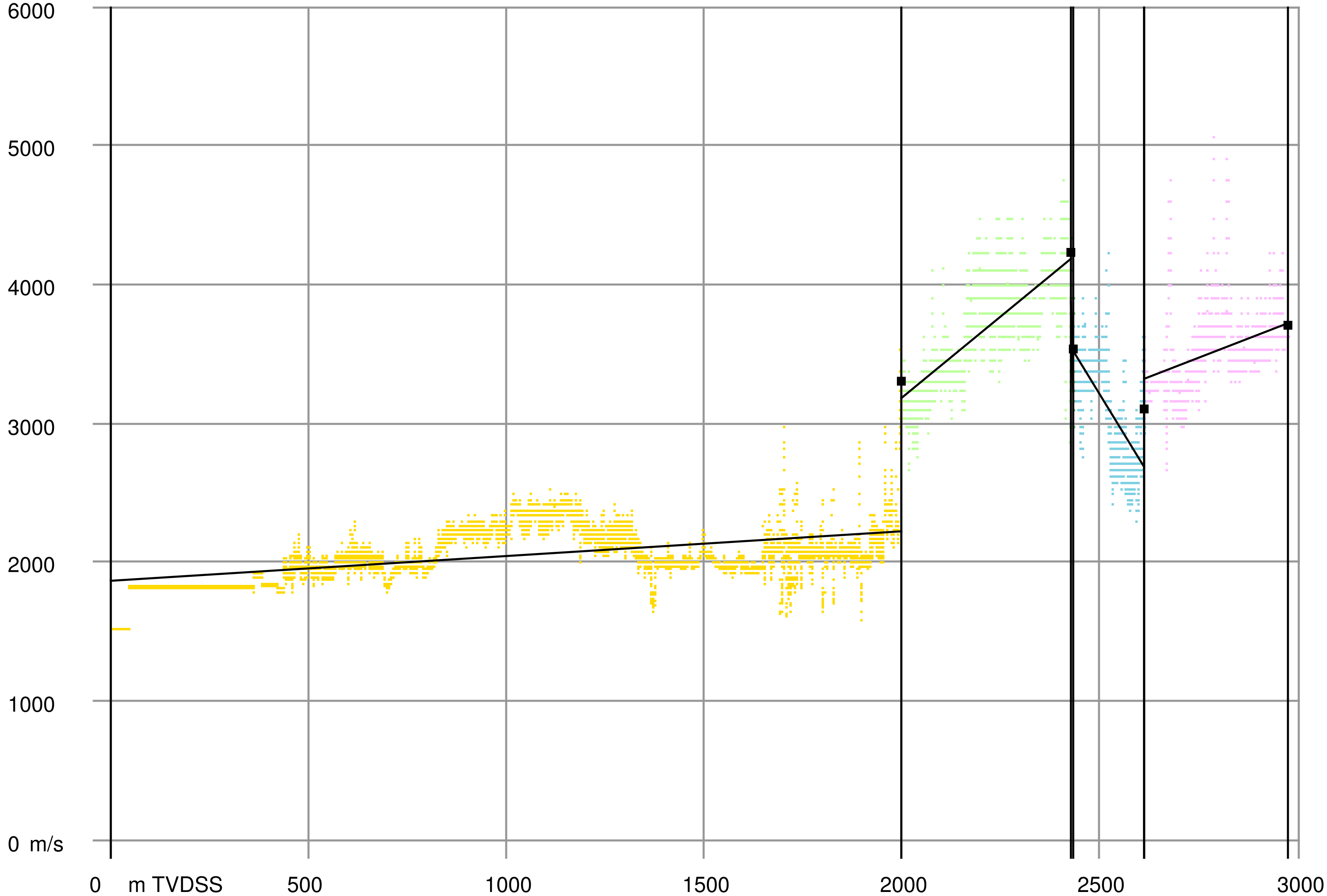

Calibrated instantaneous velocities and linearisation per layer at borehole: BKZ-01

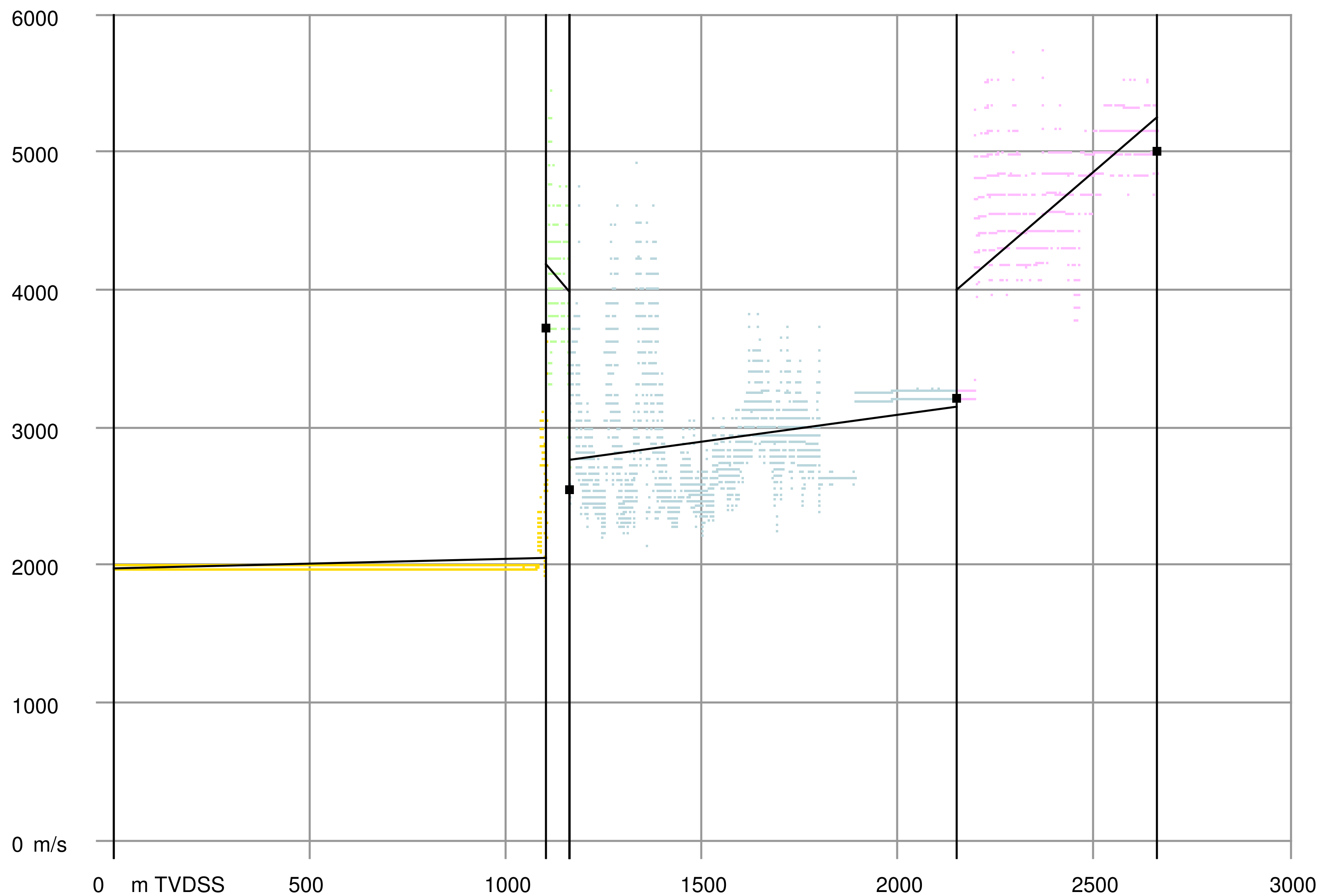

Calibrated instantaneous velocities and linearisation per layer at borehole: BRA-01

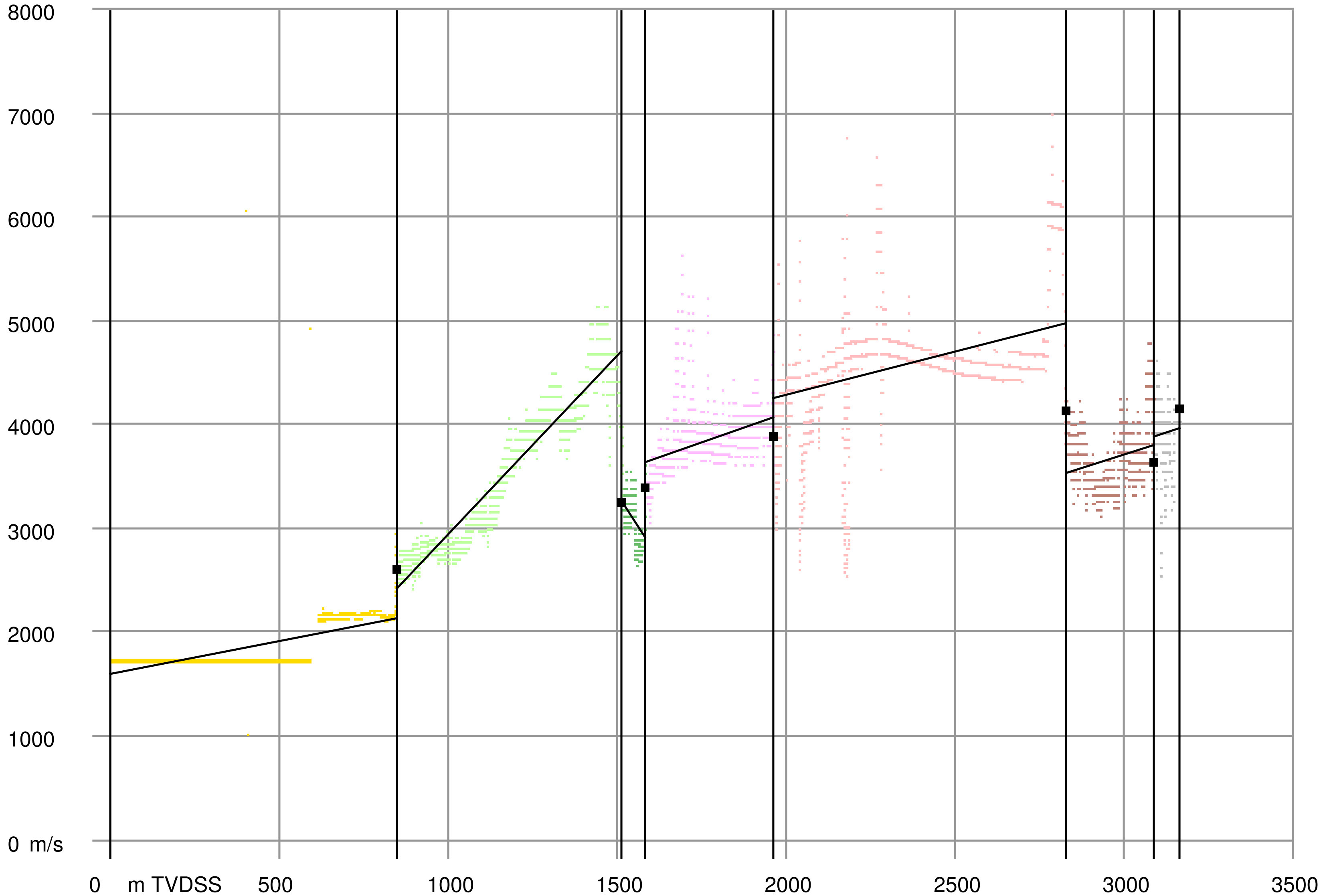

Calibrated instantaneous velocities and linearisation per layer at borehole: BTL-01

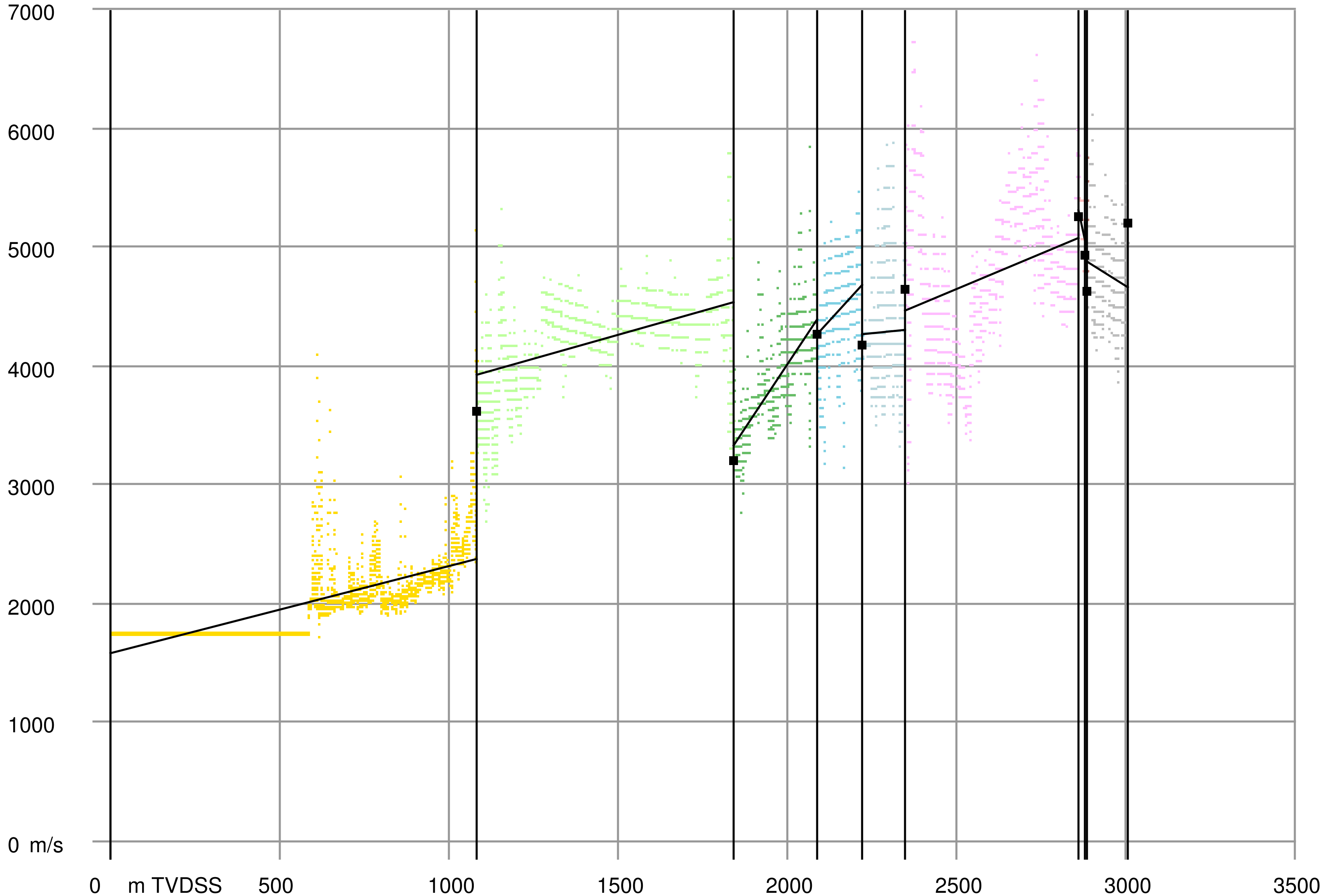

Calibrated instantaneous velocities and linearisation per layer at borehole: D12-01

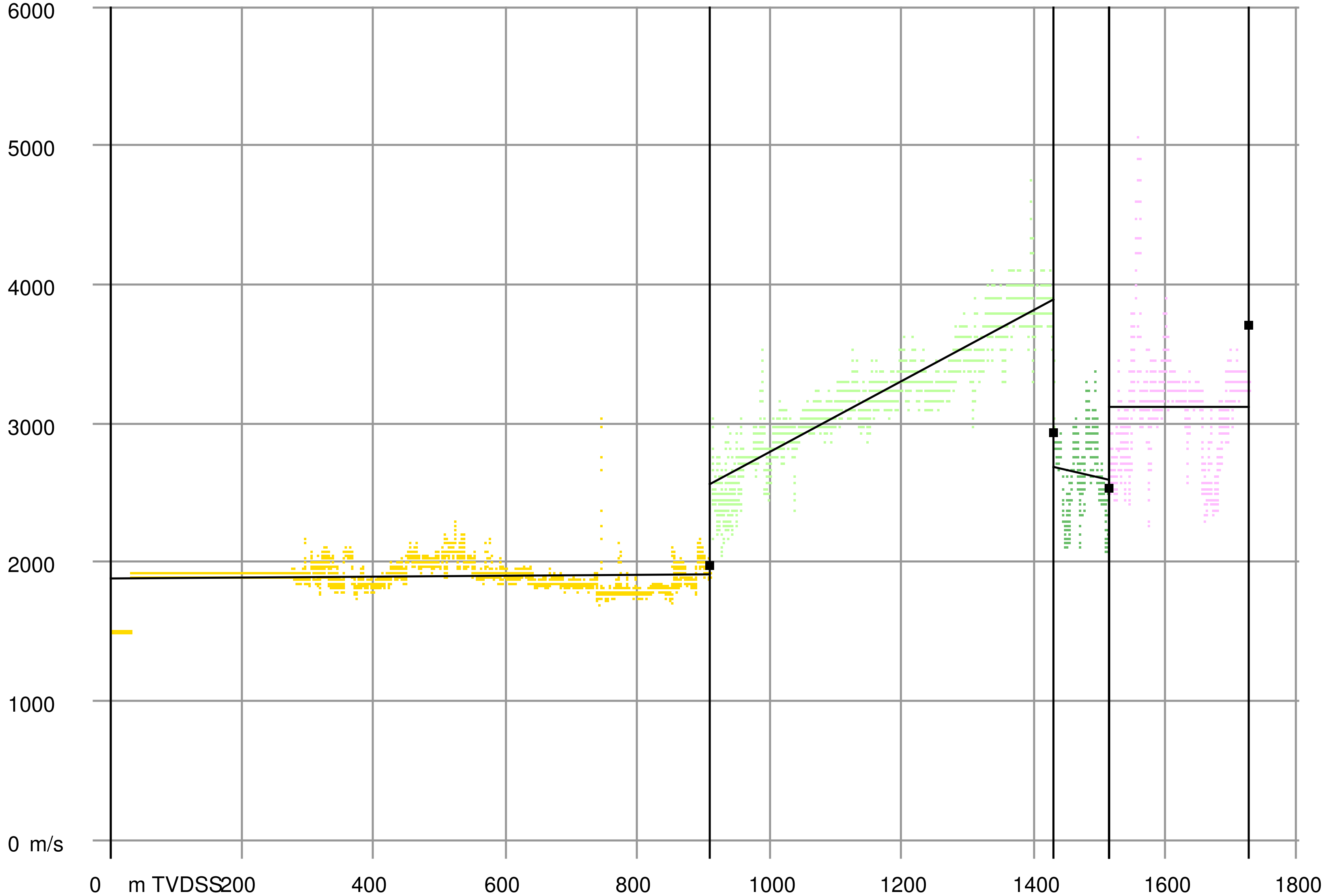

Calibrated instantaneous velocities and linearisation per layer at borehole: D12-03

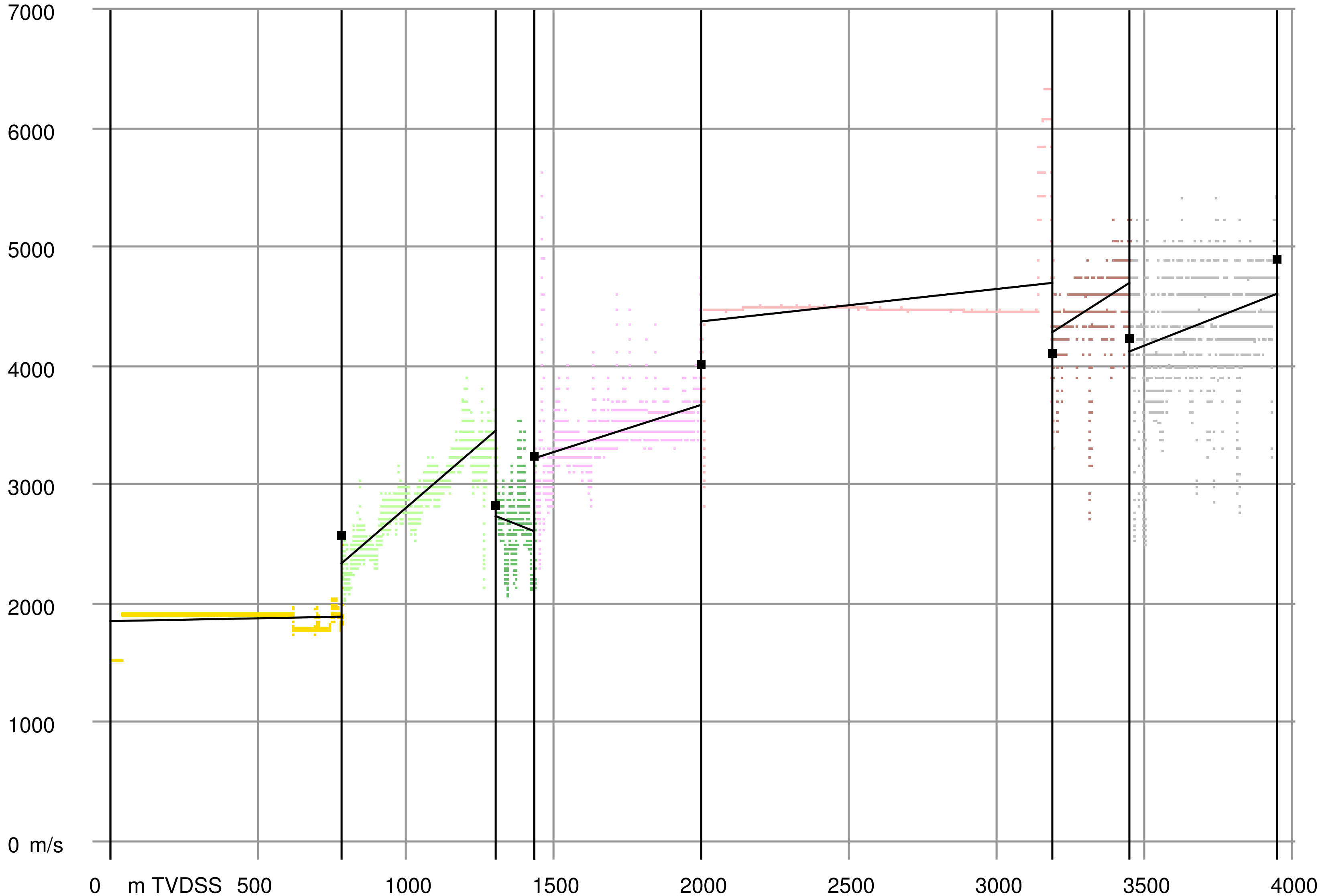

Calibrated instantaneous velocities and linearisation per layer at borehole: D12-04

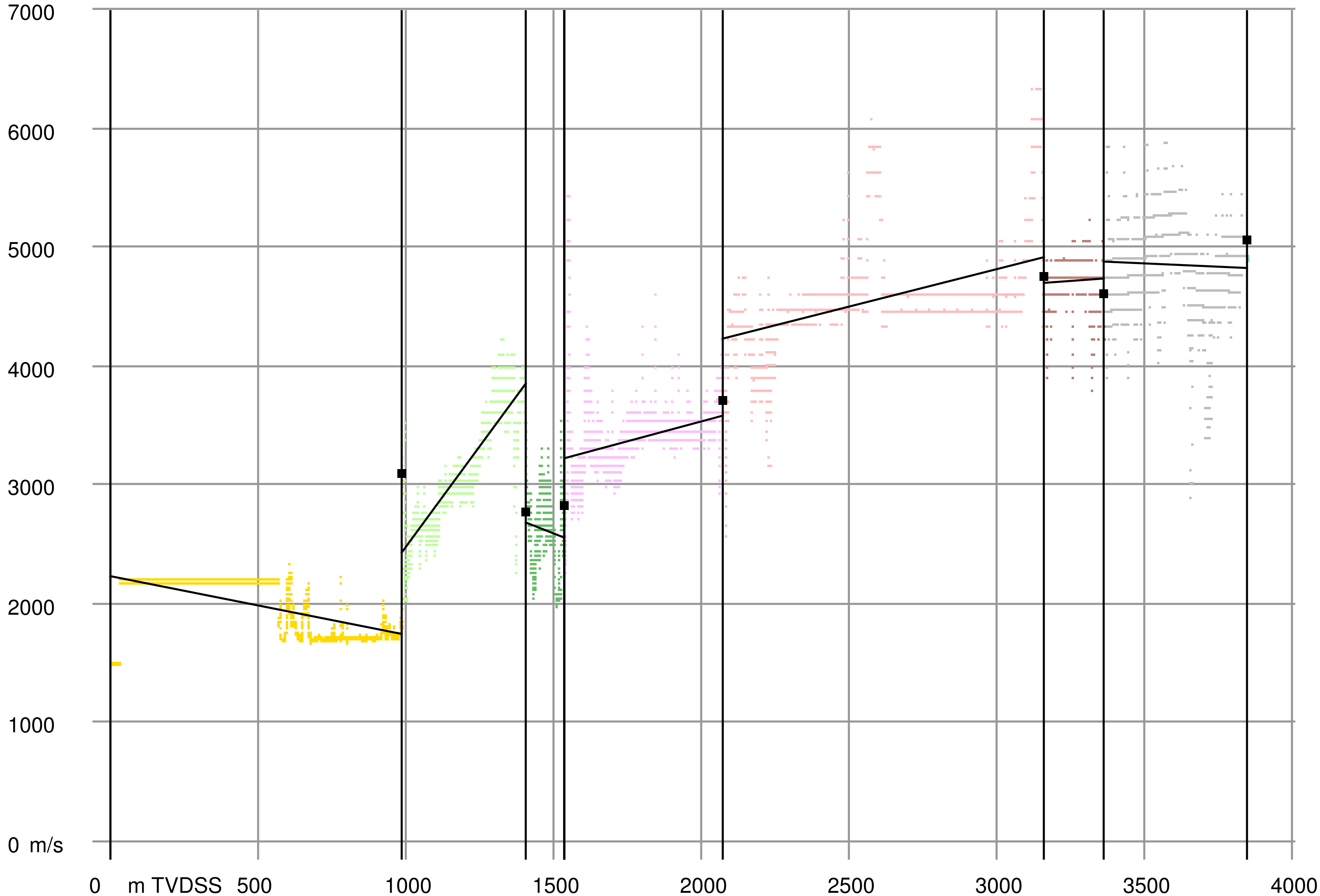

Calibrated instantaneous velocities and linearisation per layer at borehole: D15-02

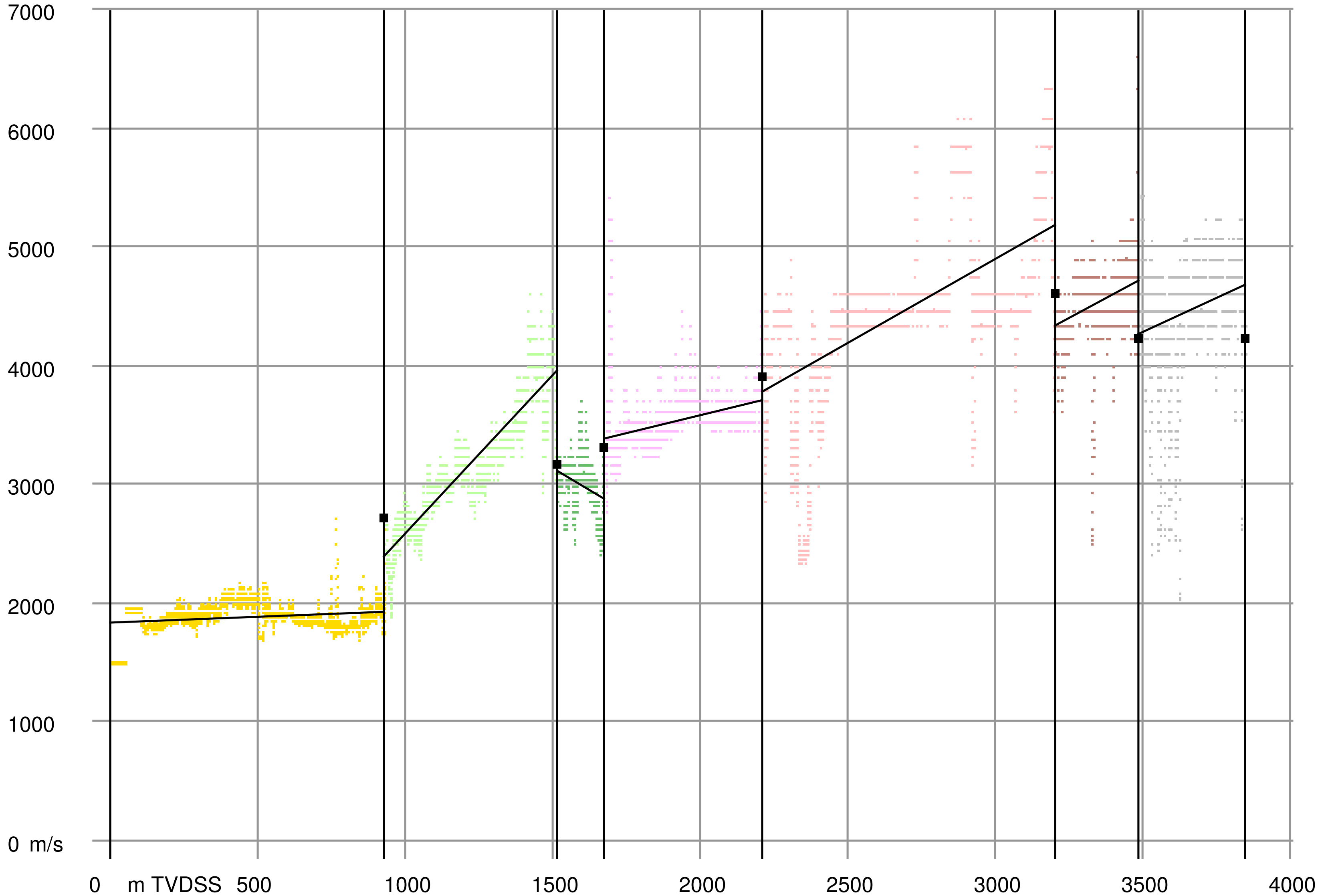

Calibrated instantaneous velocities and linearisation per layer at borehole: E02-02

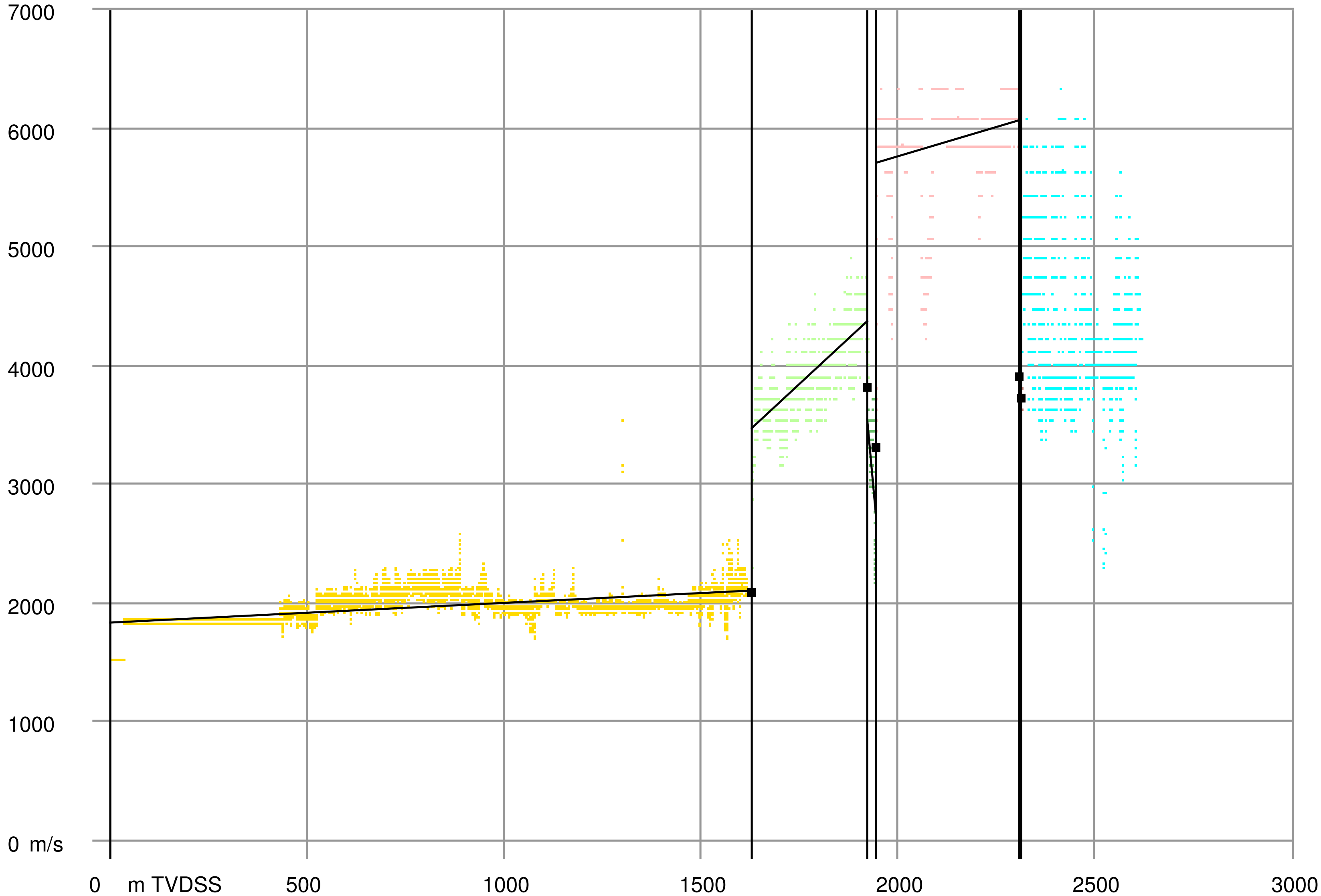

Calibrated instantaneous velocities and linearisation per layer at borehole: E04-01

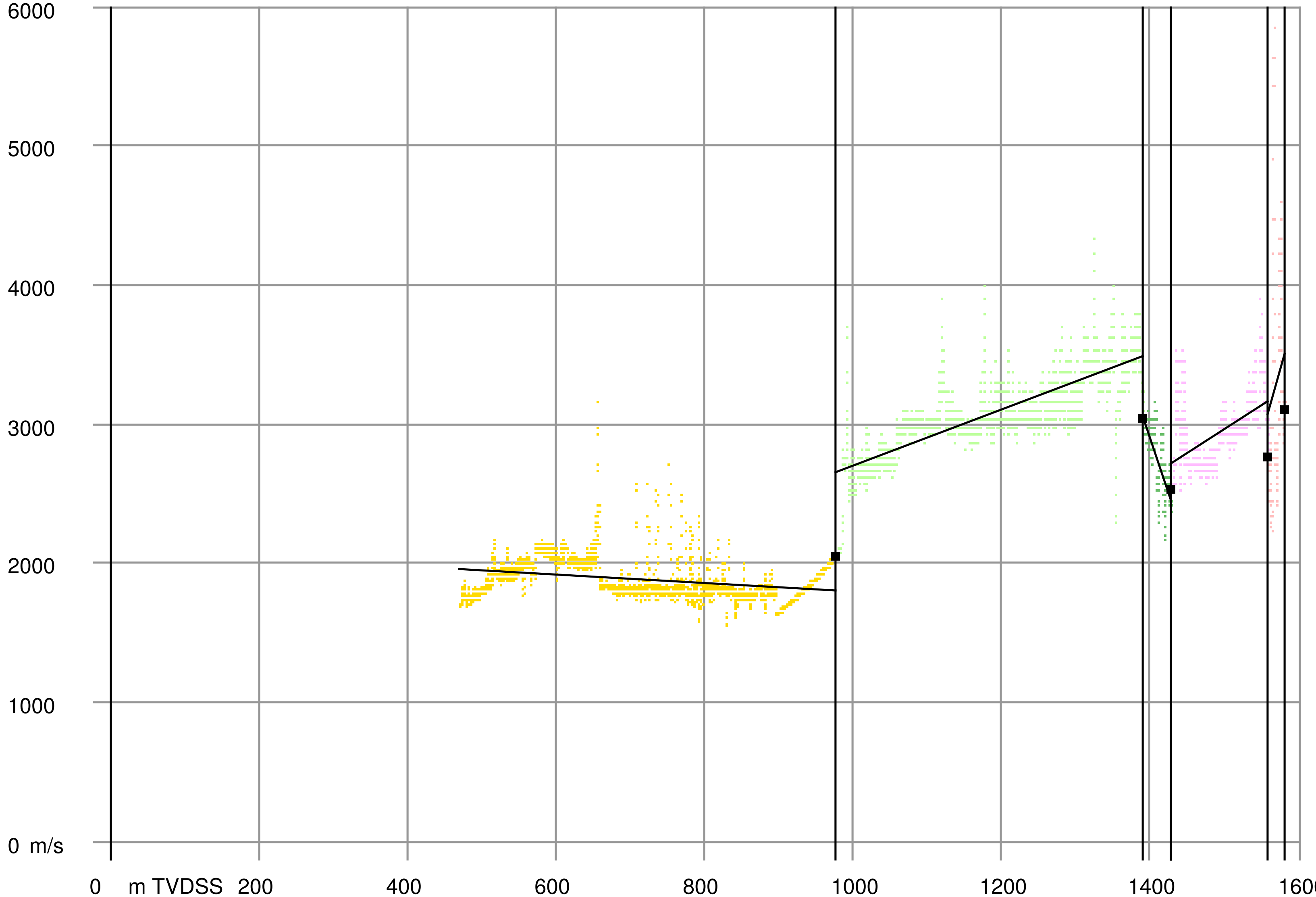

Calibrated instantaneous velocities and linearisation per layer at borehole: E10-01

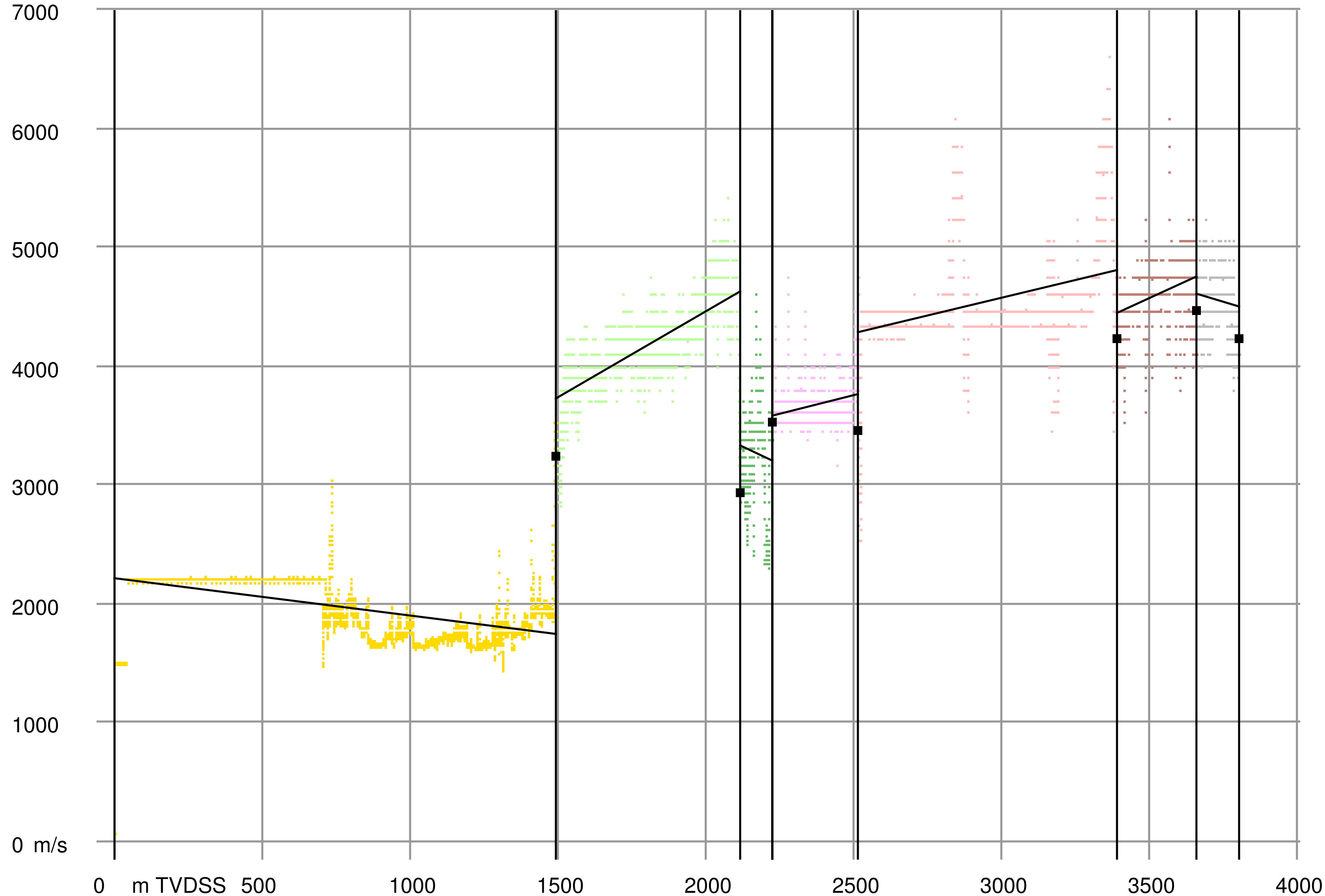

Calibrated instantaneous velocities and linearisation per layer at borehole: E18-02

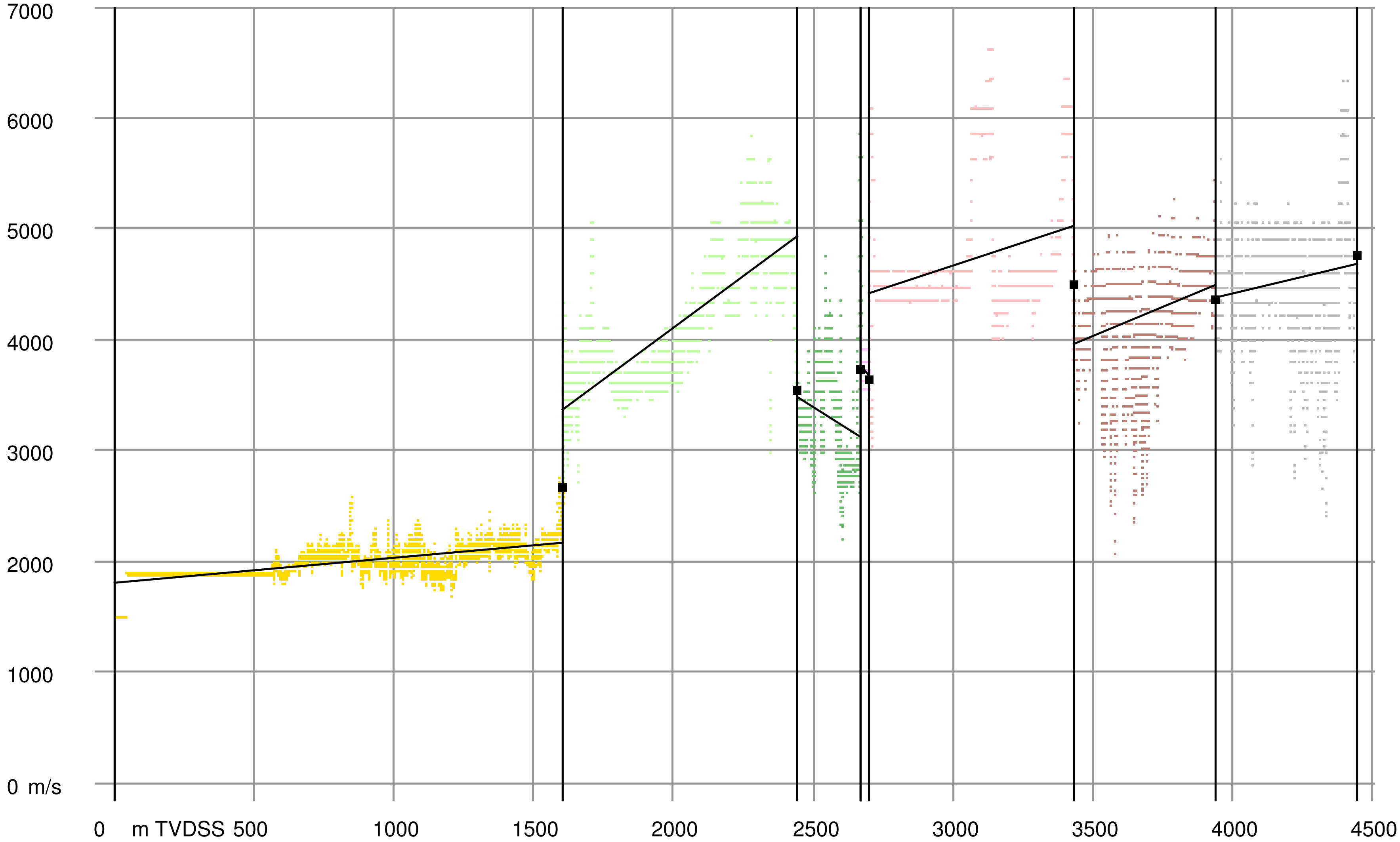

Calibrated instantaneous velocities and linearisation per layer at borehole: F01-01

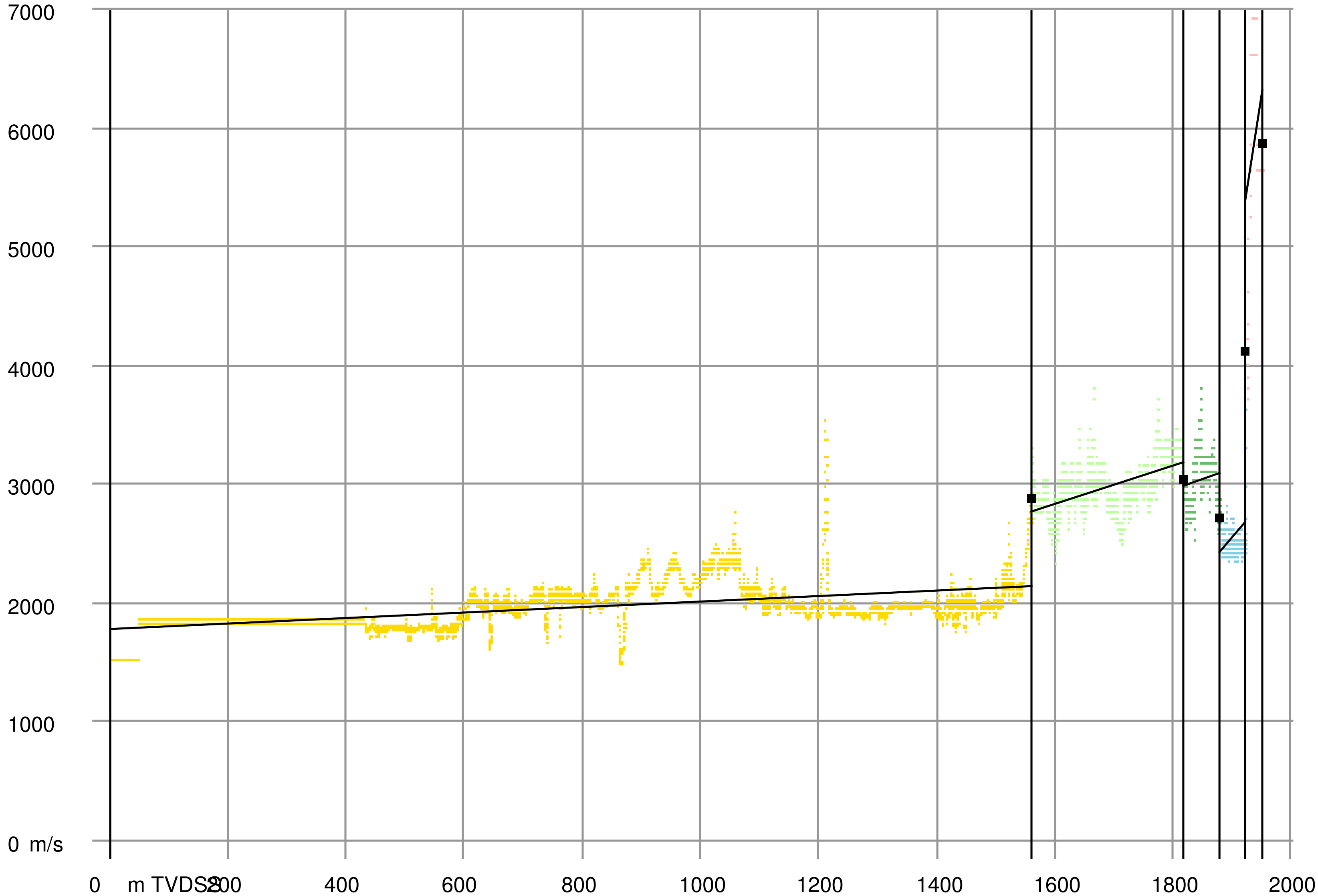

Calibrated instantaneous velocities and linearisation per layer at borehole: F05-03

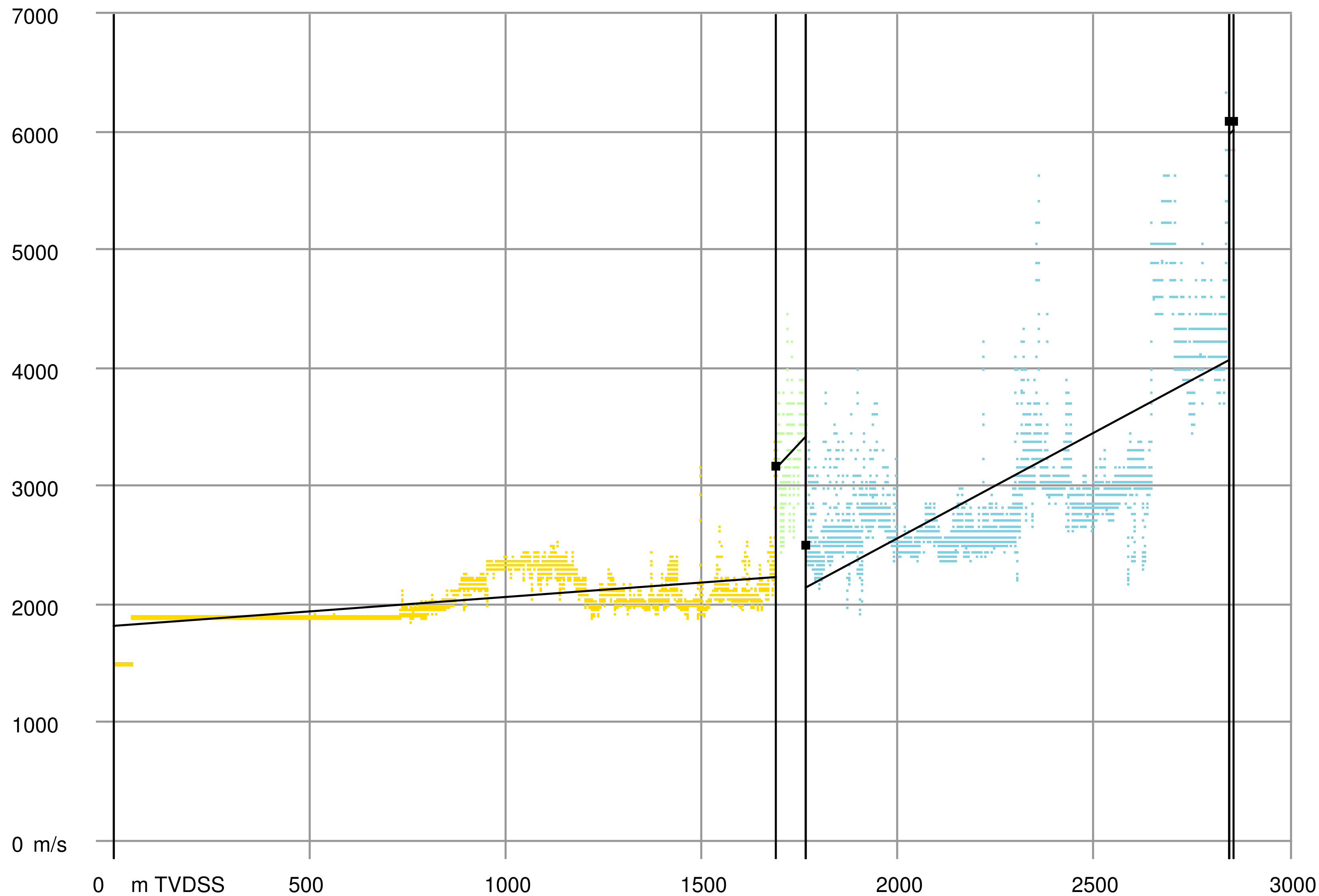

Calibrated instantaneous velocities and linearisation per layer at borehole: F12-03

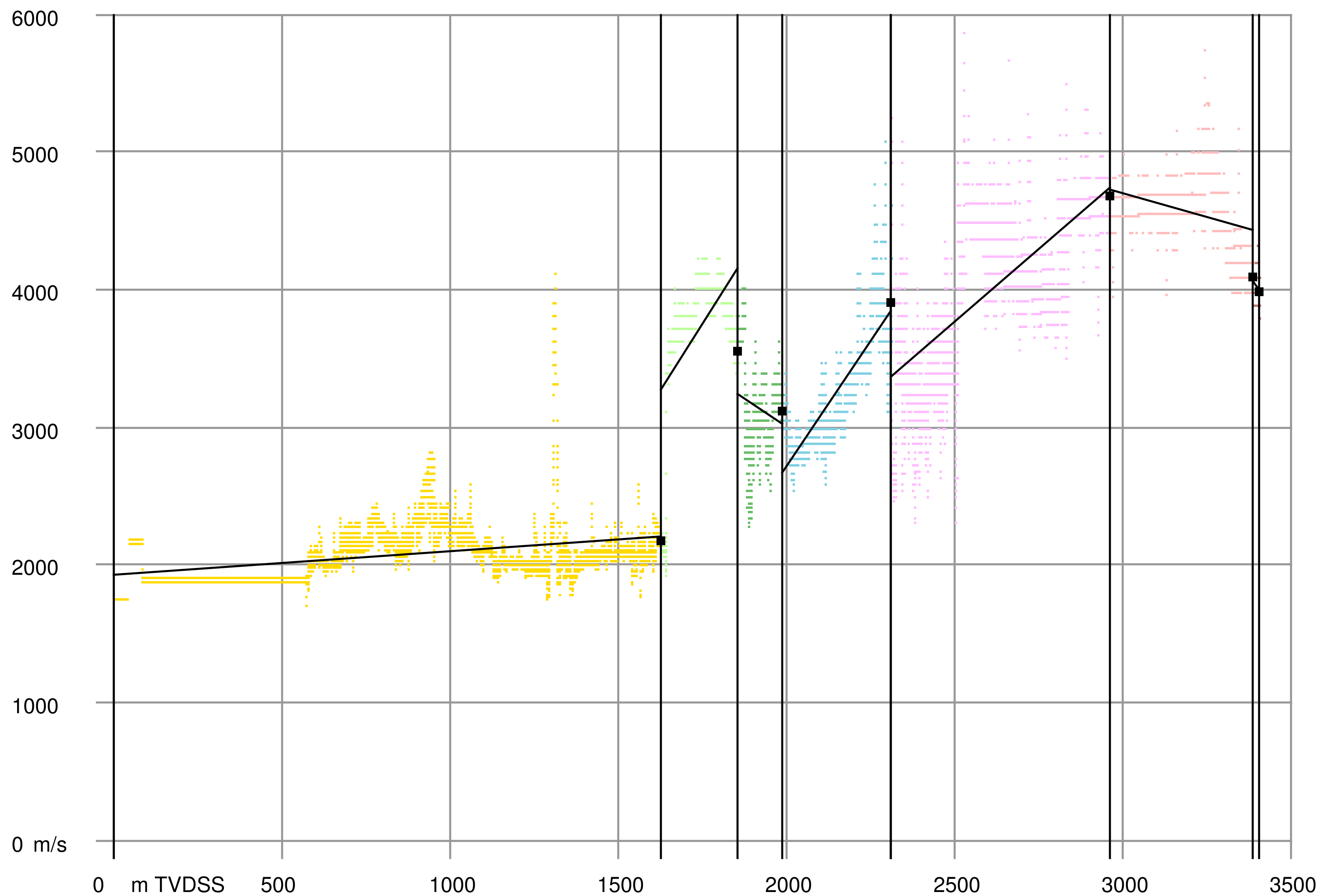

Calibrated instantaneous velocities and linearisation per layer at borehole: F15-07

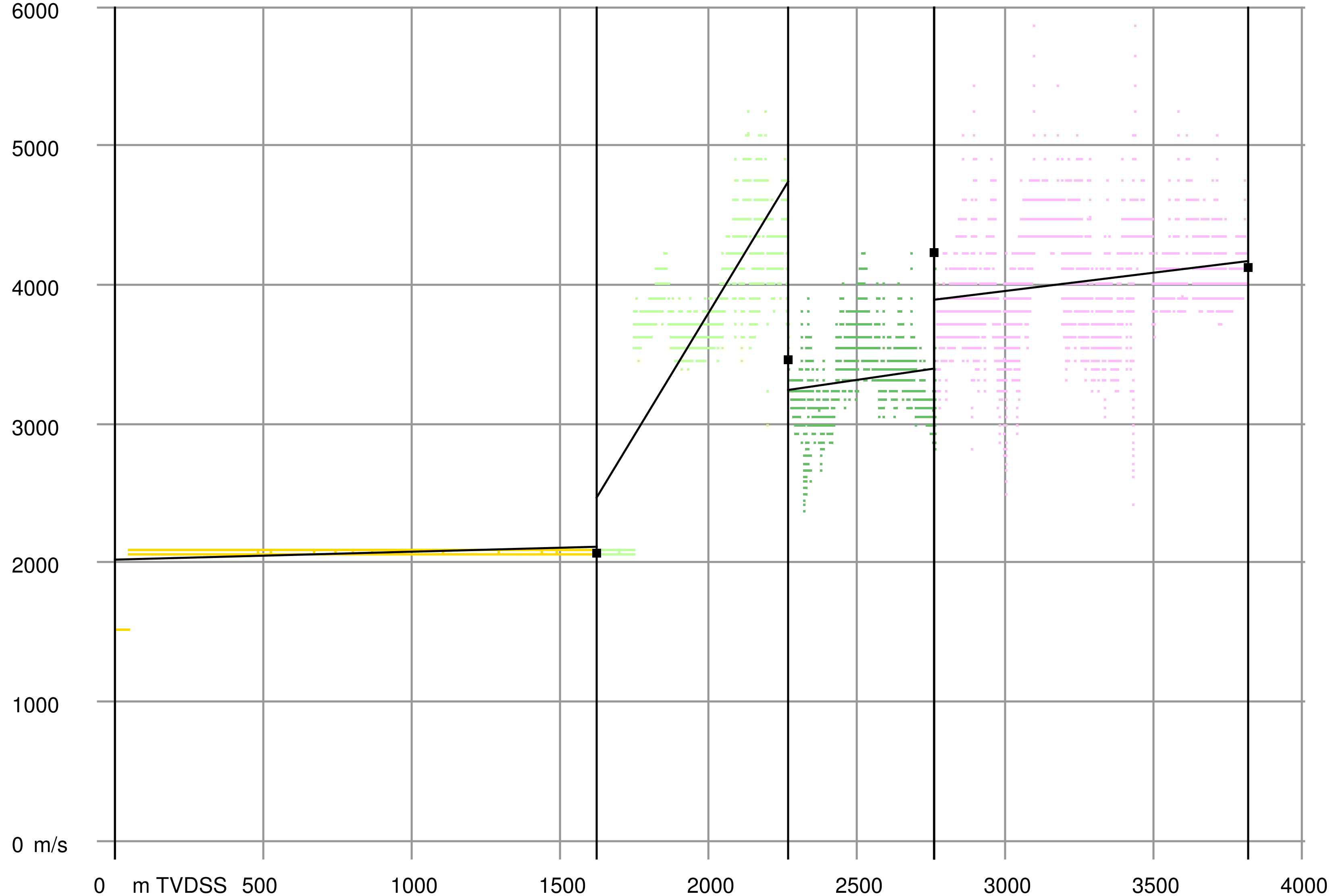

Calibrated instantaneous velocities and linearisation per layer at borehole: F17-06

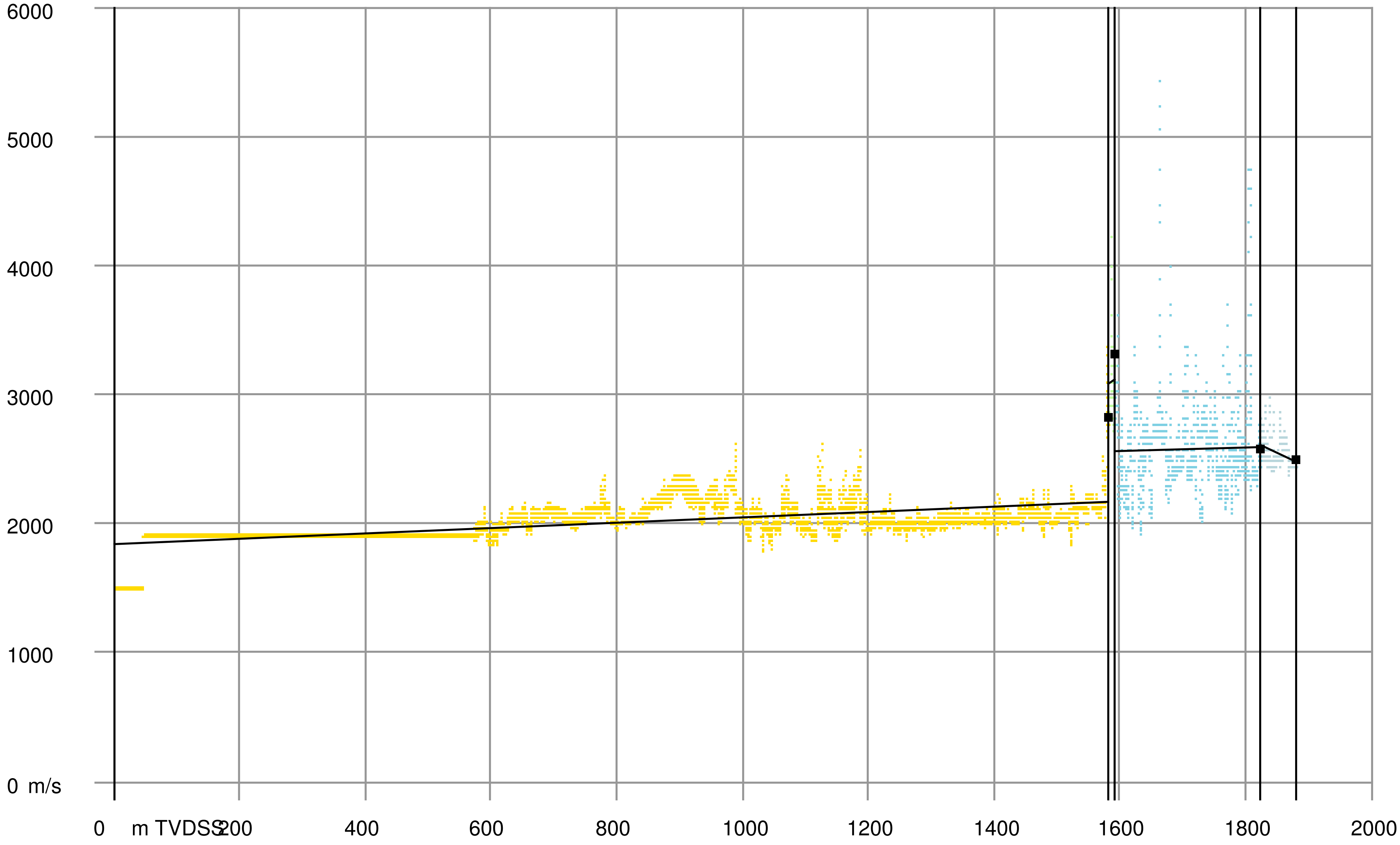

Calibrated instantaneous velocities and linearisation per layer at borehole: G11-02

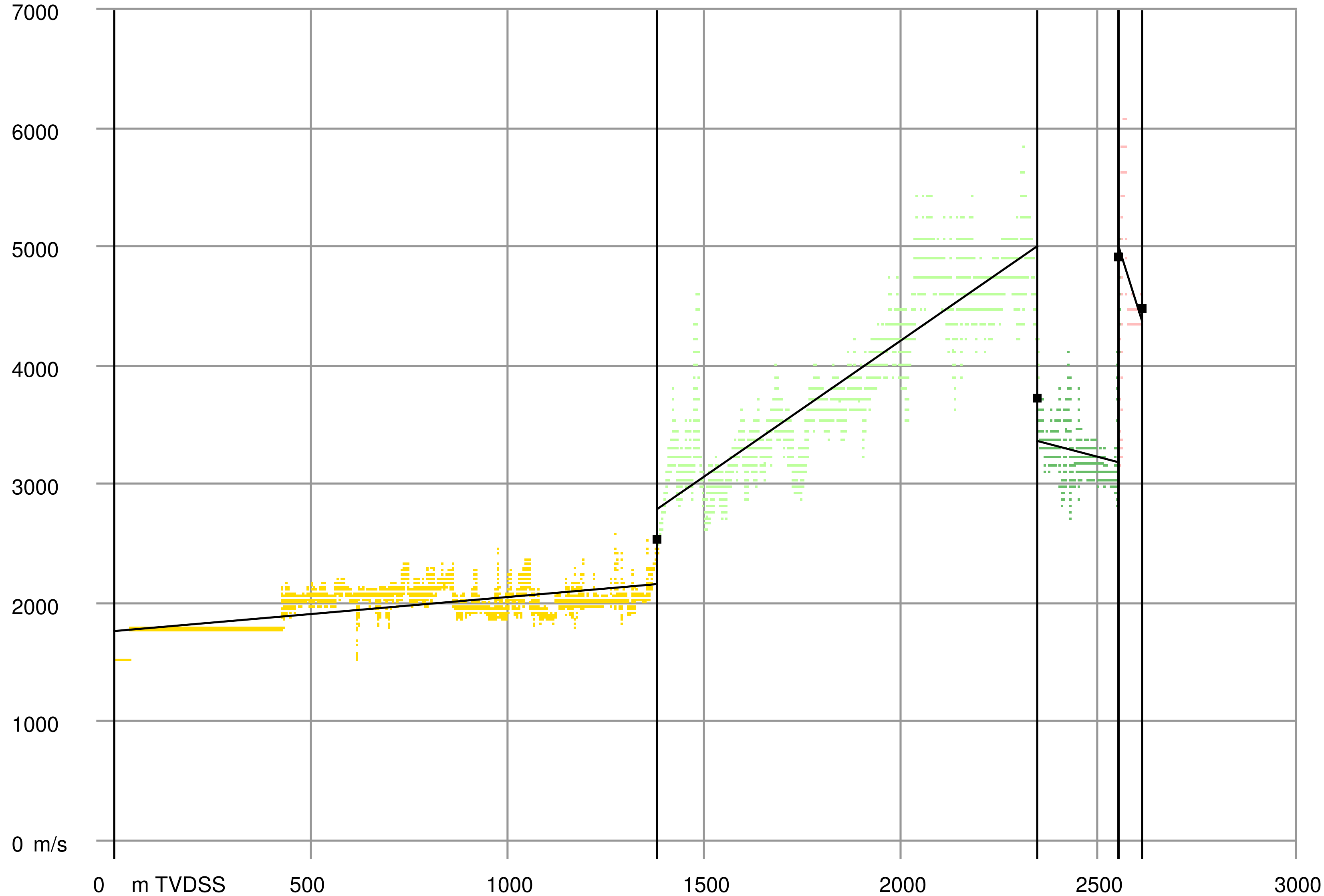

Calibrated instantaneous velocities and linearisation per layer at borehole: G16-01

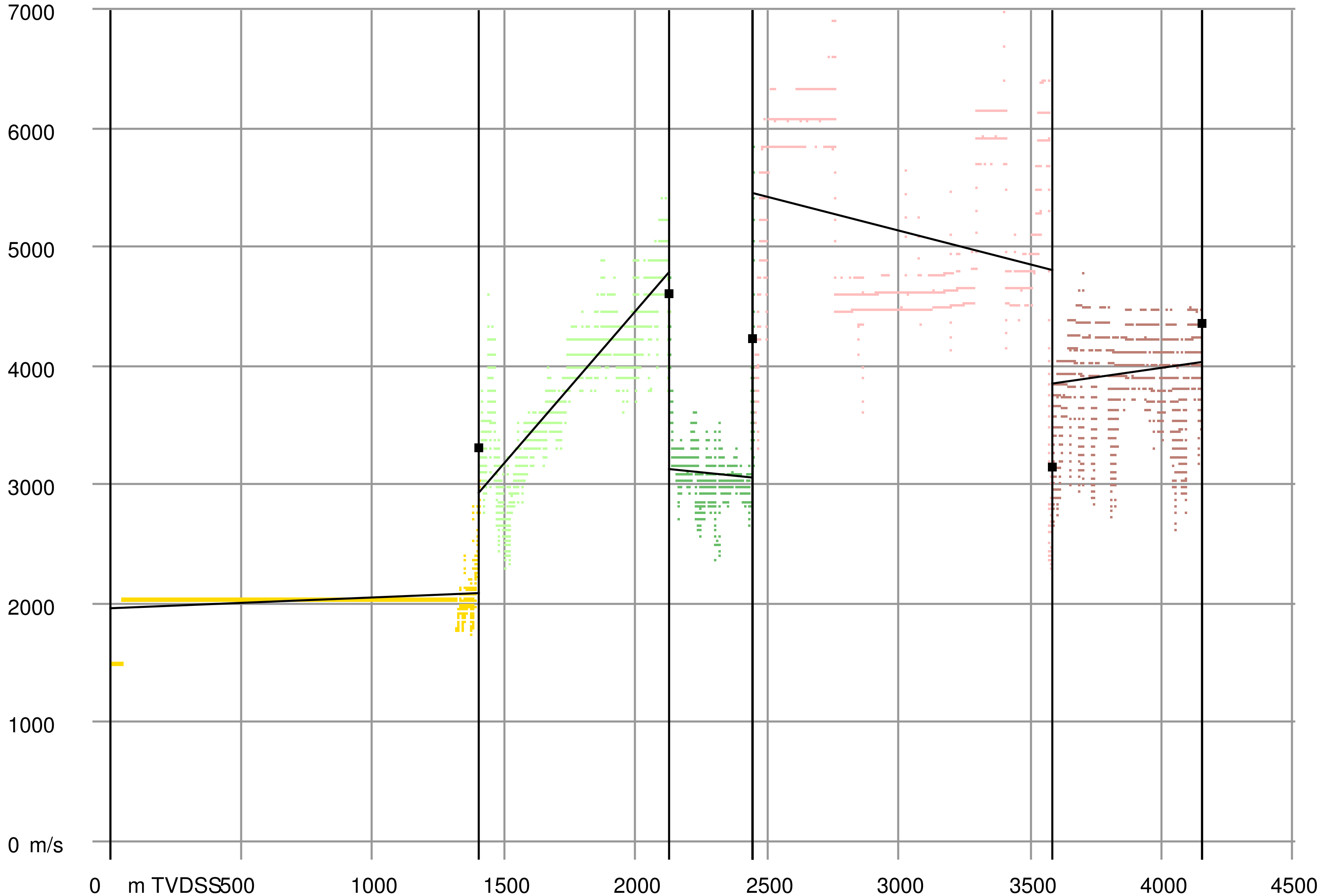

Calibrated instantaneous velocities and linearisation per layer at borehole: G17-02

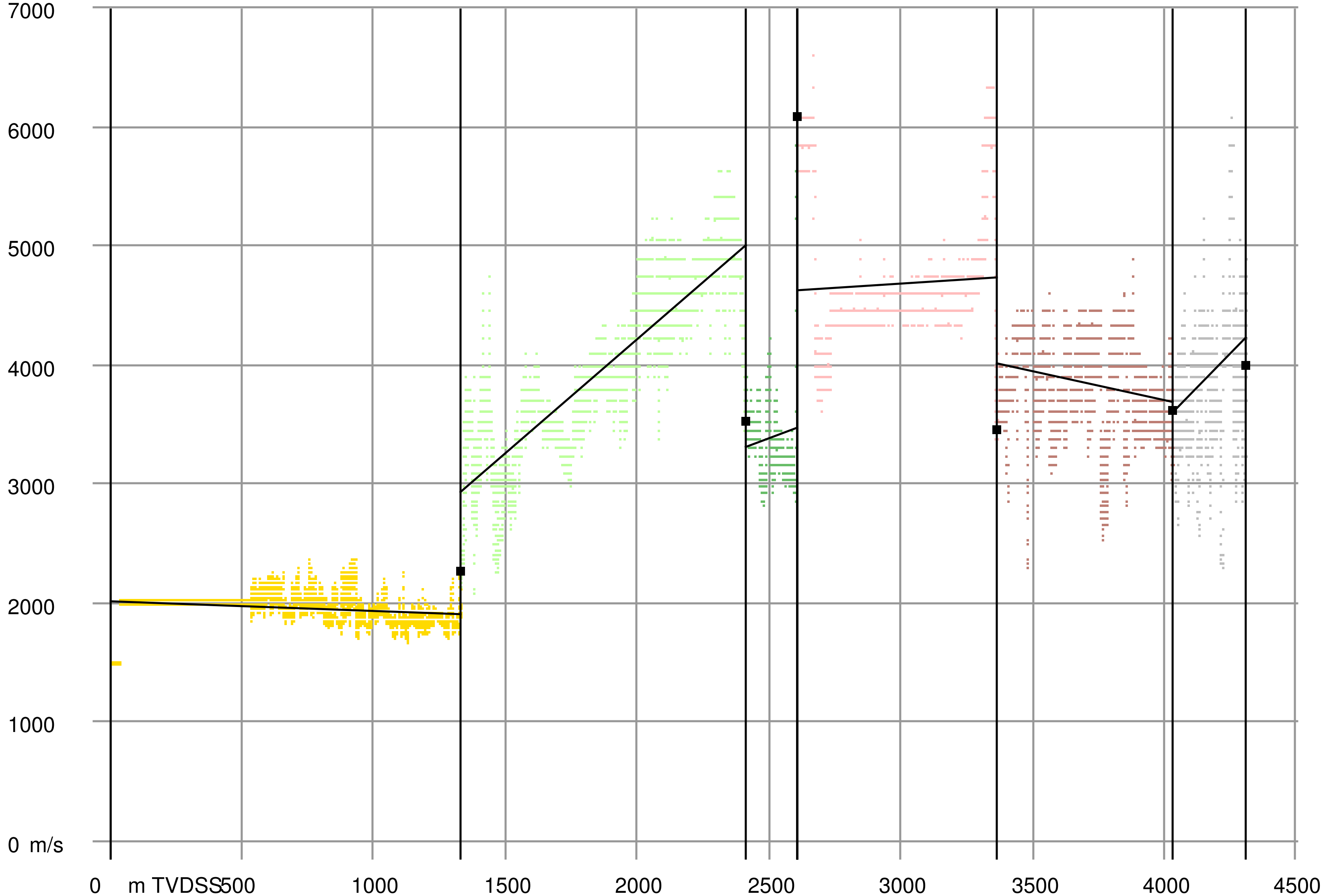

Calibrated instantaneous velocities and linearisation per layer at borehole: G18-01

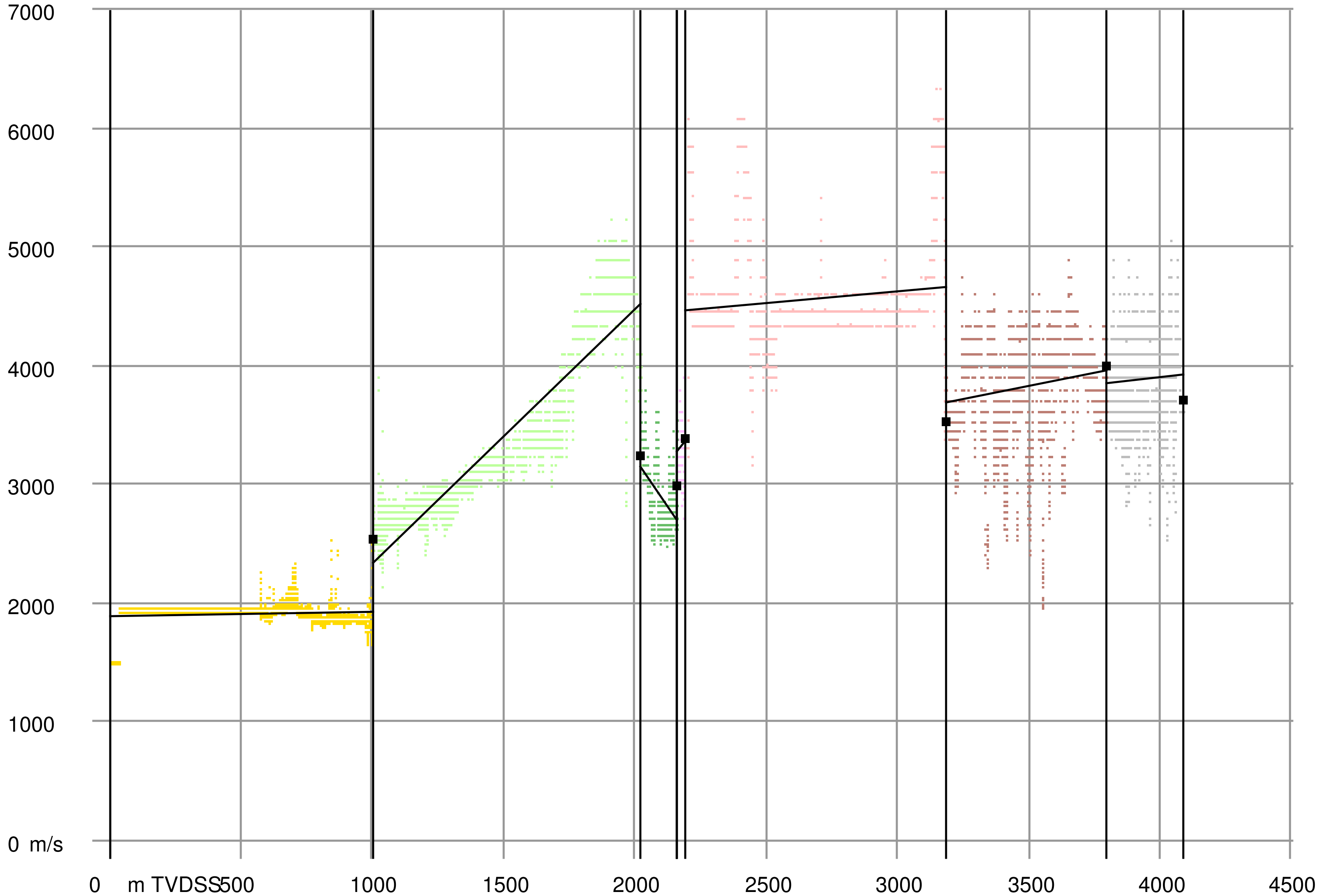

Calibrated instantaneous velocities and linearisation per layer at borehole: H16-01

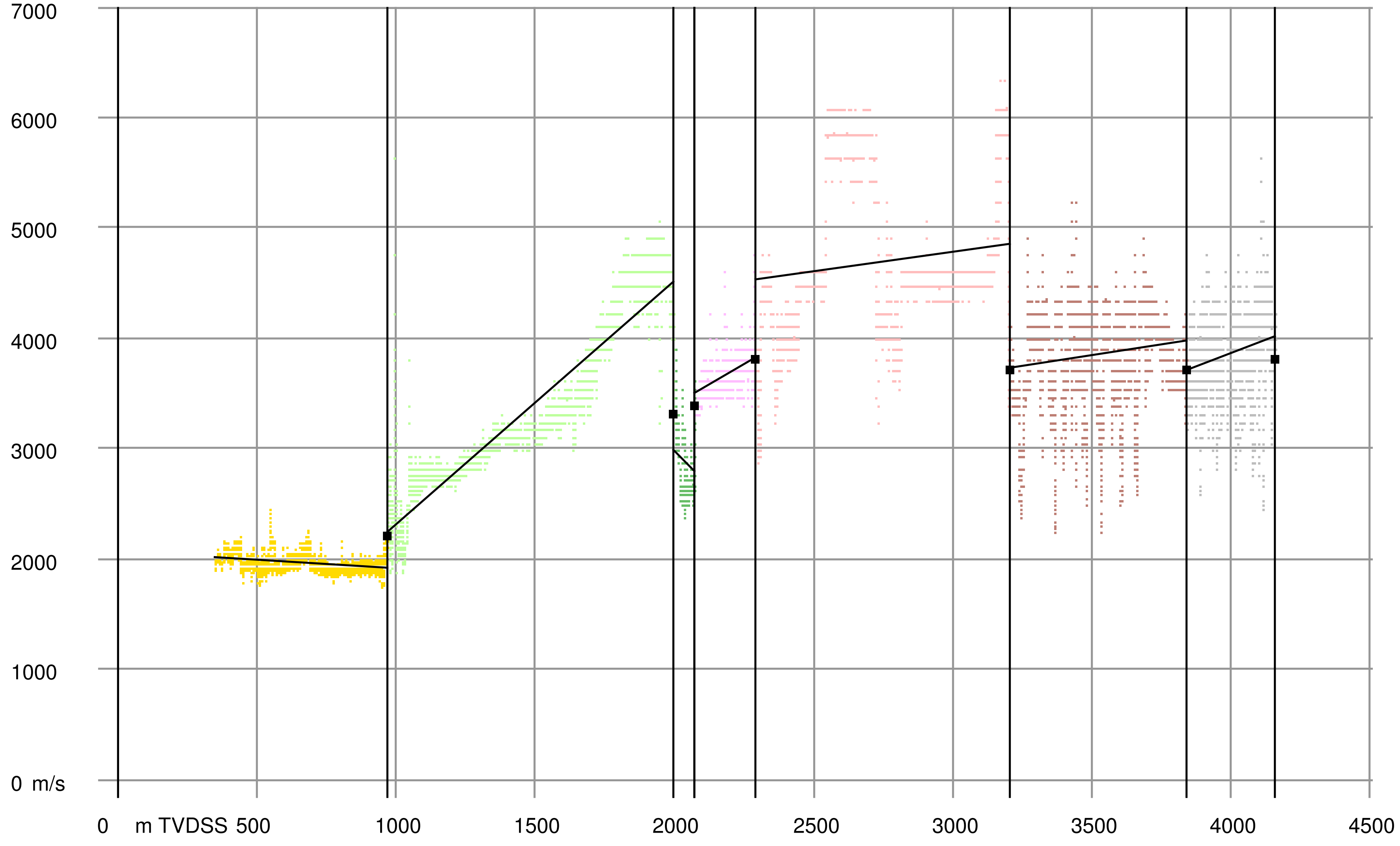

Calibrated instantaneous velocities and linearisation per layer at borehole: HST-02-S1

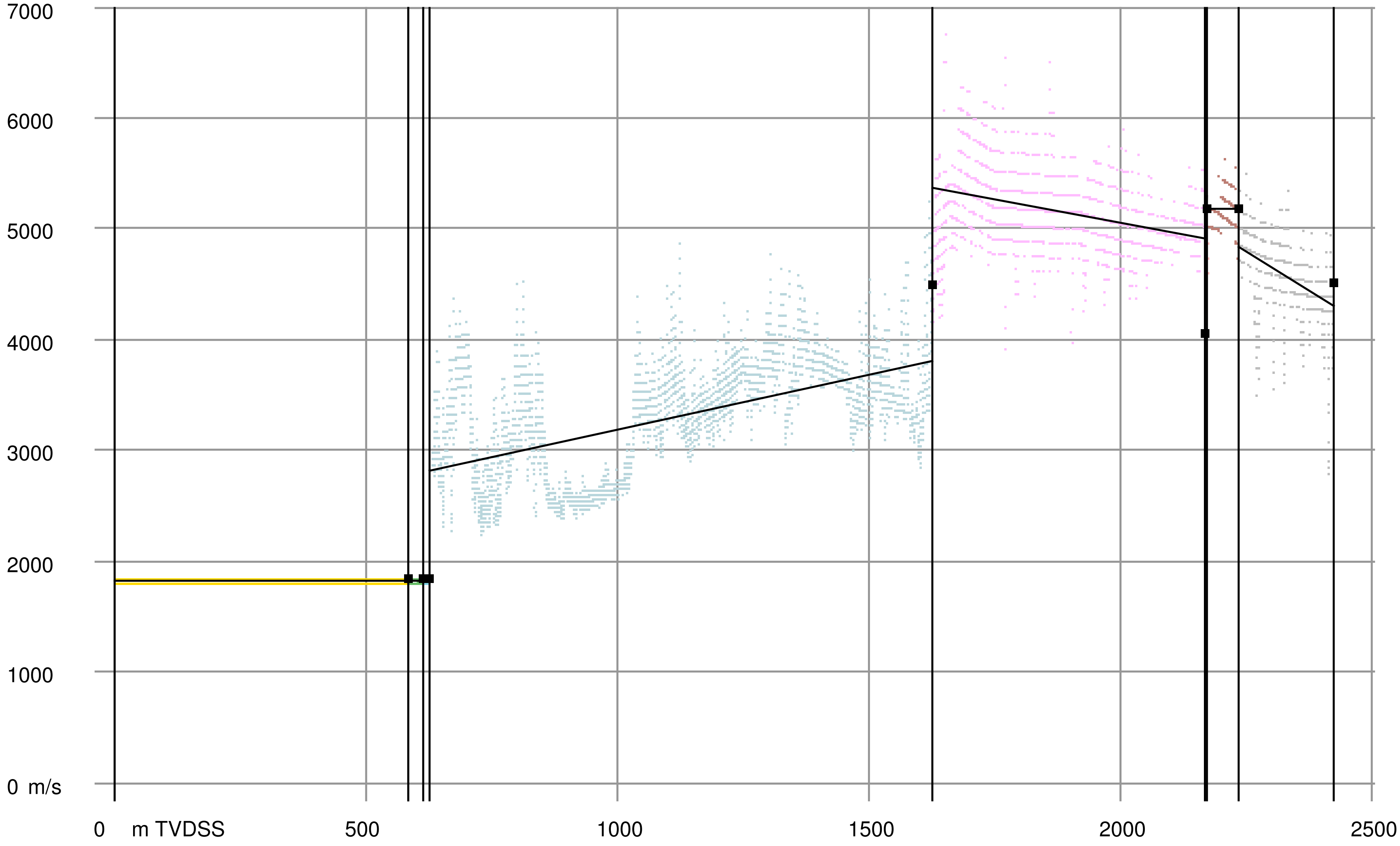

Calibrated instantaneous velocities and linearisation per layer at borehole: J03-02

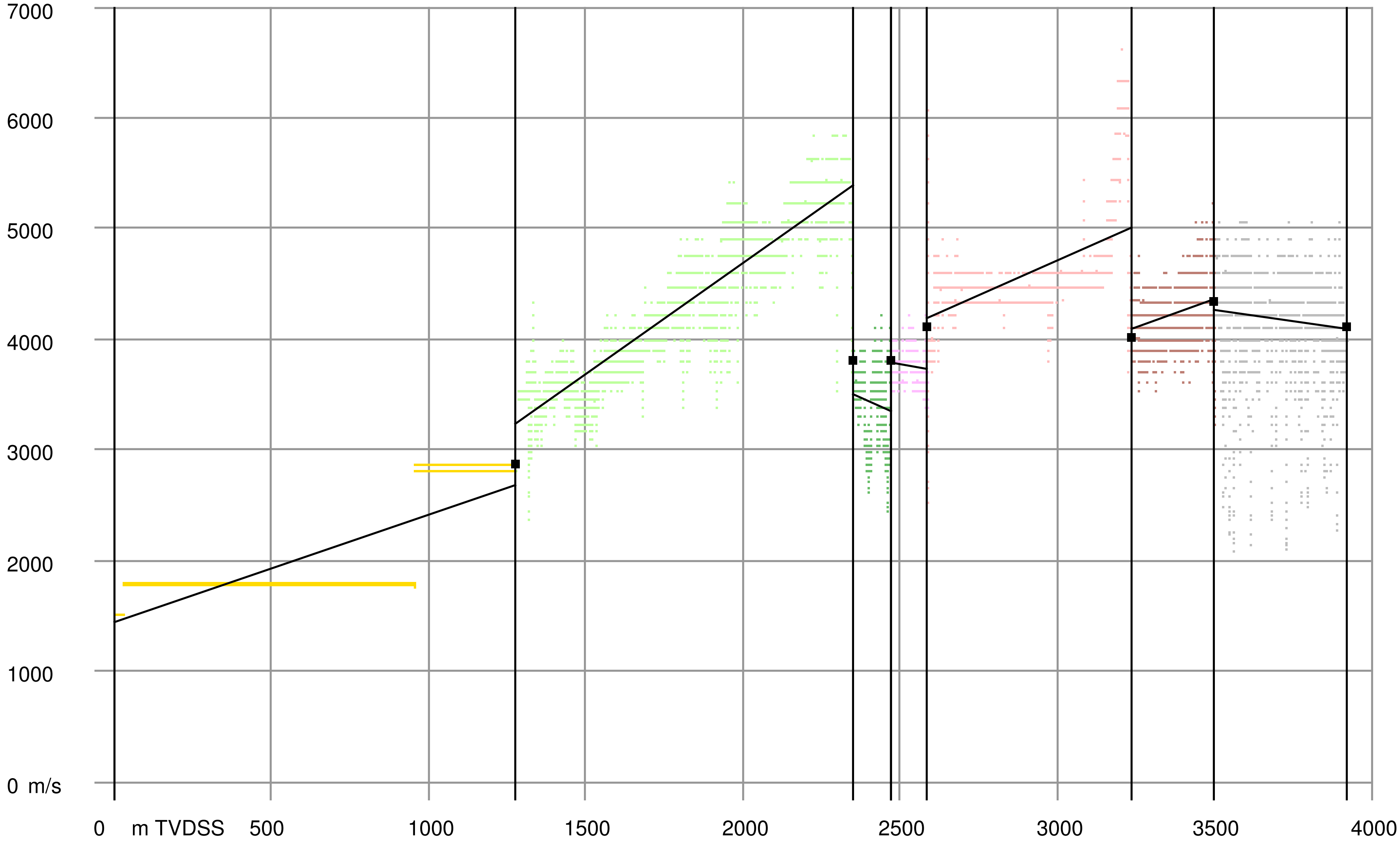

Calibrated instantaneous velocities and linearisation per layer at borehole: J06-A-01

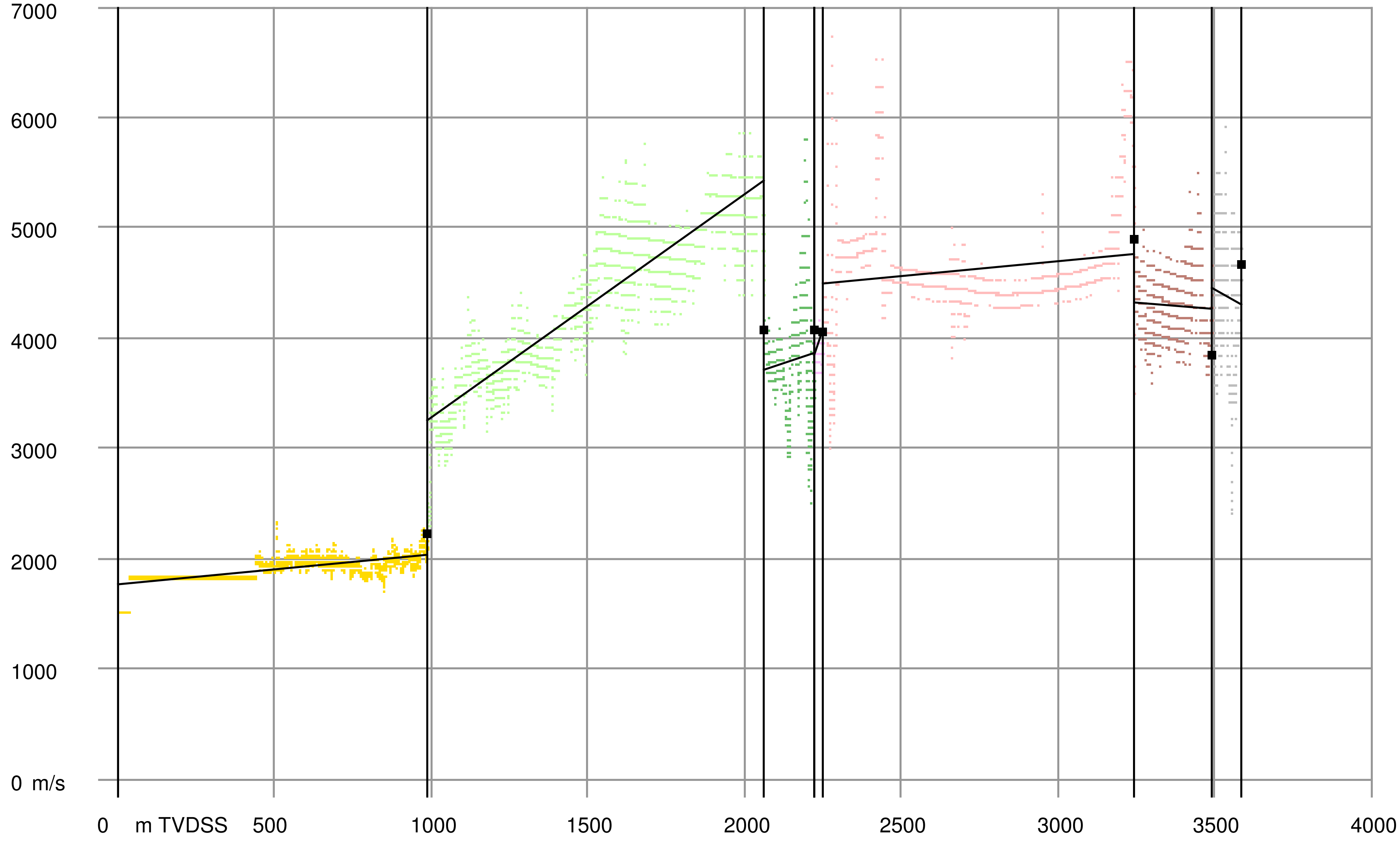

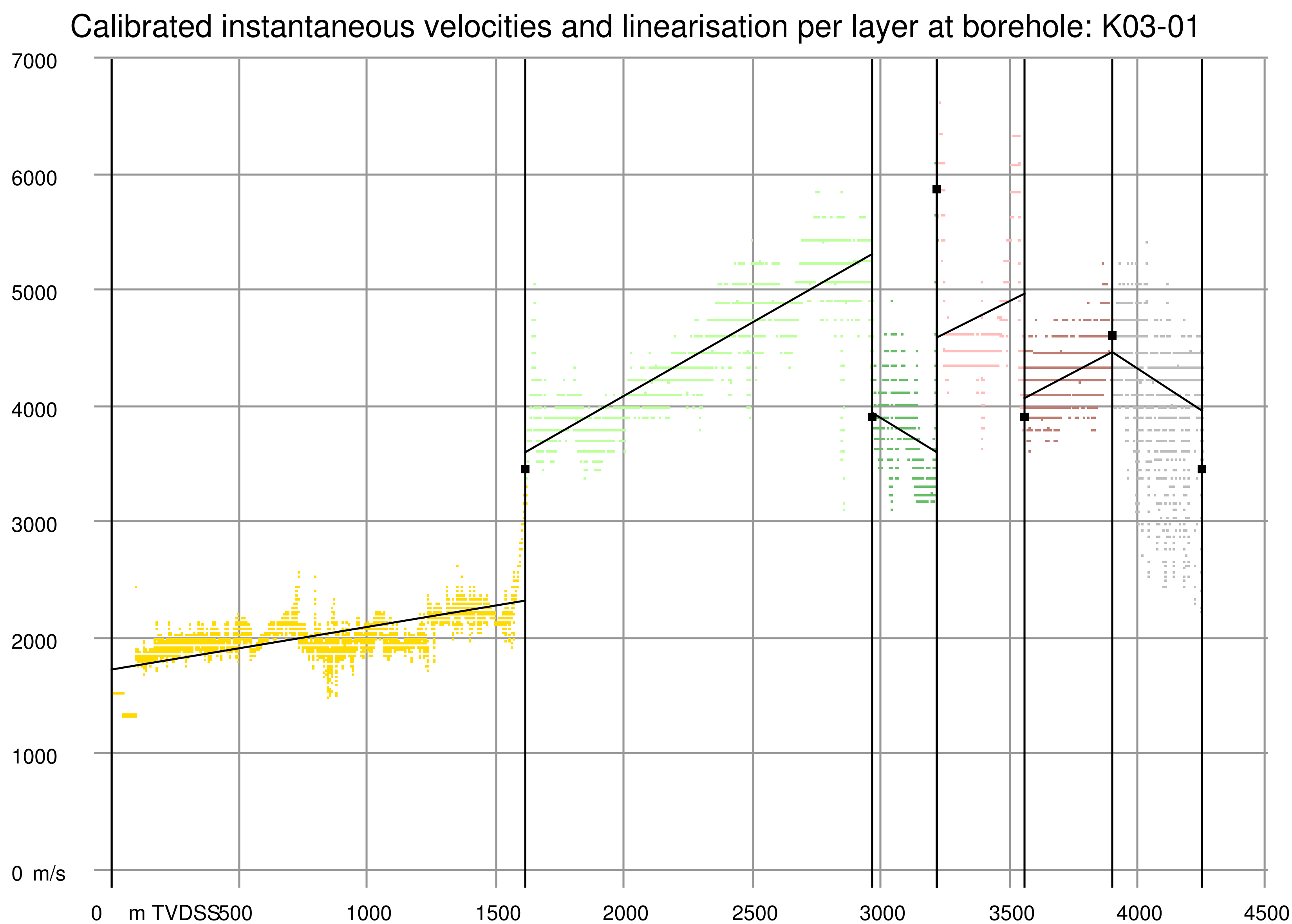
Calibrated instantaneous velocities and linearisation per layer at borehole: K03-01
7000
6000
5000
4000
3000
2000
1000
0 m/s
0
m TVDSS
500
1000
1500
2000
2500
3000
3500
4000
4500

Calibrated instantaneous velocities and linearisation per layer at borehole: K06-06

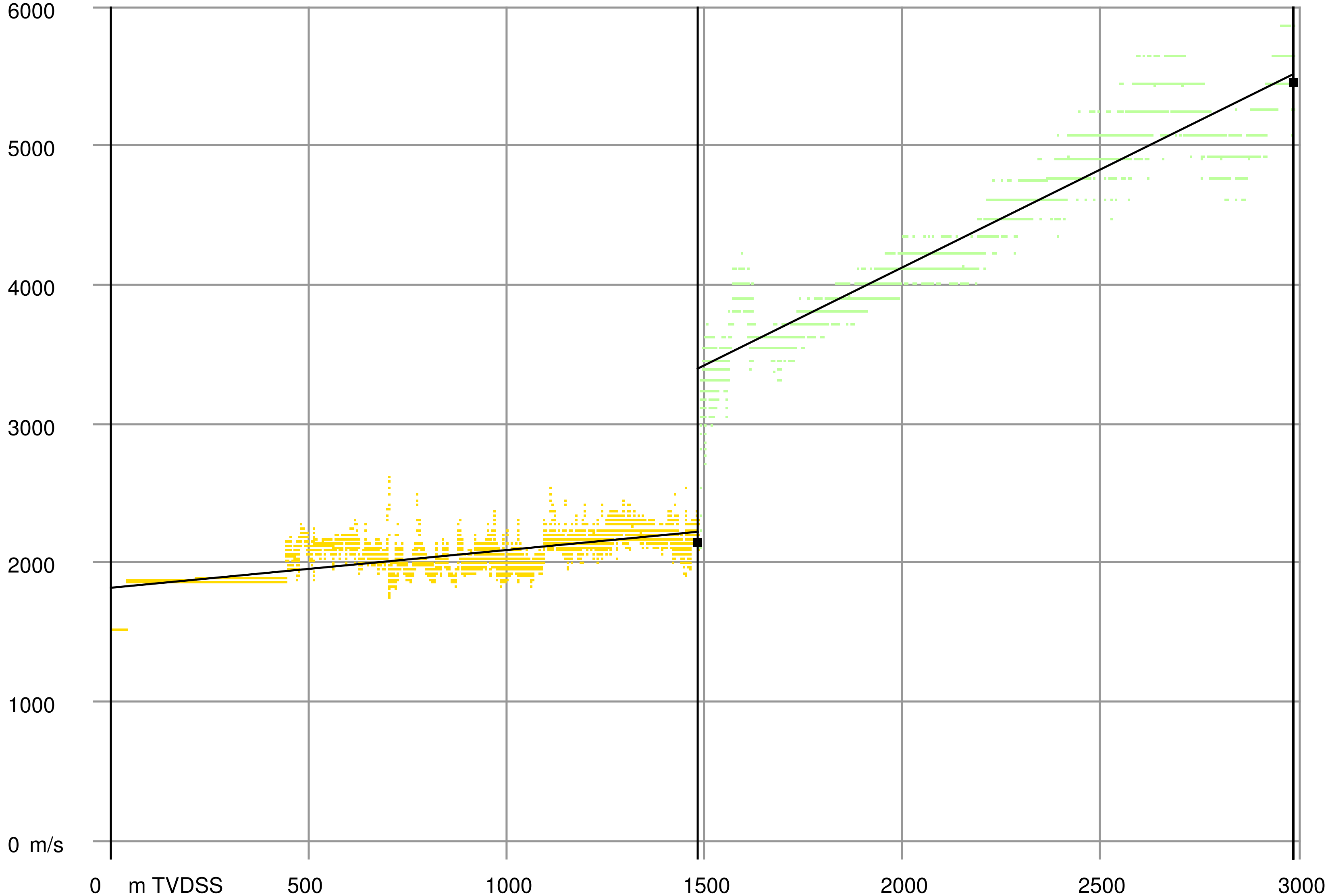

Calibrated instantaneous velocities and linearisation per layer at borehole: K06-08

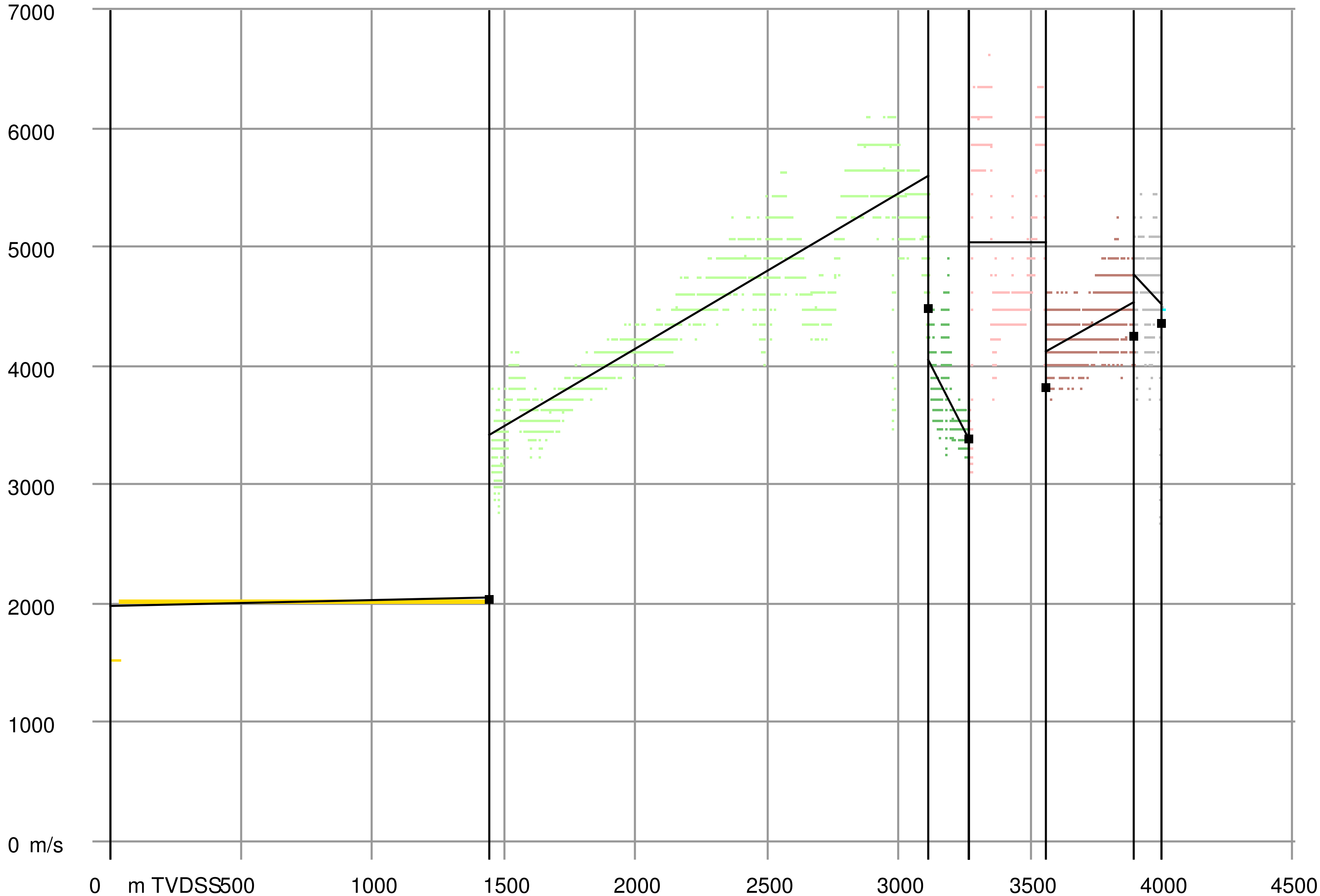

Calibrated instantaneous velocities and linearisation per layer at borehole: K06-N-01

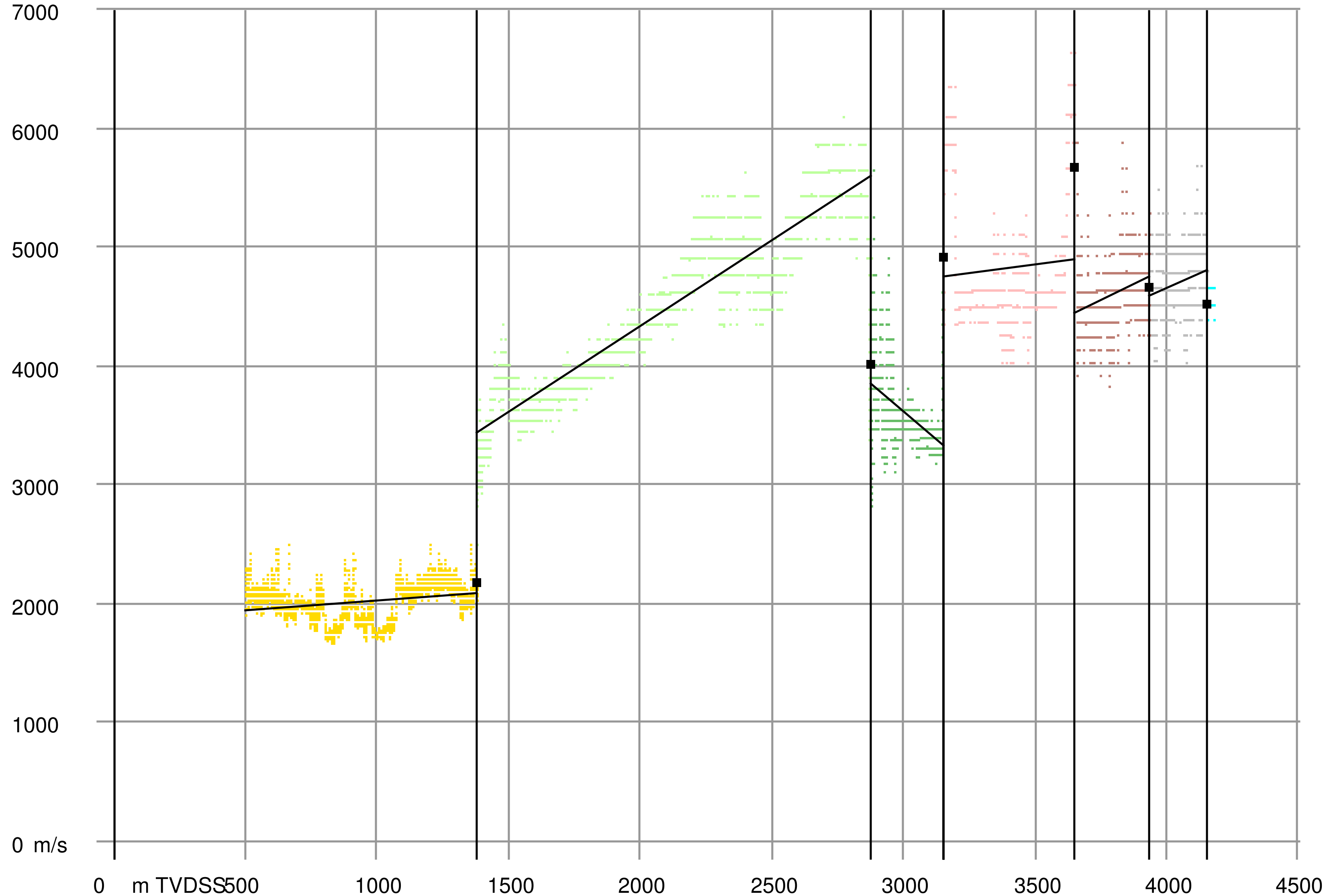

Calibrated instantaneous velocities and linearisation per layer at borehole: K10-11

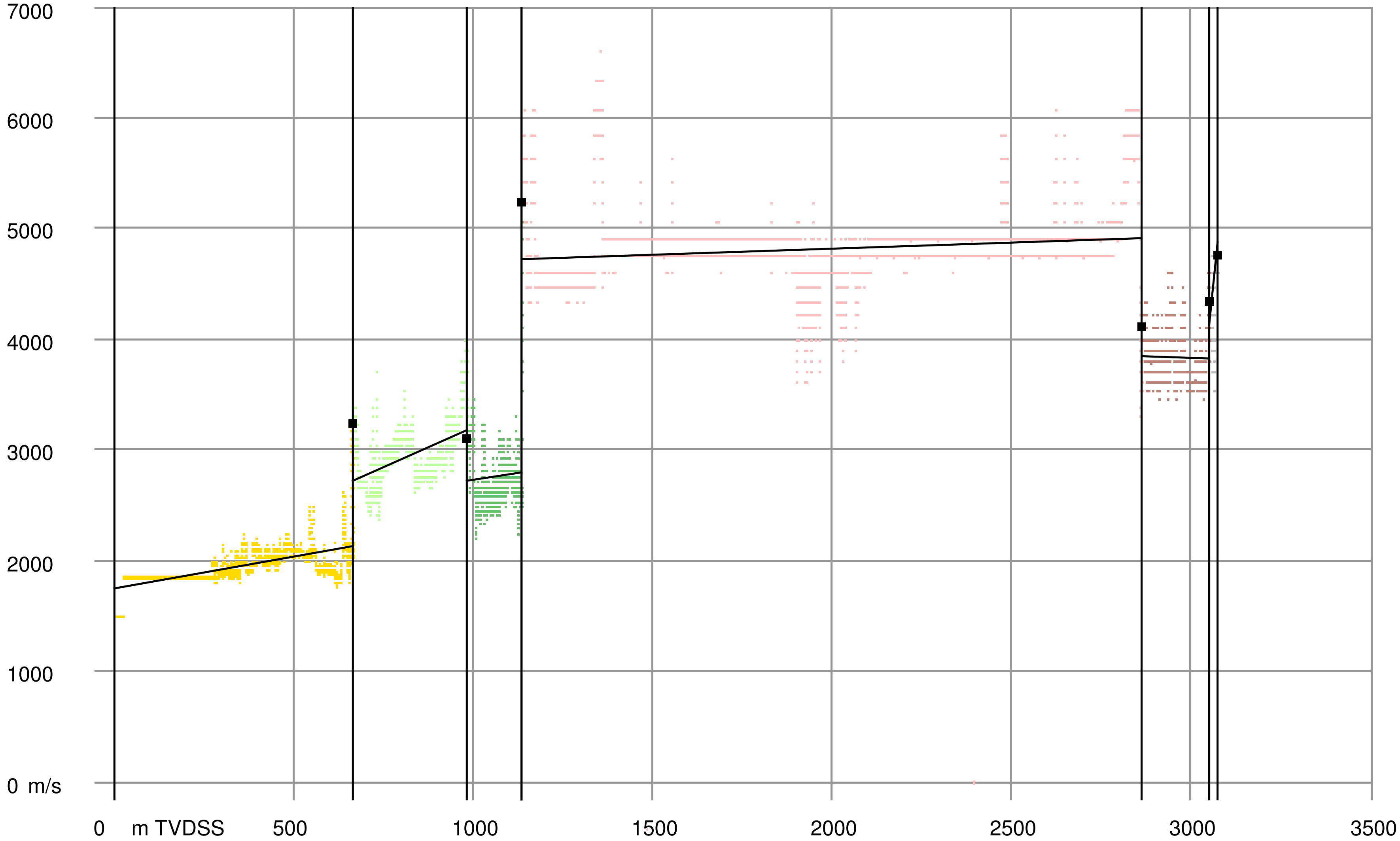

Calibrated instantaneous velocities and linearisation per layer at borehole: K10-12

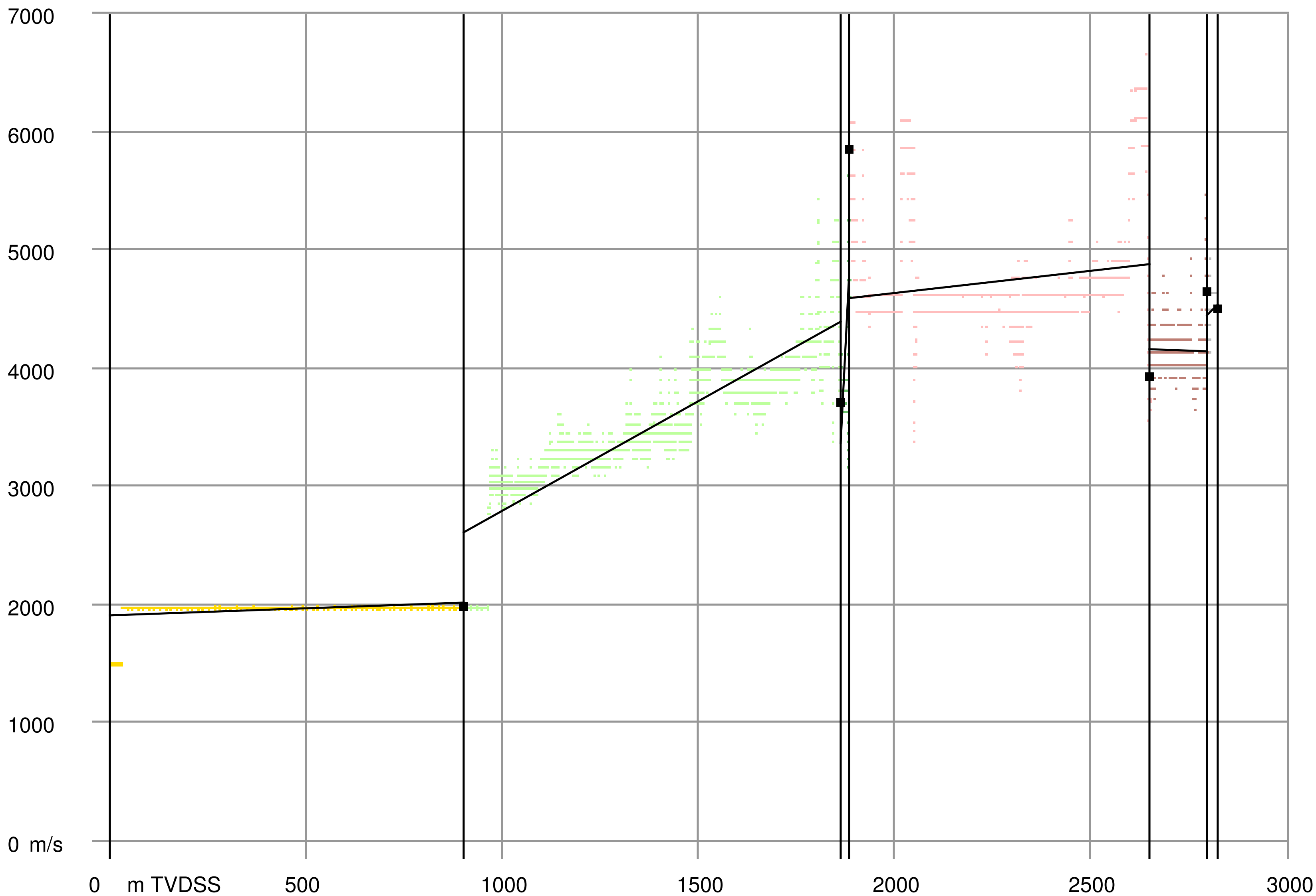

Calibrated instantaneous velocities and linearisation per layer at borehole: K10-V-02

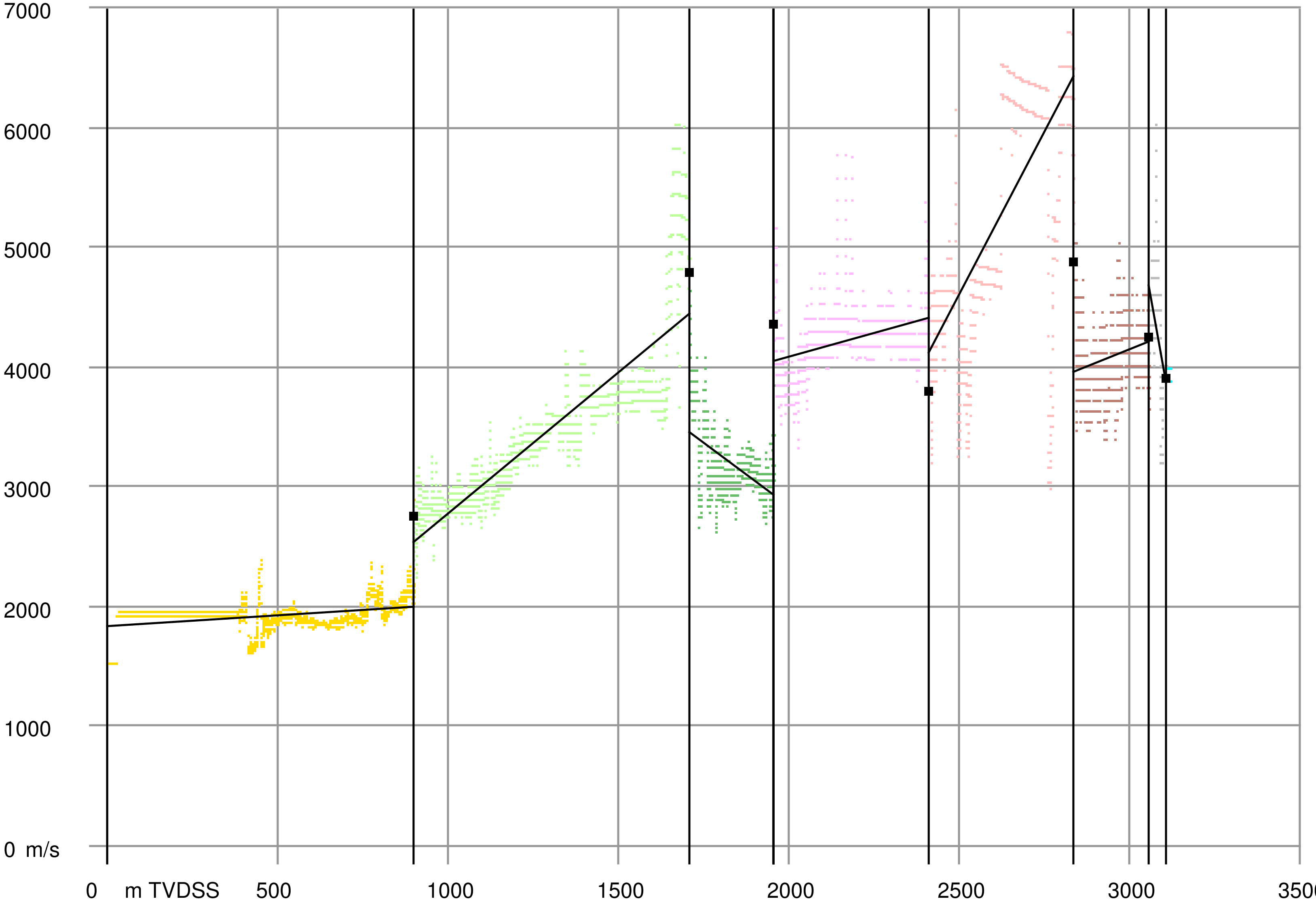

Calibrated instantaneous velocities and linearisation per layer at borehole: K11-09

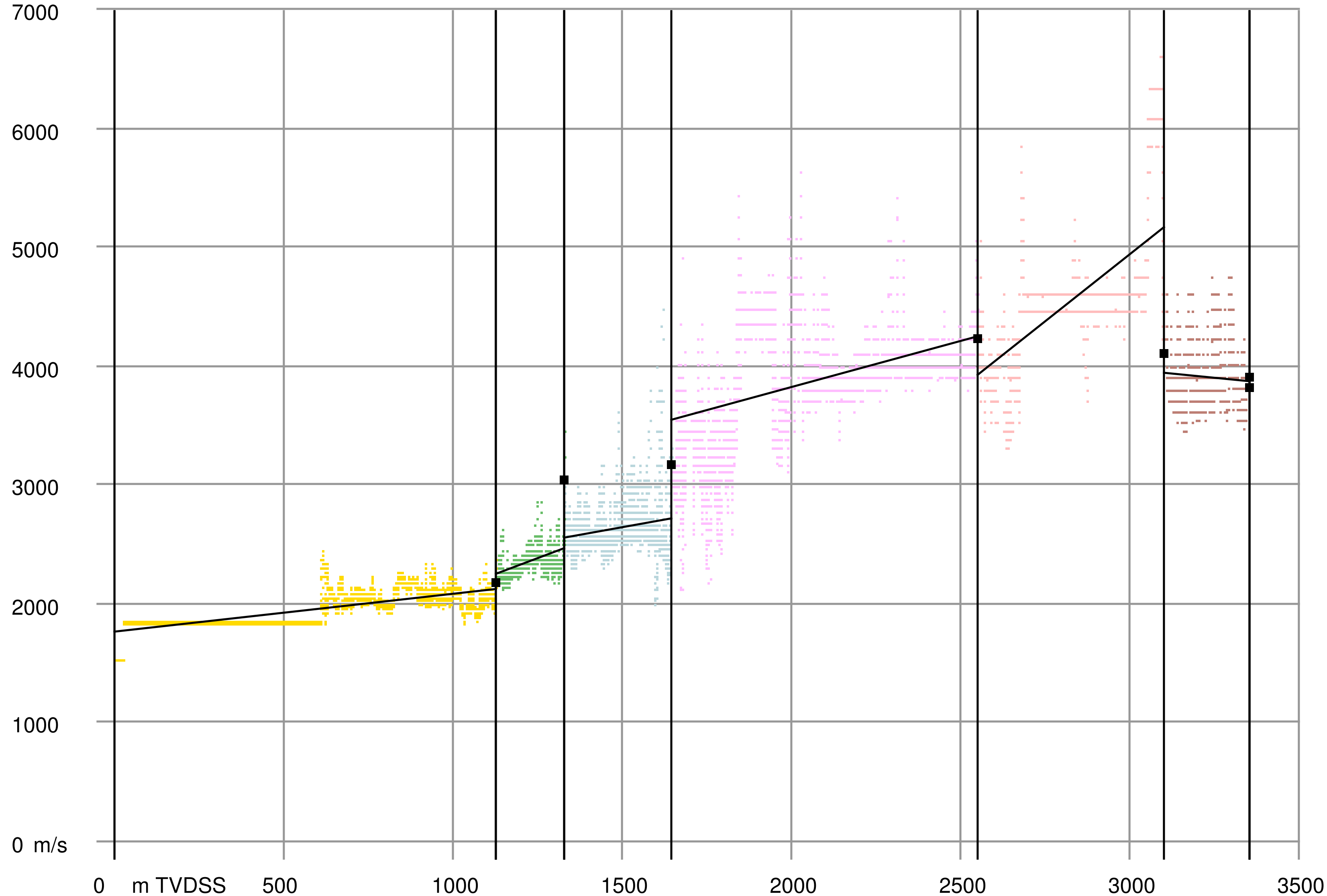

Calibrated instantaneous velocities and linearisation per layer at borehole: K11-11

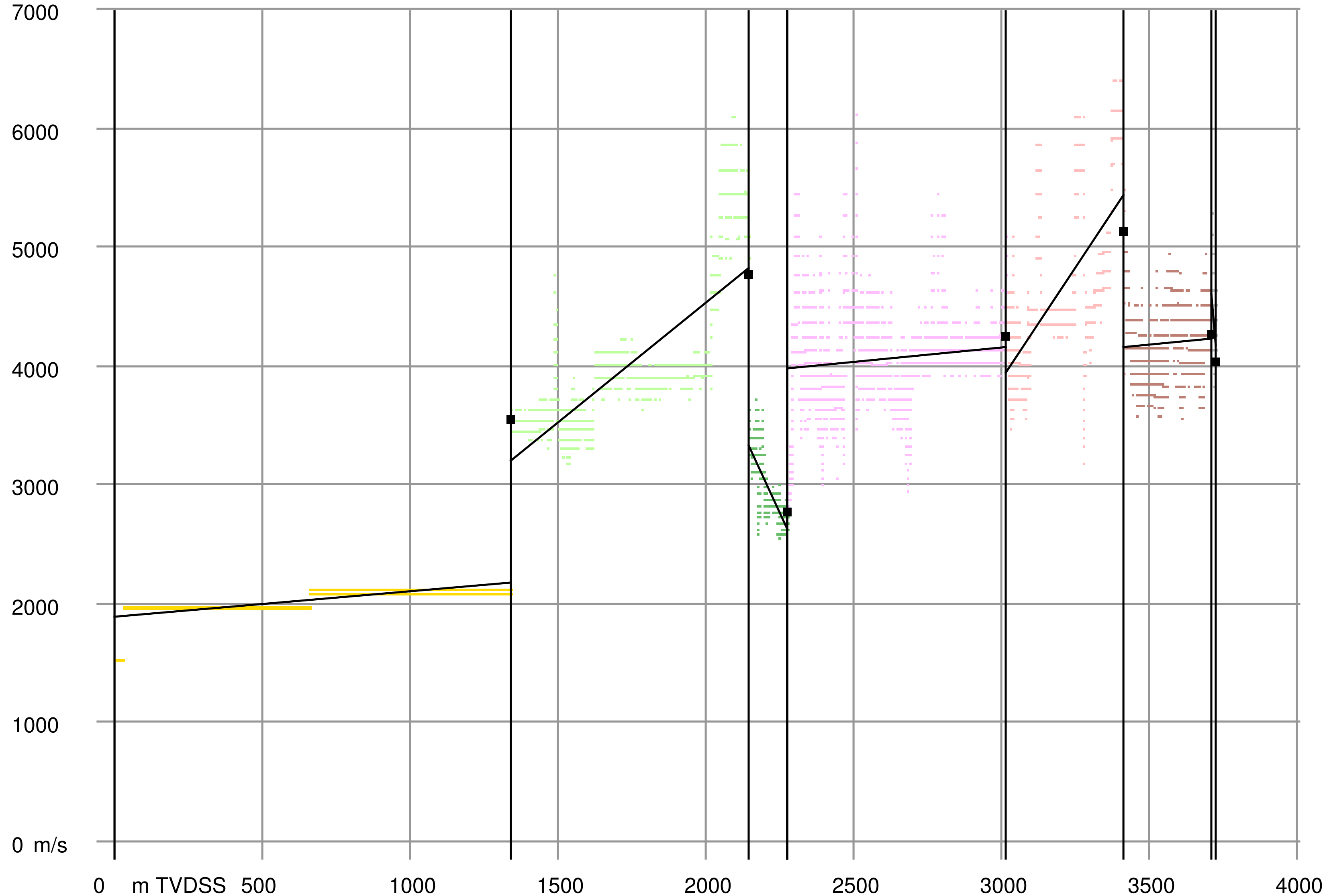

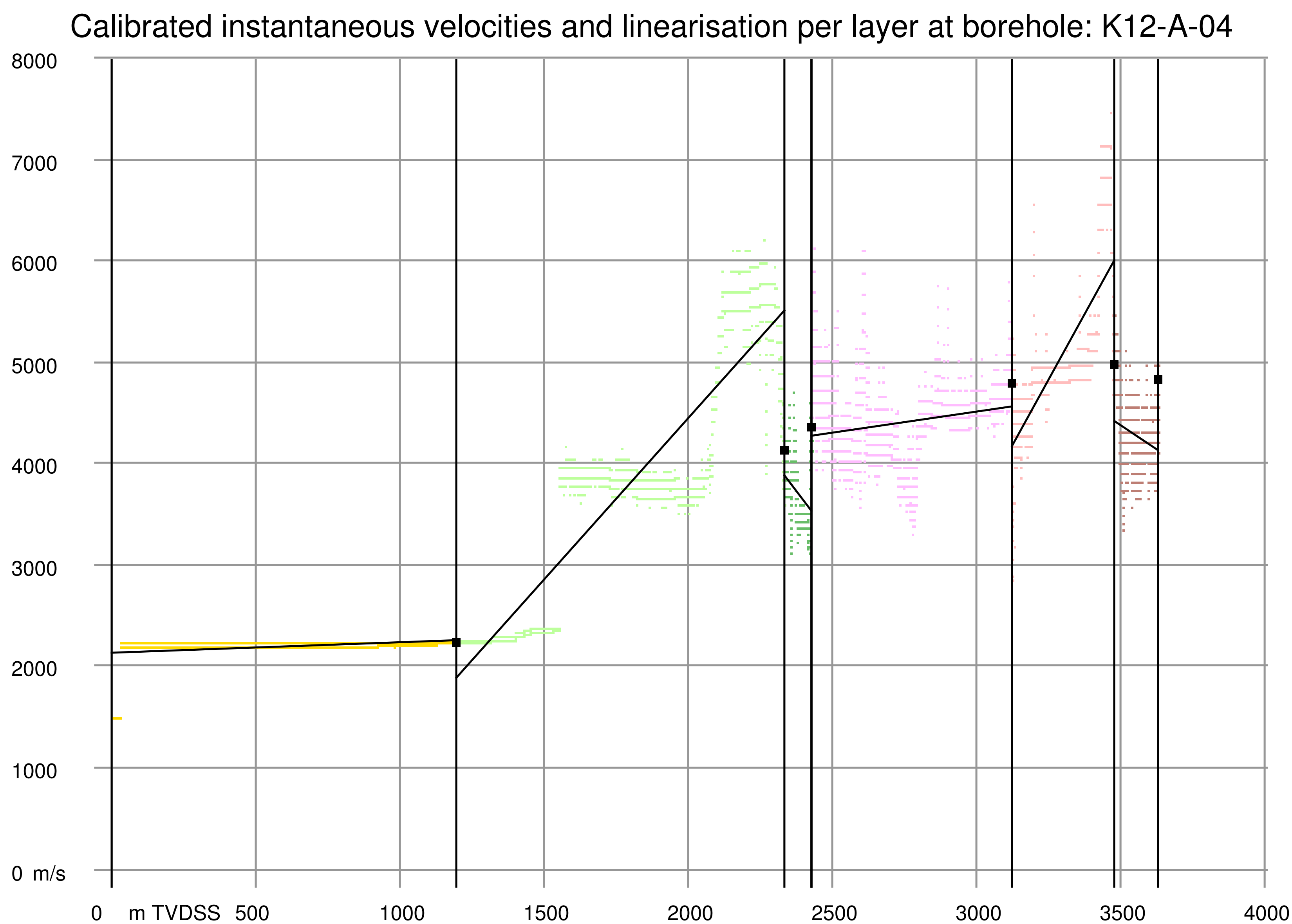

Calibrated instantaneous velocities and linearisation per layer at borehole: K12-A-04
8000
7000
6000
5000
4000
3000
2000
1000
0 m/s
0
m TVDSS
500
1000
1500
2000
2500
3000
3500
4000

Calibrated instantaneous velocities and linearisation per layer at borehole: K12-B-03

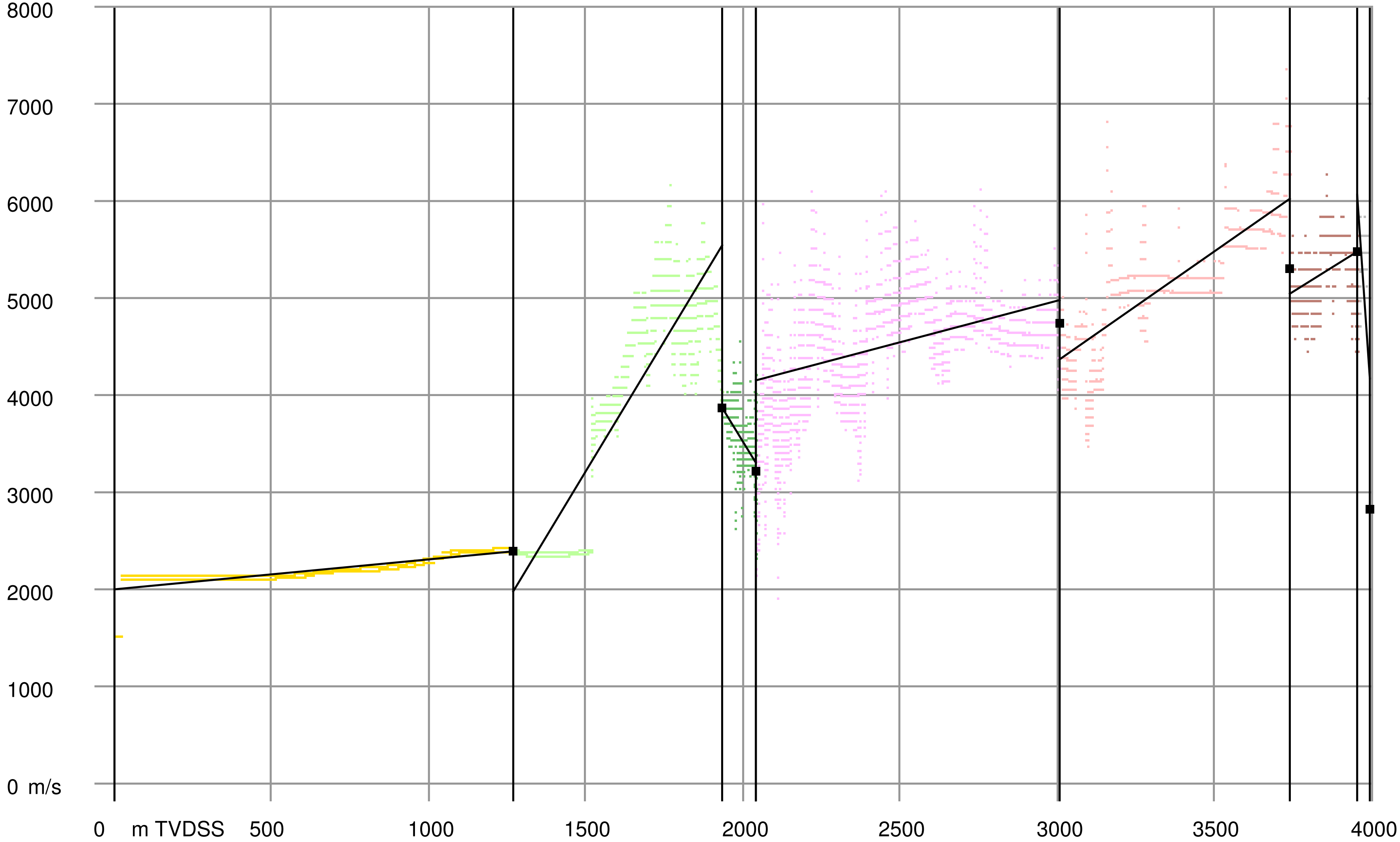

Calibrated instantaneous velocities and linearisation per layer at borehole: K12-B-05

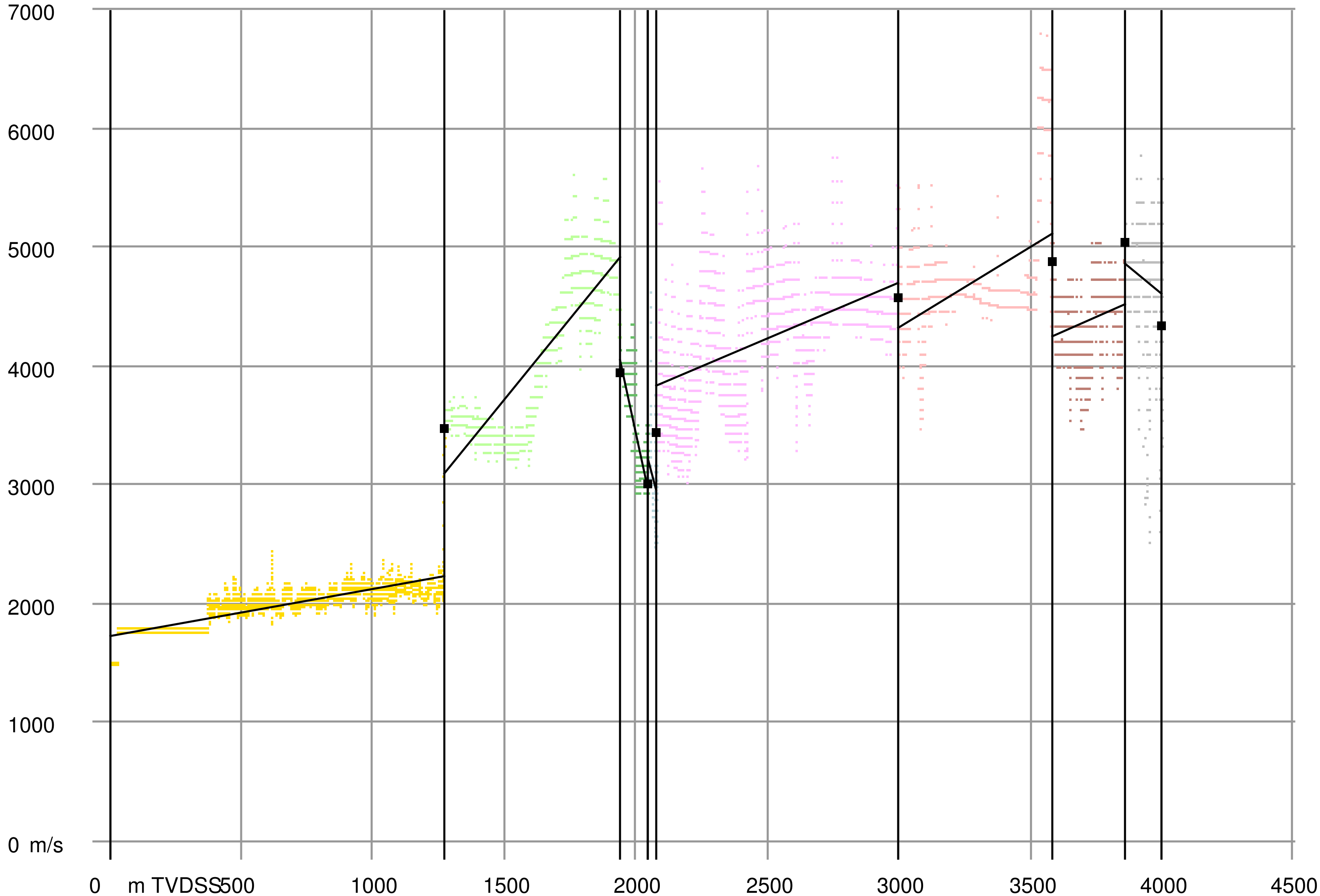

Calibrated instantaneous velocities and linearisation per layer at borehole: K12-B-06

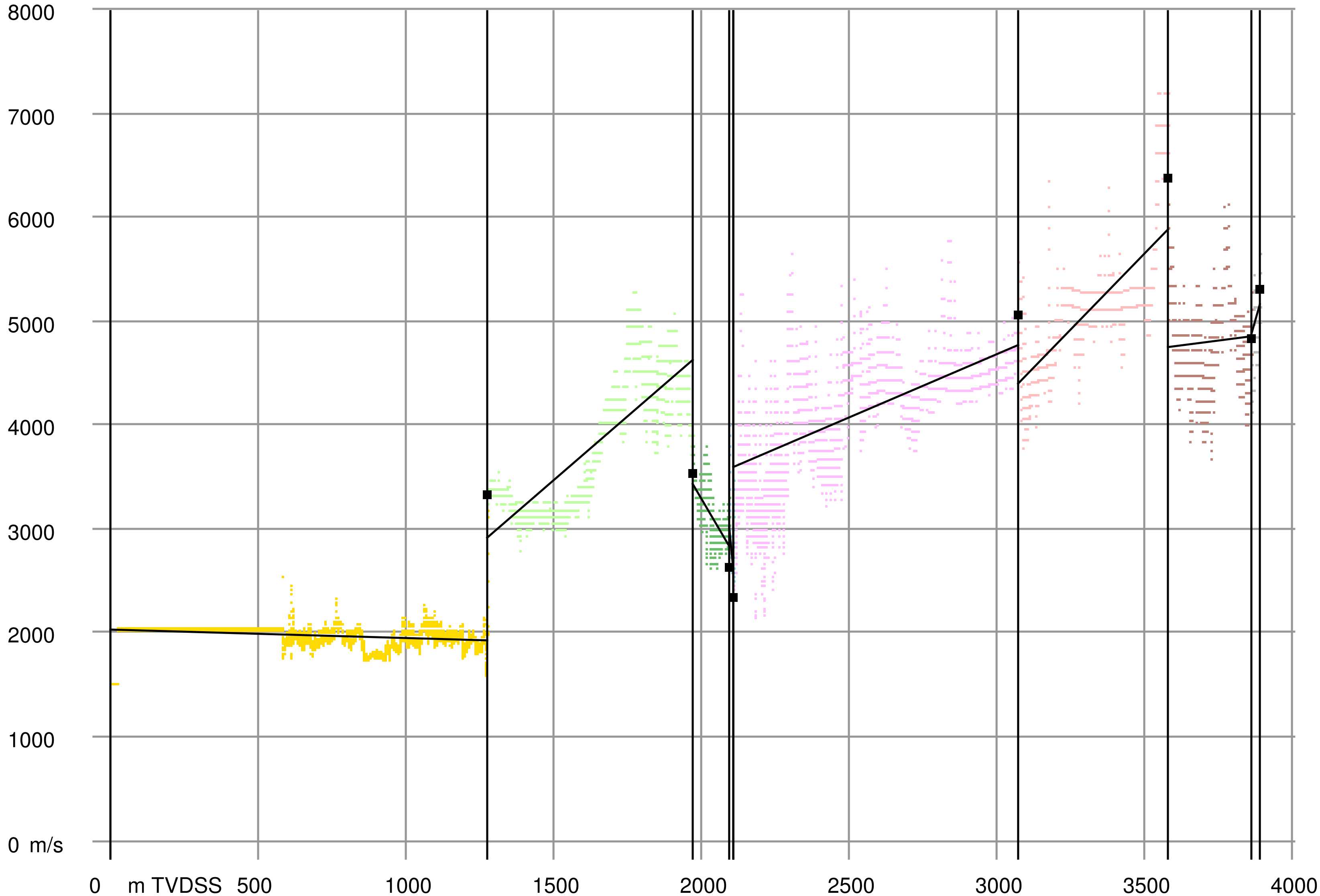

Calibrated instantaneous velocities and linearisation per layer at borehole: K13-14

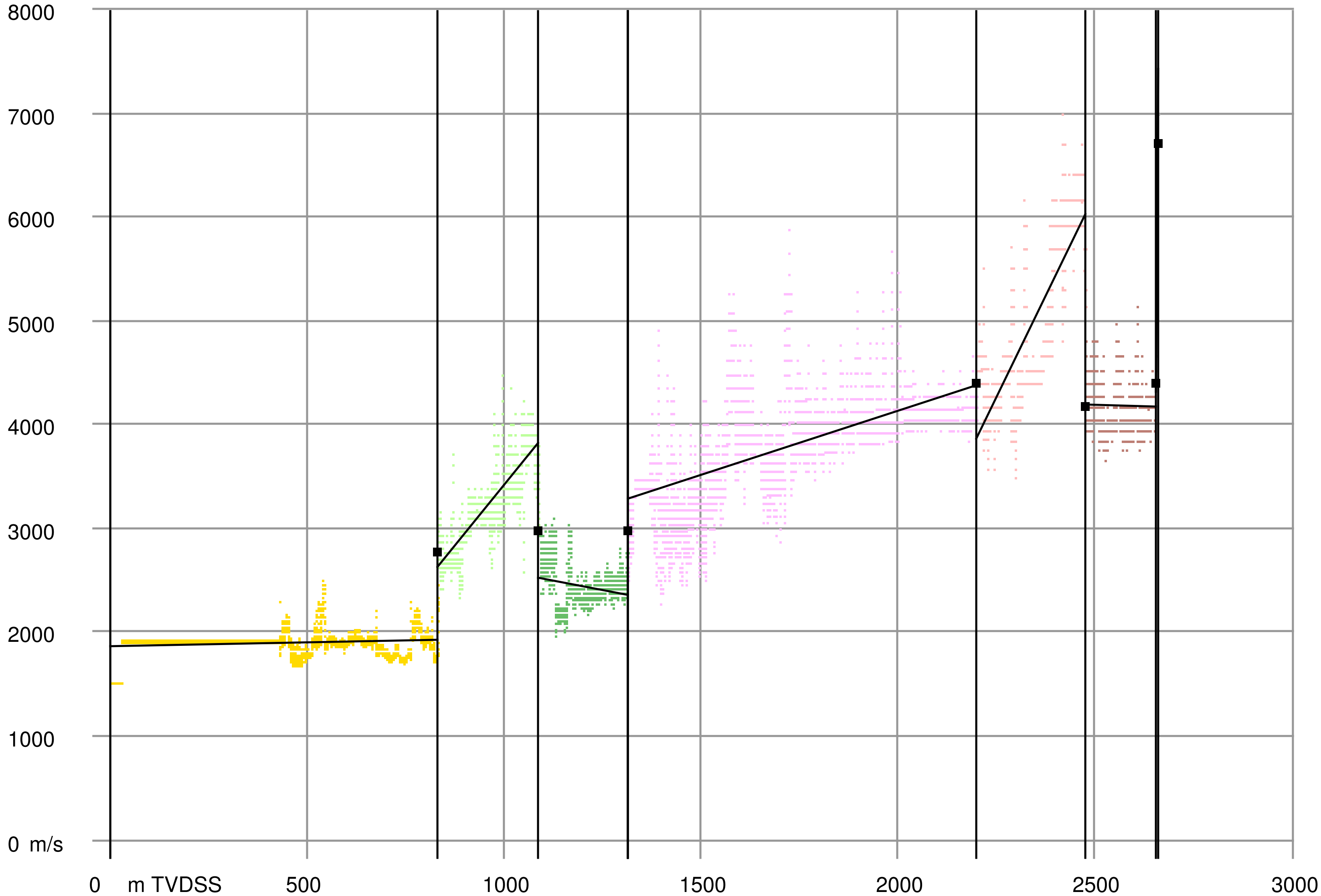

Calibrated instantaneous velocities and linearisation per layer at borehole: K16-04

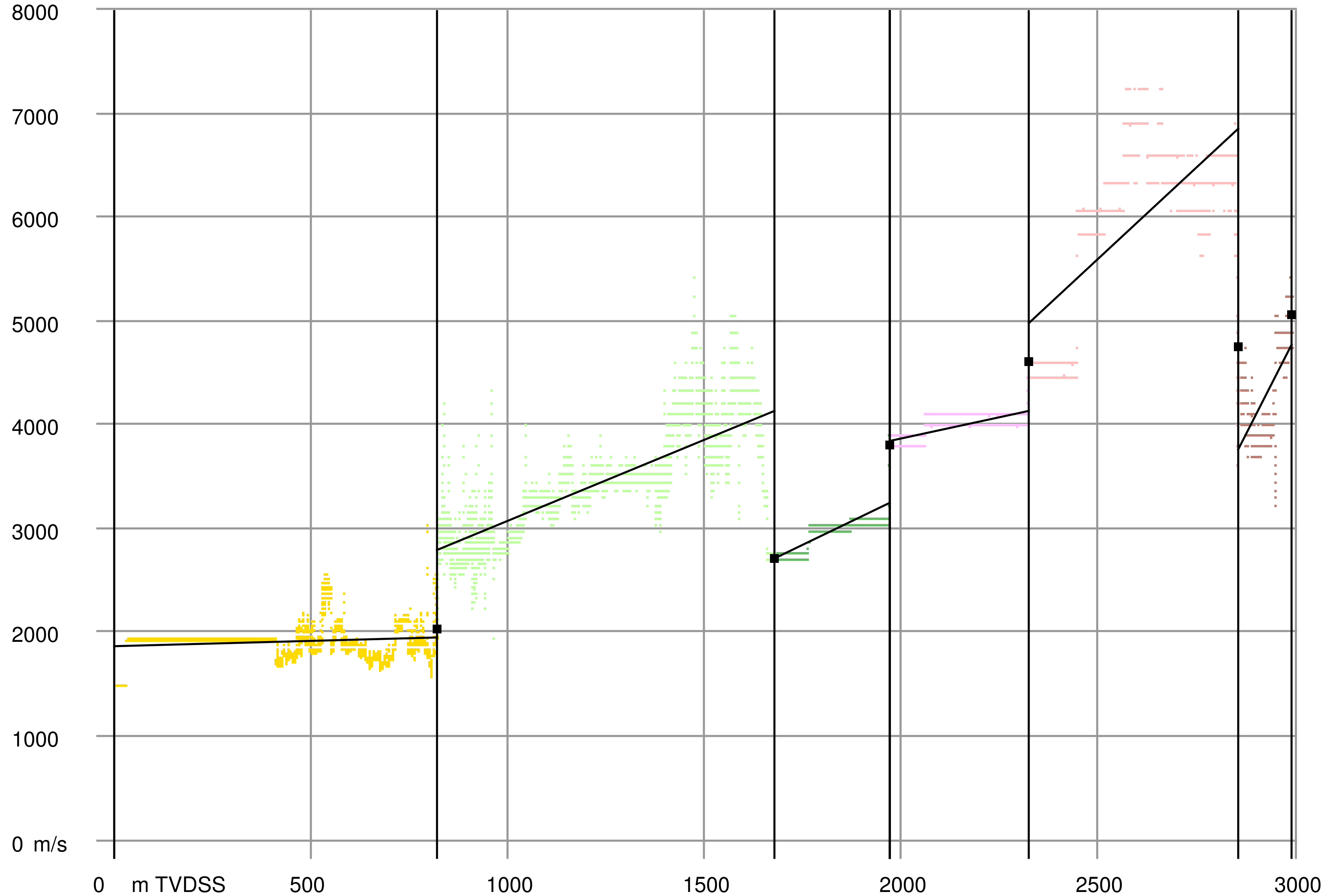

Calibrated instantaneous velocities and linearisation per layer at borehole: K18-KOT-05

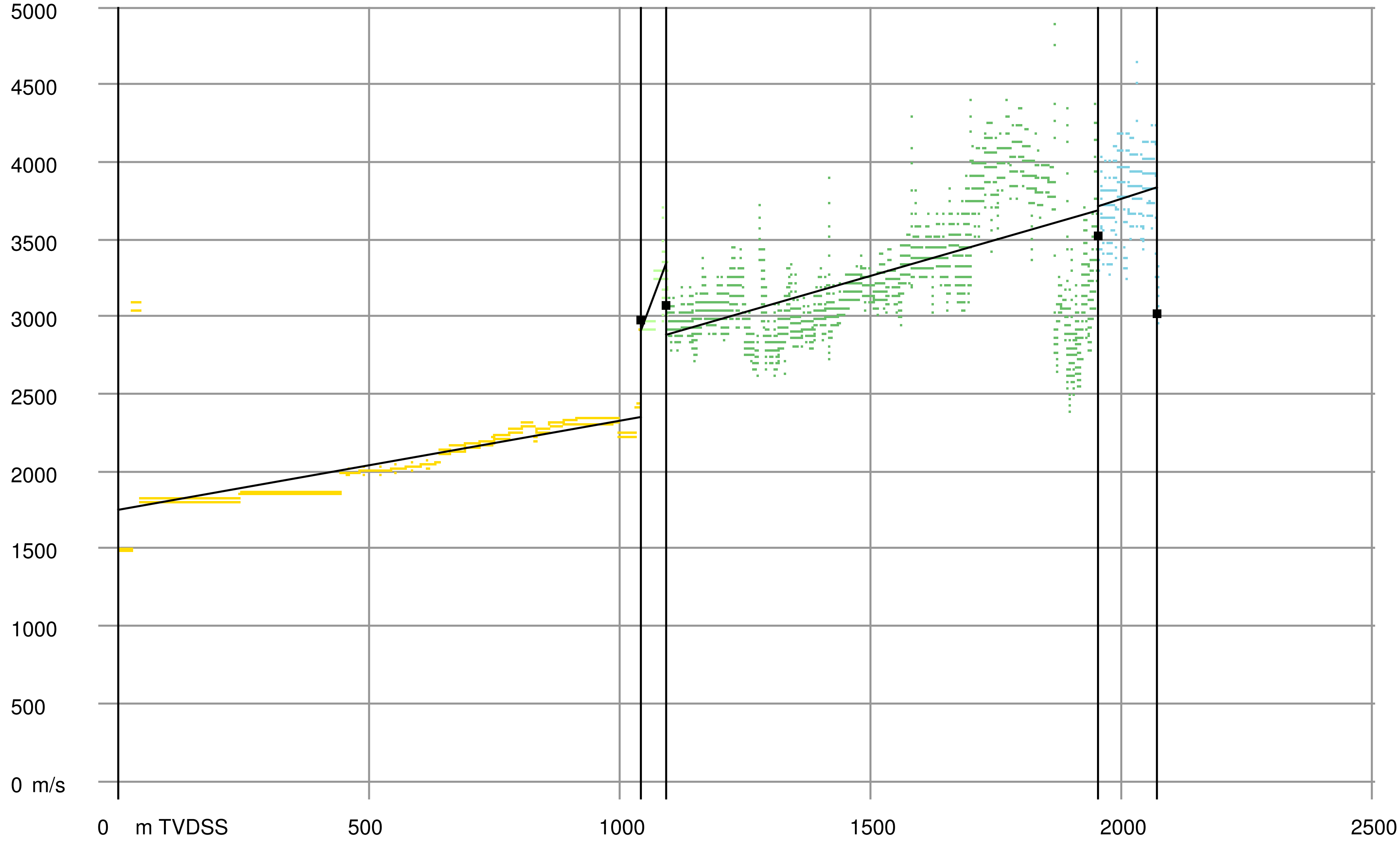

Calibrated instantaneous velocities and linearisation per layer at borehole: K18-KOT-07-1

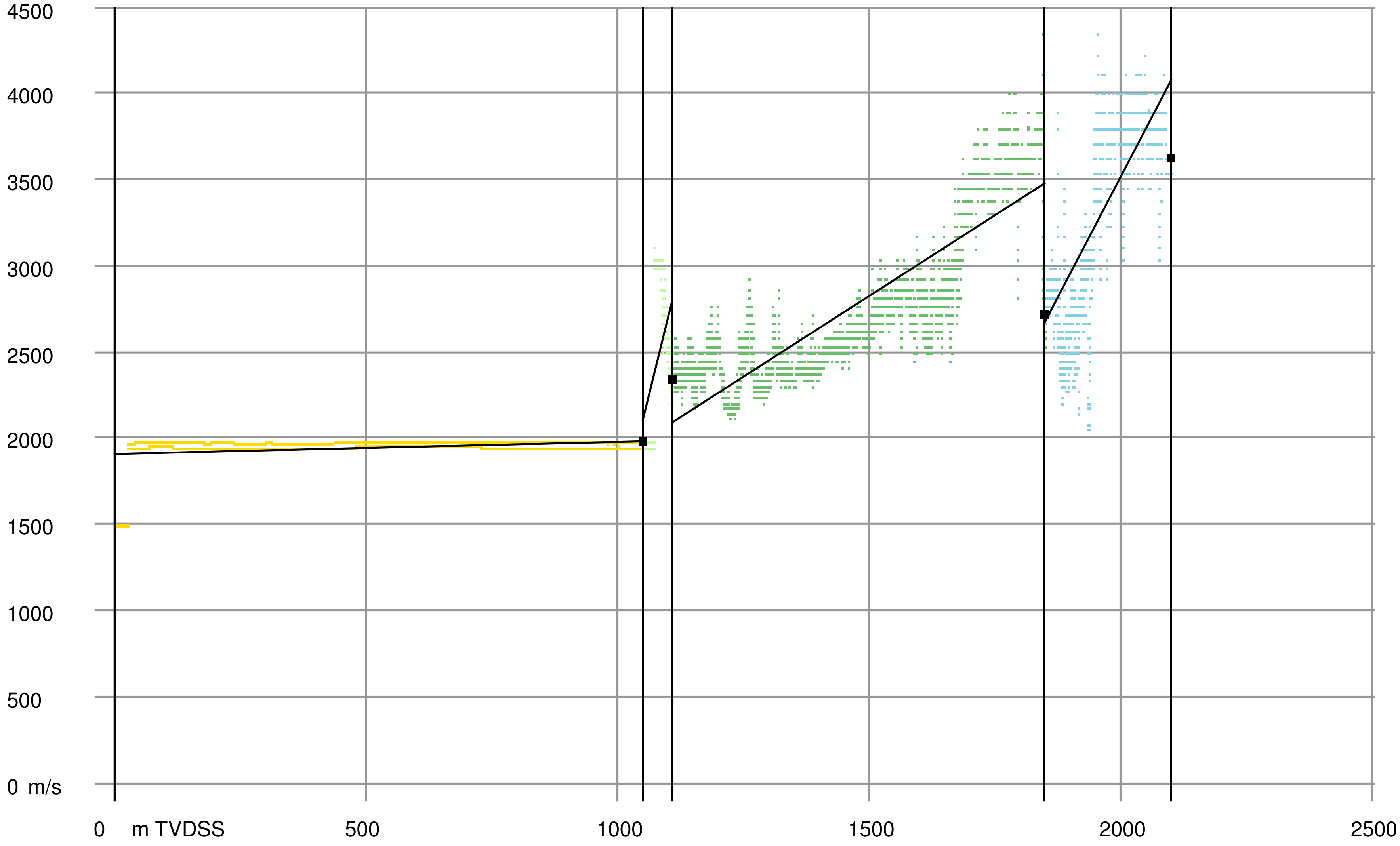

Calibrated instantaneous velocities and linearisation per layer at borehole: K18-KOT-08-0

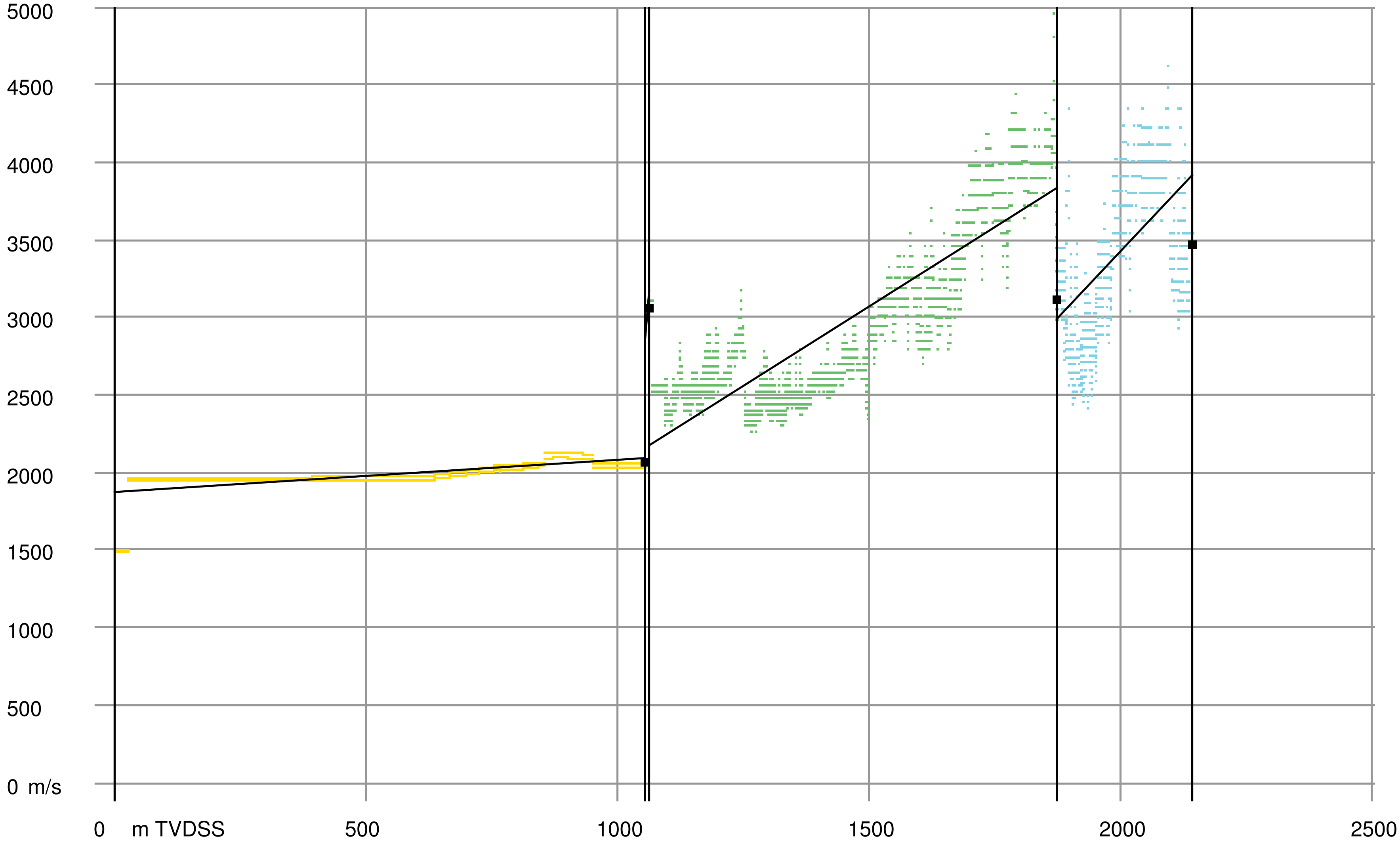

Calibrated instantaneous velocities and linearisation per layer at borehole: K18-KOT-09-1

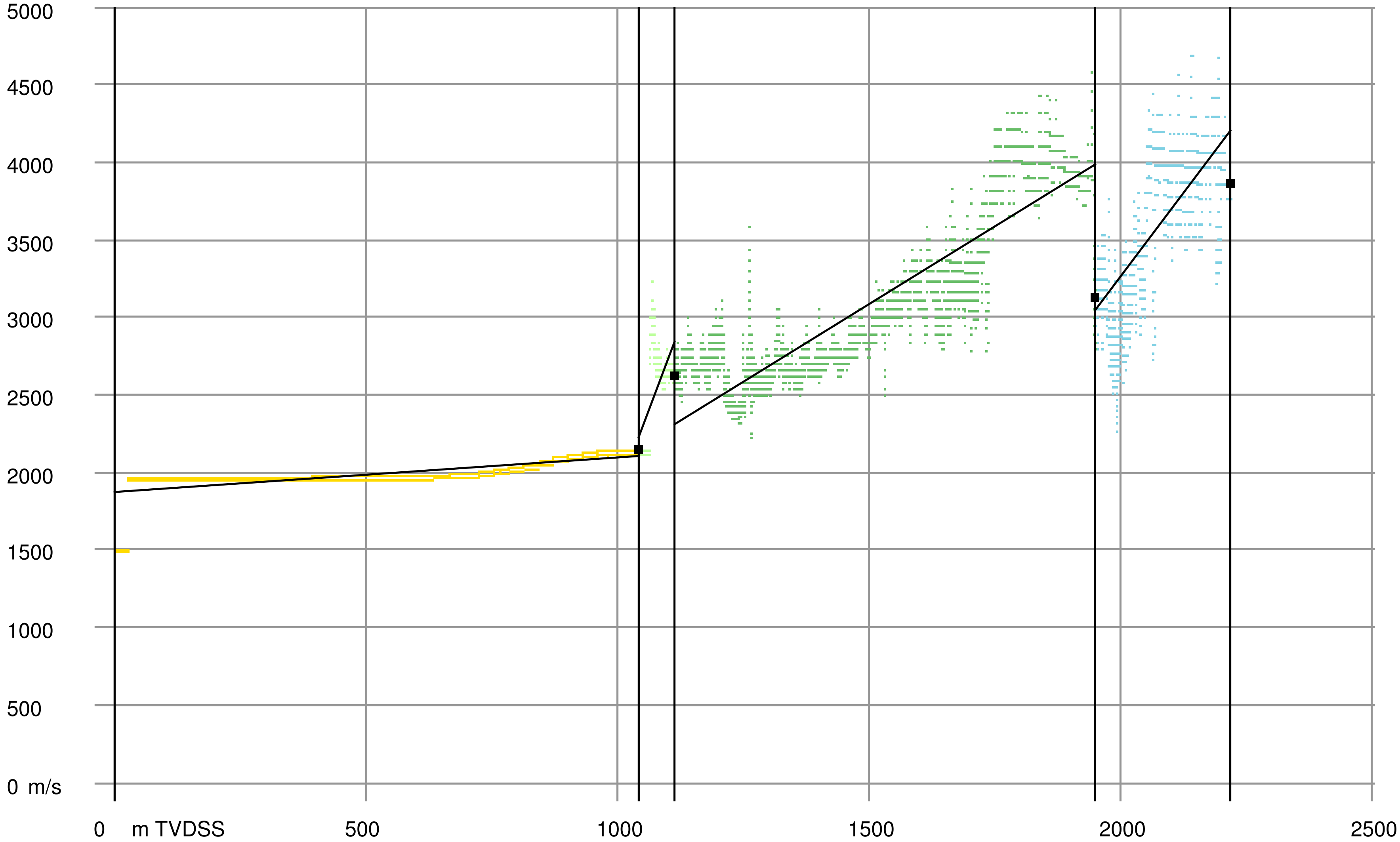

Calibrated instantaneous velocities and linearisation per layer at borehole: KDZ-02

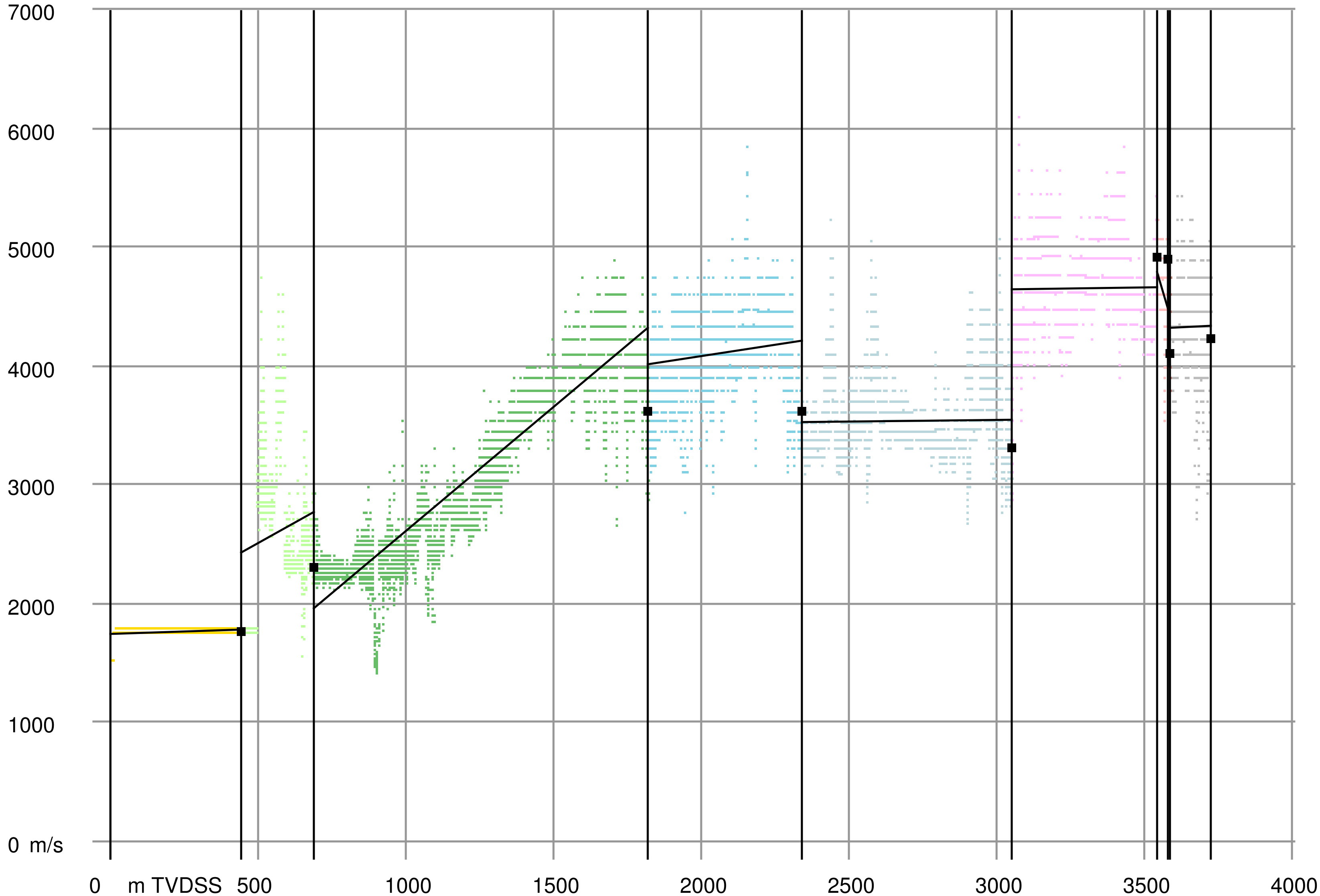

Calibrated instantaneous velocities and linearisation per layer at borehole: KGB-01

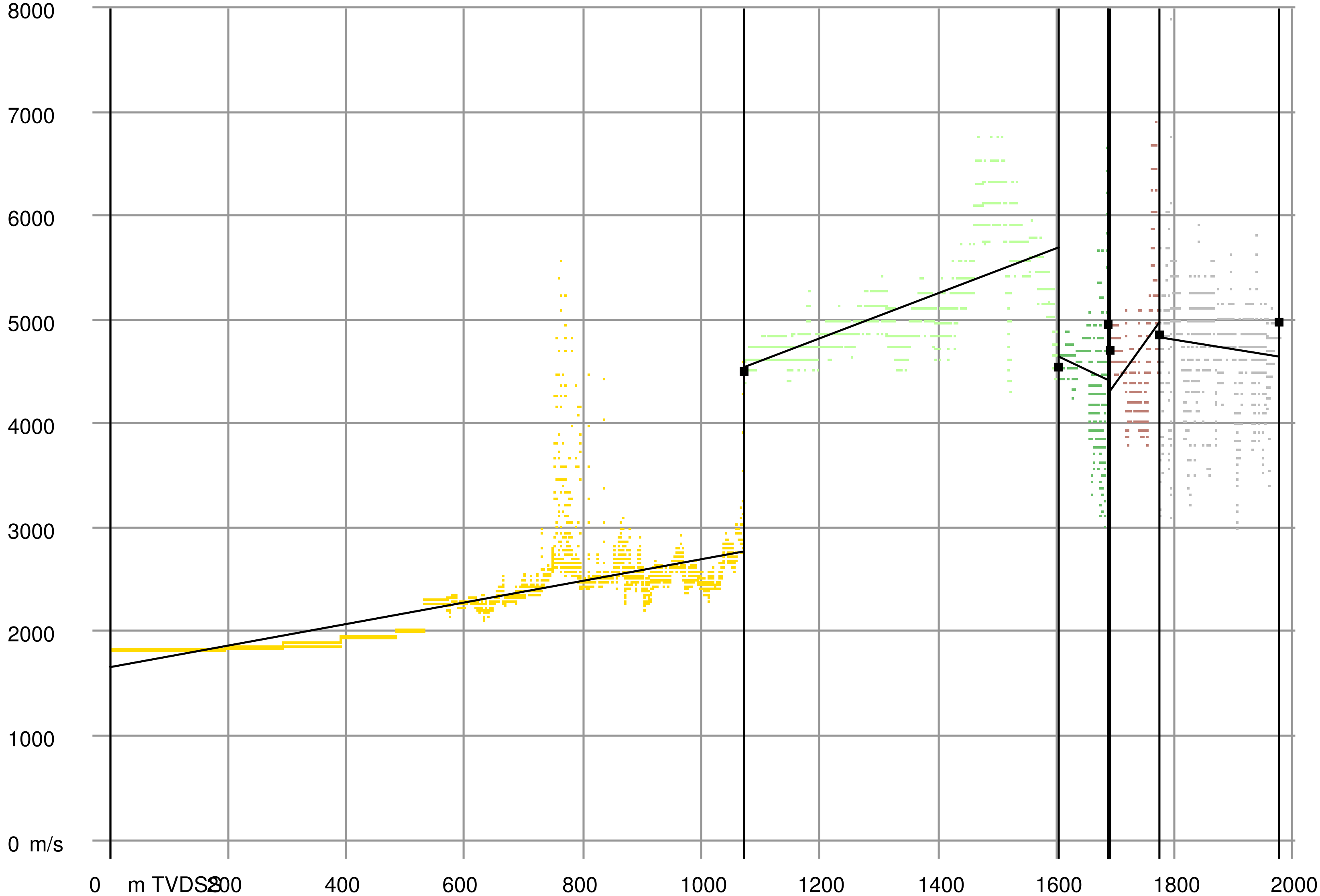

Calibrated instantaneous velocities and linearisation per layer at borehole: L03-03

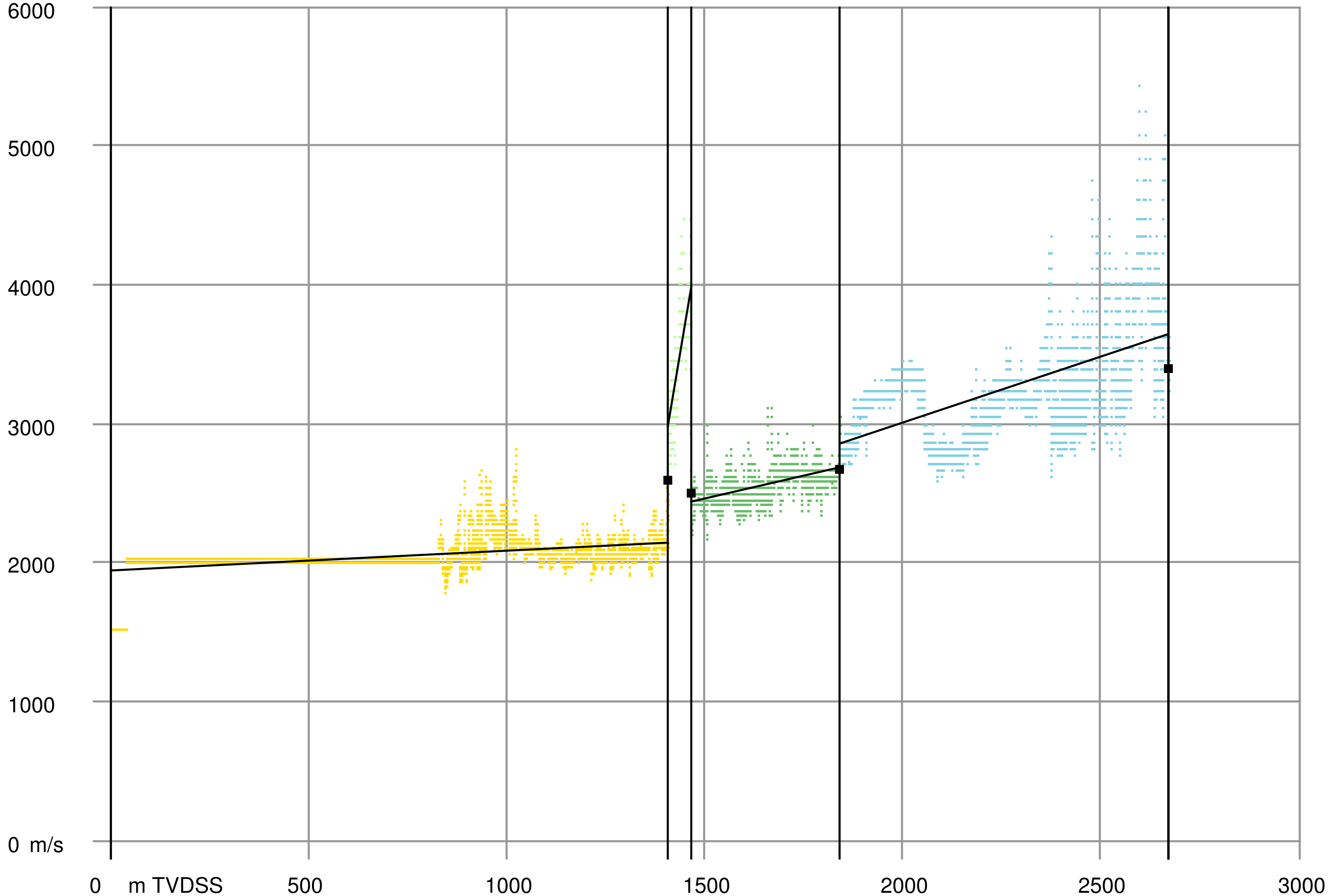

Calibrated instantaneous velocities and linearisation per layer at borehole: L03-04

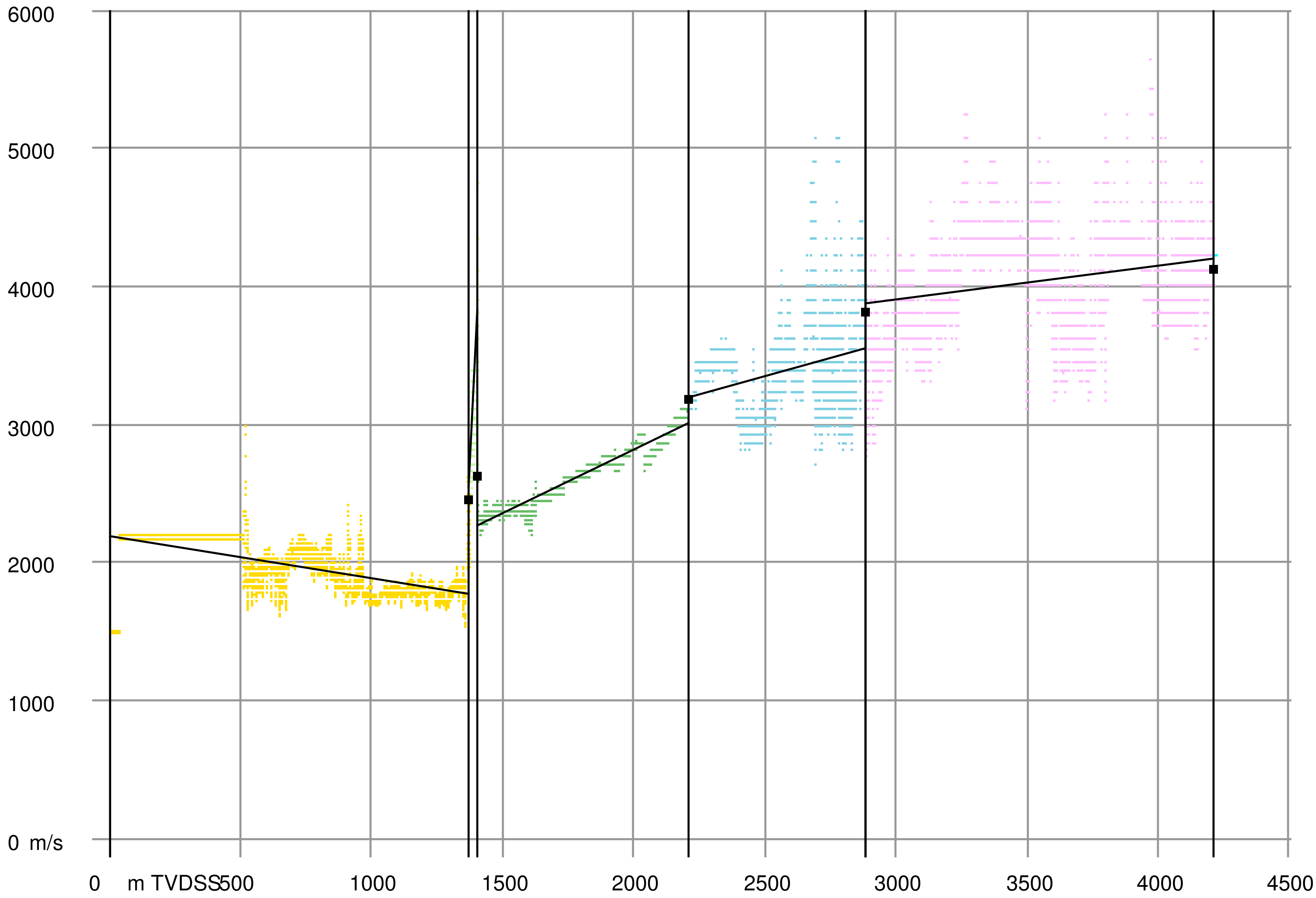

Calibrated instantaneous velocities and linearisation per layer at borehole: L04-06

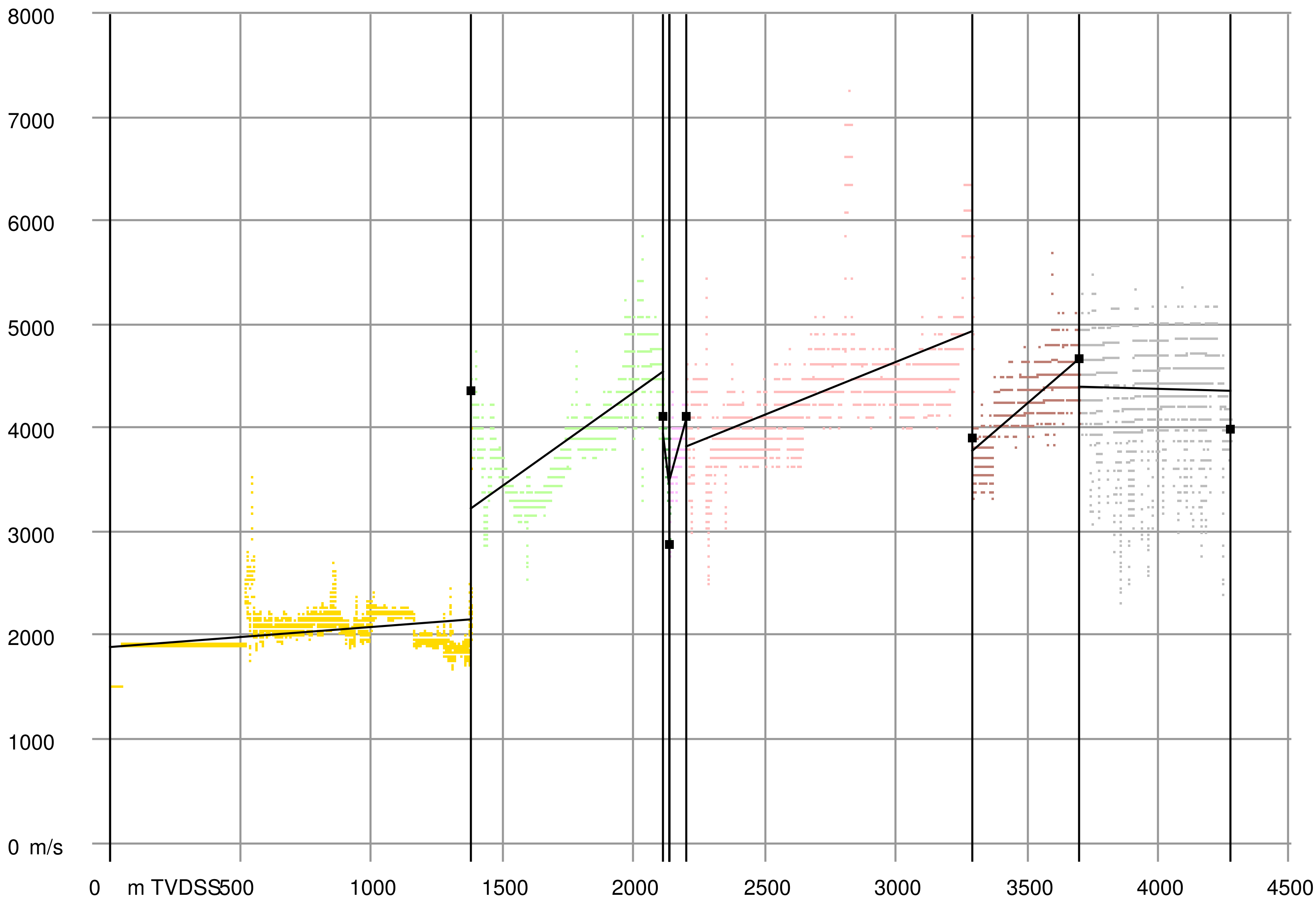

Calibrated instantaneous velocities and linearisation per layer at borehole: L05-04

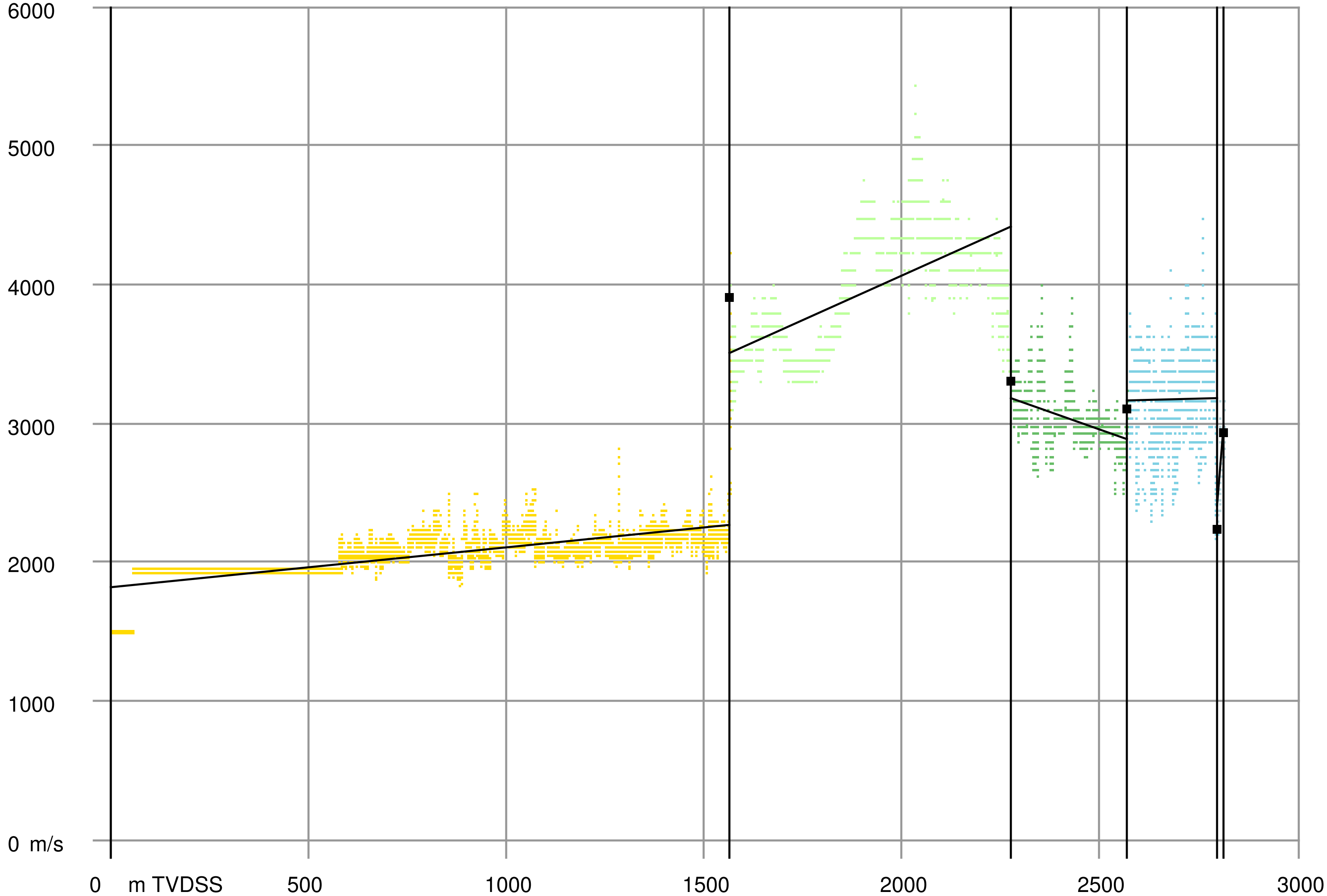

Calibrated instantaneous velocities and linearisation per layer at borehole: L05-05

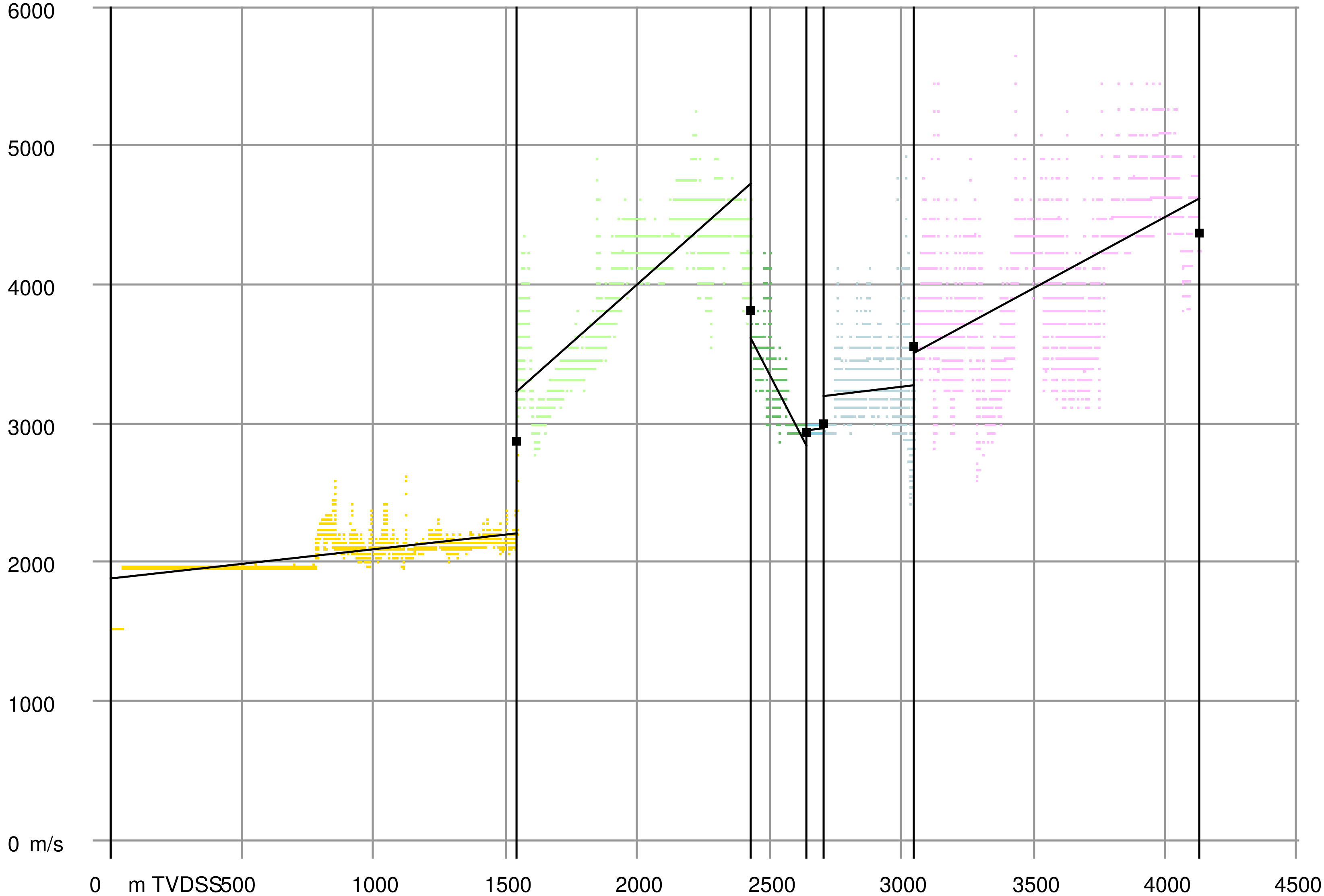

Calibrated instantaneous velocities and linearisation per layer at borehole: L06-01

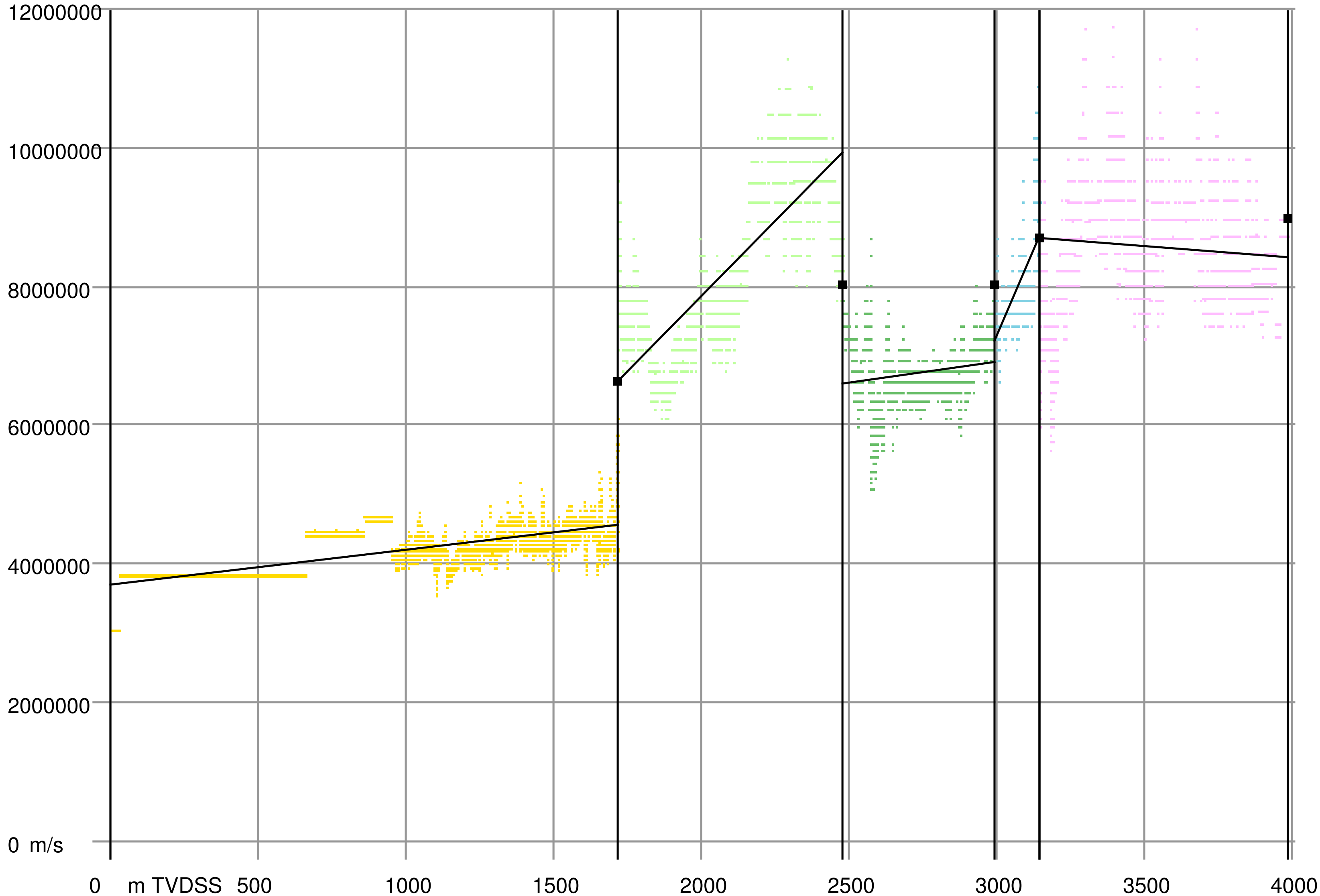

Calibrated instantaneous velocities and linearisation per layer at borehole: L08-04

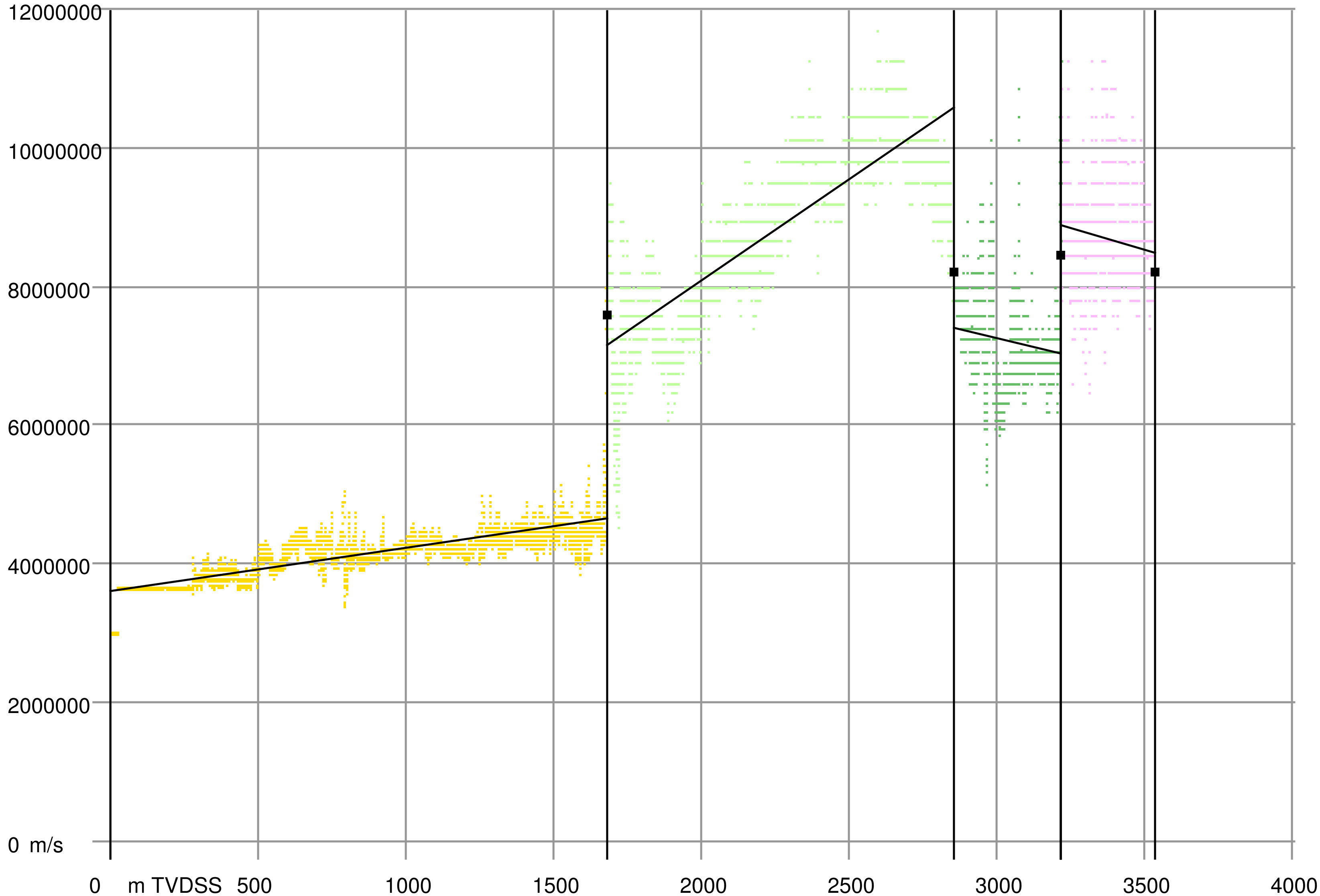

Calibrated instantaneous velocities and linearisation per layer at borehole: L08-11

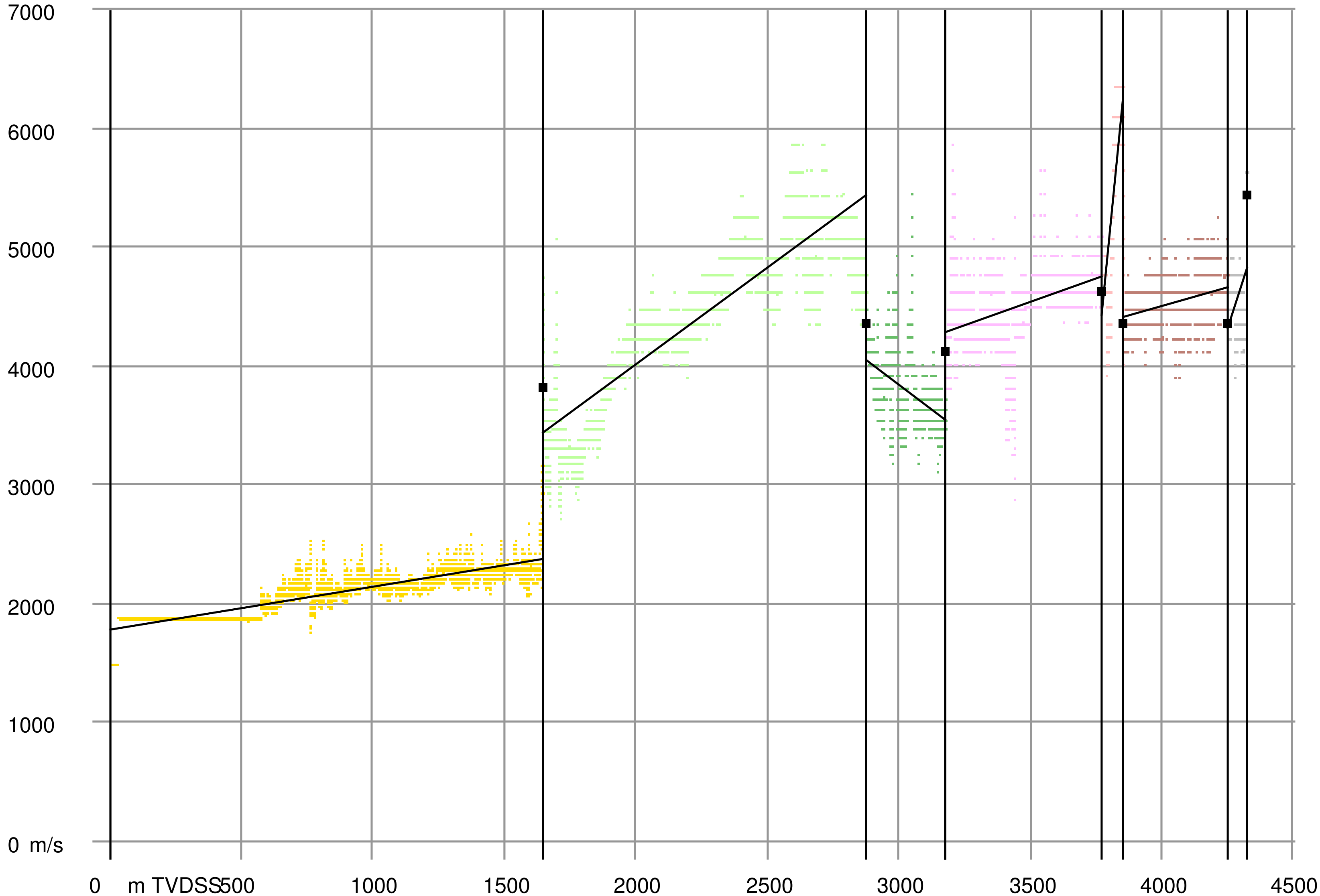

Calibrated instantaneous velocities and linearisation per layer at borehole: L09-02

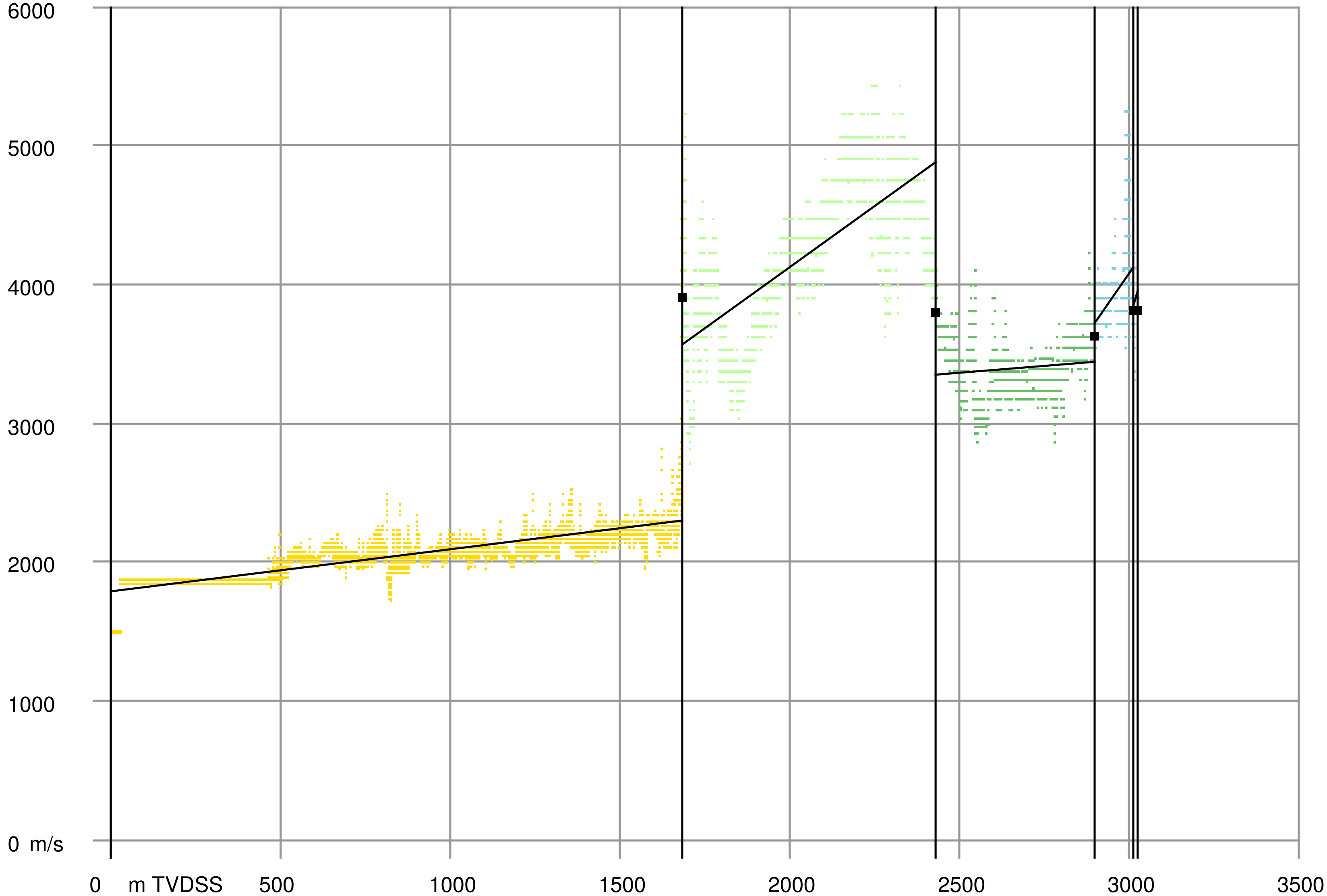

Calibrated instantaneous velocities and linearisation per layer at borehole: L09-04

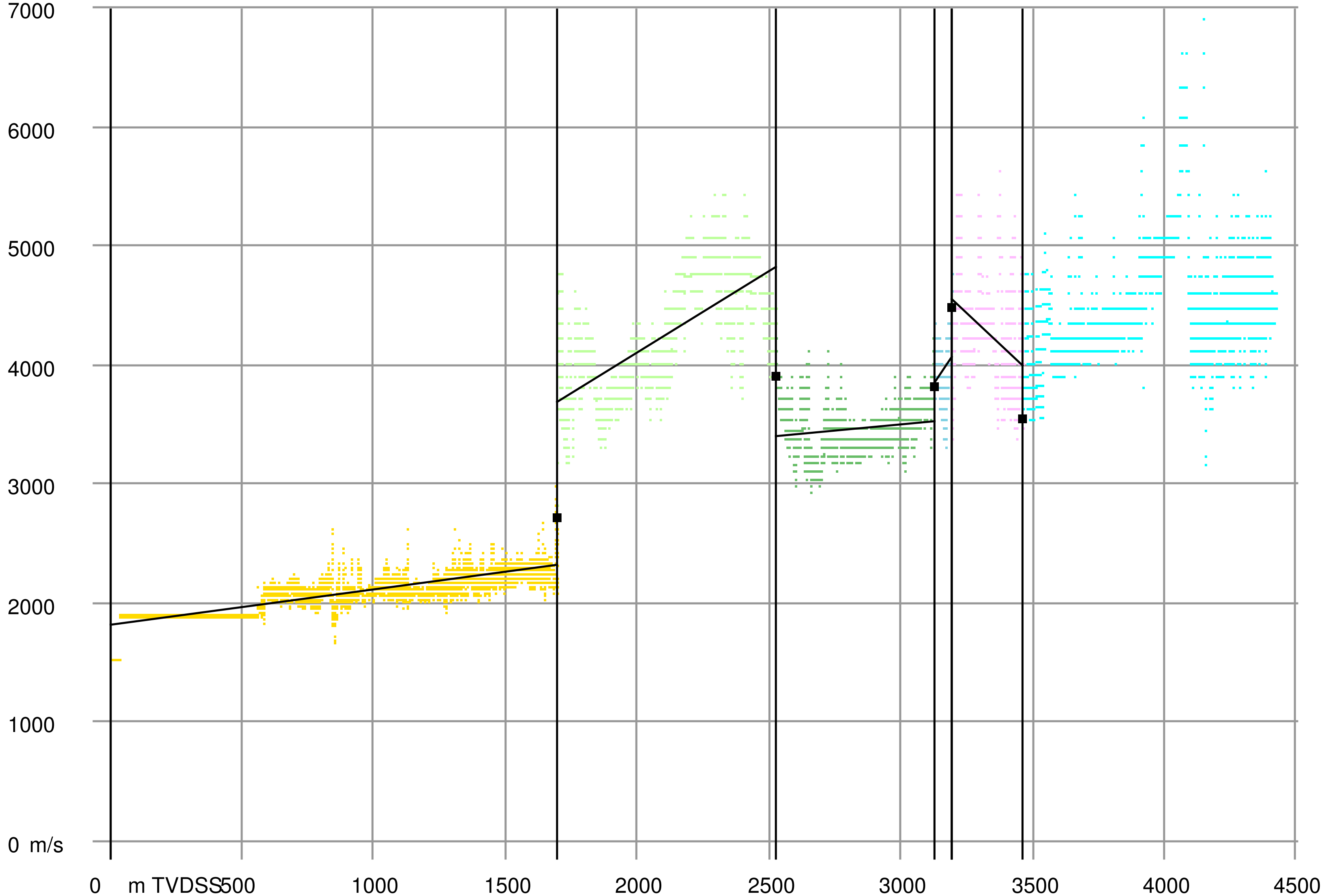

Calibrated instantaneous velocities and linearisation per layer at borehole: L10-22

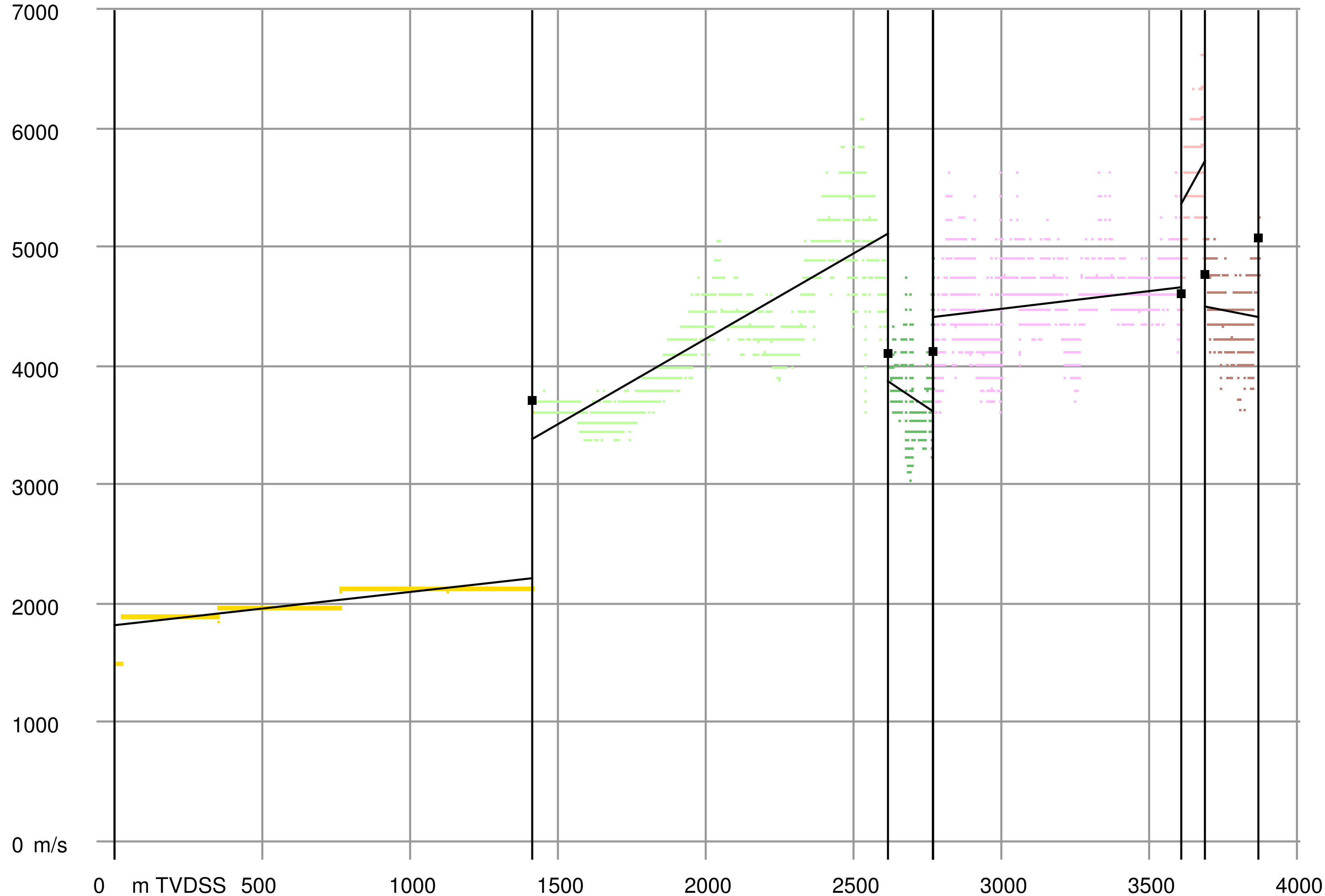

Calibrated instantaneous velocities and linearisation per layer at borehole: L10-24

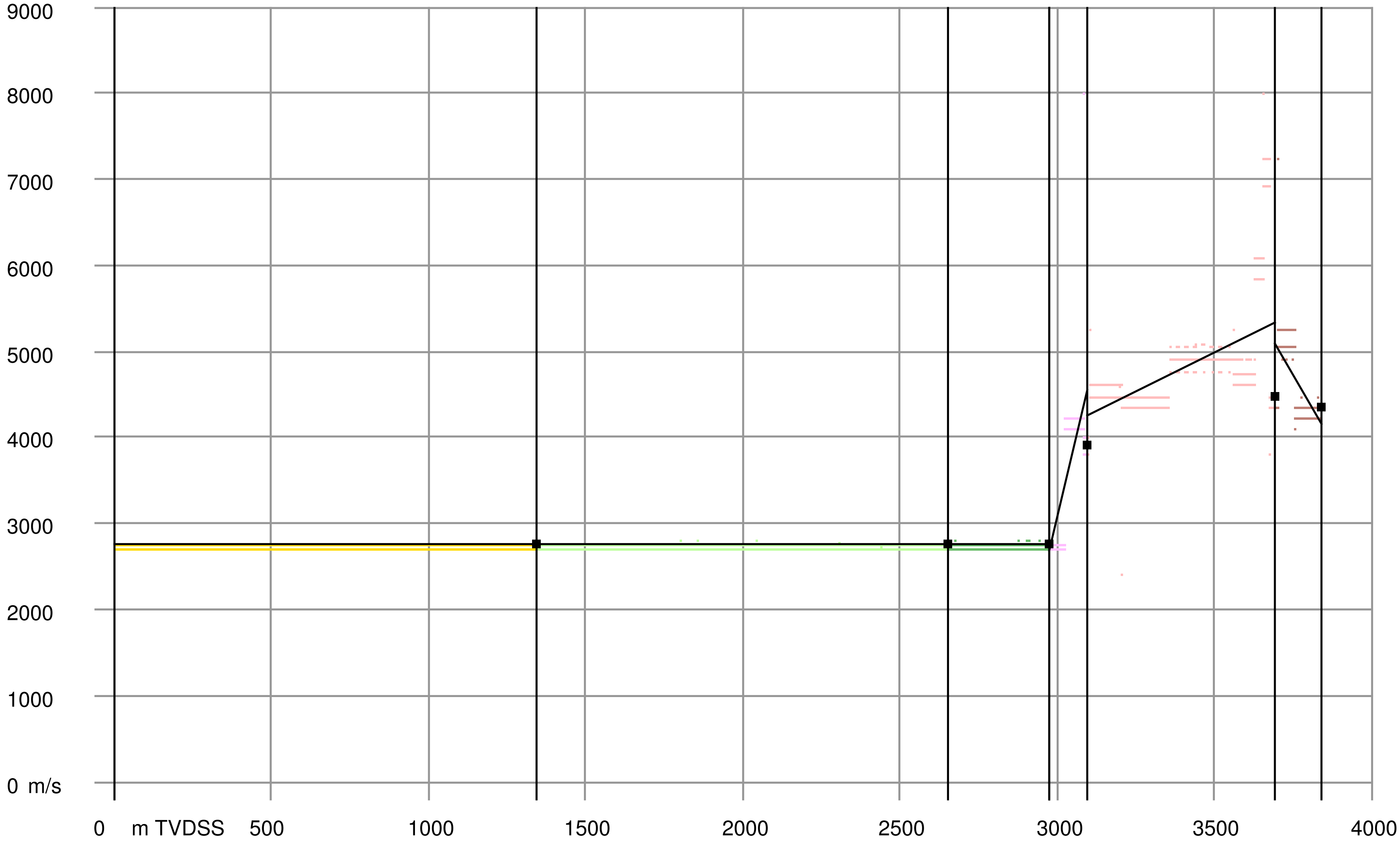

Calibrated instantaneous velocities and linearisation per layer at borehole: L10-27

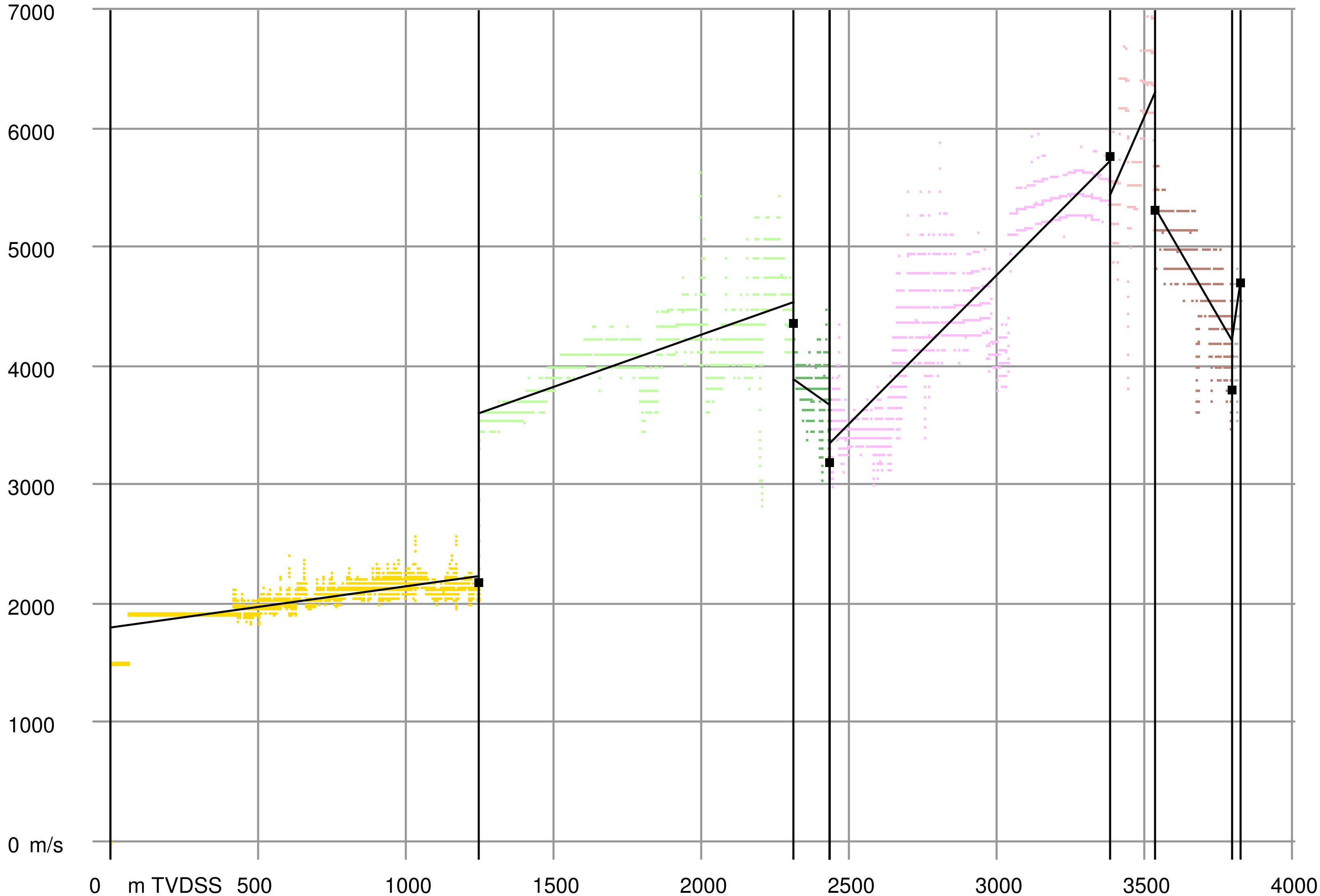

Calibrated instantaneous velocities and linearisation per layer at borehole: L10-29

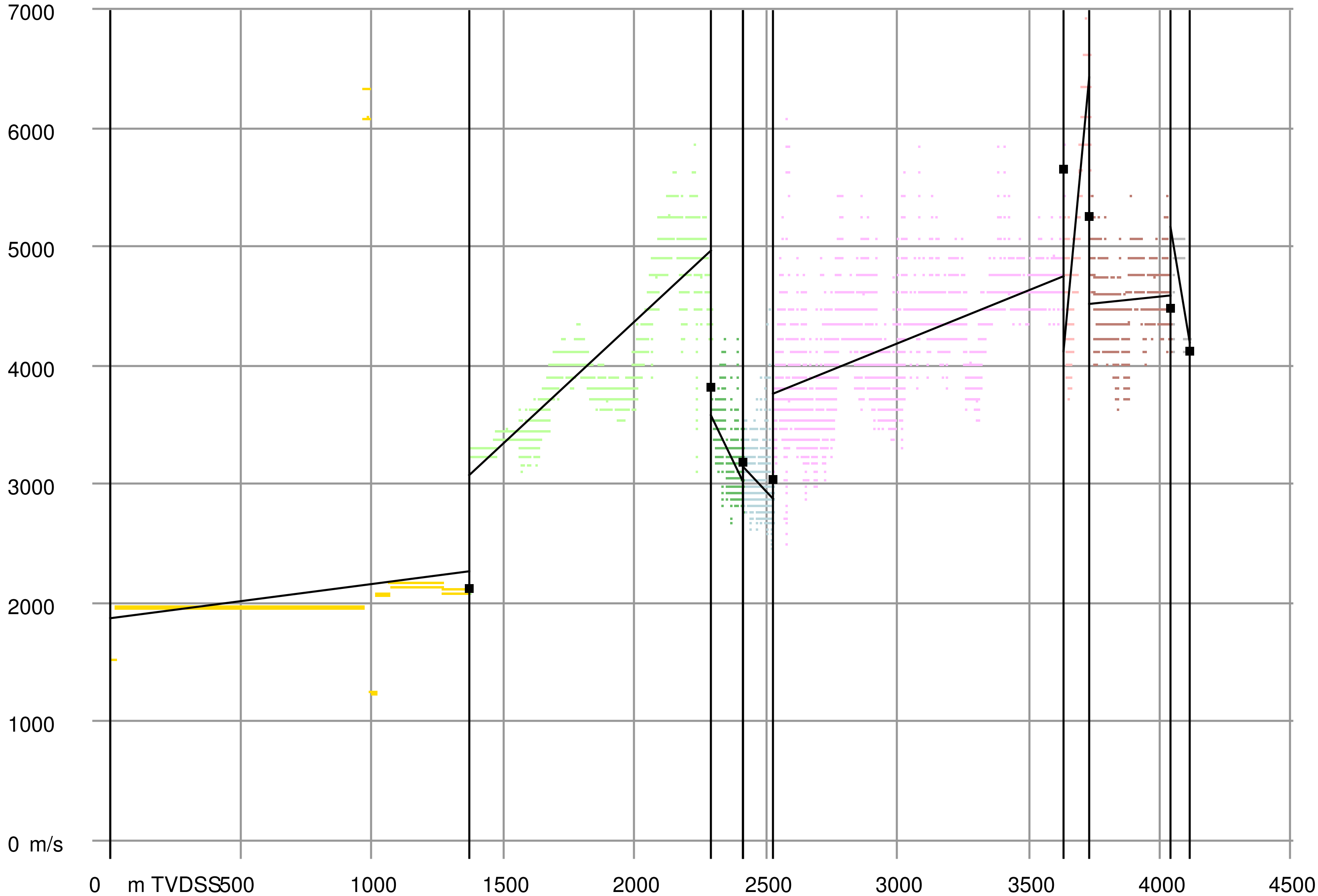

Calibrated instantaneous velocities and linearisation per layer at borehole: L10-F-01

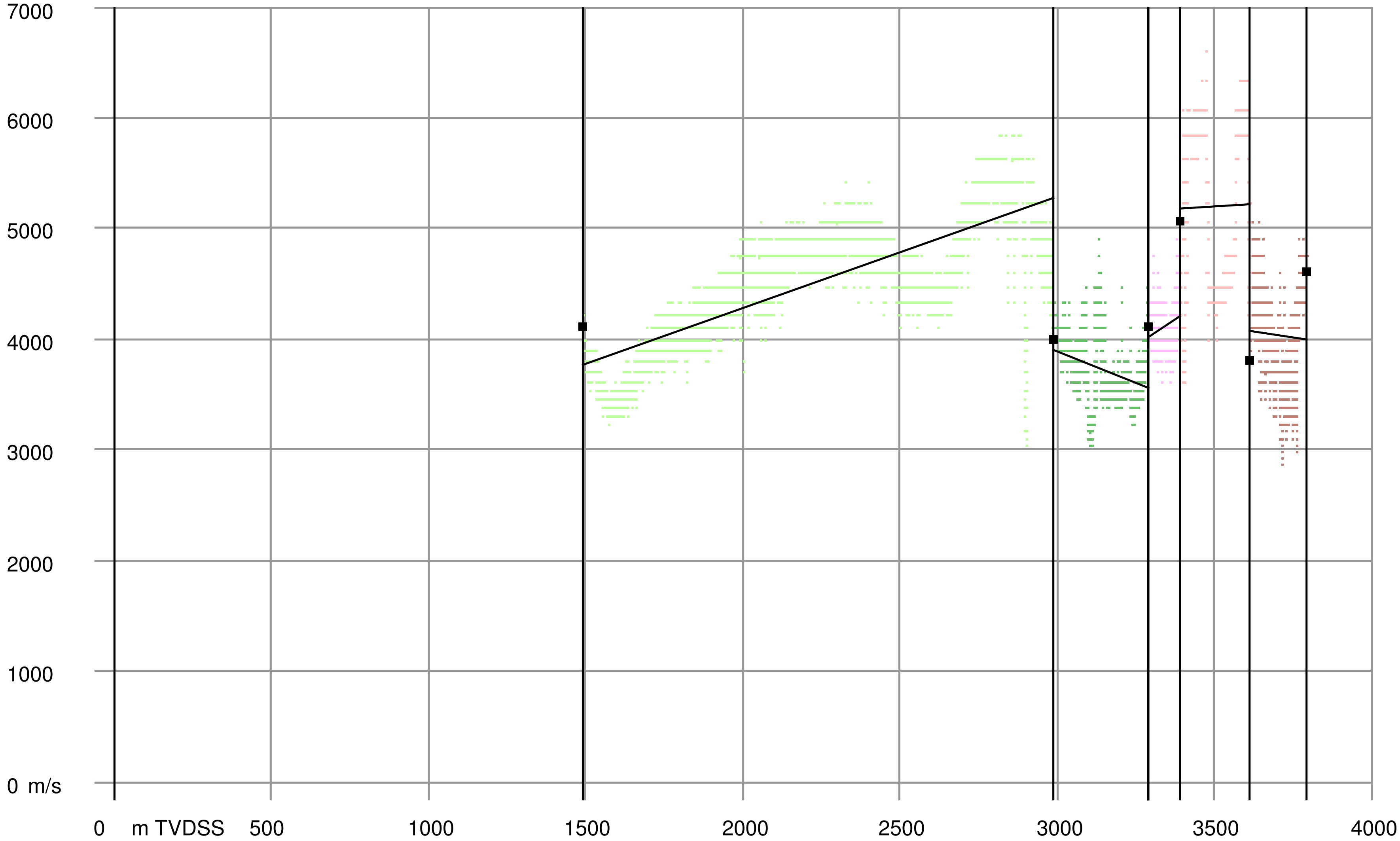

Calibrated instantaneous velocities and linearisation per layer at borehole: L10-G-01

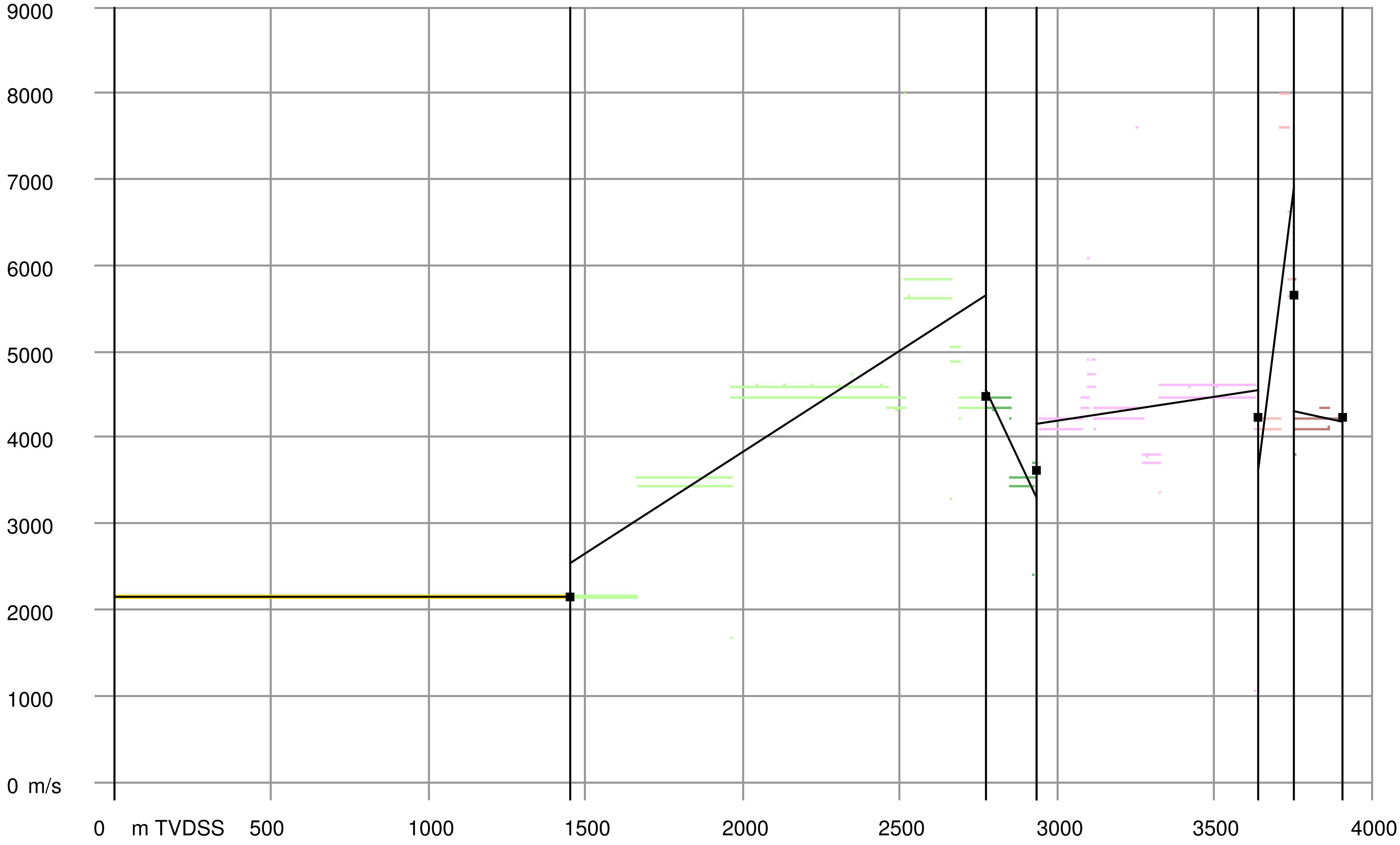

Calibrated instantaneous velocities and linearisation per layer at borehole: L10-K-01-S1

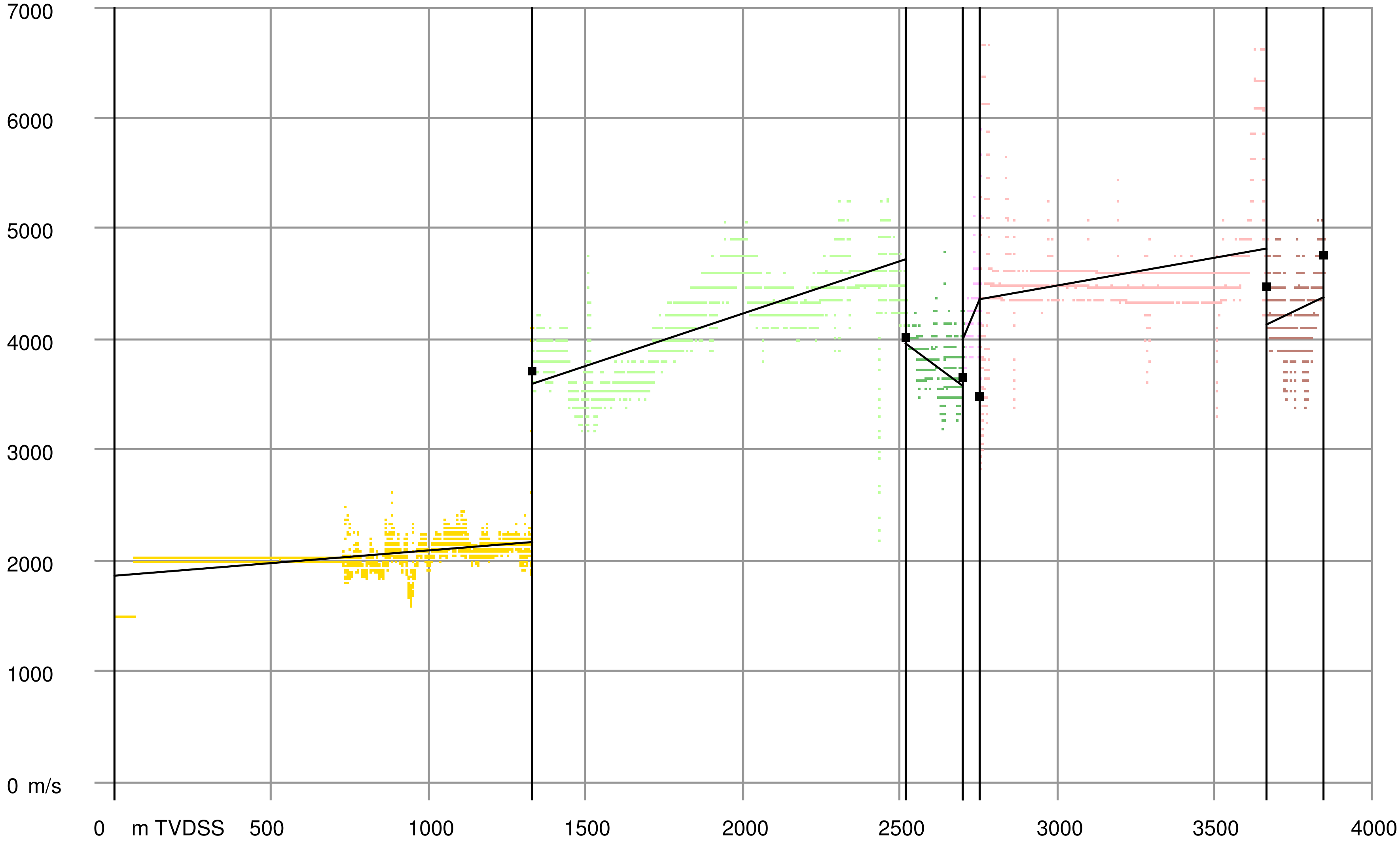

Calibrated instantaneous velocities and linearisation per layer at borehole: L10-K-01-S2

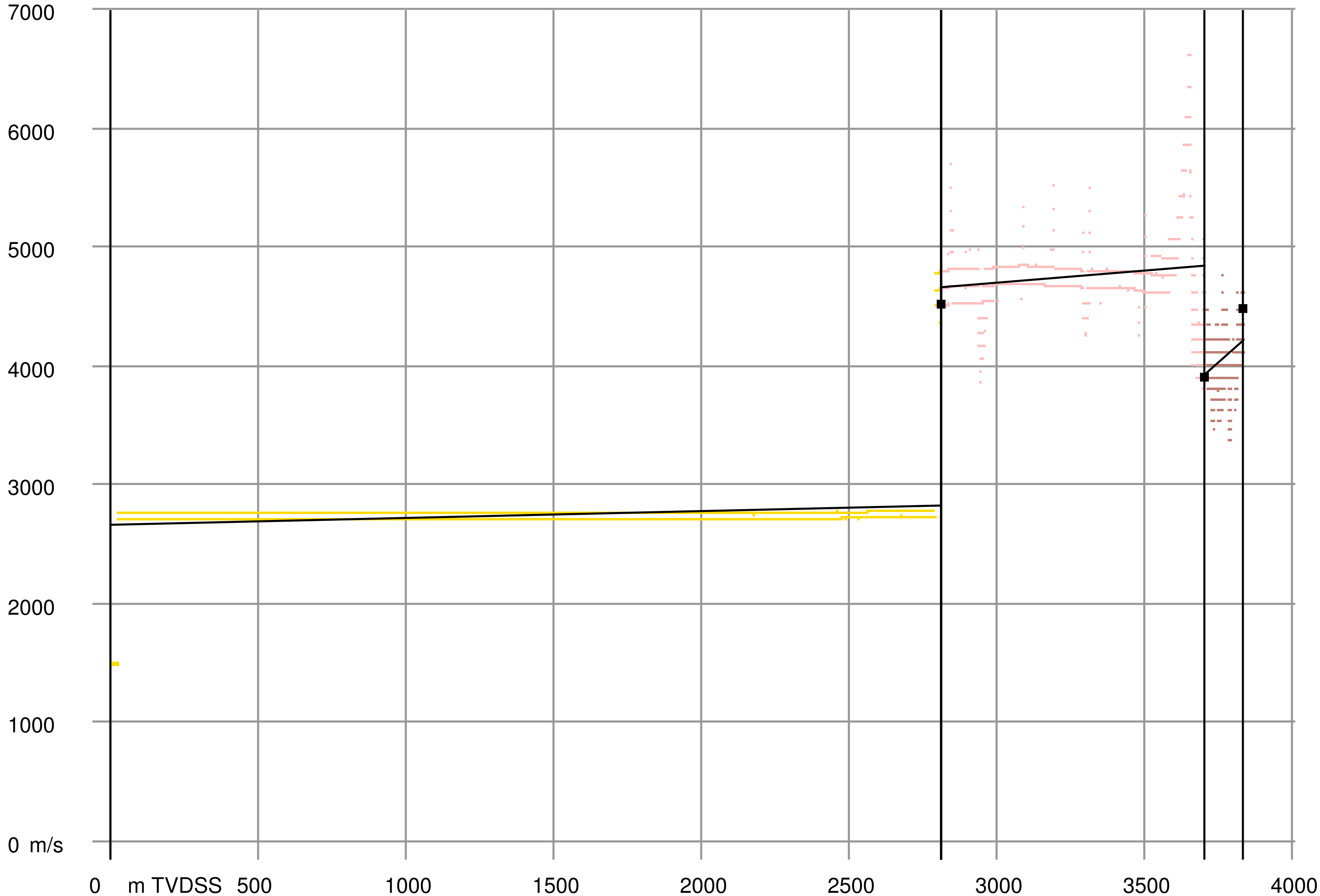

Calibrated instantaneous velocities and linearisation per layer at borehole: L10-K-02

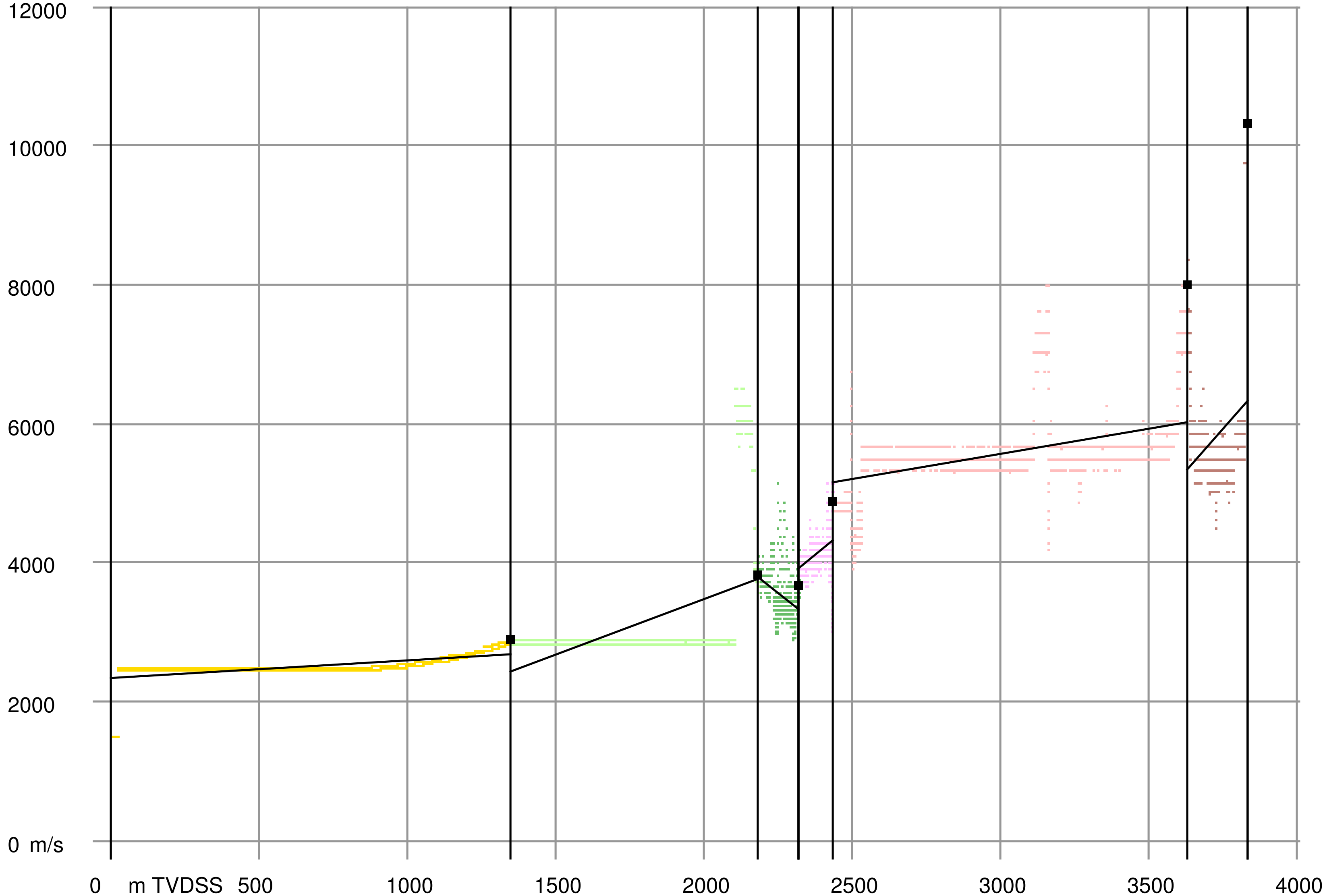

Calibrated instantaneous velocities and linearisation per layer at borehole: L10-L-02

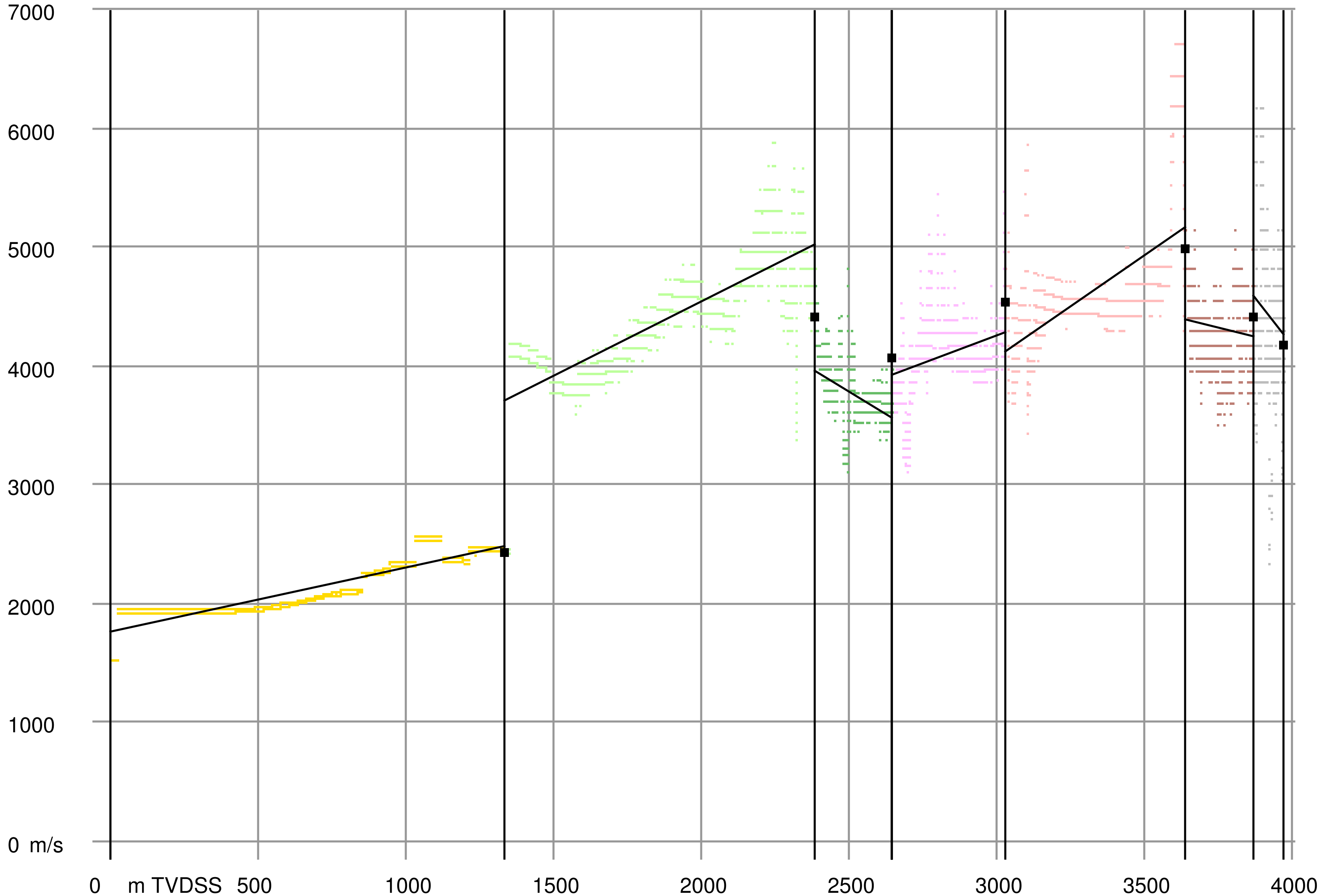

Calibrated instantaneous velocities and linearisation per layer at borehole: L11-08

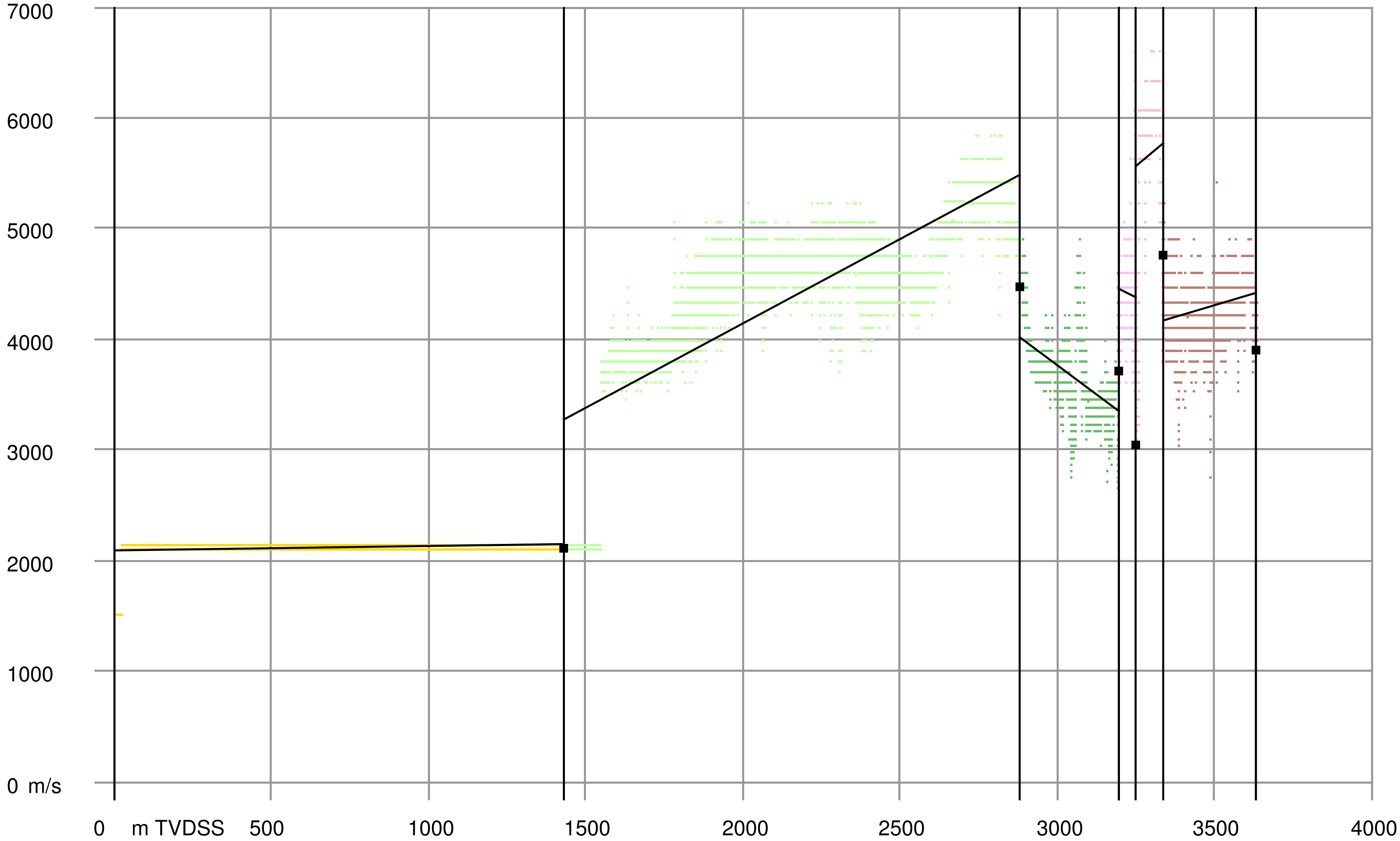

Calibrated instantaneous velocities and linearisation per layer at borehole: L13-05

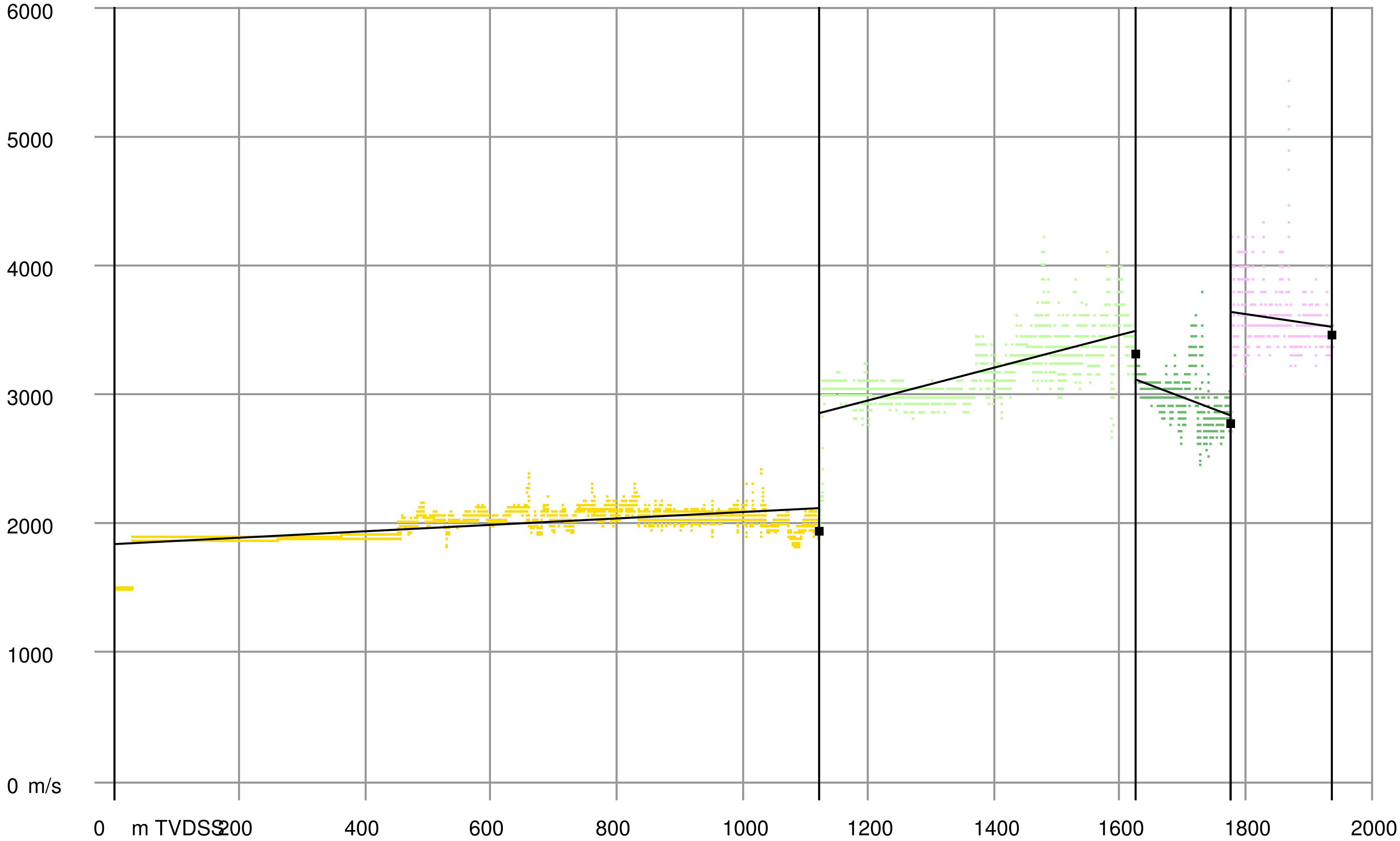

Calibrated instantaneous velocities and linearisation per layer at borehole: L13-06

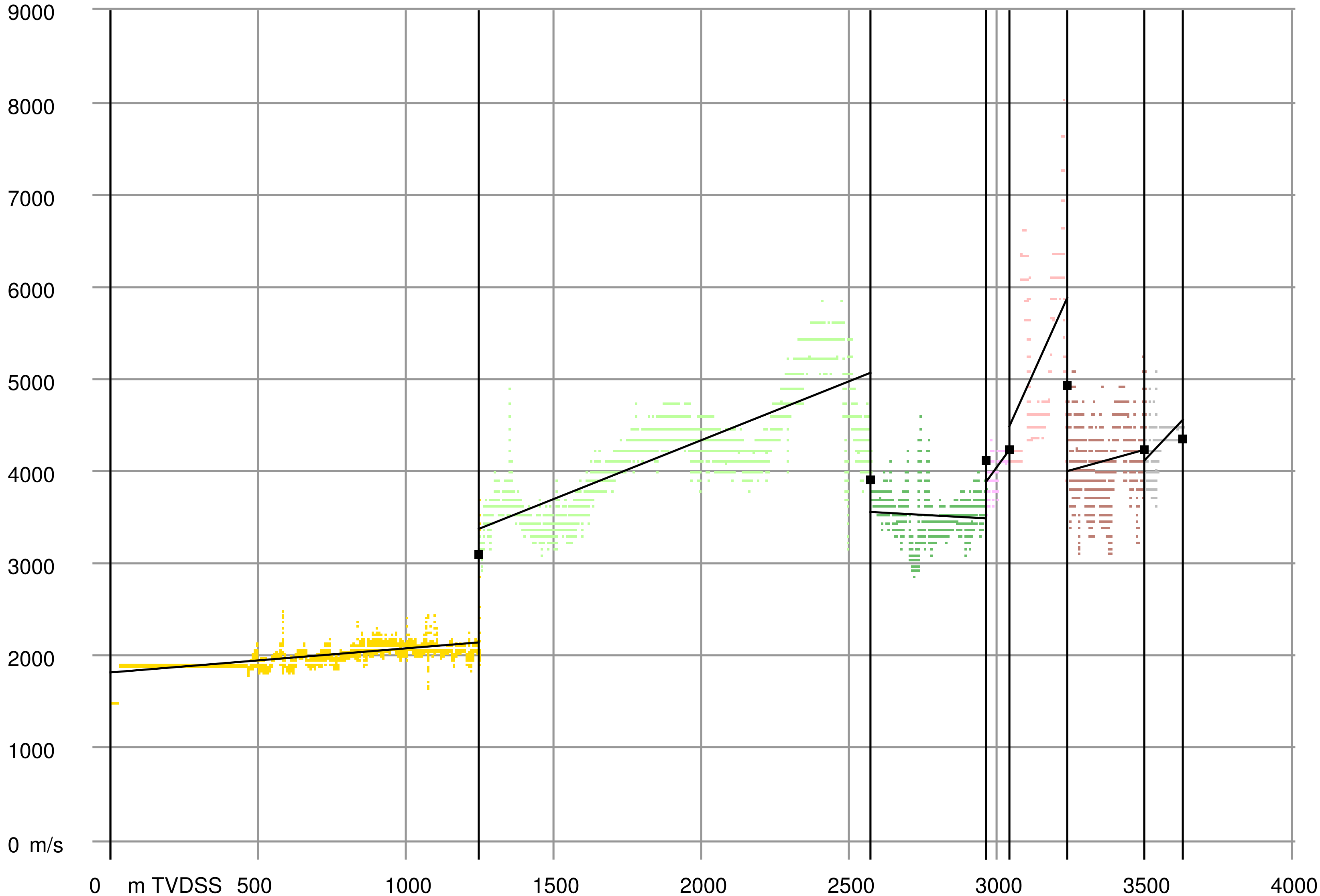

Calibrated instantaneous velocities and linearisation per layer at borehole: L13-FD-101

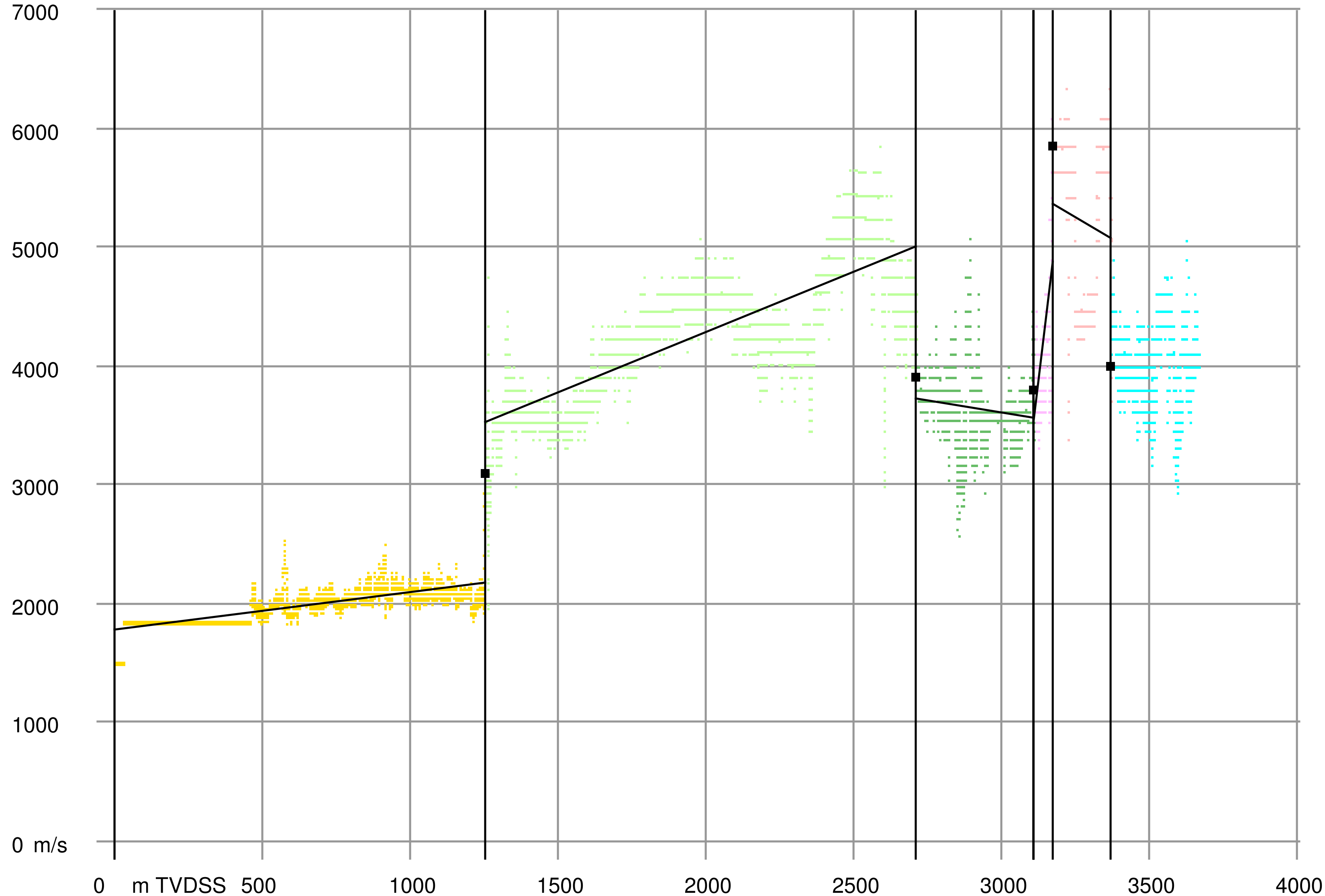

Calibrated instantaneous velocities and linearisation per layer at borehole: L14-05

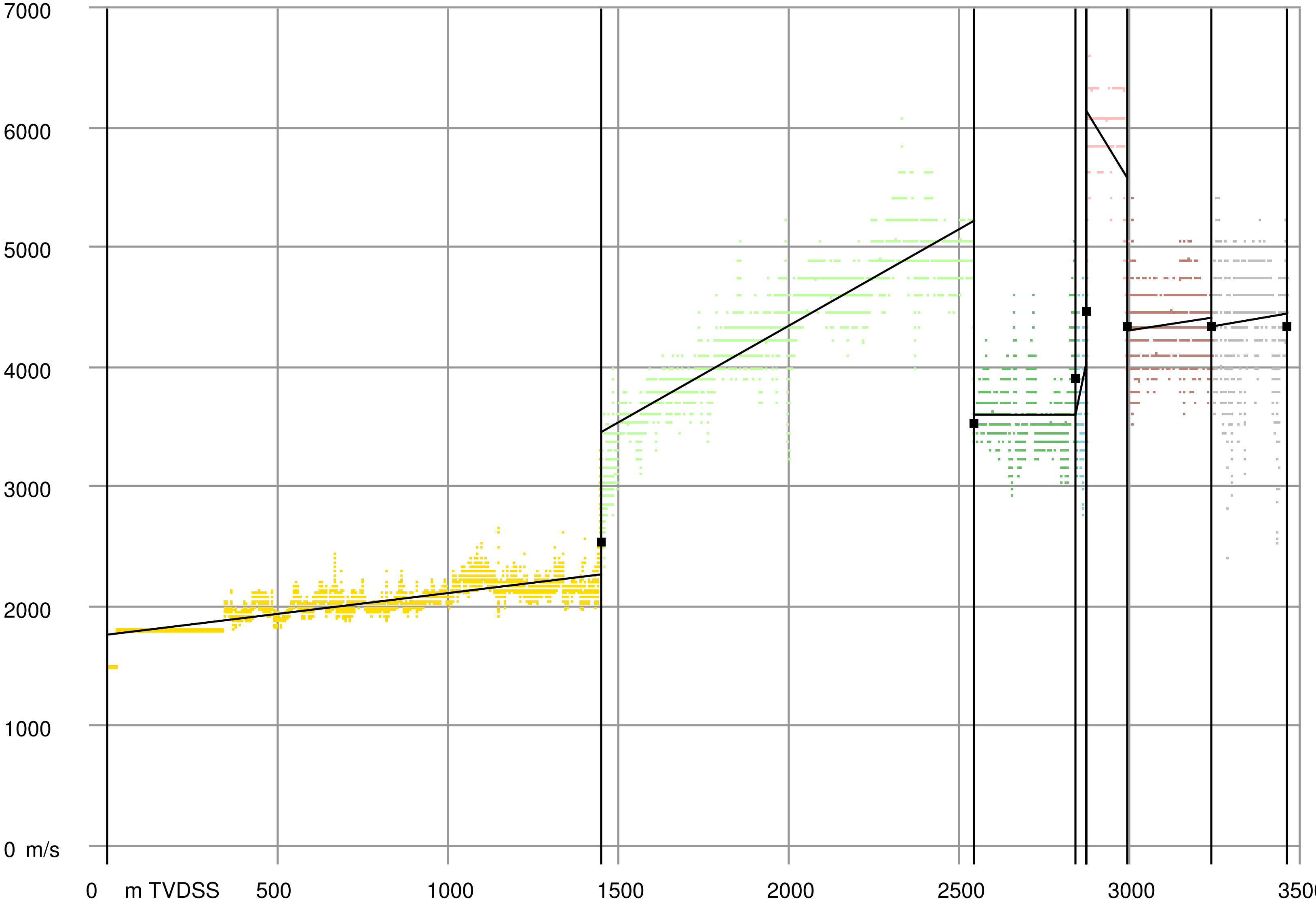

Calibrated instantaneous velocities and linearisation per layer at borehole: L16-LOG-04-S

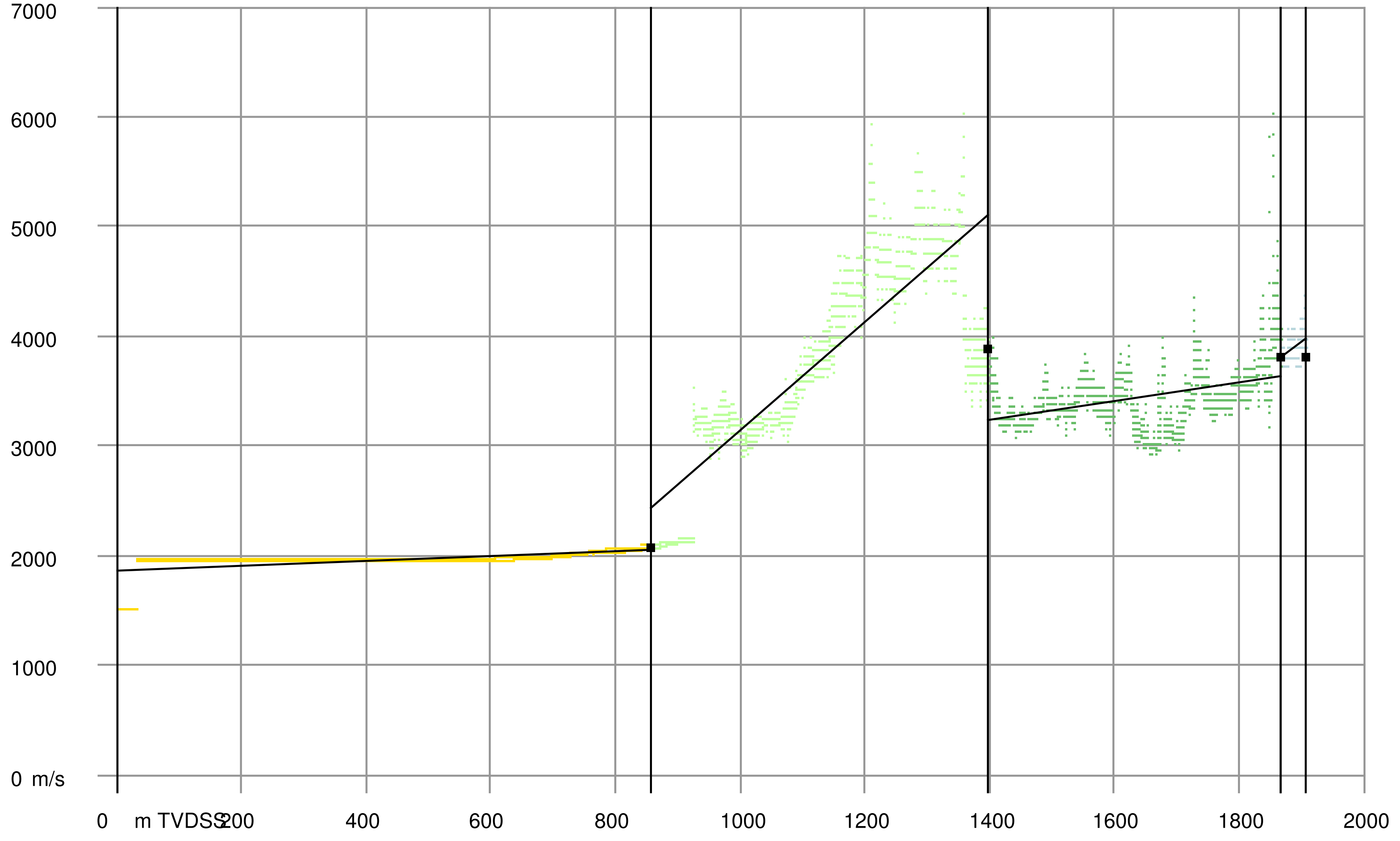

Calibrated instantaneous velocities and linearisation per layer at borehole: M04-01

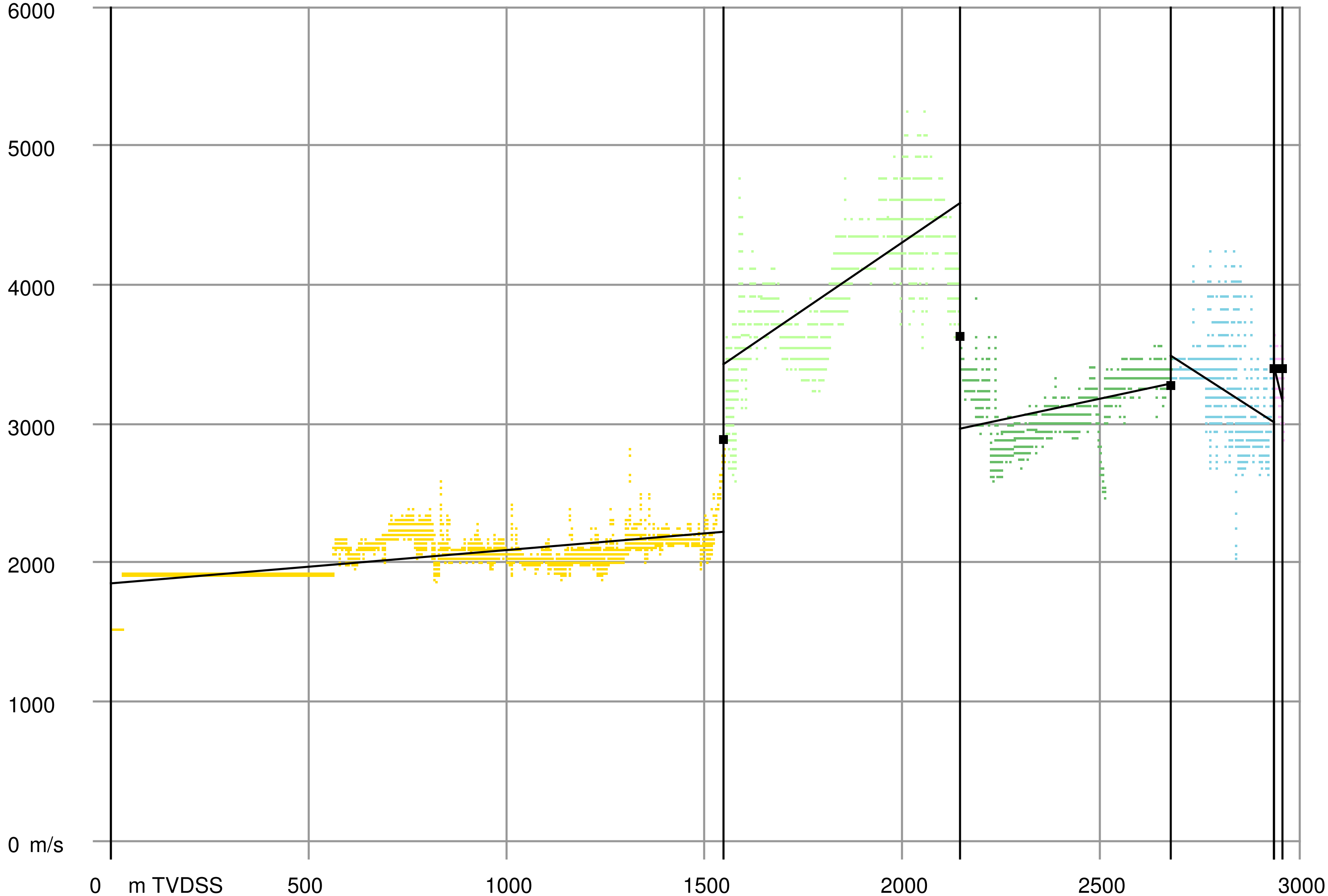

Calibrated instantaneous velocities and linearisation per layer at borehole: M04-02

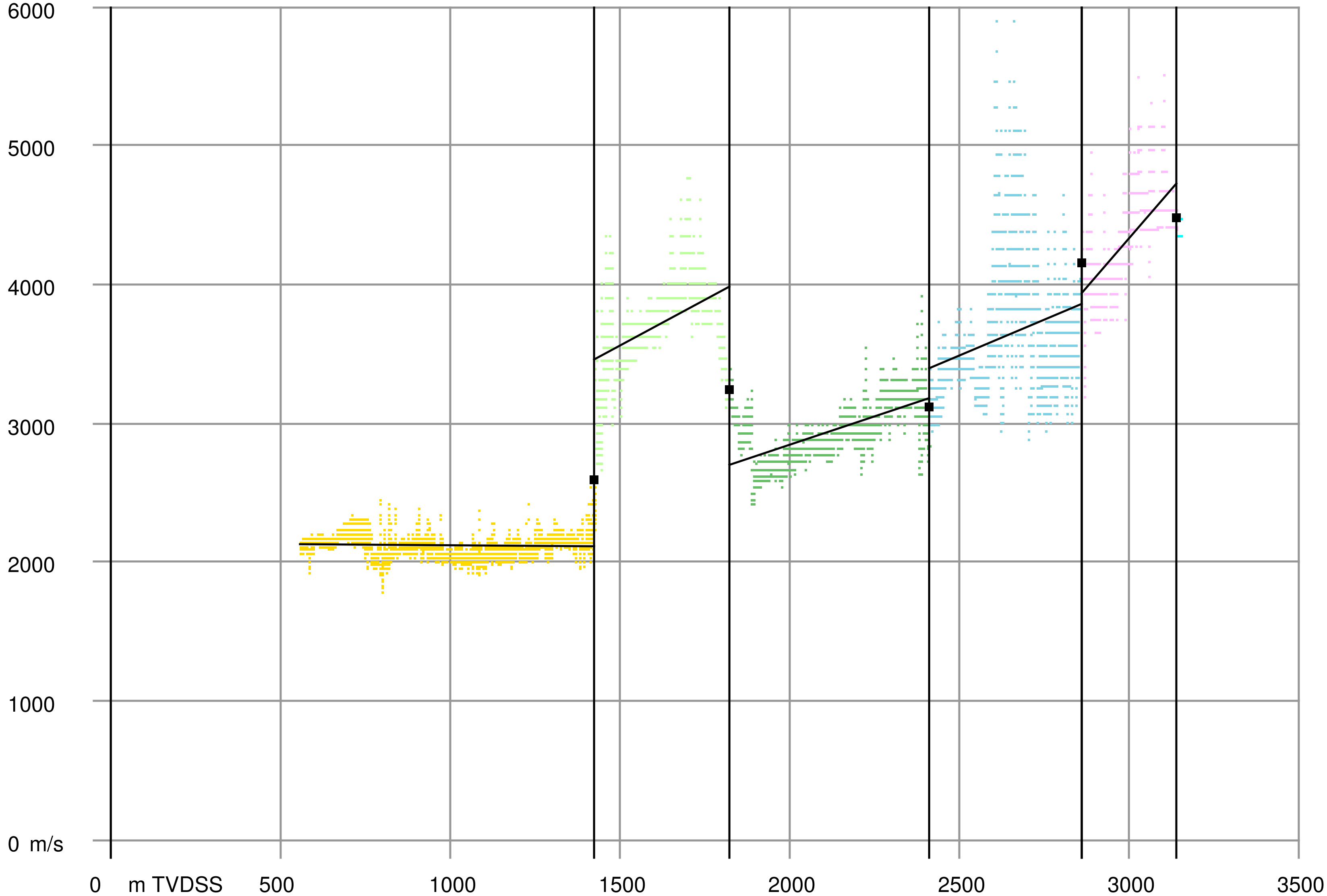

Calibrated instantaneous velocities and linearisation per layer at borehole: M10-03

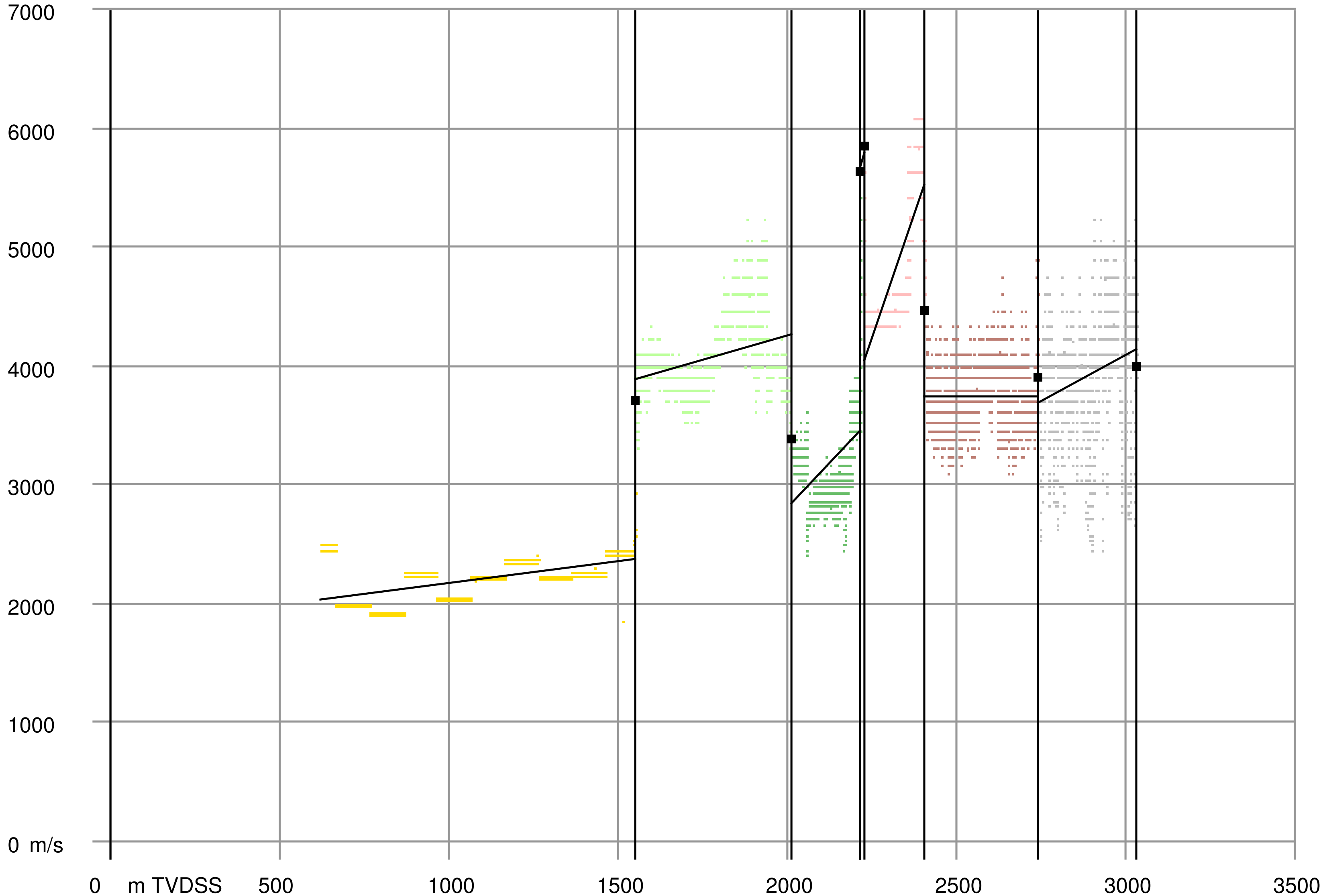

Calibrated instantaneous velocities and linearisation per layer at borehole: M10-04

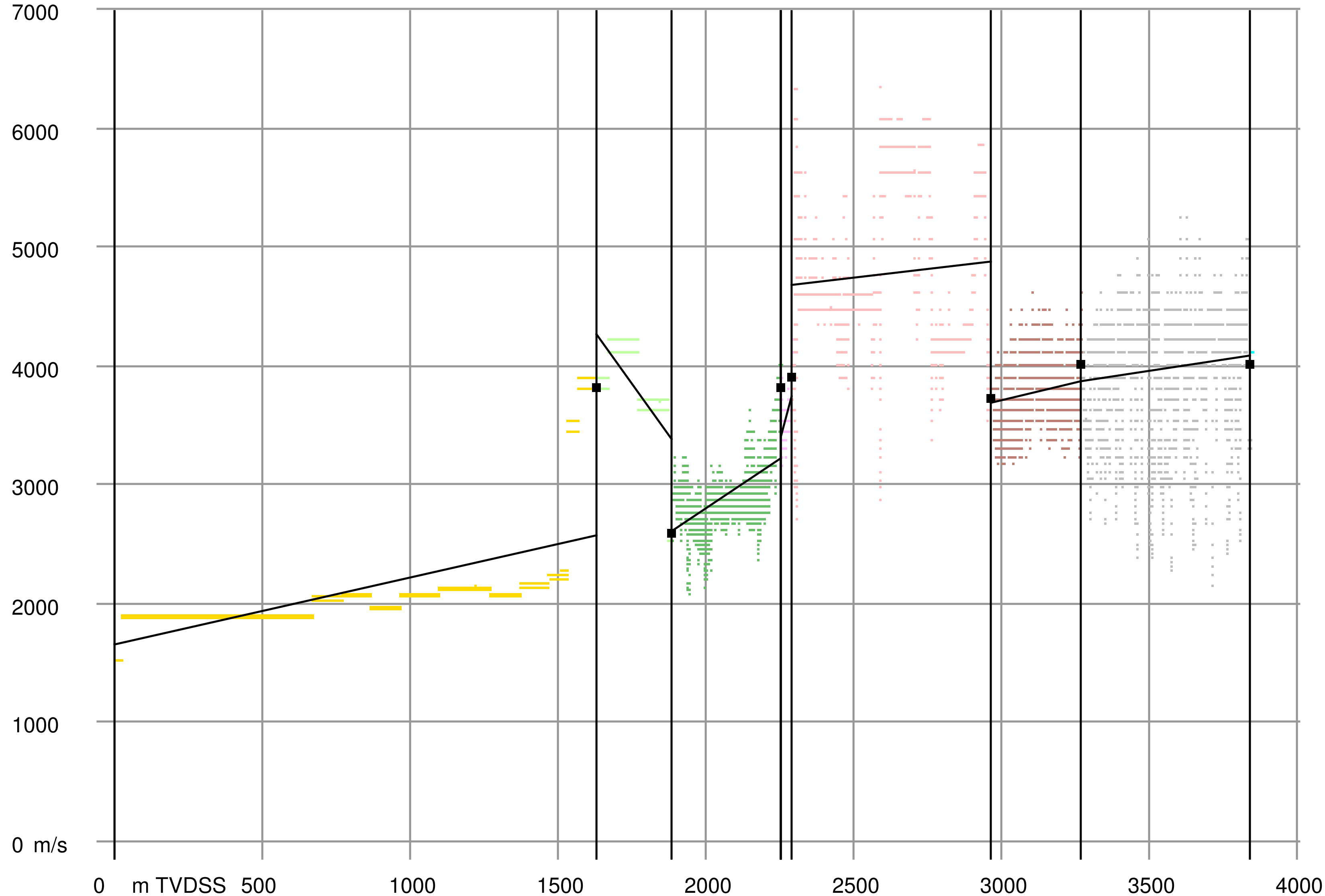

Calibrated instantaneous velocities and linearisation per layer at borehole: MRK-01

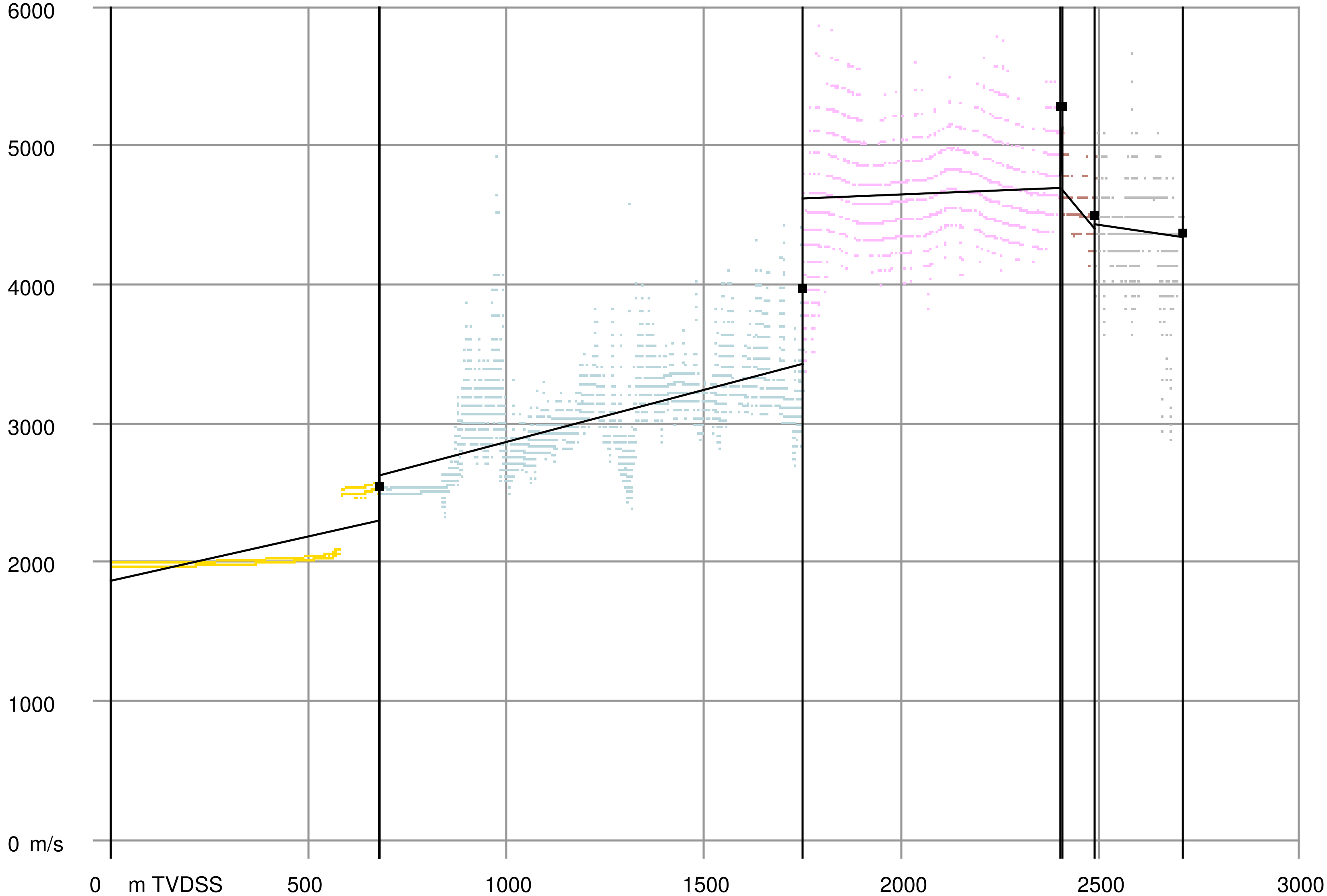

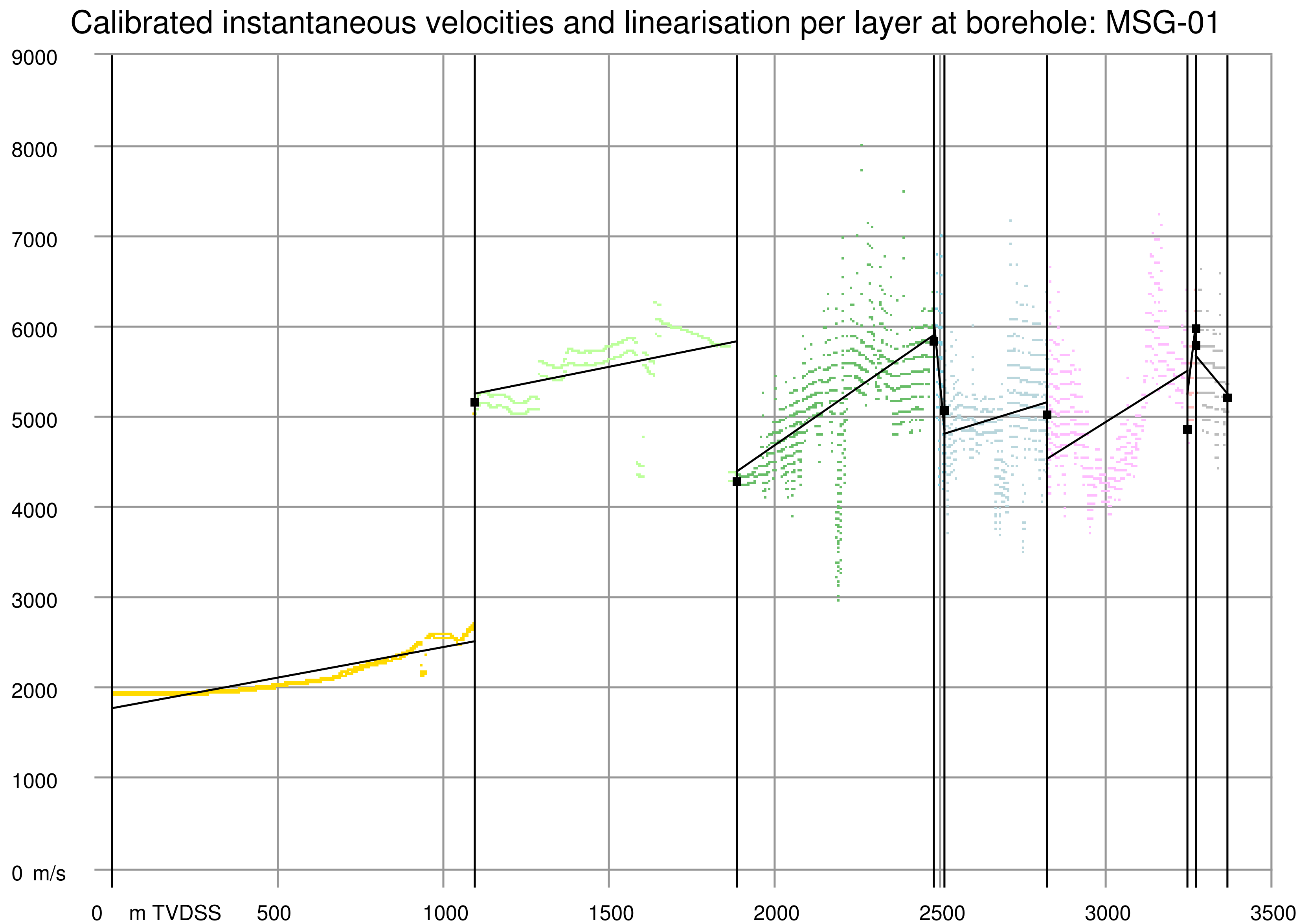
Calibrated instantaneous velocities and linearisation per layer at borehole: MSG-01
9000
8000
7000
6000
5000
4000
3000
2000
1000
0 m/s
0
m TVDSS
500
1000
1500
2000
2500
3000
3500

Calibrated instantaneous velocities and linearisation per layer at borehole: NRZ-01

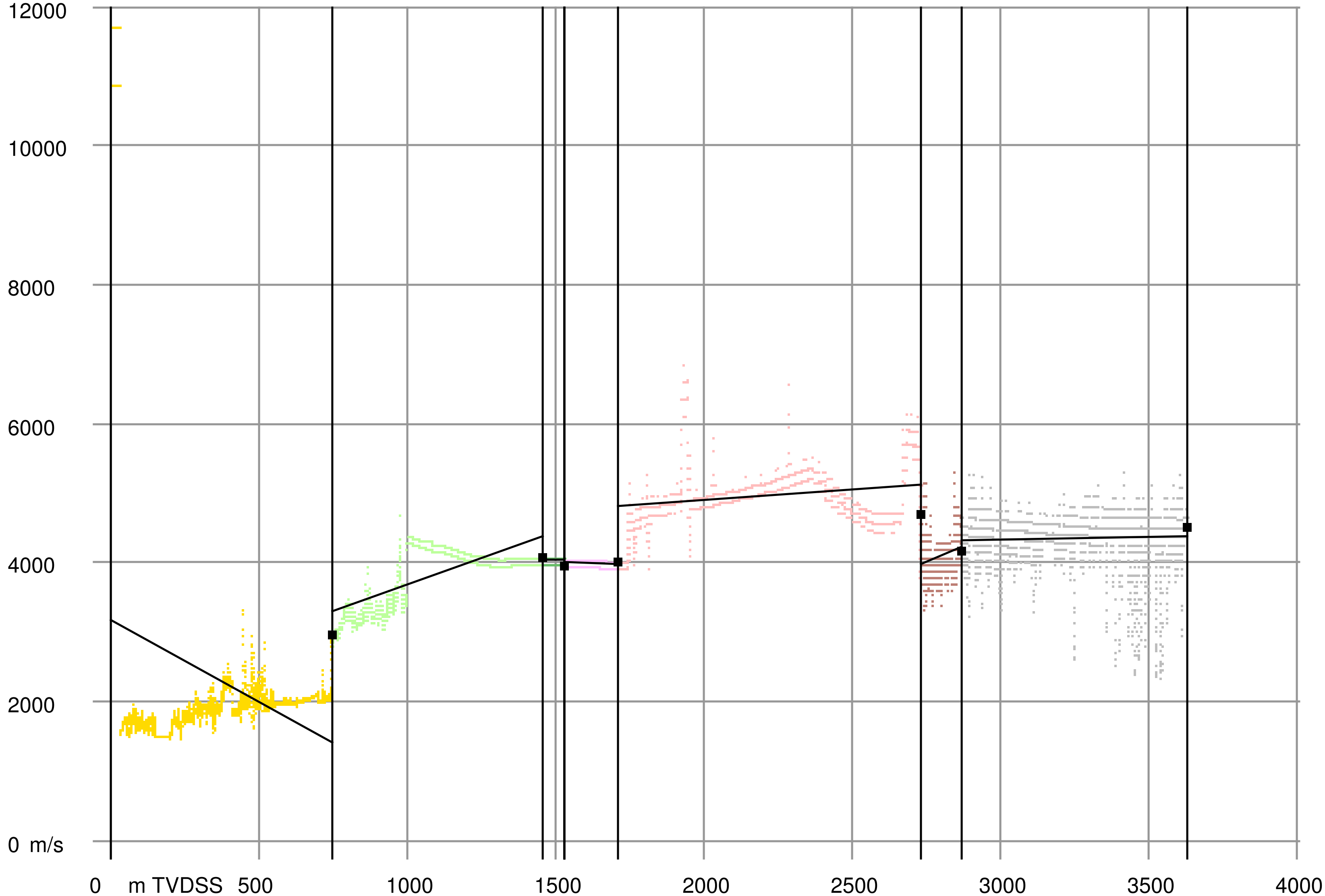

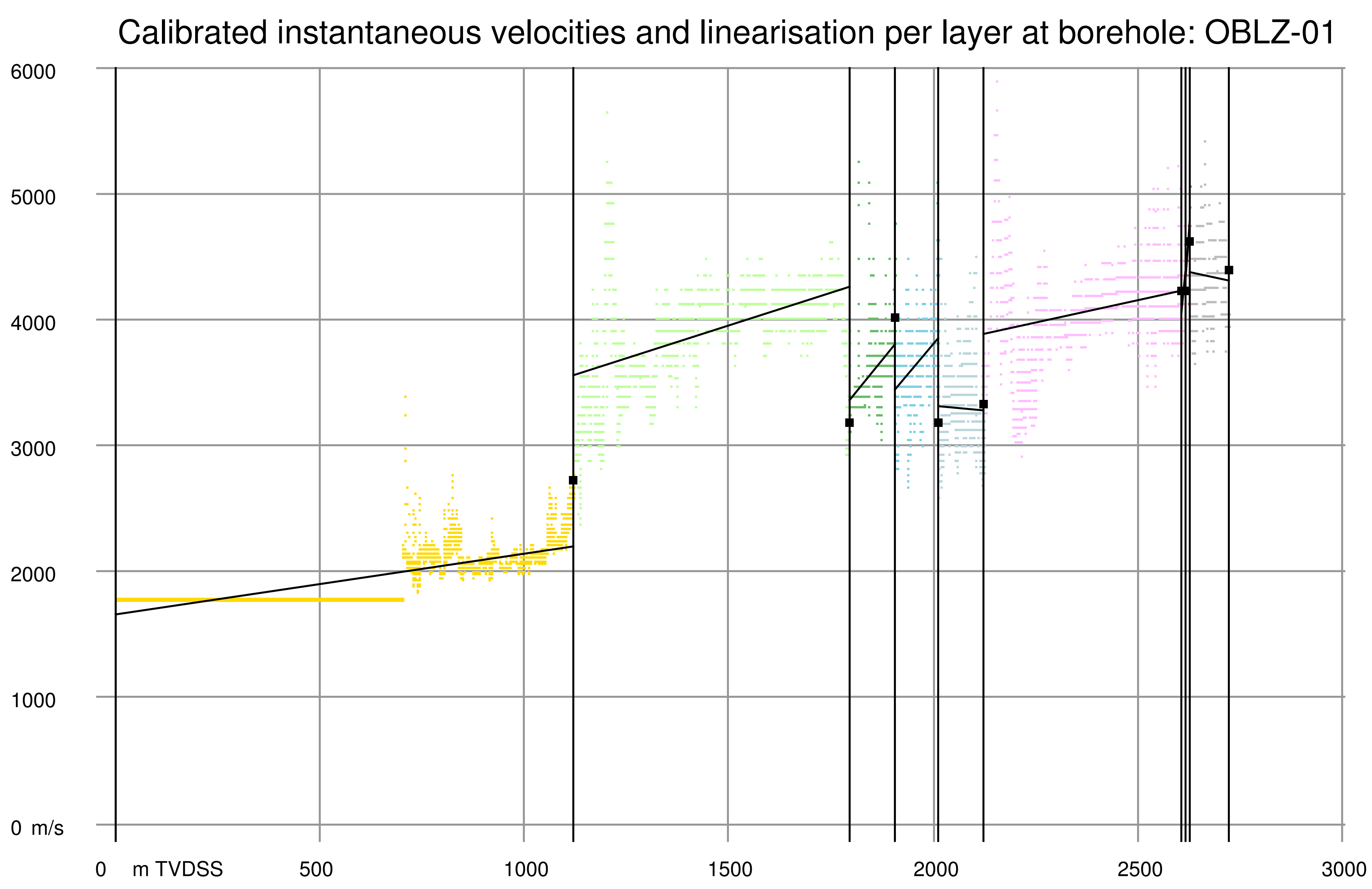
Calibrated instantaneous velocities and linearisation per layer at borehole: OBLZ-01
6000
5000
4000
3000
2000
1000
0 m/s
0
m TVDSS
500
1000
1500
2000
2500
3000

Calibrated instantaneous velocities and linearisation per layer at borehole: P02-04

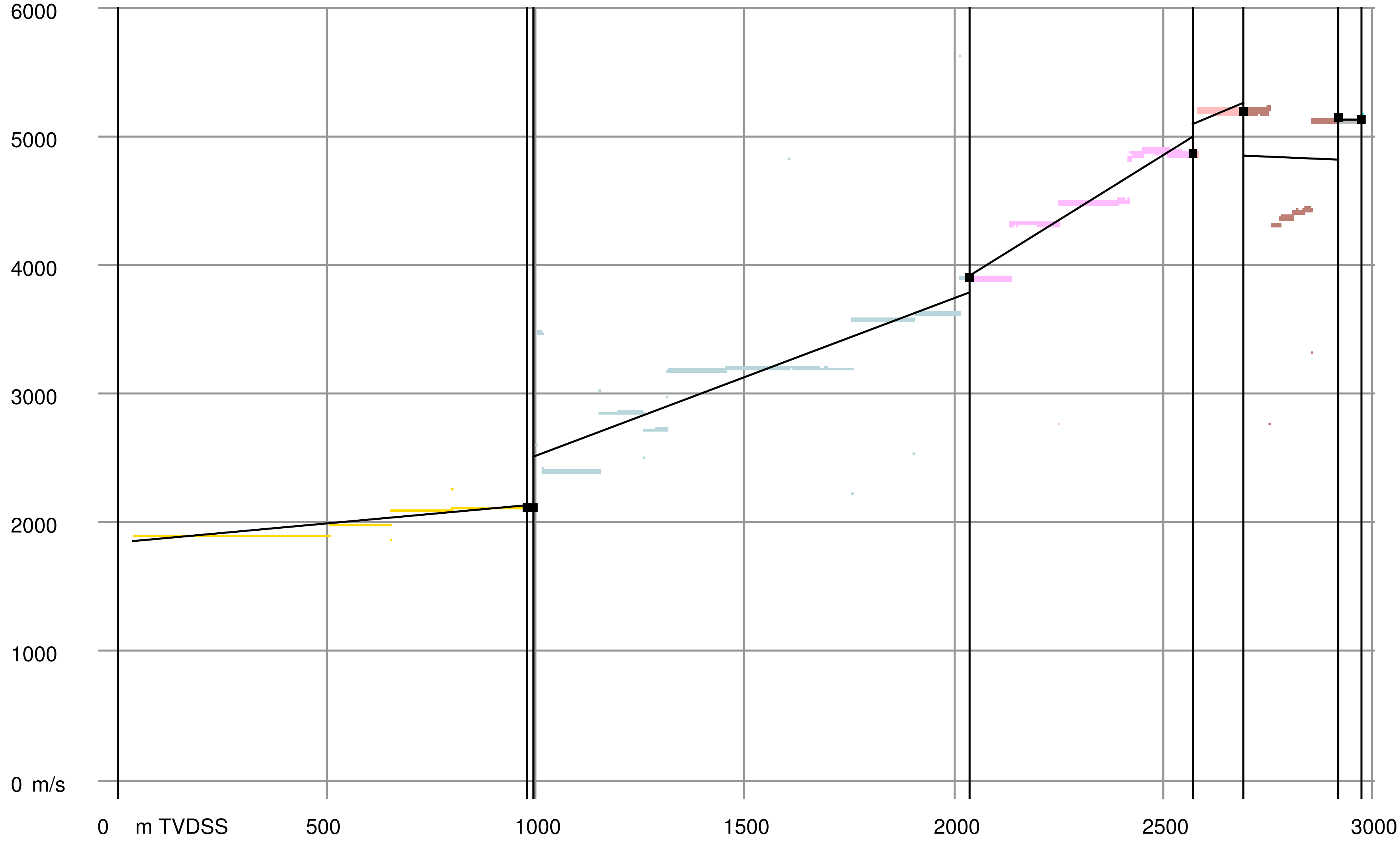

Calibrated instantaneous velocities and linearisation per layer at borehole: P02-07

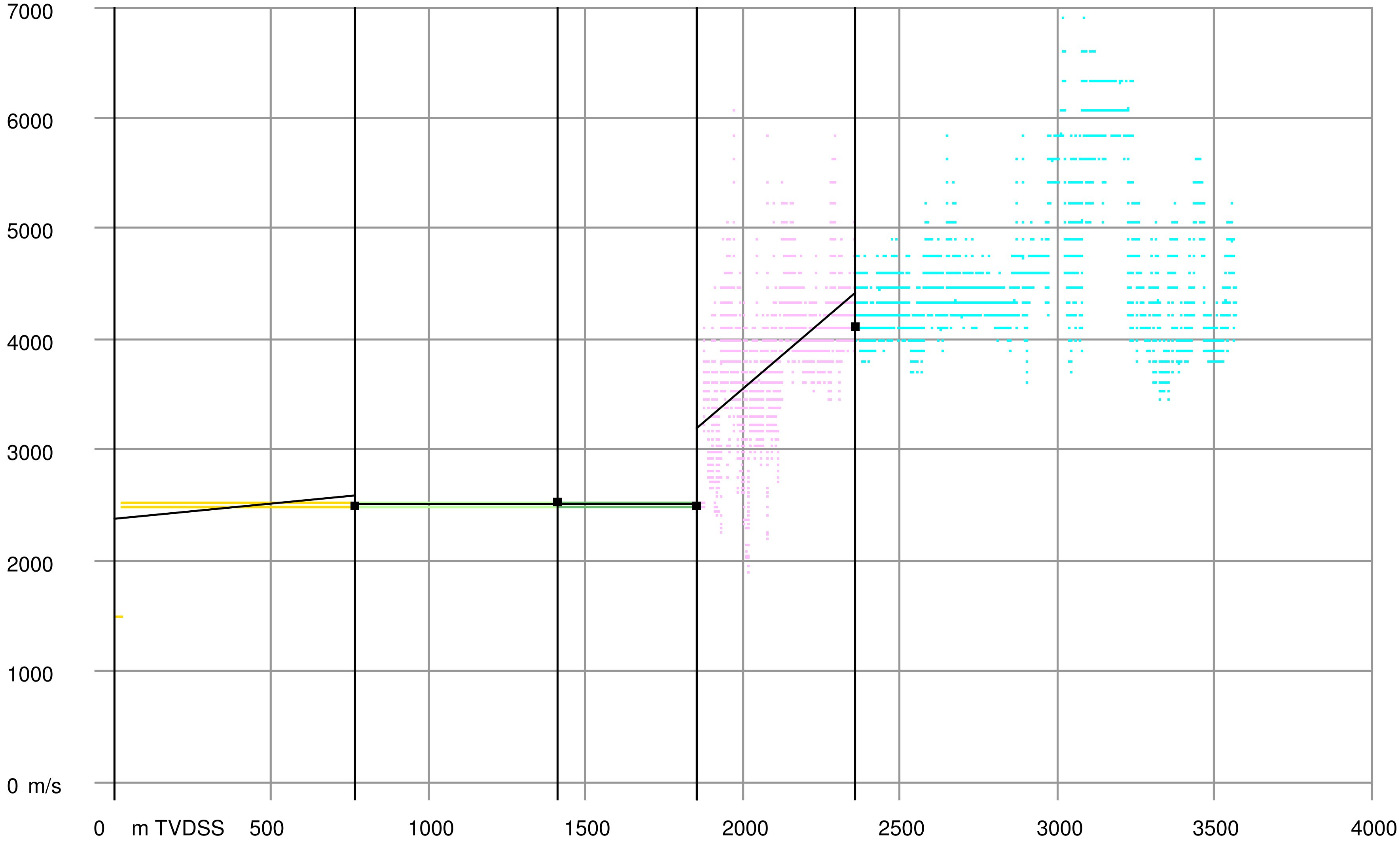

Calibrated instantaneous velocities and linearisation per layer at borehole: P05-05

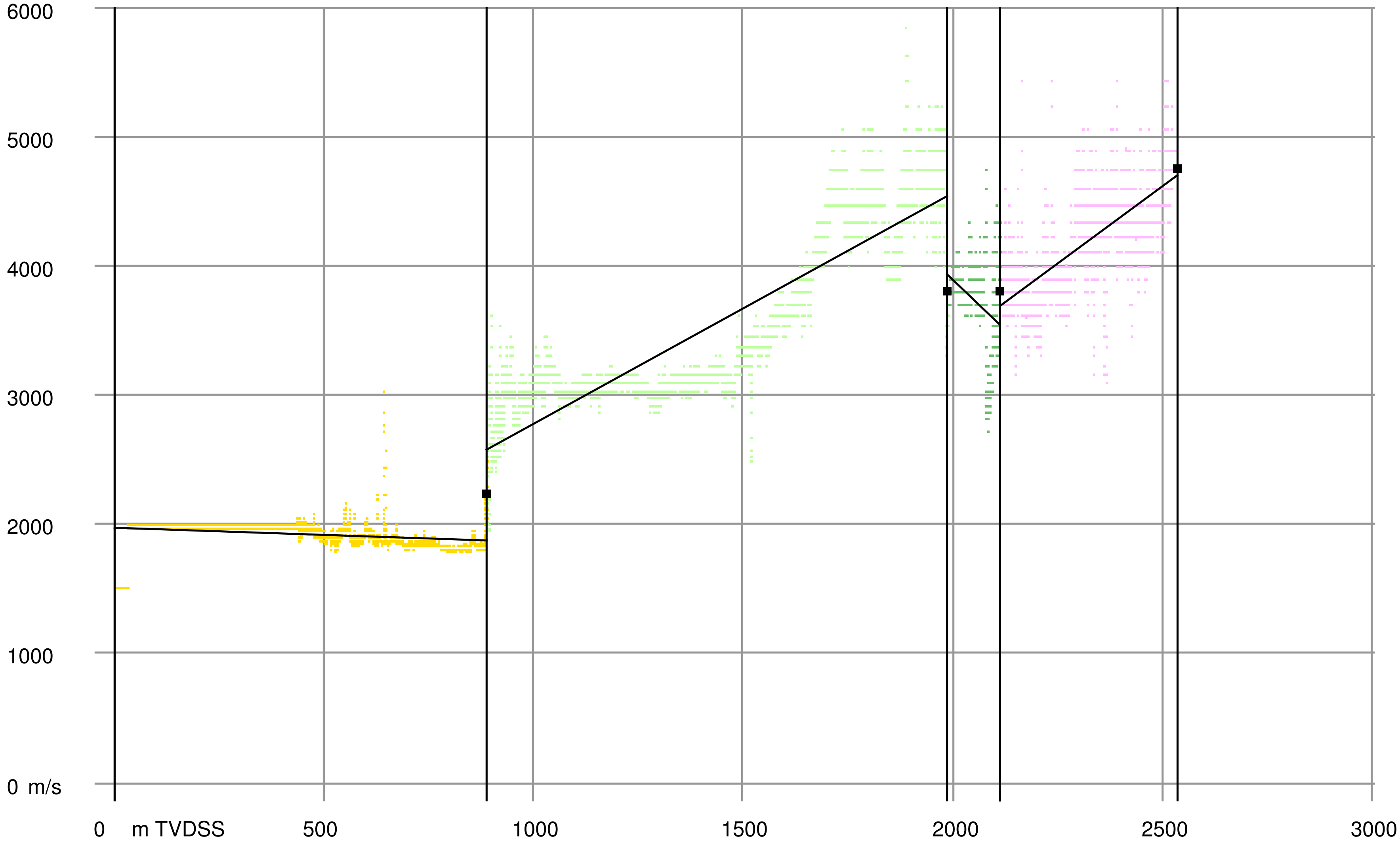

Calibrated instantaneous velocities and linearisation per layer at borehole: P06-A-01

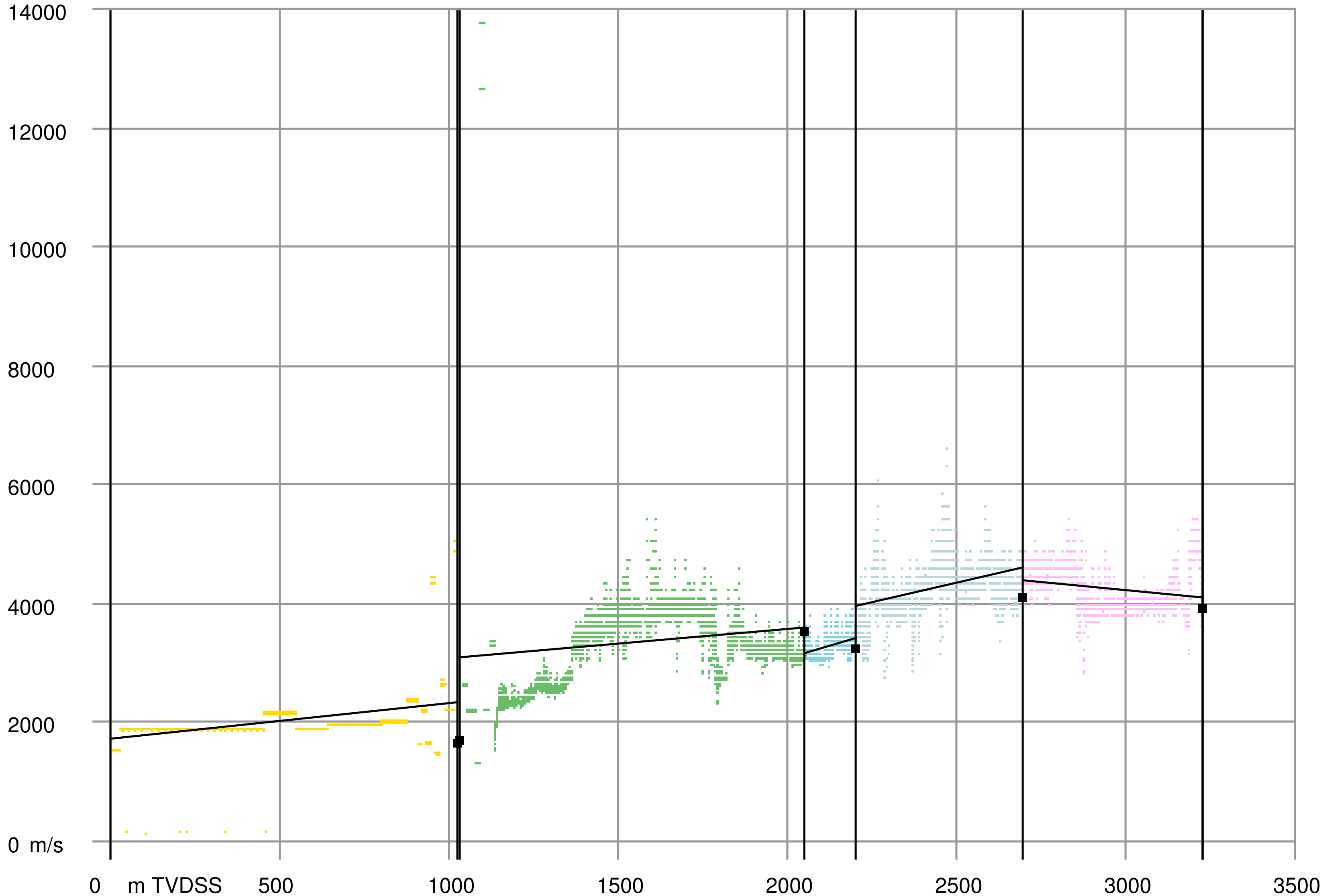

Calibrated instantaneous velocities and linearisation per layer at borehole: P06-A-02

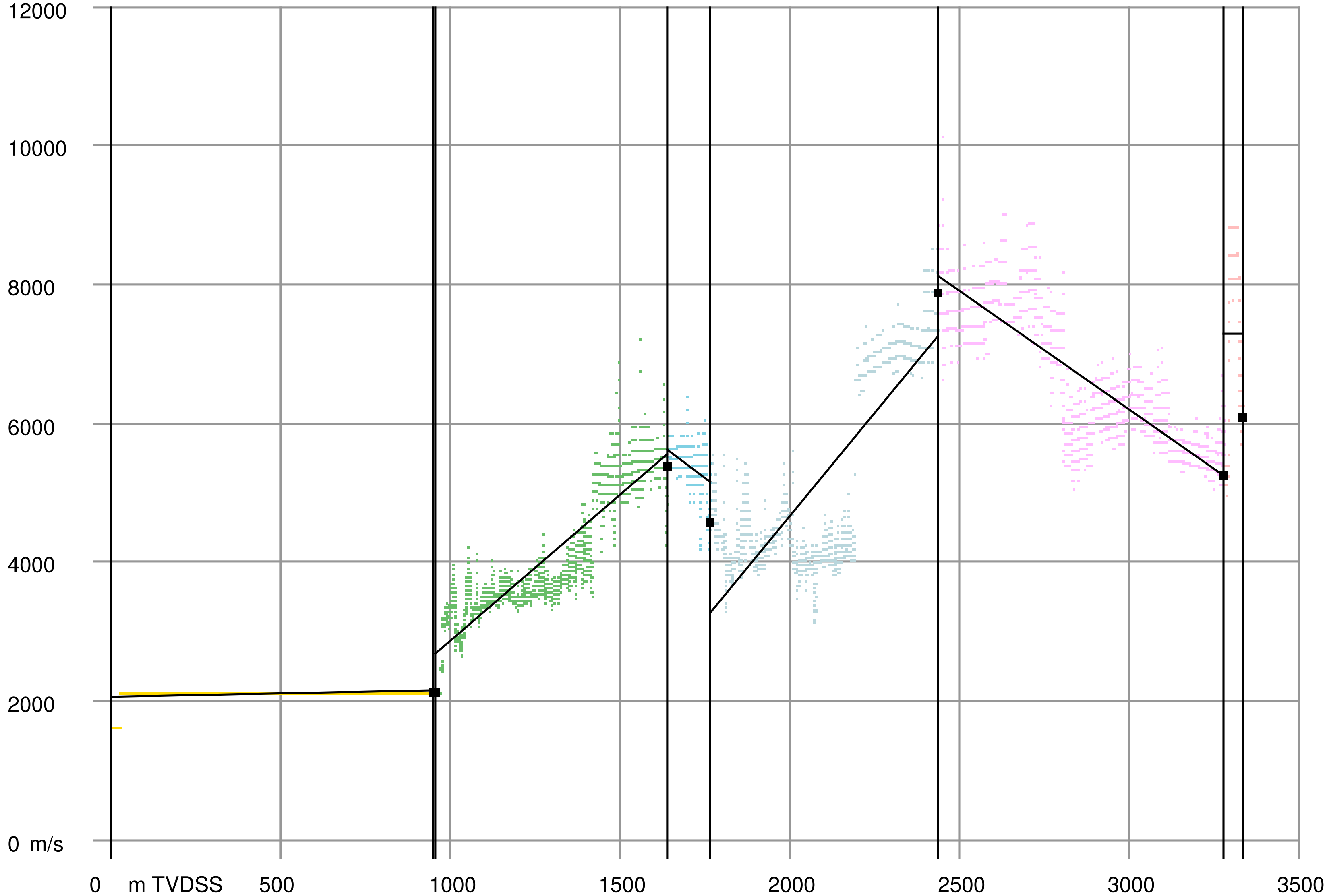

Calibrated instantaneous velocities and linearisation per layer at borehole: P06-A-03

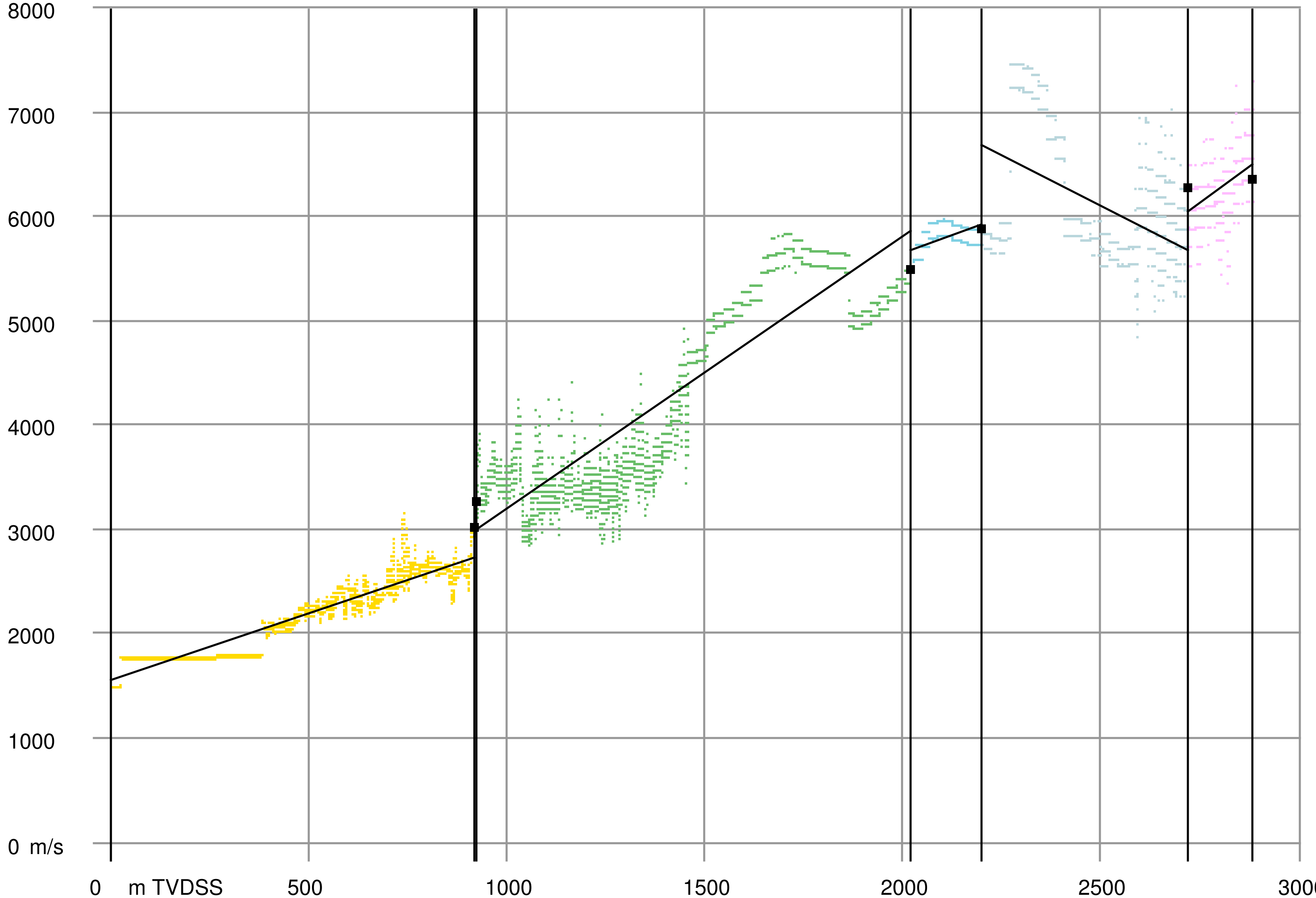

Calibrated instantaneous velocities and linearisation per layer at borehole: P06-A-04

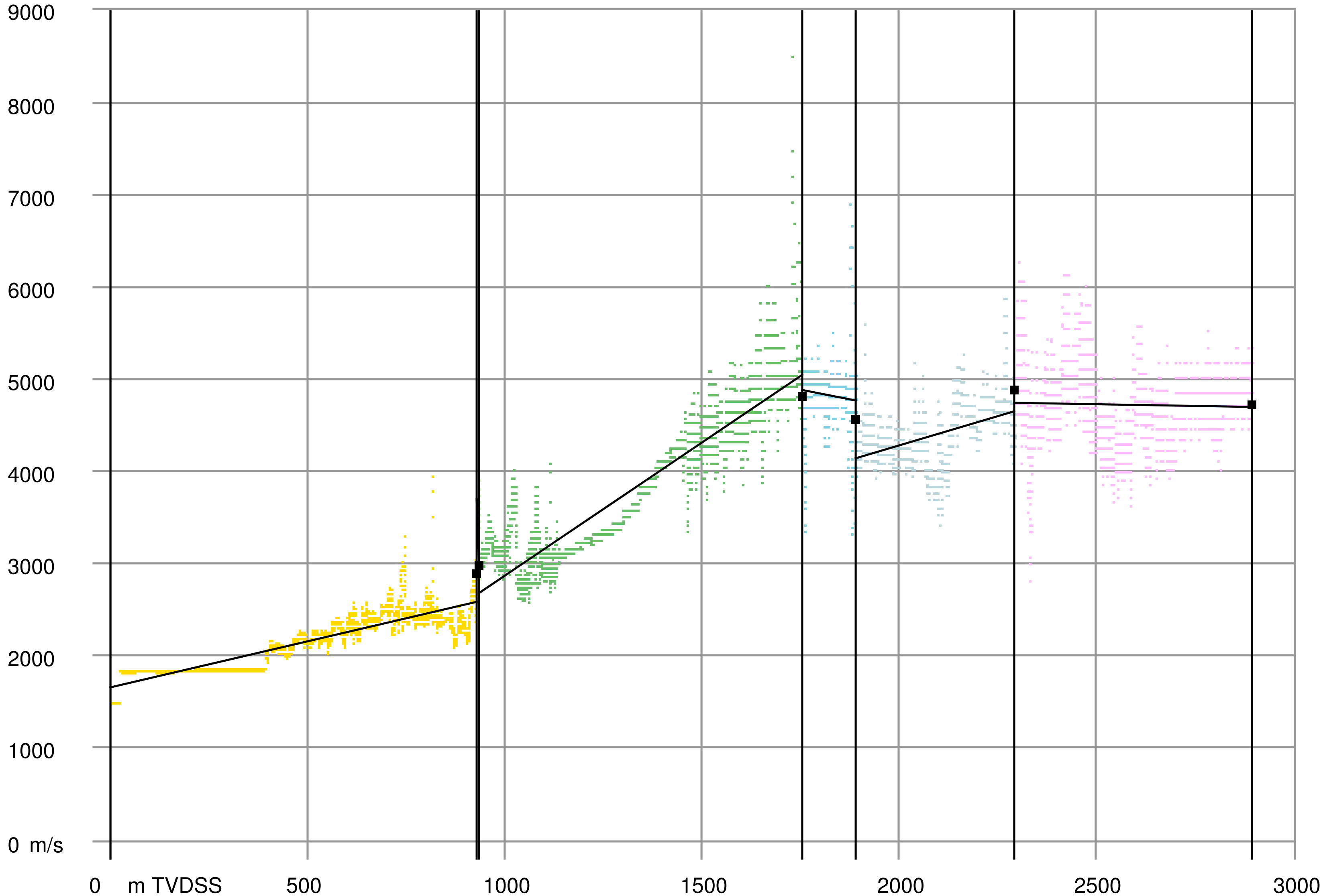

Calibrated instantaneous velocities and linearisation per layer at borehole: P06-A-06

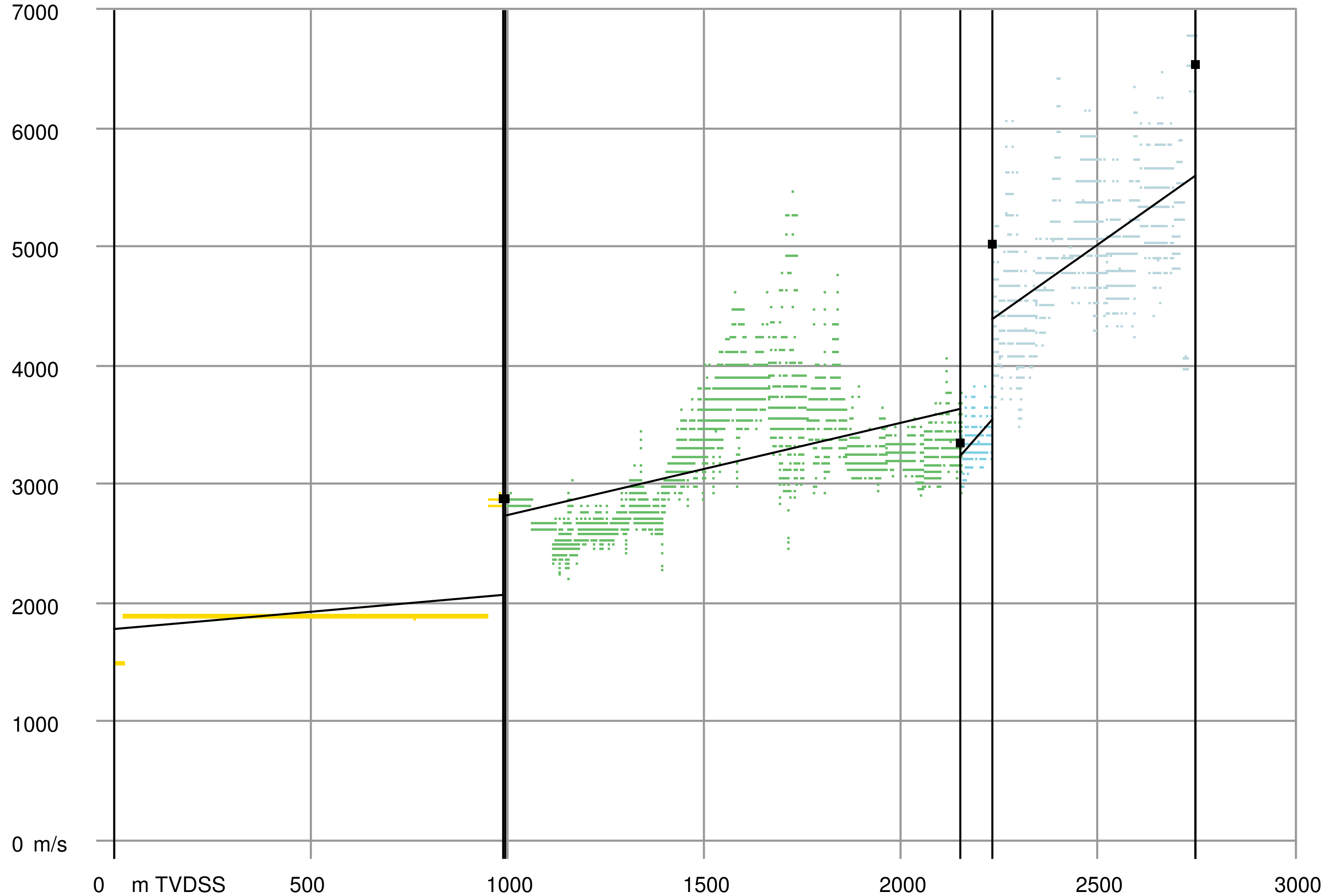

Calibrated instantaneous velocities and linearisation per layer at borehole: P06-B-01

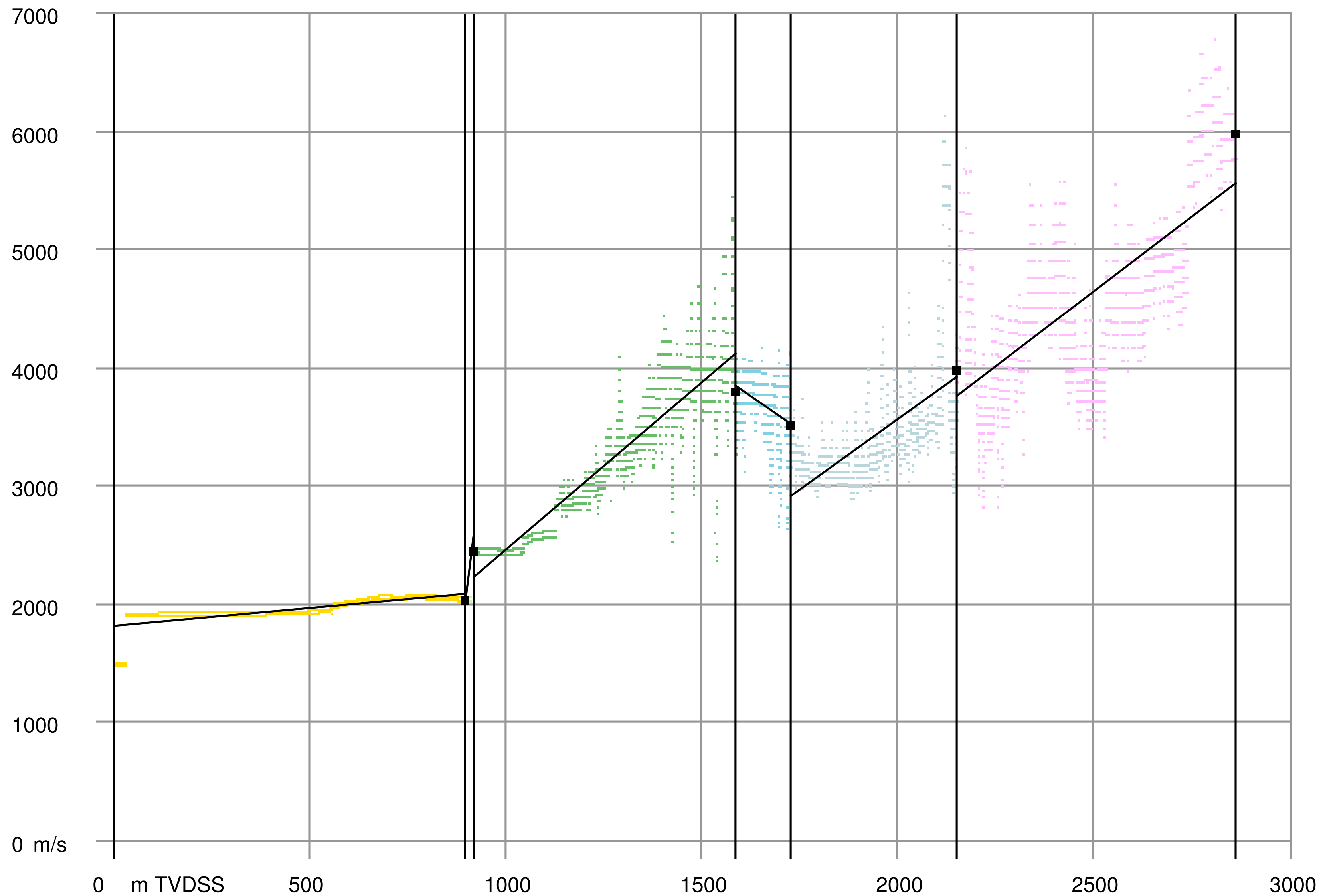

Calibrated instantaneous velocities and linearisation per layer at borehole: P06-C-01

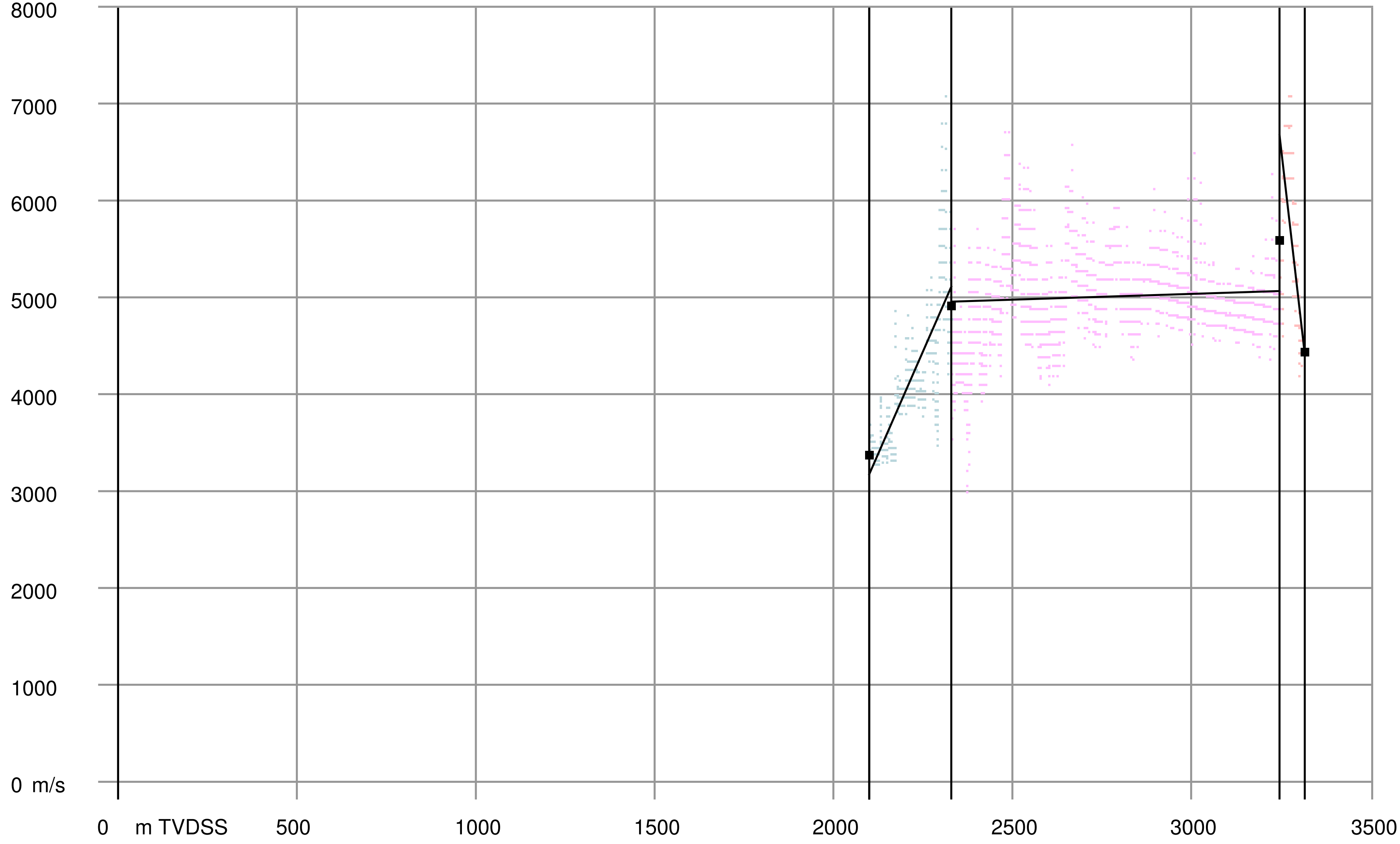

Calibrated instantaneous velocities and linearisation per layer at borehole: P06-S-01

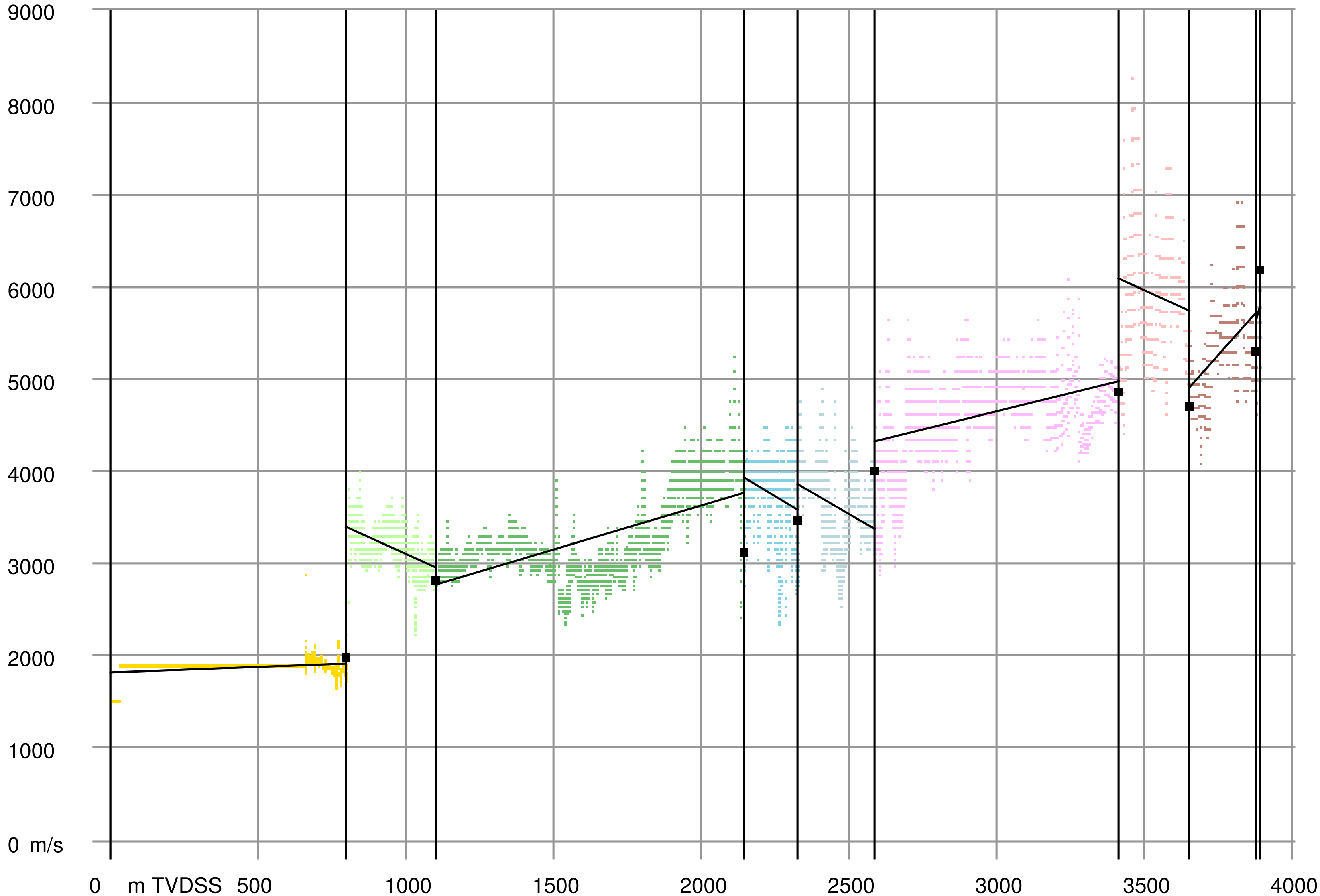

Calibrated instantaneous velocities and linearisation per layer at borehole: P08-02

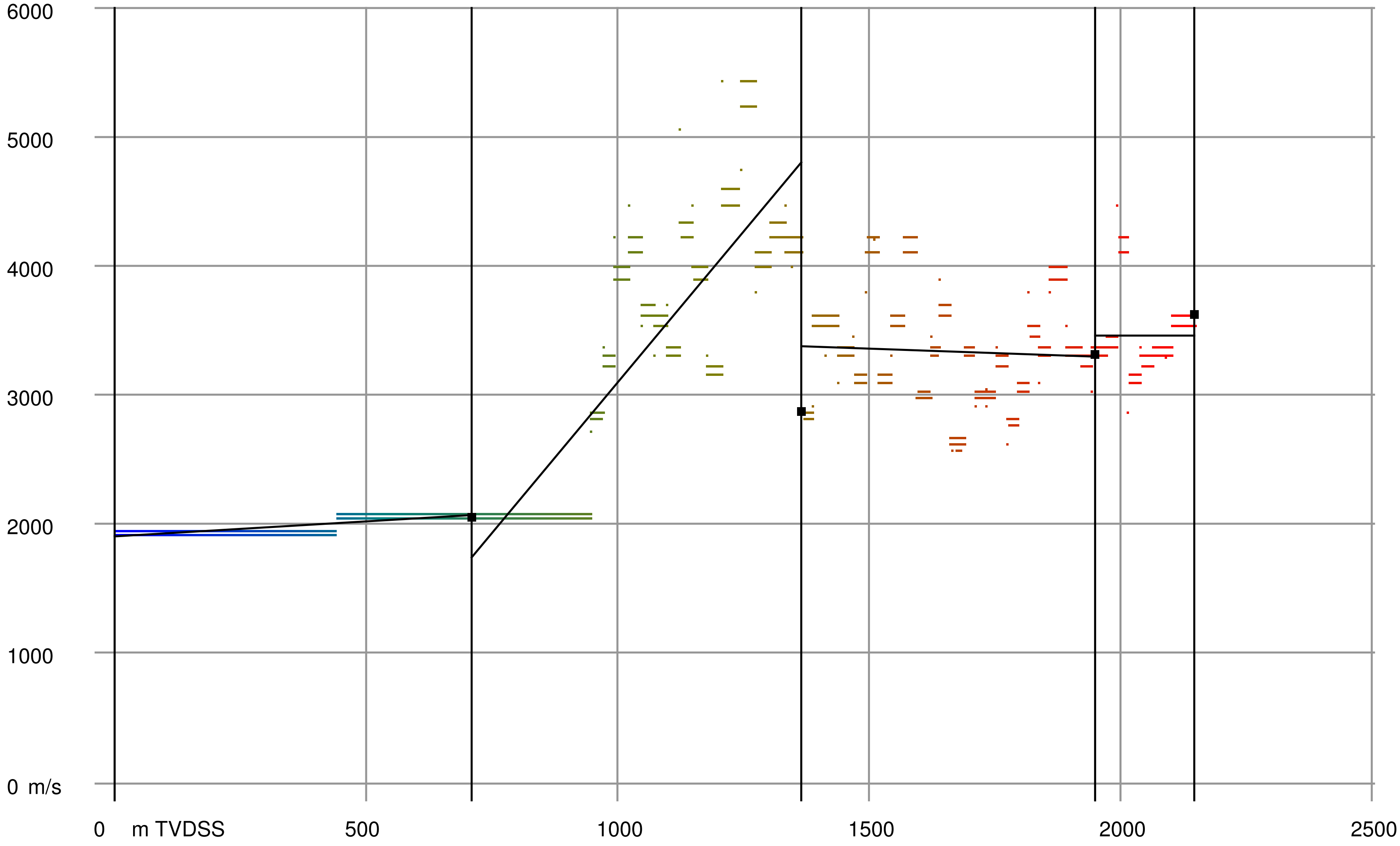

Calibrated instantaneous velocities and linearisation per layer at borehole: P08-04

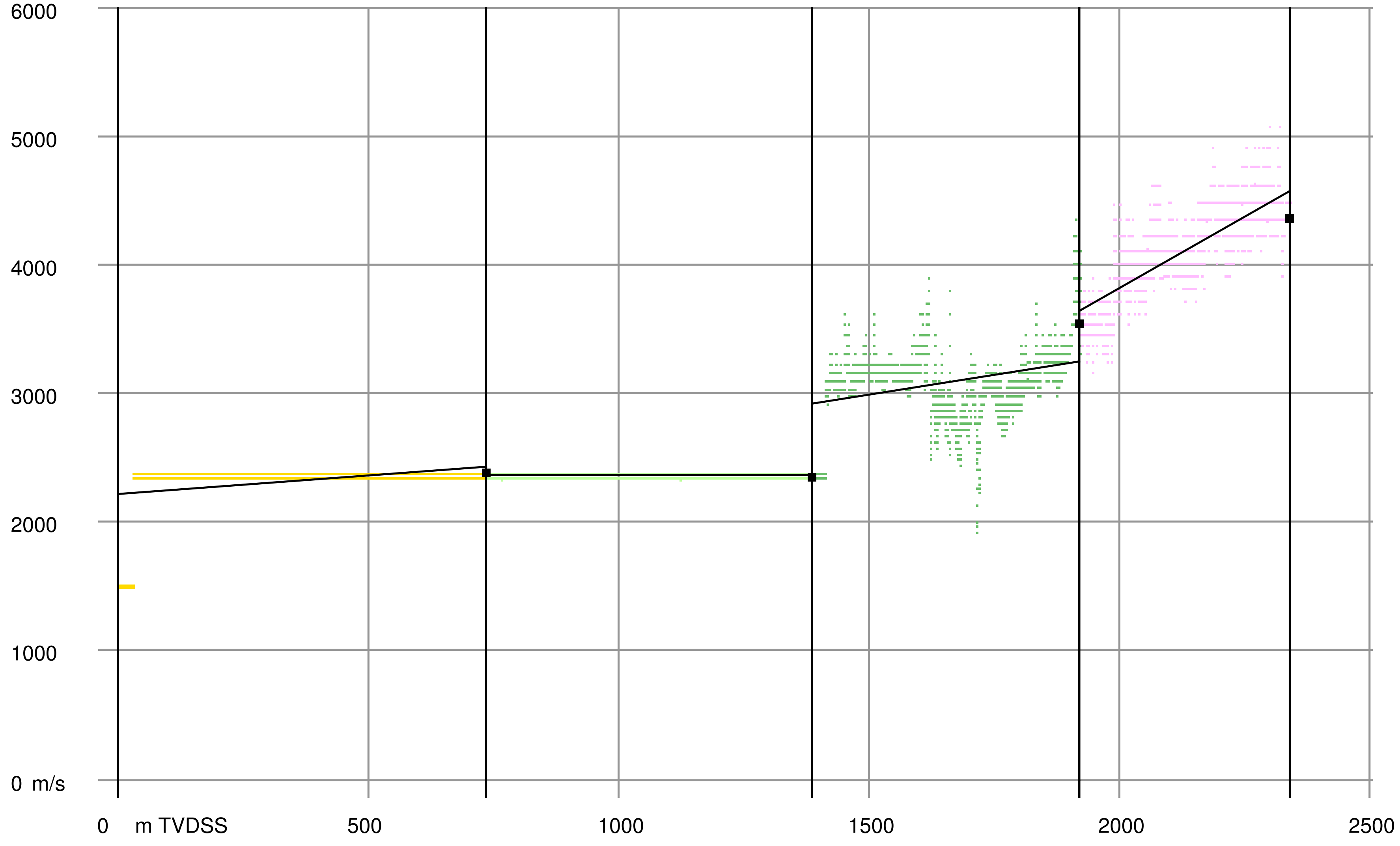

Calibrated instantaneous velocities and linearisation per layer at borehole: P08-05-S1

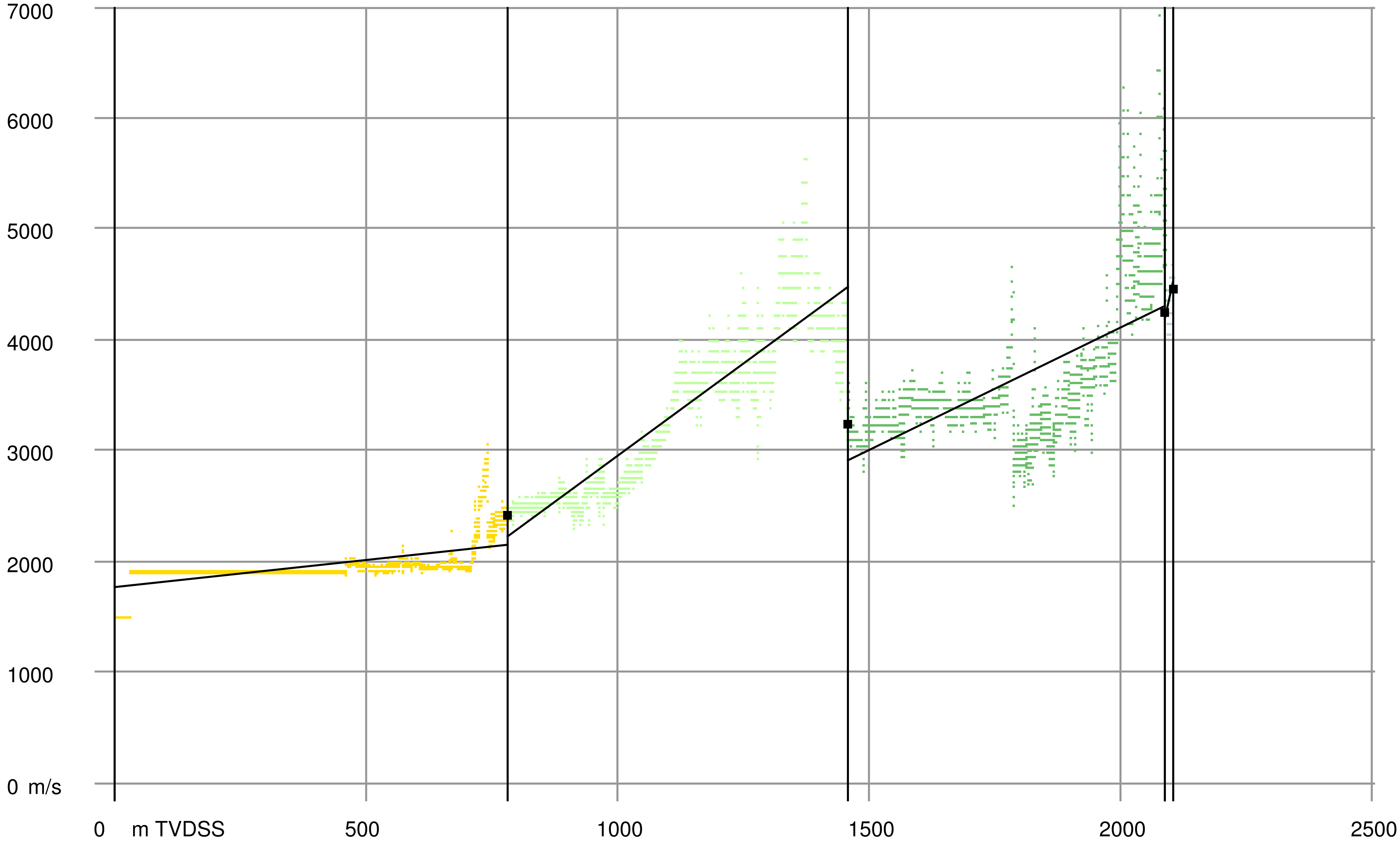

Calibrated instantaneous velocities and linearisation per layer at borehole: P09-02

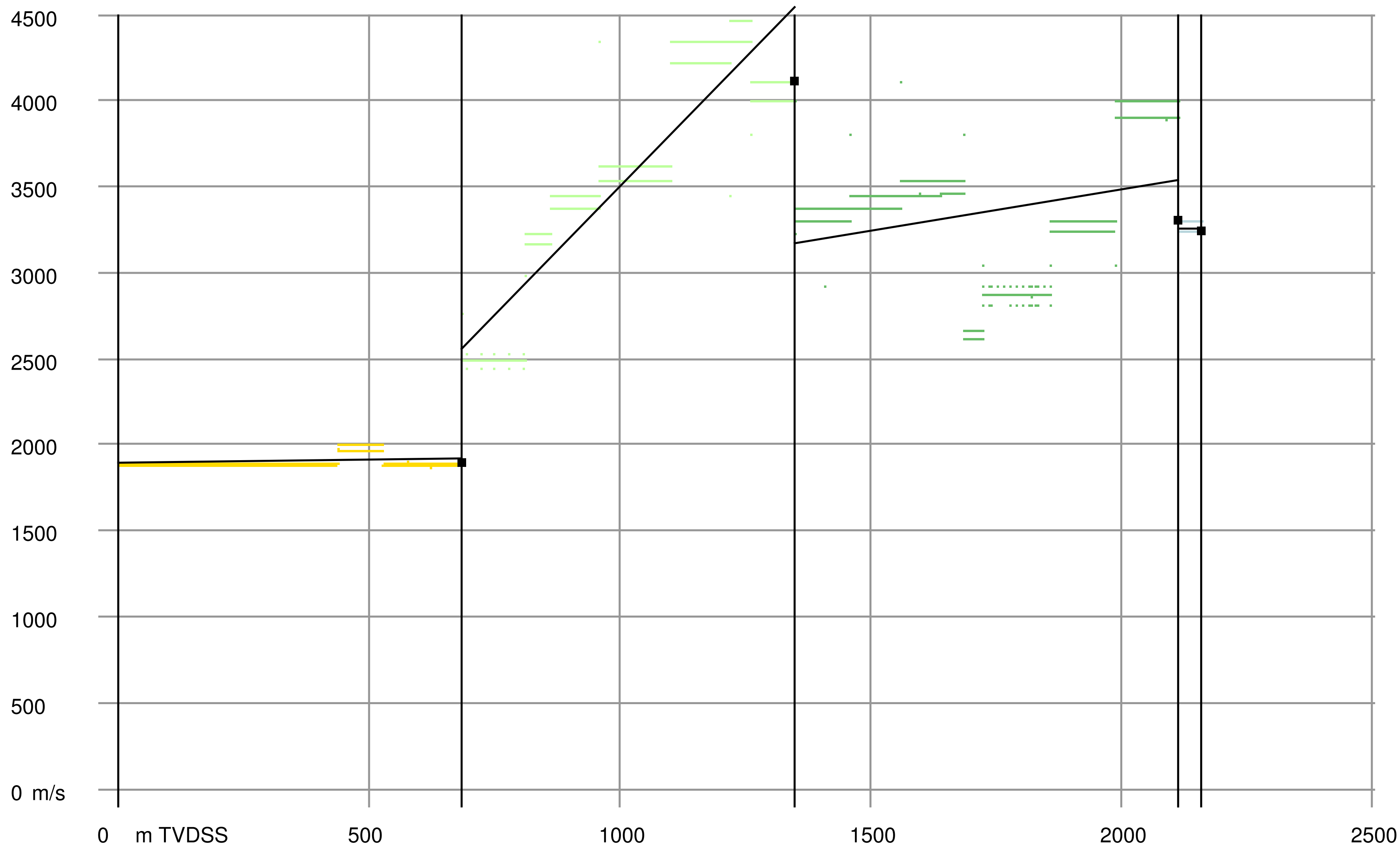

Calibrated instantaneous velocities and linearisation per layer at borehole: P12-07

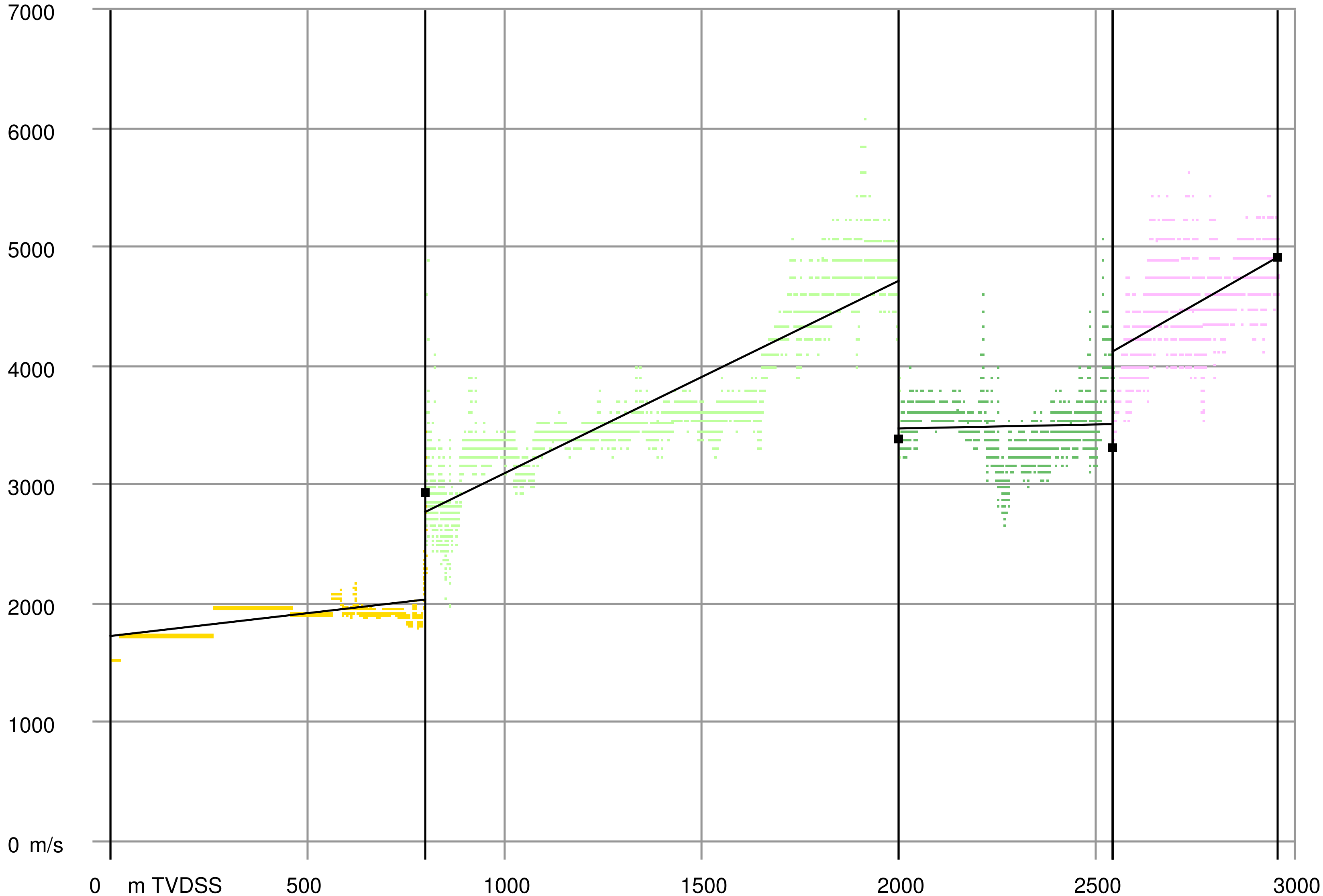

Calibrated instantaneous velocities and linearisation per layer at borehole: P12-12

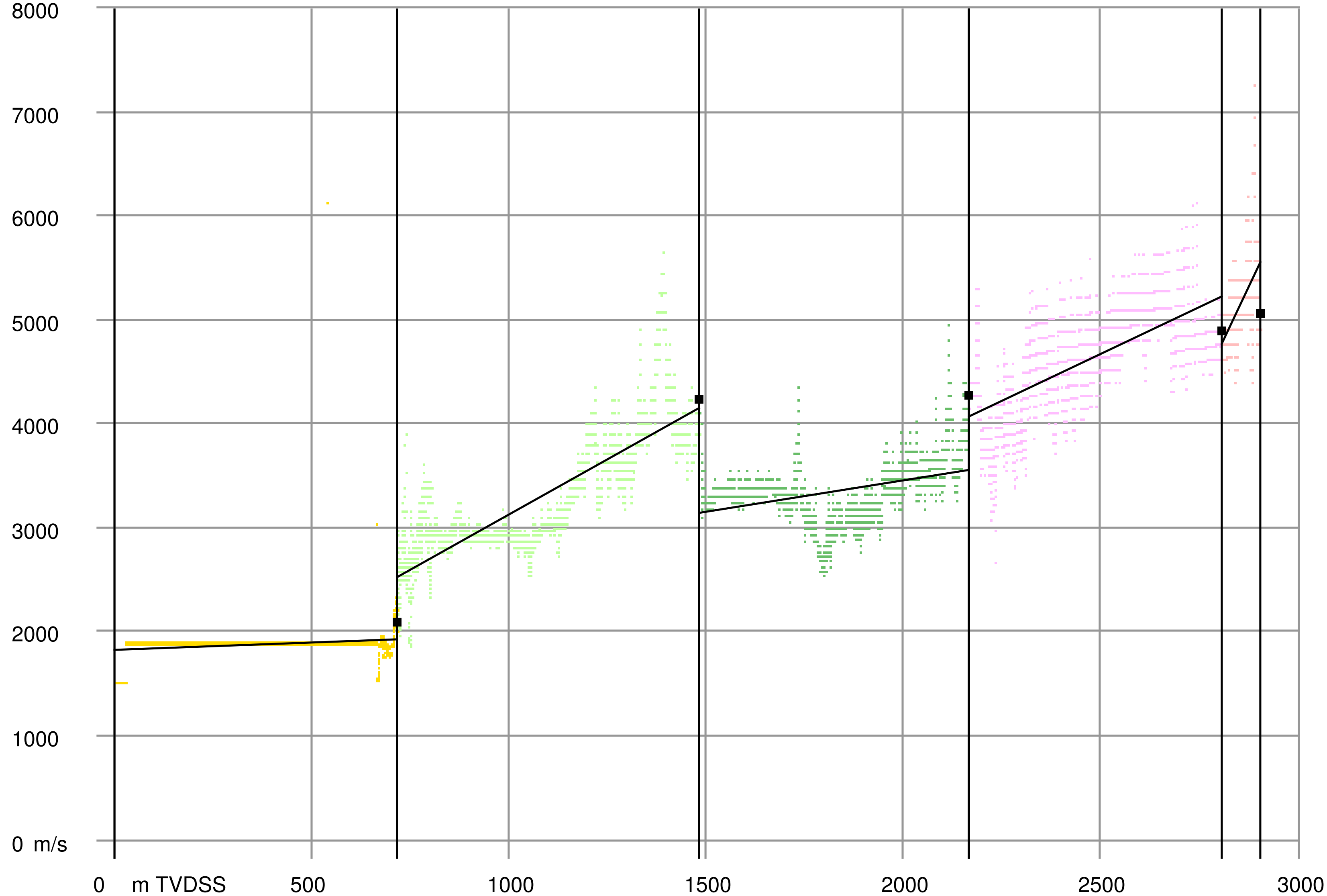

Calibrated instantaneous velocities and linearisation per layer at borehole: P12-C-06

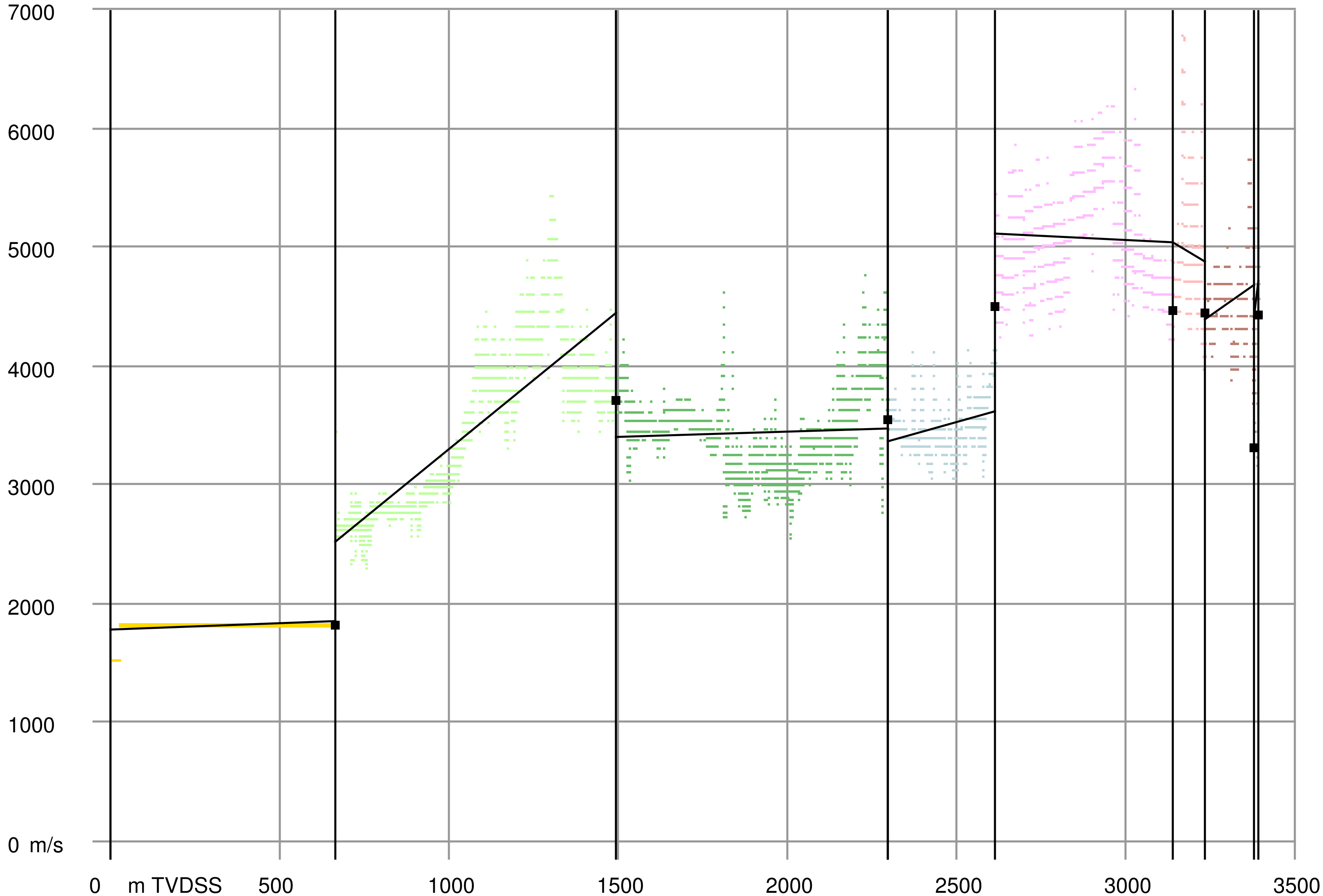

Calibrated instantaneous velocities and linearisation per layer at borehole: P14-A-01

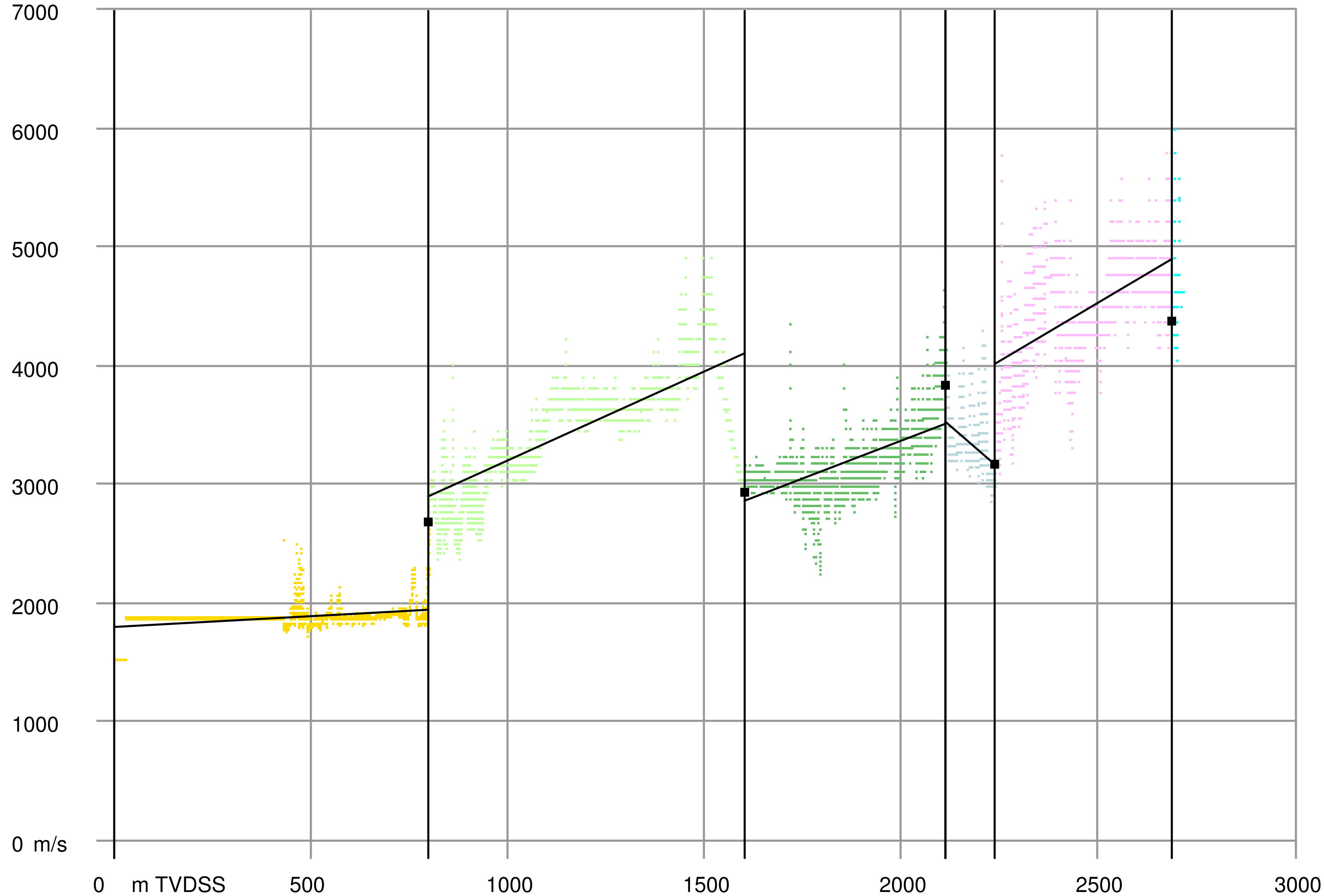

Calibrated instantaneous velocities and linearisation per layer at borehole: P16-01

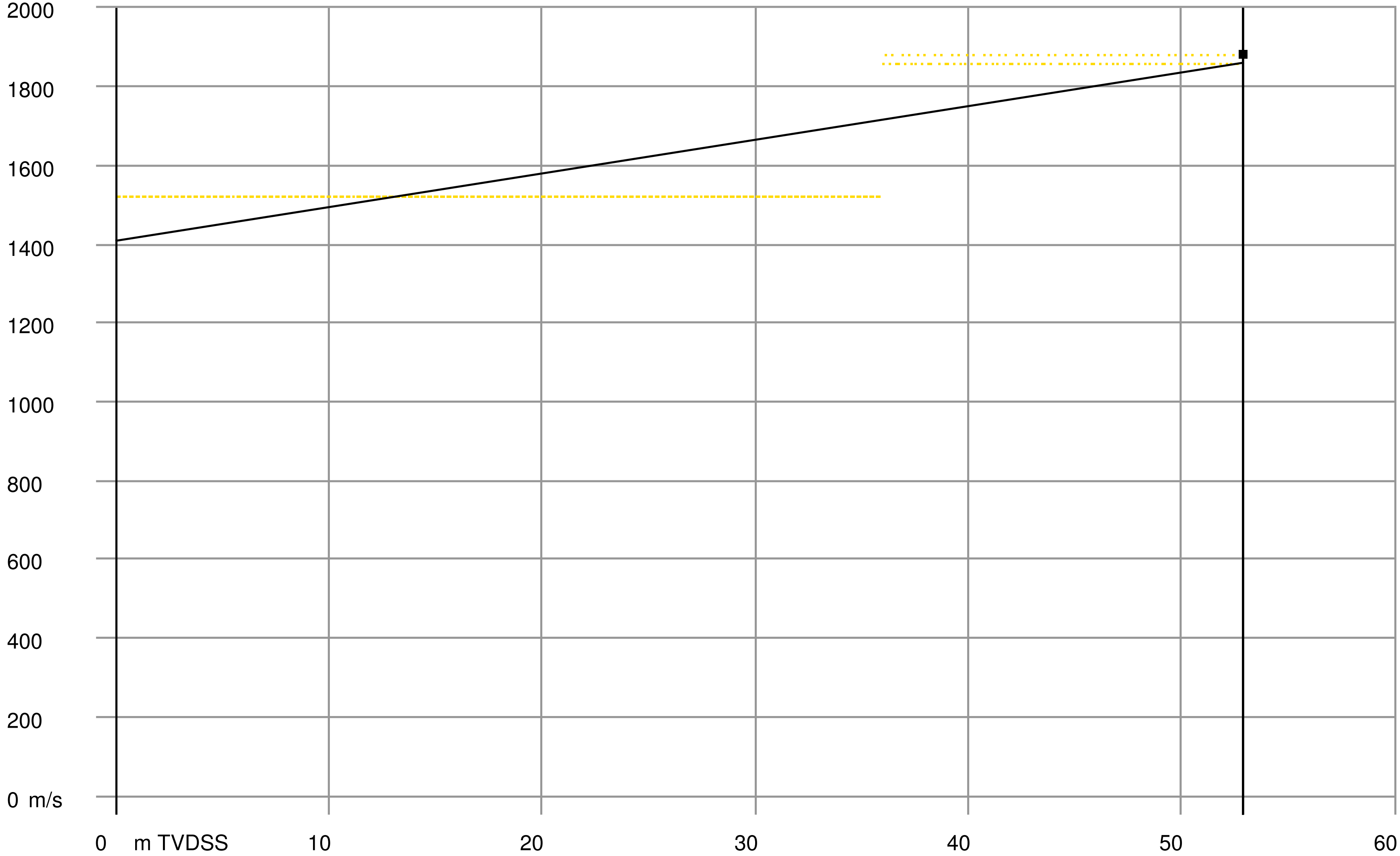

Calibrated instantaneous velocities and linearisation per layer at borehole: PKP-01

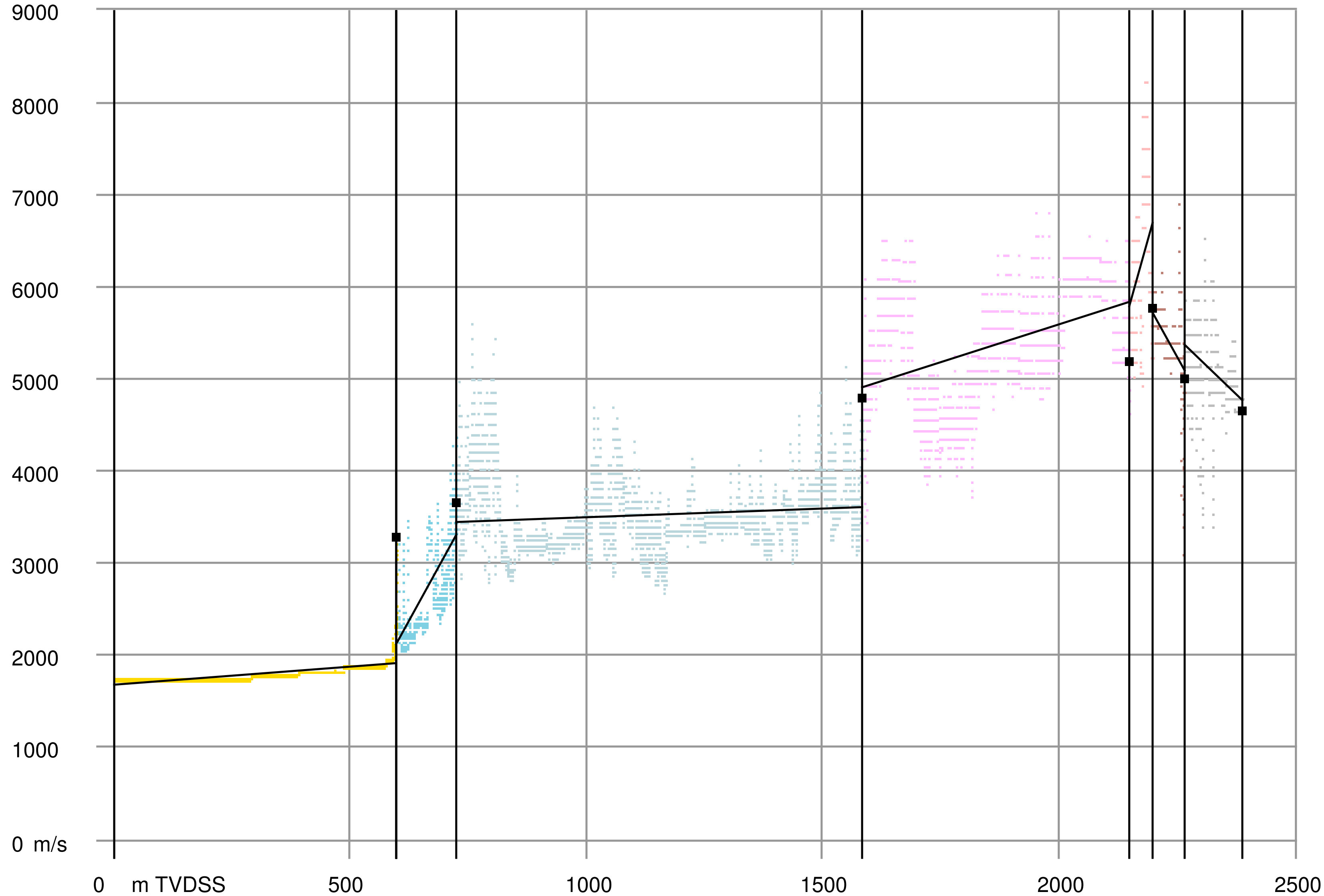

Calibrated instantaneous velocities and linearisation per layer at borehole: PRN-01

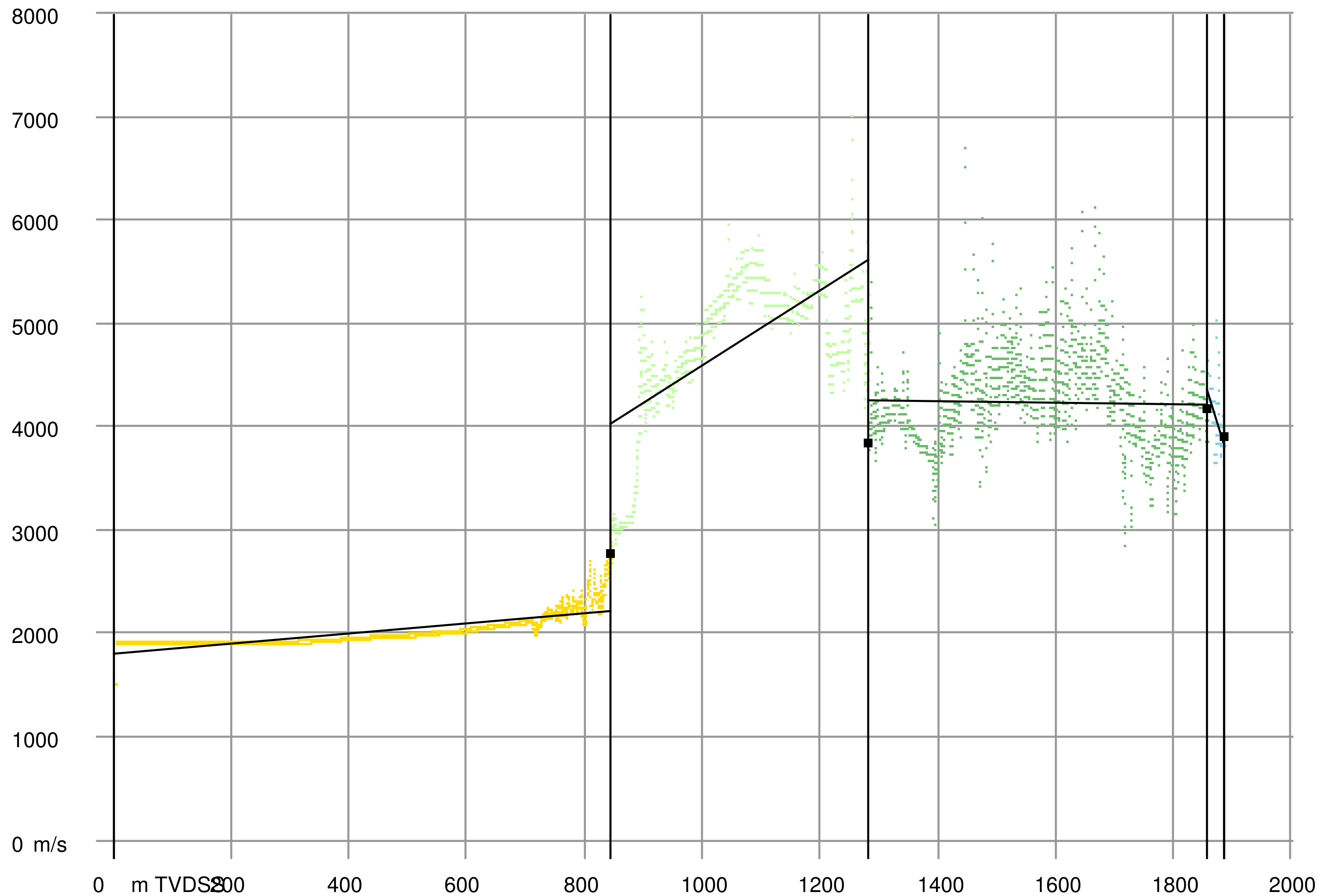

Calibrated instantaneous velocities and linearisation per layer at borehole: Q02-04

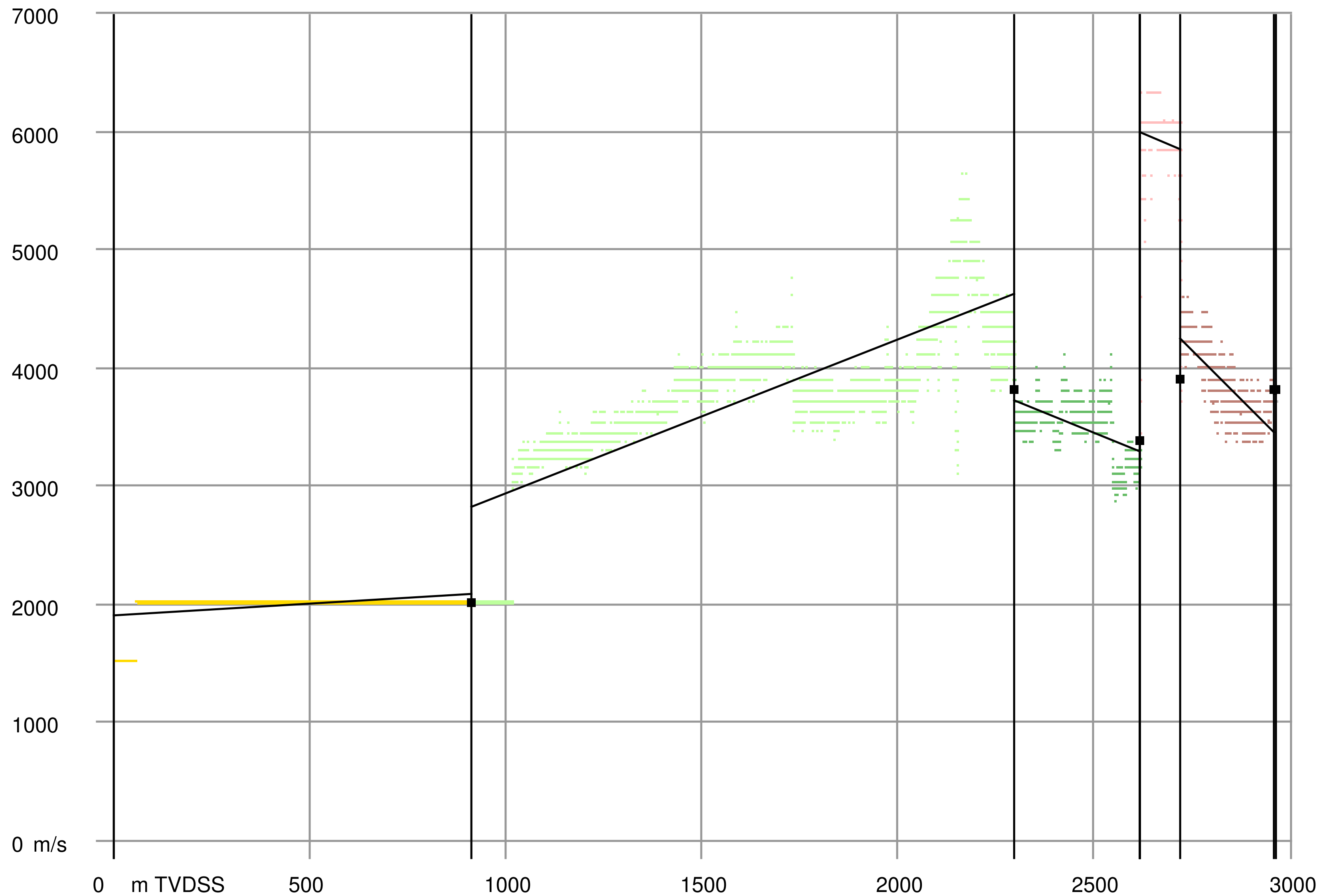

Calibrated instantaneous velocities and linearisation per layer at borehole: Q04-04

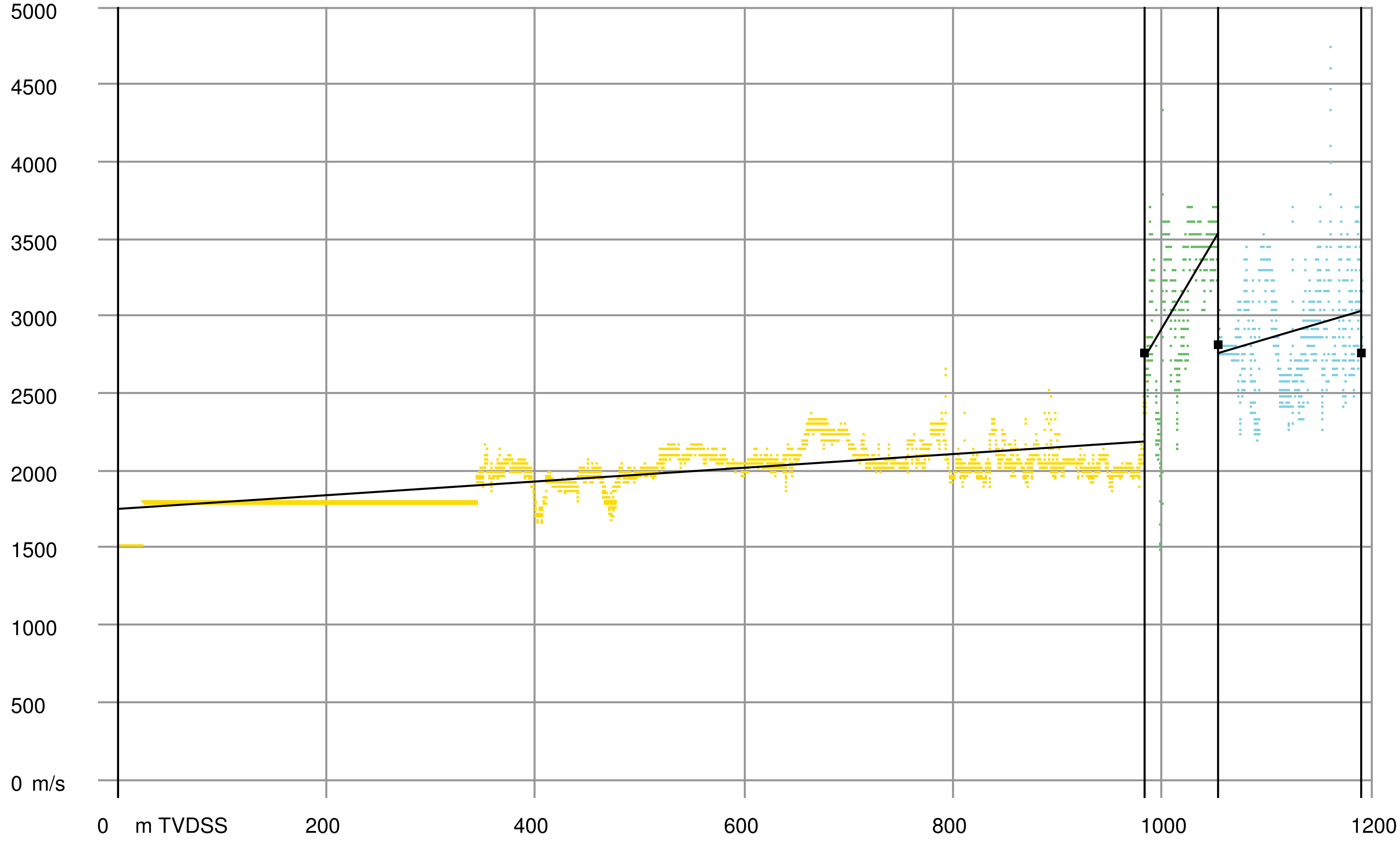

Calibrated instantaneous velocities and linearisation per layer at borehole: Q05-01

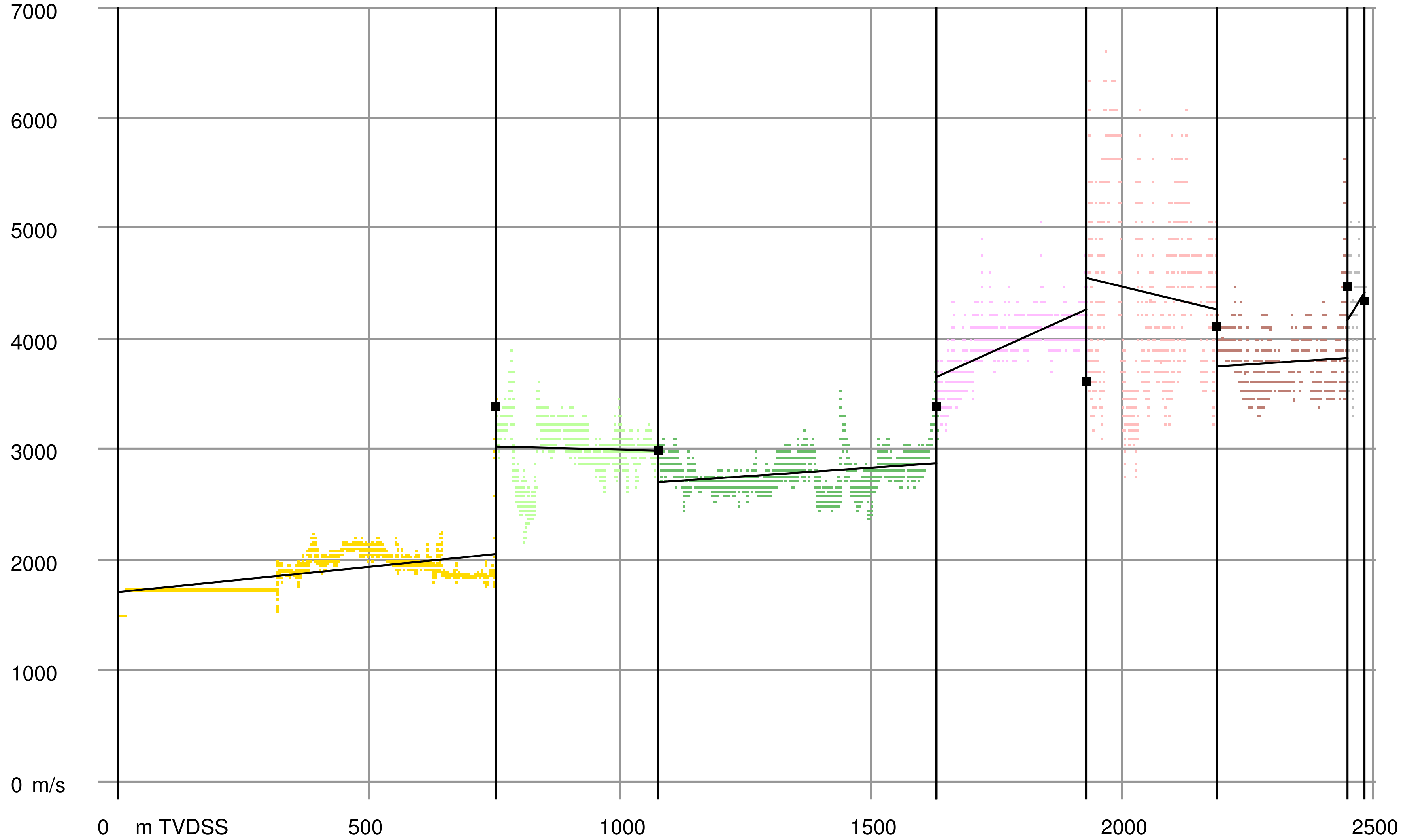

Calibrated instantaneous velocities and linearisation per layer at borehole: Q05-05

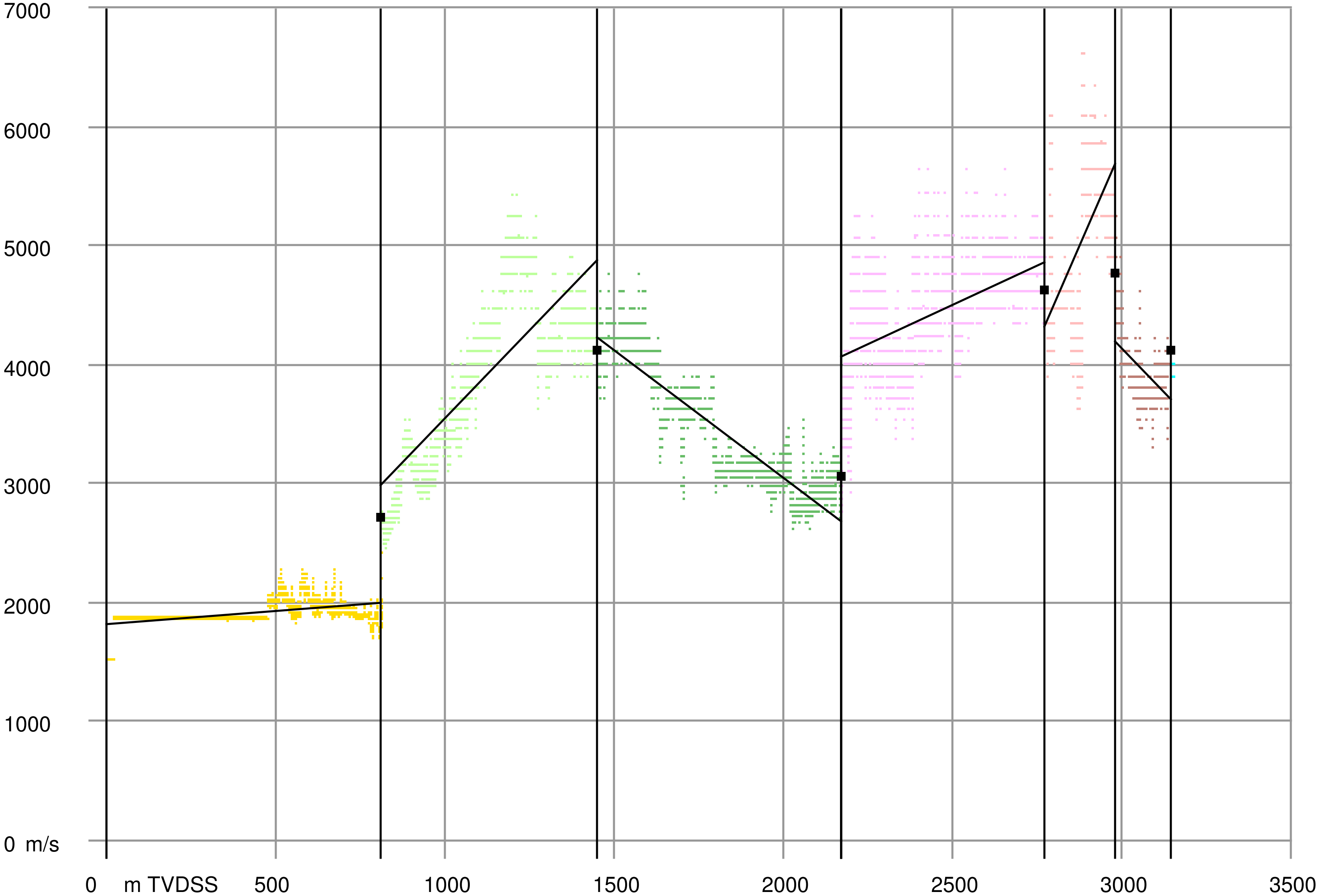

Calibrated instantaneous velocities and linearisation per layer at borehole: Q07-04

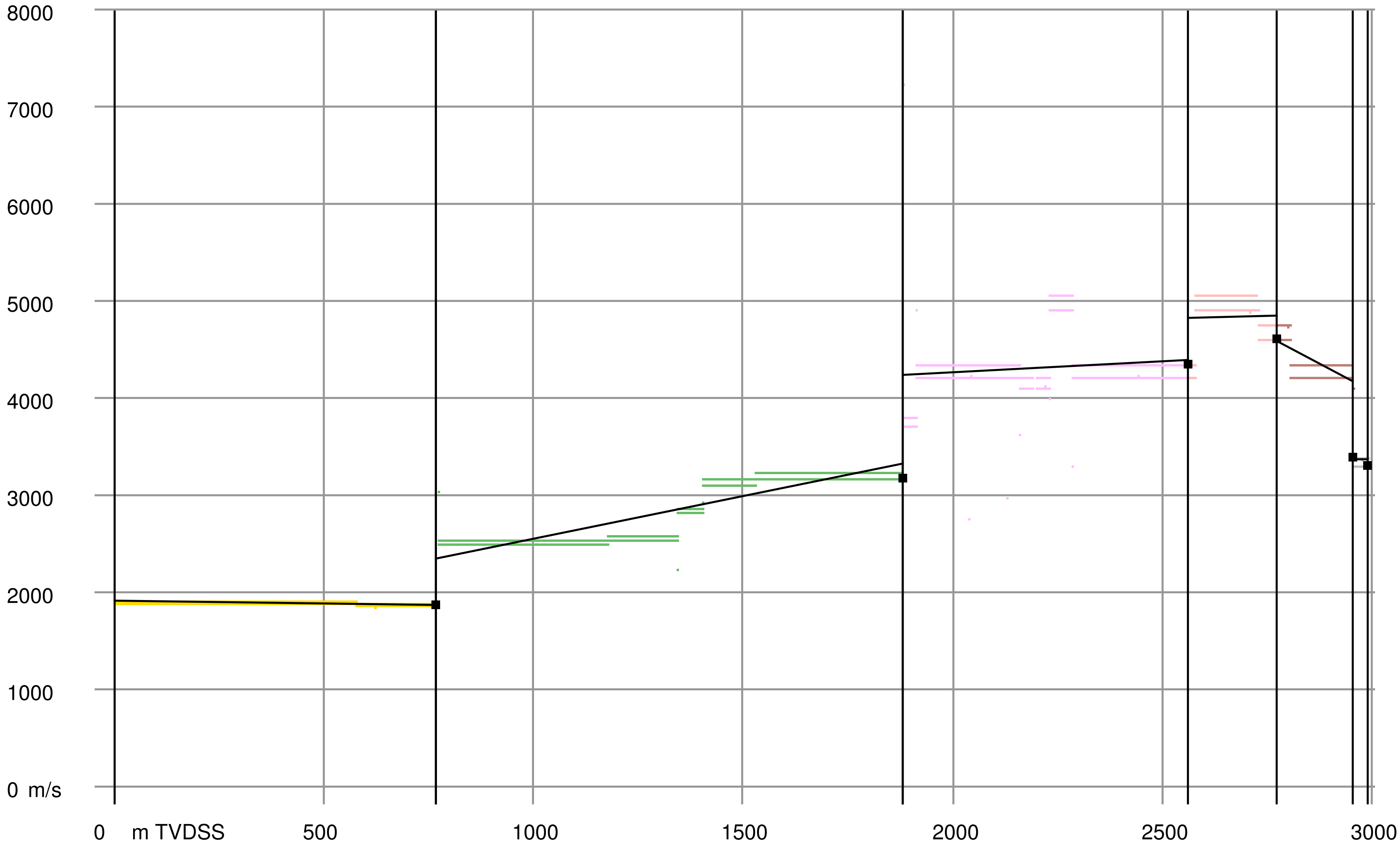

Calibrated instantaneous velocities and linearisation per layer at borehole: Q08-06

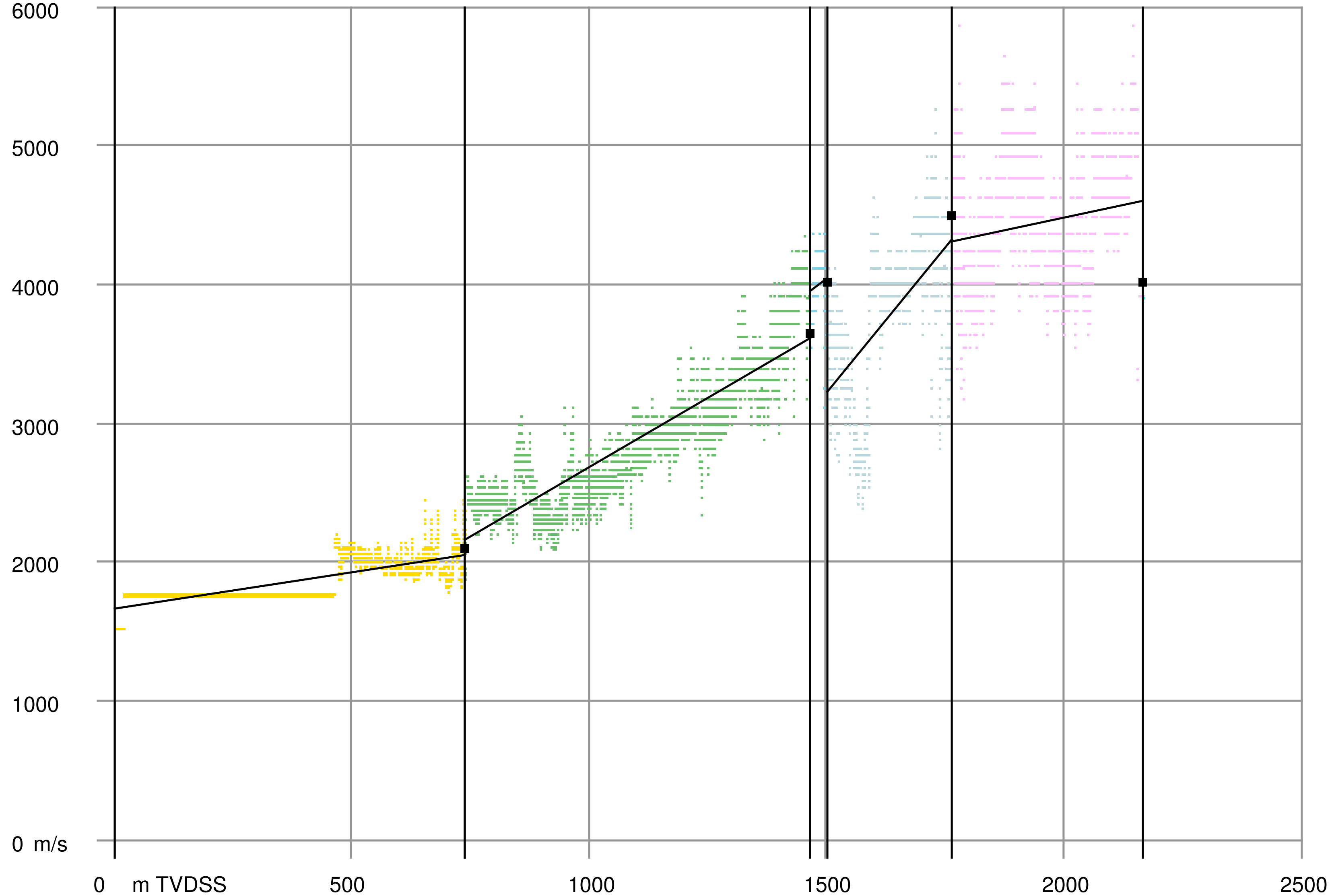

Calibrated instantaneous velocities and linearisation per layer at borehole: Q08-B-01

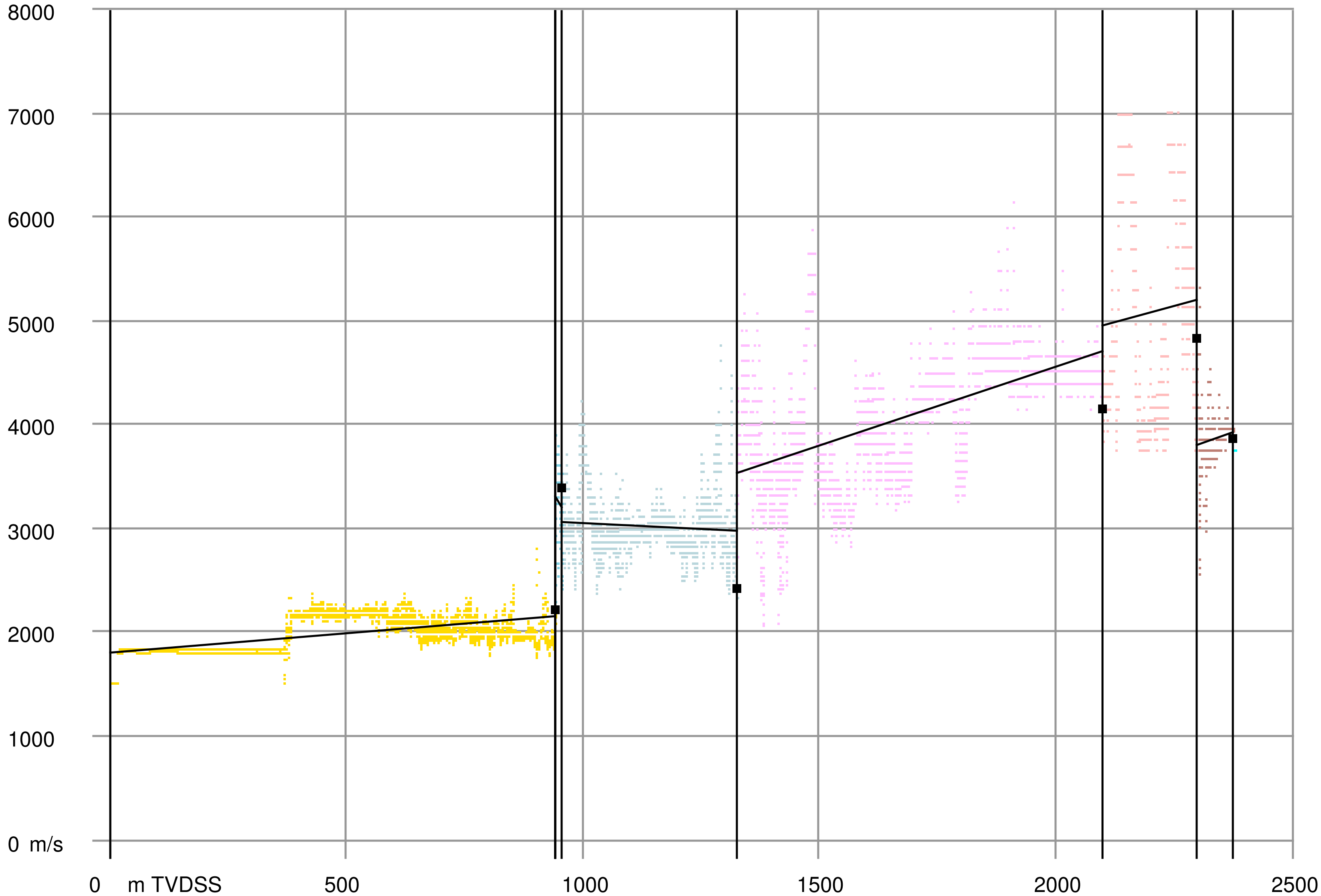

Calibrated instantaneous velocities and linearisation per layer at borehole: Q10-03

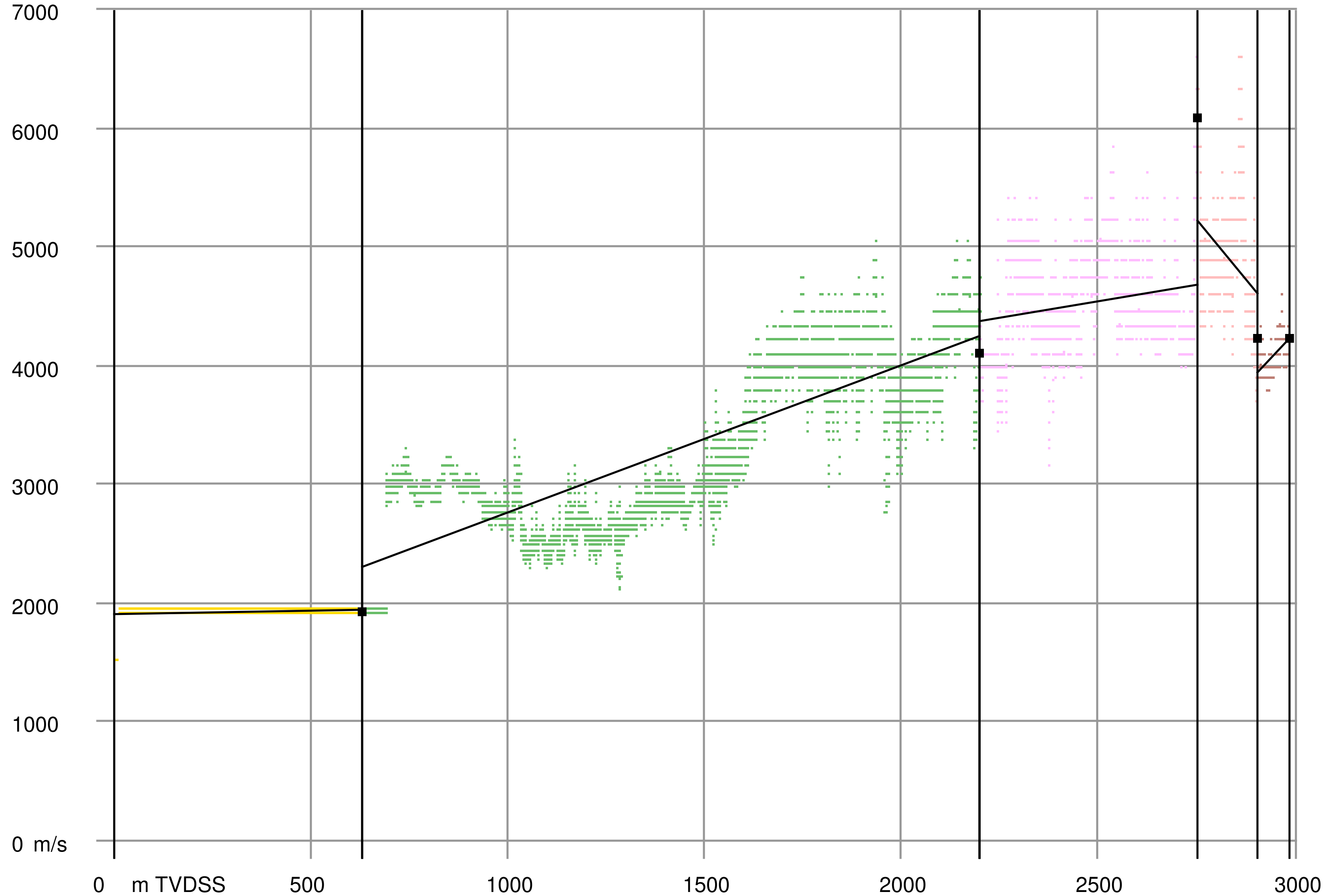

Calibrated instantaneous velocities and linearisation per layer at borehole: Q13-04

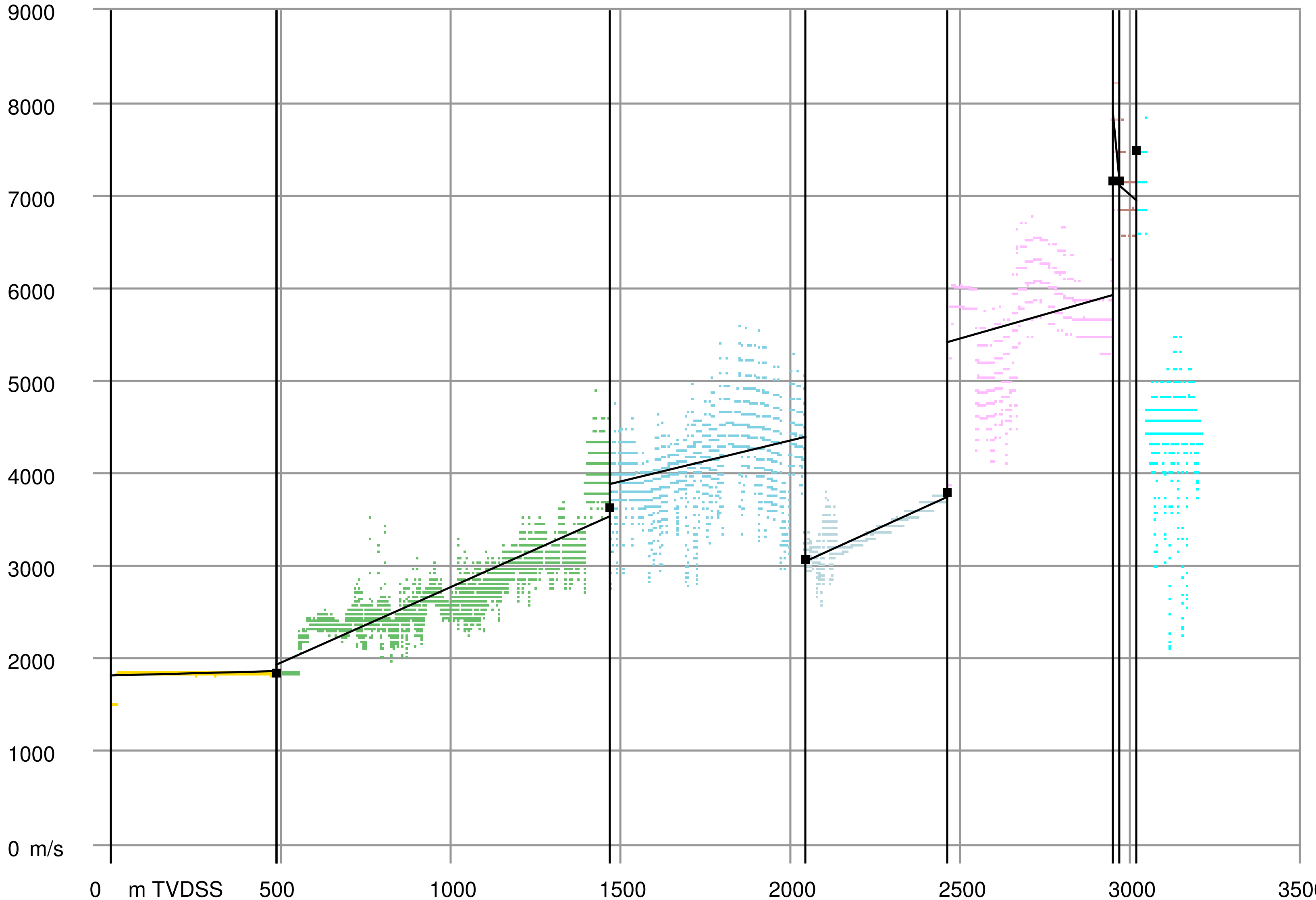

Calibrated instantaneous velocities and linearisation per layer at borehole: Q13-05

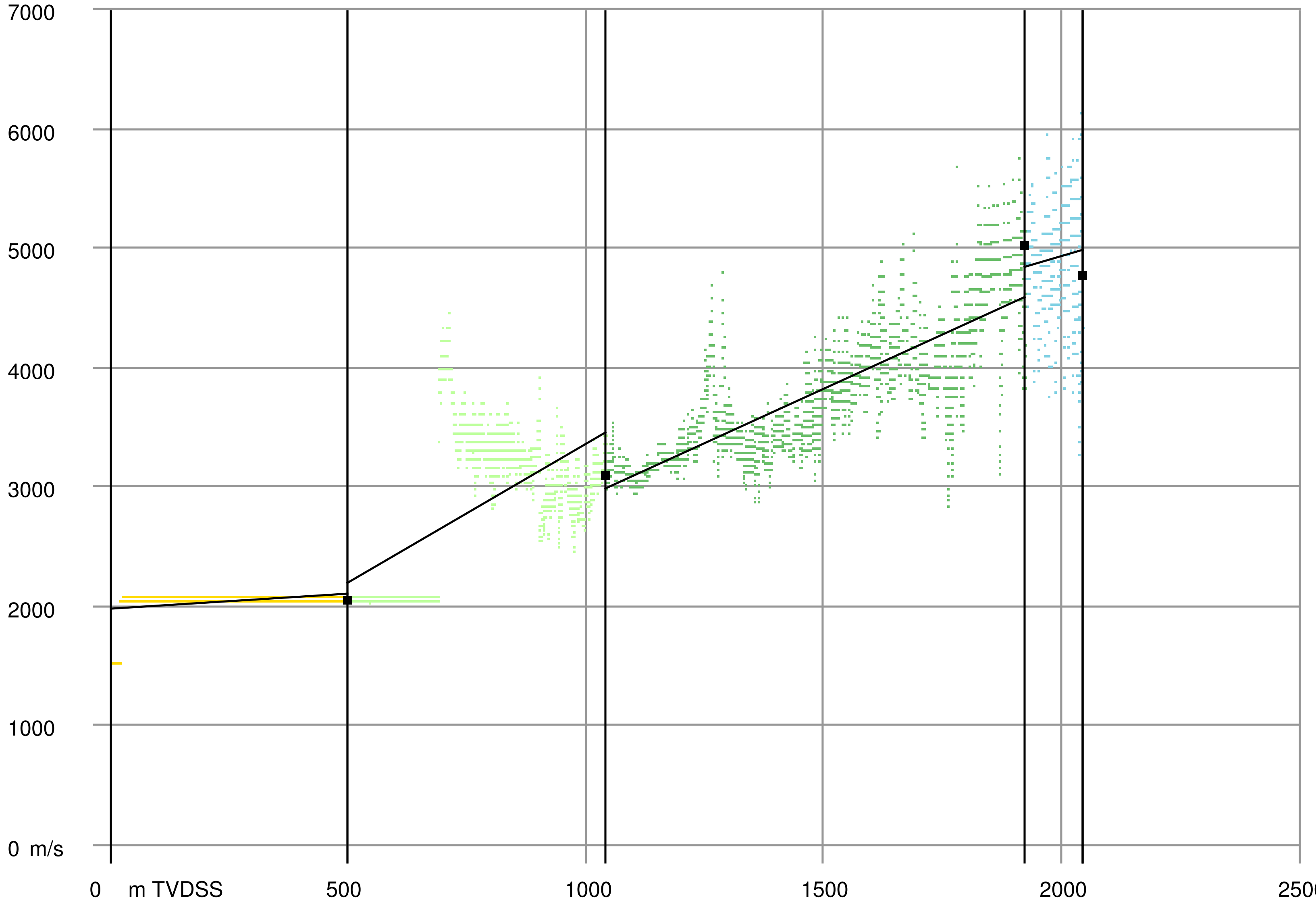

Calibrated instantaneous velocities and linearisation per layer at borehole: Q16-03

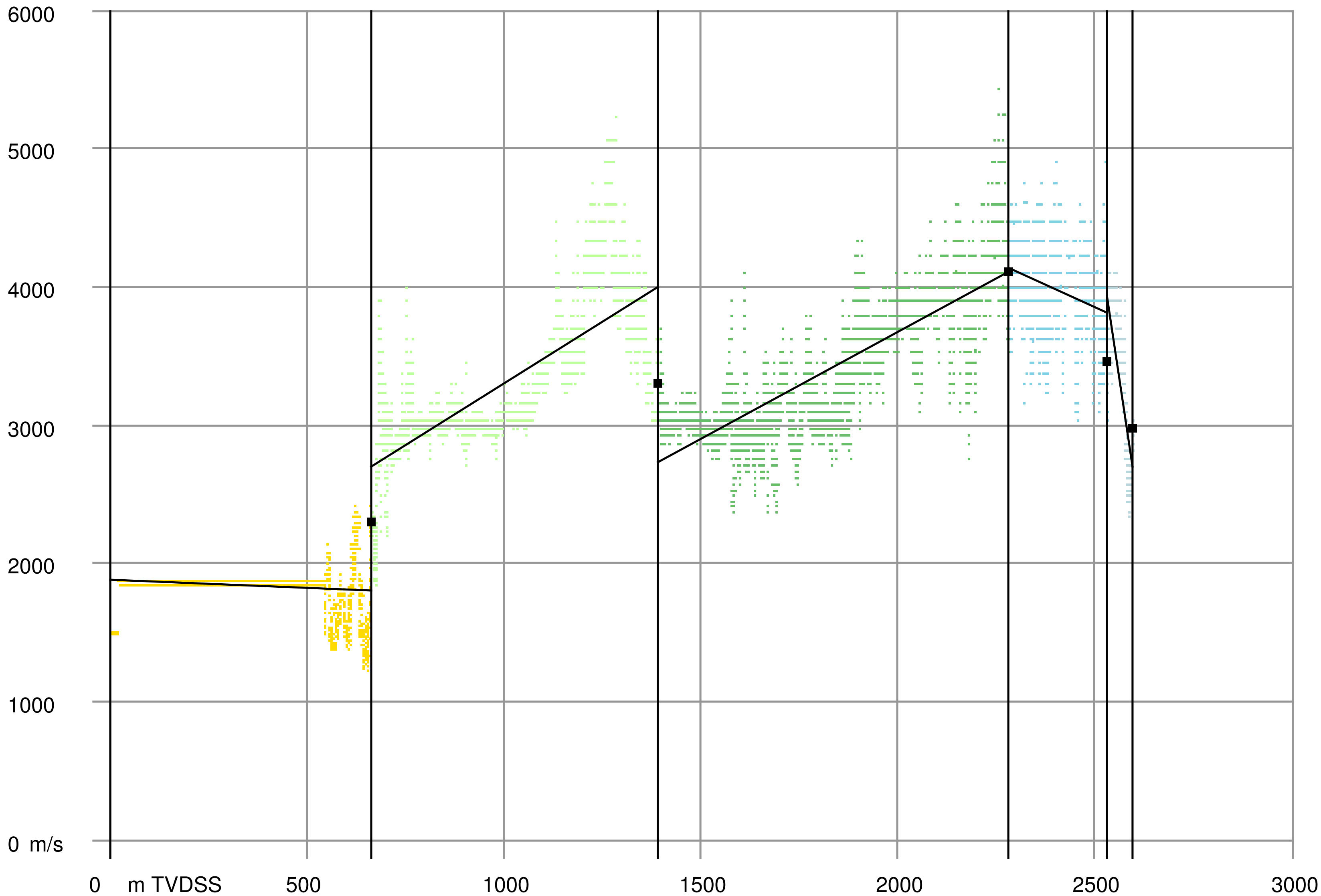

Calibrated instantaneous velocities and linearisation per layer at borehole: Q16-FA-101

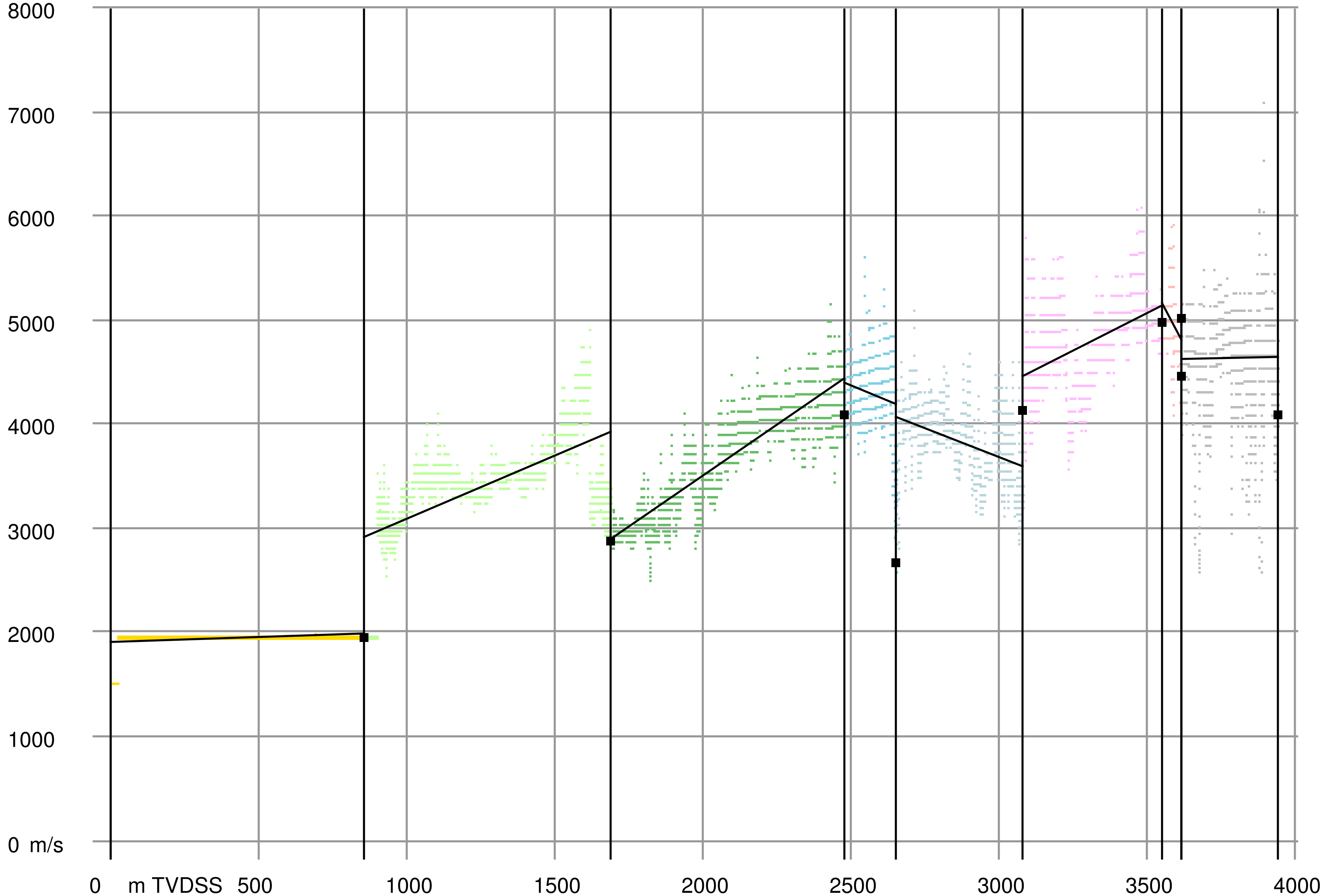

Calibrated instantaneous velocities and linearisation per layer at borehole: WWN-02

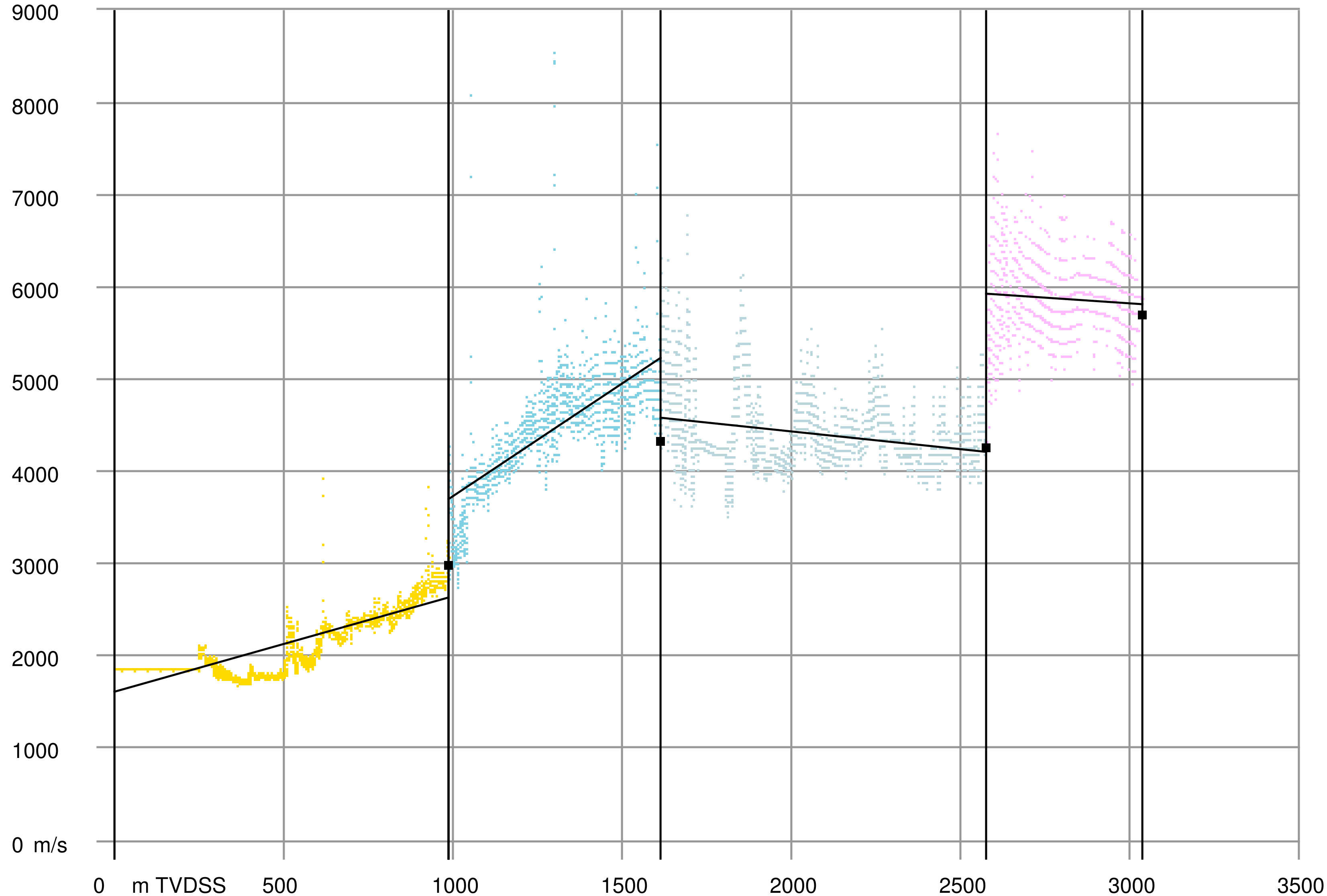

Calibrated instantaneous velocities and linearisation per layer at borehole: ZVH-01

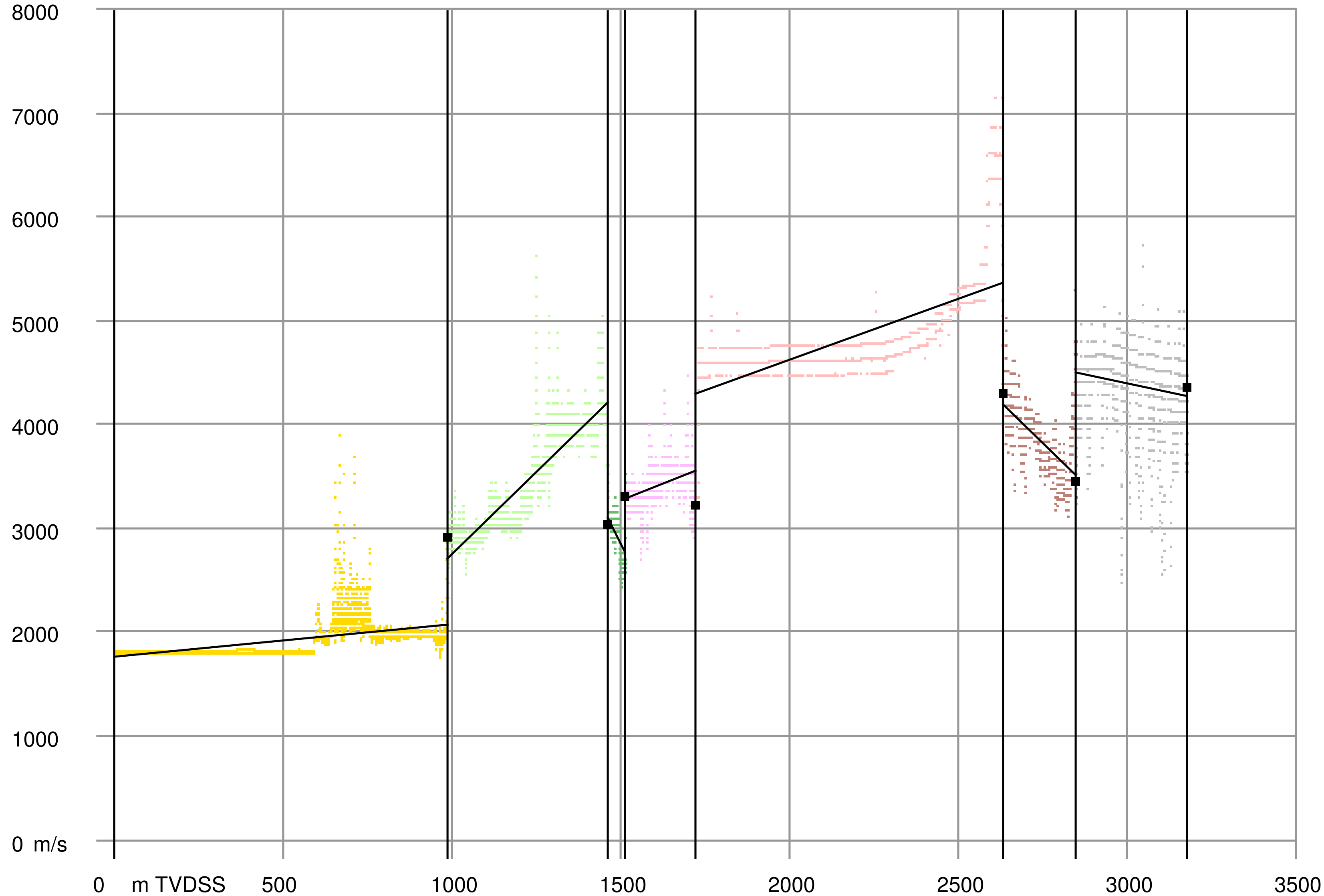

C Linearisation data (v0 and k) of VOLONZ-processed DCS logs

The data is available on CD.

Table C. 1: Explanation of abbreviations used in Appendix C

Abbreviation	**Description**
Status	V_{int} is accepted or rejected for V_{int}-z_{mid} analysis and geostatistical modelling. SNET>DCS: DCS data is used in stead of SNET data
UWI	Borehole identifier
Borehole	Name of the borehole
Layer	Lithostratigraphic layer
E_t	Location (Easting) of the borehole at the top of the layer
N_t	Location (Northing) of the borehole at the top of the layer
z_t	Depth of the top of the layer [m]
z_b	Depth of the base of the layer [m]
TWT_t	Two way traveltime to the top of the layer
TWT_b	Two way traveltime to the base of the layer
ΔT	One way traveltime vertical through layer
E_b	Location (Easting) of the borehole at the bottom of the layer
N_b	Location (Northing) of the borehole at the bottom of the layer
E_0	Location (Easting) of the borehole at reference surface
N_0	Location (Northing) of the borehole at reference surface
E_b-E_0	Deviation (Easting)
N_b-N_0	Deviation (Northing)
Δz	True vertical thickness [m]
E_{mid}	Location (Easting) of the borehole at the mid-depth of the layer
N_{mid}	Location (Northing) of the borehole at the mid-depth of the layer
z_{mid}	Mid-depth of the layer [m]
V_{int}	Interval velocity [m/s]
k	[/s] (calculated by VOLONZ)
dk	[/s] (calculated by VOLONZ)
v_0	[m/s] (calculated by VOLONZ)
dv_0	[m/s] (calculated by VOLONZ)
V_{av}	[m/s] (calculated by VOLONZ)

D Results of VELMOD-1 Phase 1

The data is available on CD.

Table D. 1: Explanation of abbreviations used in Appendix D

Abbreviation	**Description**
DCS/SNET	Which dataset is used for the borehole
UWI	Borehole identifier
Borehole	Name of the borehole
E_t	Location (Easting) of the borehole at the top of the layer
N_t	Location (Northing) of the borehole at the top of the layer
z_t	Depth of the top of the layer [m]
z_b	Depth of the base of the layer [m]
ΔT	One way traveltime vertical through layer
T_b	One way traveltime to the base of the layer
E_{mid}	Location (Easting) of the borehole at the mid-depth of the layer
N_{mid}	Location (Northing) of the borehole at the mid-depth of the layer
z_{mid}	Mid-depth of the layer [m]
V_{int}	Interval velocity [m/s]
v_0	[m/s] (calculated by VOLONZ for DCS boreholes)
k	[/s] (calculated by VOLONZ for DCS boreholes)
$\Delta T_{predicted}$ method A	One way traveltime vertical through layer, calculated from predicted V_0 and K in method A [ms]
V_0 method B	[m/s]
K method B	[/s]

E Isochore maps and time maps of the bases of the lithostratigraphic layers.

On the next pages the isochore maps and time maps of the bases of the lithostratigraphic layers are shown. These maps are also available on CD.

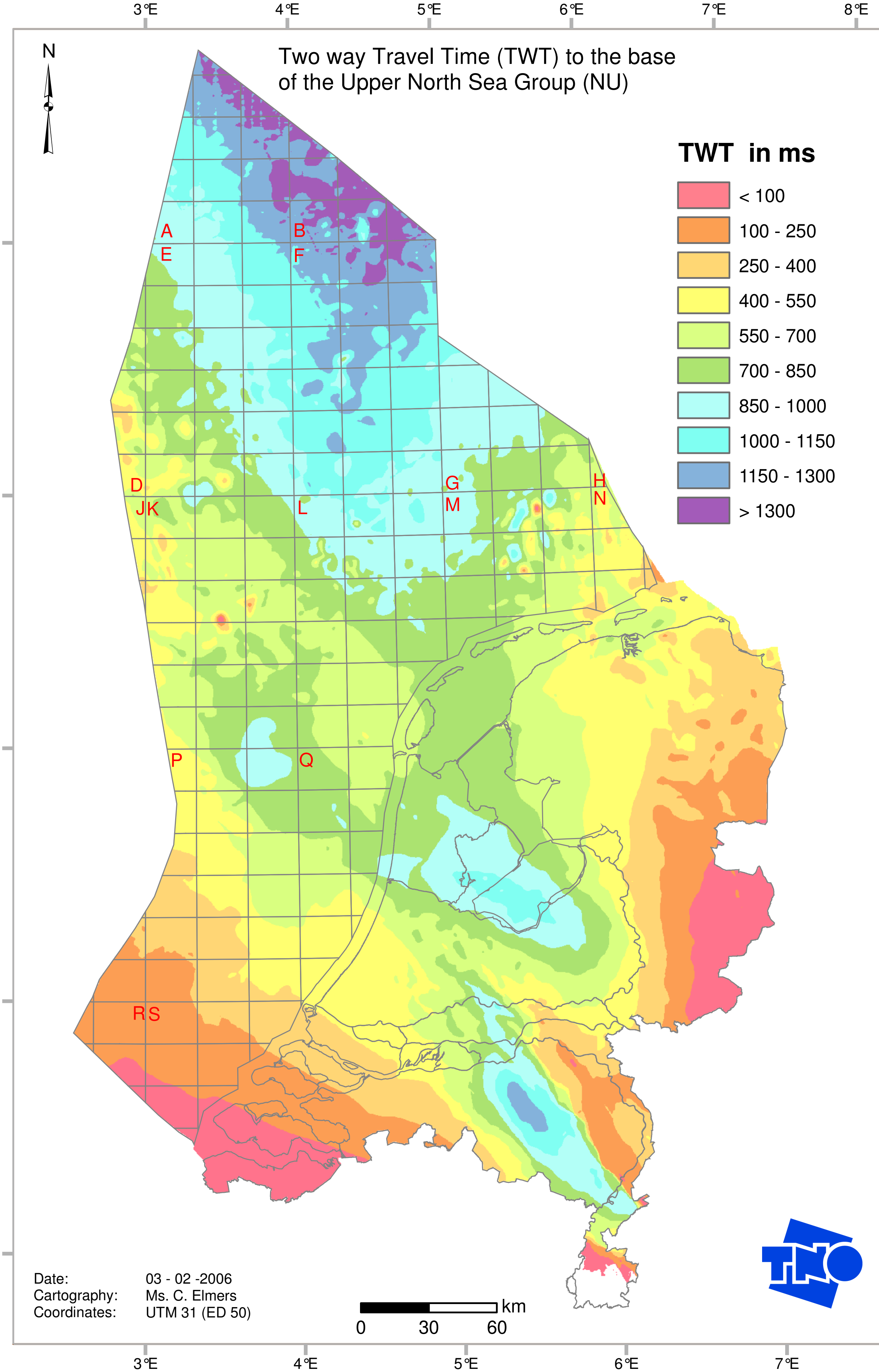
Two way Travel Time (TWT) to the base
of the Upper North Sea Group (NU)
TWT in ms
< 100
100 - 250
250 - 400
400 - 550
550 - 700
700 - 850
850 - 1000
1000 - 1150
1150 - 1300
> 1300
N
A
B
E
F
D
JK
L
G
M
H
N
P
Q
RS
3°E
4°E
5°E
6°E
7°E
8°E
51°N
52°N
53°N
54°N
55°N
Date: 03 - 02 -2006
Cartography: Ms. C. Elmers
Coordinates: UTM 31 (ED 50)
km
0
30
60

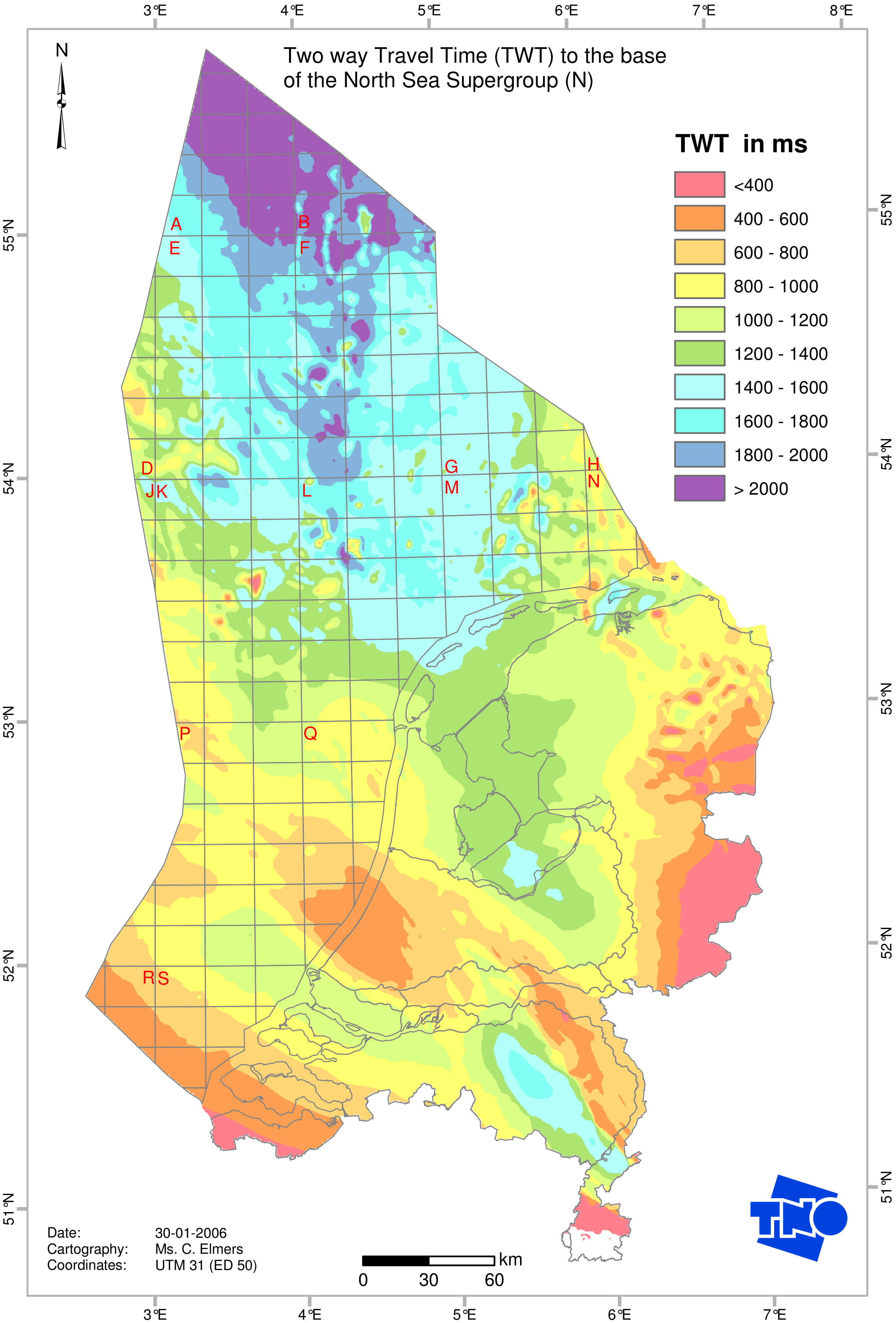
Two way Travel Time (TWT) to the base
of the North Sea Supergroup (N)
TWT in ms
<400
400 - 600
600 - 800
800 - 1000
1000 - 1200
1200 - 1400
1400 - 1600
1600 - 1800
1800 - 2000
> 2000
N
3°E
4°E
5°E
6°E
7°E
8°E
55°N
54°N
53°N
52°N
51°N
A
B
E
F
D
JK
L
G
M
H
N
P
Q
RS
Date: 30-01-2006
Cartography: Ms. C. Elmers
Coordinates: UTM 31 (ED 50)
0
30
60
km
TNO

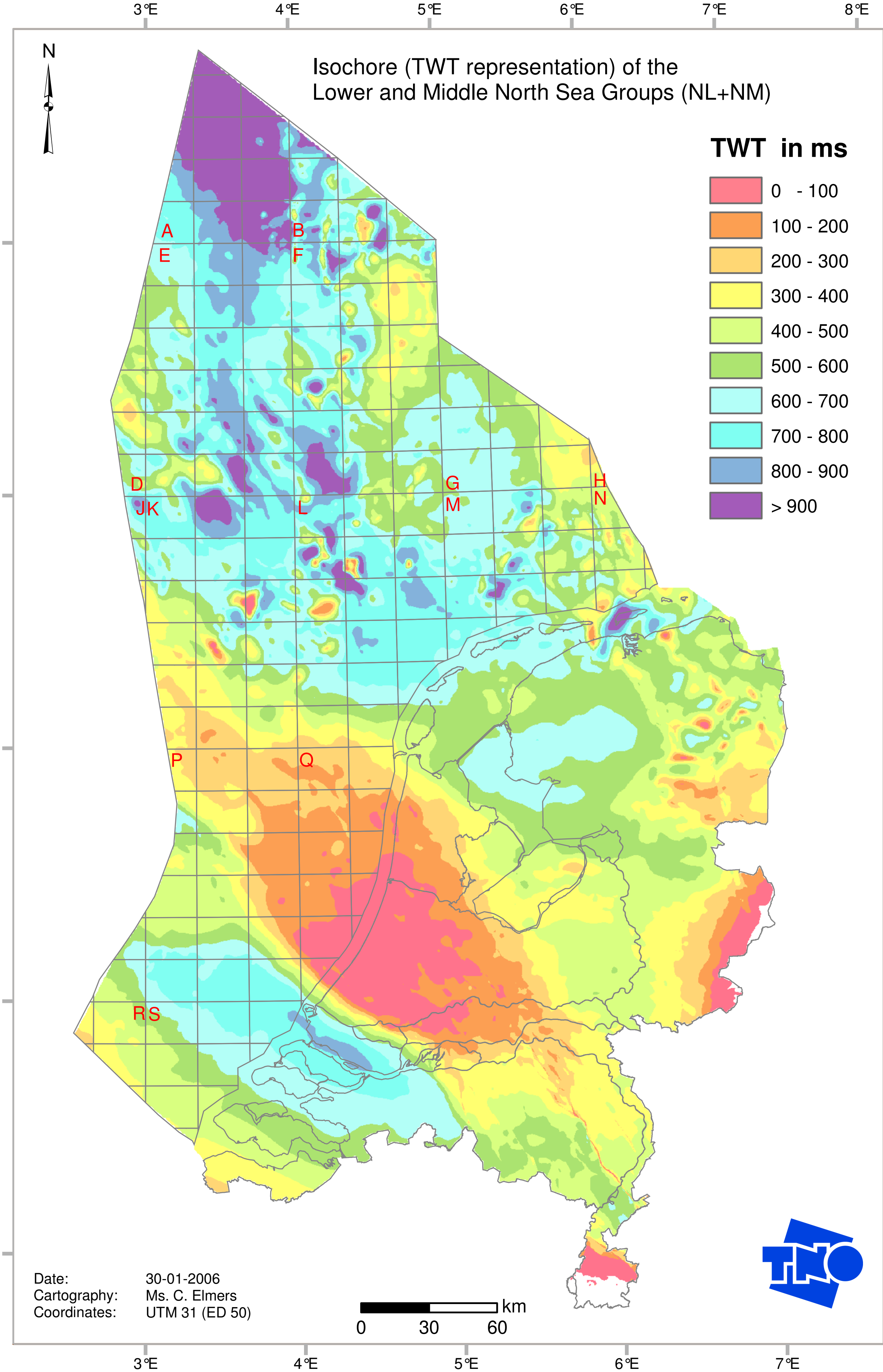

Isochore (TWT representation) of the
Lower and Middle North Sea Groups (NL+NM)
TWT in ms
0 - 100
100 - 200
200 - 300
300 - 400
400 - 500
500 - 600
600 - 700
700 - 800
800 - 900
> 900
N
A
E
B
F
D
JK
L
G
M
H
N
P
Q
RS
3°E
4°E
5°E
6°E
7°E
8°E
55°N
54°N
53°N
52°N
51°N
km
0
30
60
Date: 30-01-2006
Cartography: Ms. C. Elmers
Coordinates: UTM 31 (ED 50)
TNO

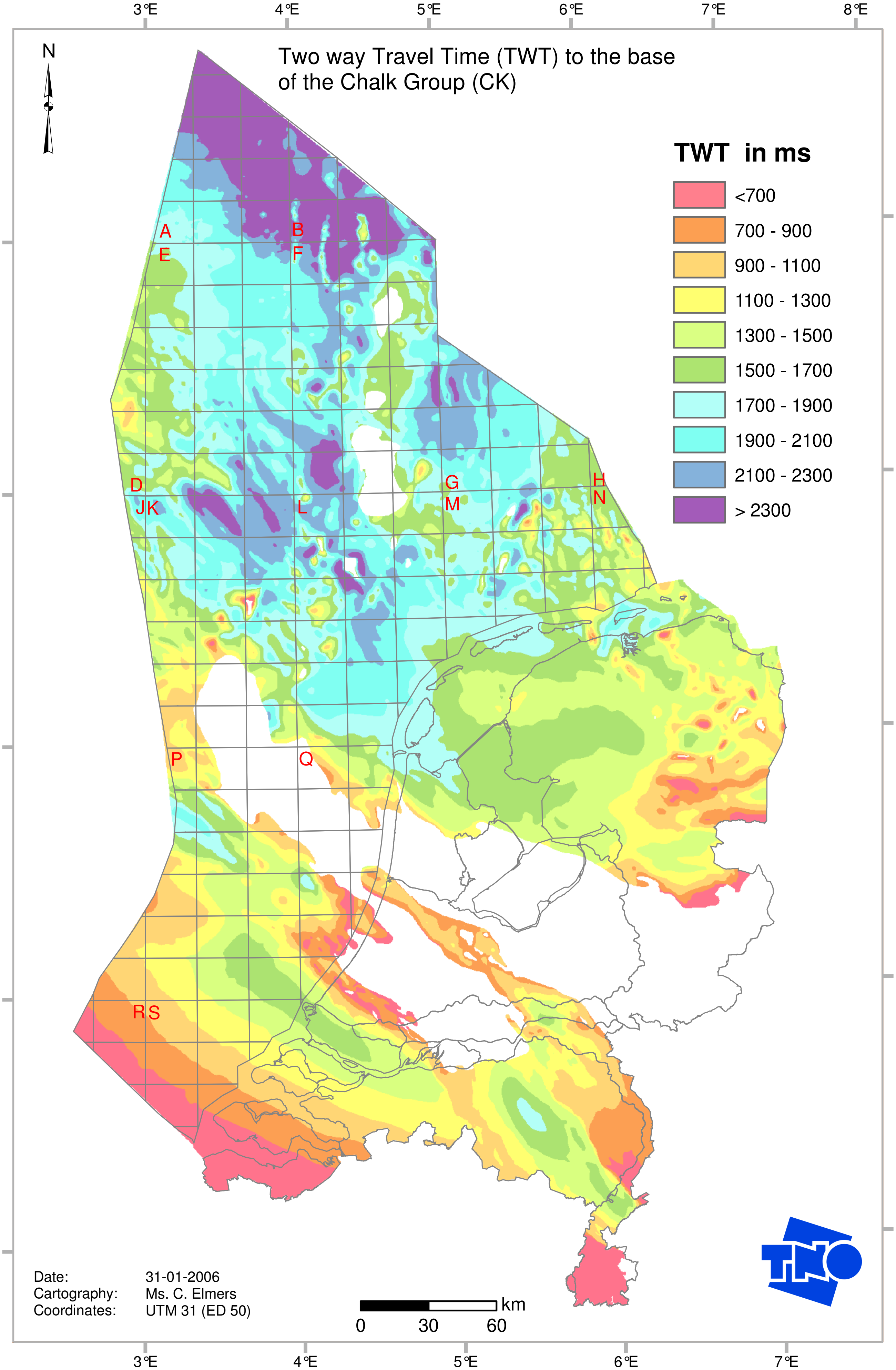

Two way Travel Time (TWT) to the base
of the Chalk Group (CK)
N
TWT in ms
<700
700 - 900
900 - 1100
1100 - 1300
1300 - 1500
1500 - 1700
1700 - 1900
1900 - 2100
2100 - 2300
> 2300
3°E
4°E
5°E
6°E
7°E
8°E
55°N
54°N
53°N
52°N
51°N
A
E
B
F
D
JK
L
G
M
H
N
P
Q
RS
Date: 31-01-2006
Cartography: Ms. C. Elmers
Coordinates: UTM 31 (ED 50)
km
0 30 60

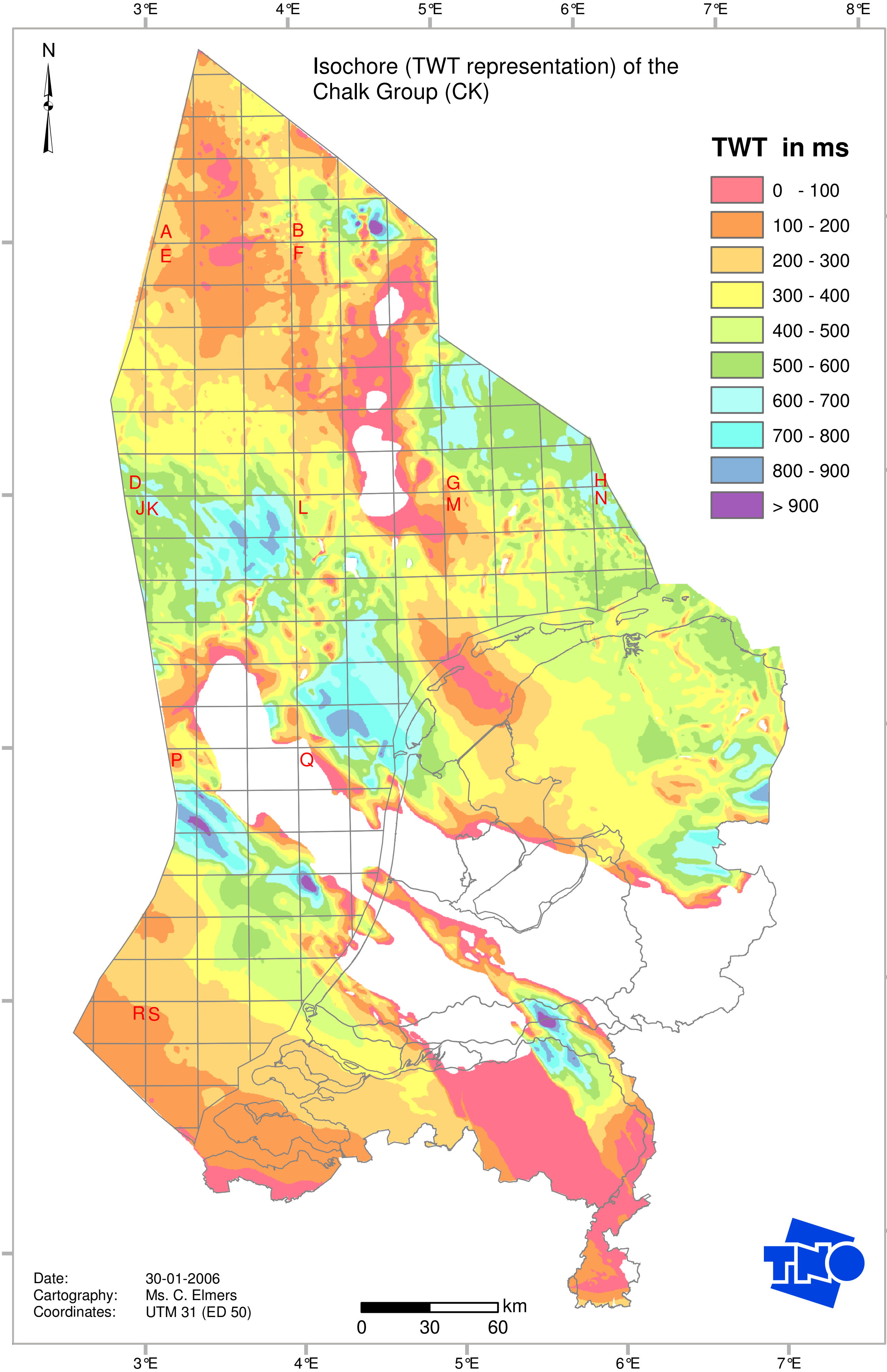

Isochore (TWT representation) of the
Chalk Group (CK)
TWT in ms
0 - 100
100 - 200
200 - 300
300 - 400
400 - 500
500 - 600
600 - 700
700 - 800
800 - 900
> 900
N
A
B
E
F
D
JK
L
G
M
H
N
P
Q
RS
3°E
4°E
5°E
6°E
7°E
8°E
51°N
52°N
53°N
54°N
55°N
km
0
30
60
Date: 30-01-2006
Cartography: Ms. C. Elmers
Coordinates: UTM 31 (ED 50)

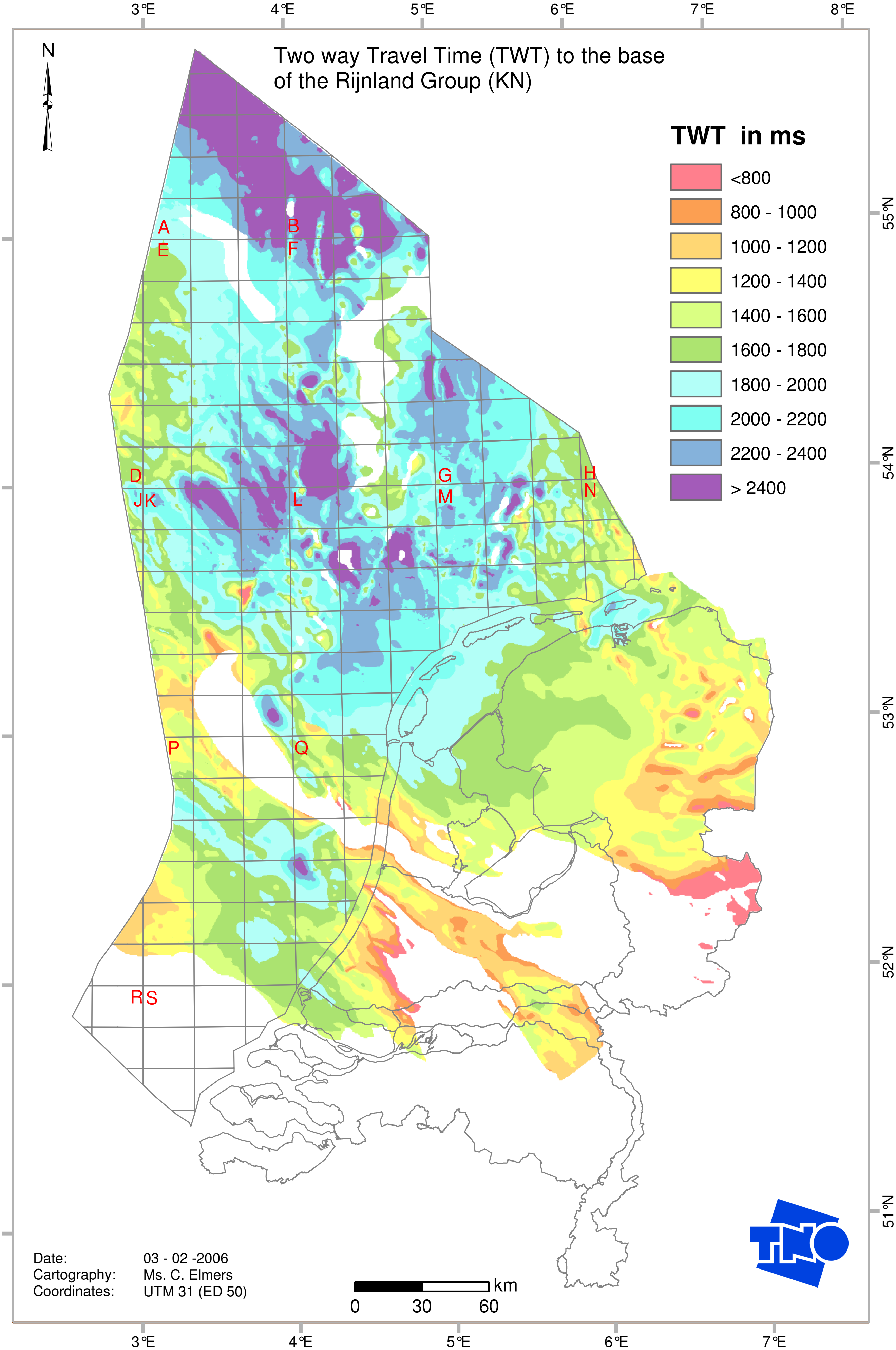

Two way Travel Time (TWT) to the base
of the Rijnland Group (KN)
TWT in ms
<800
800 - 1000
1000 - 1200
1200 - 1400
1400 - 1600
1600 - 1800
1800 - 2000
2000 - 2200
2200 - 2400
> 2400
N
A
E
B
F
D
JK
L
G
M
H
N
P
Q
RS
3°E
4°E
5°E
6°E
7°E
8°E
51°N
52°N
53°N
54°N
55°N
Date: 03 - 02 -2006
Cartography: Ms. C. Elmers
Coordinates: UTM 31 (ED 50)
0
30
60
km

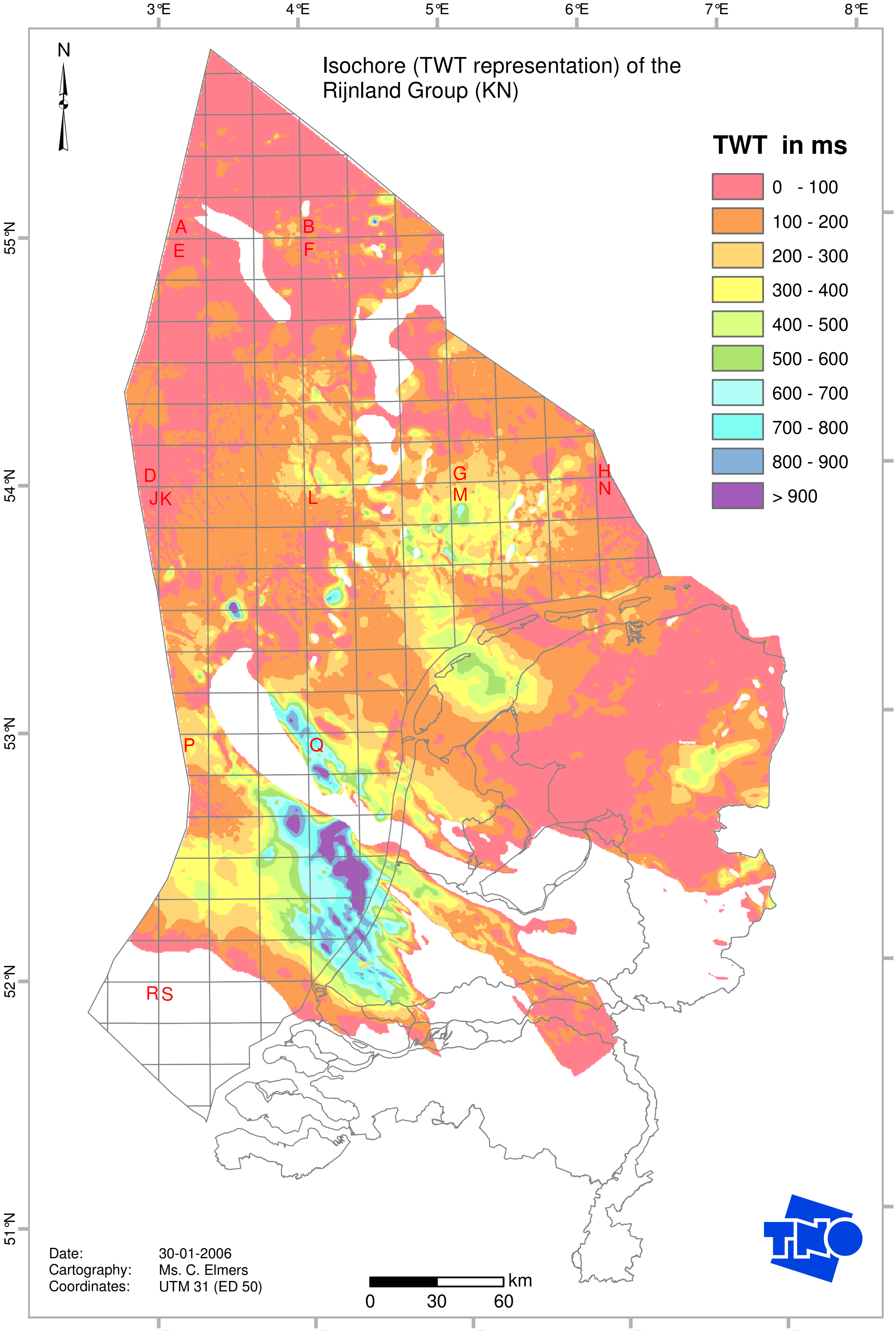

Isochore (TWT representation) of the Rijnland Group (KN)
TWT in ms
0 - 100
100 - 200
200 - 300
300 - 400
400 - 500
500 - 600
600 - 700
700 - 800
800 - 900
> 900
N
A
B
E
F
D
JK
L
G
M
H
N
P
Q
RS
3°E
4°E
5°E
6°E
7°E
8°E
51°N
52°N
53°N
54°N
55°N
0
30
60
km
Date: 30-01-2006
Cartography: Ms. C. Elmers
Coordinates: UTM 31 (ED 50)

Two way Travel Time (TWT) to the base of the Niedersachsen, Schieland and Scruff Groups (S)

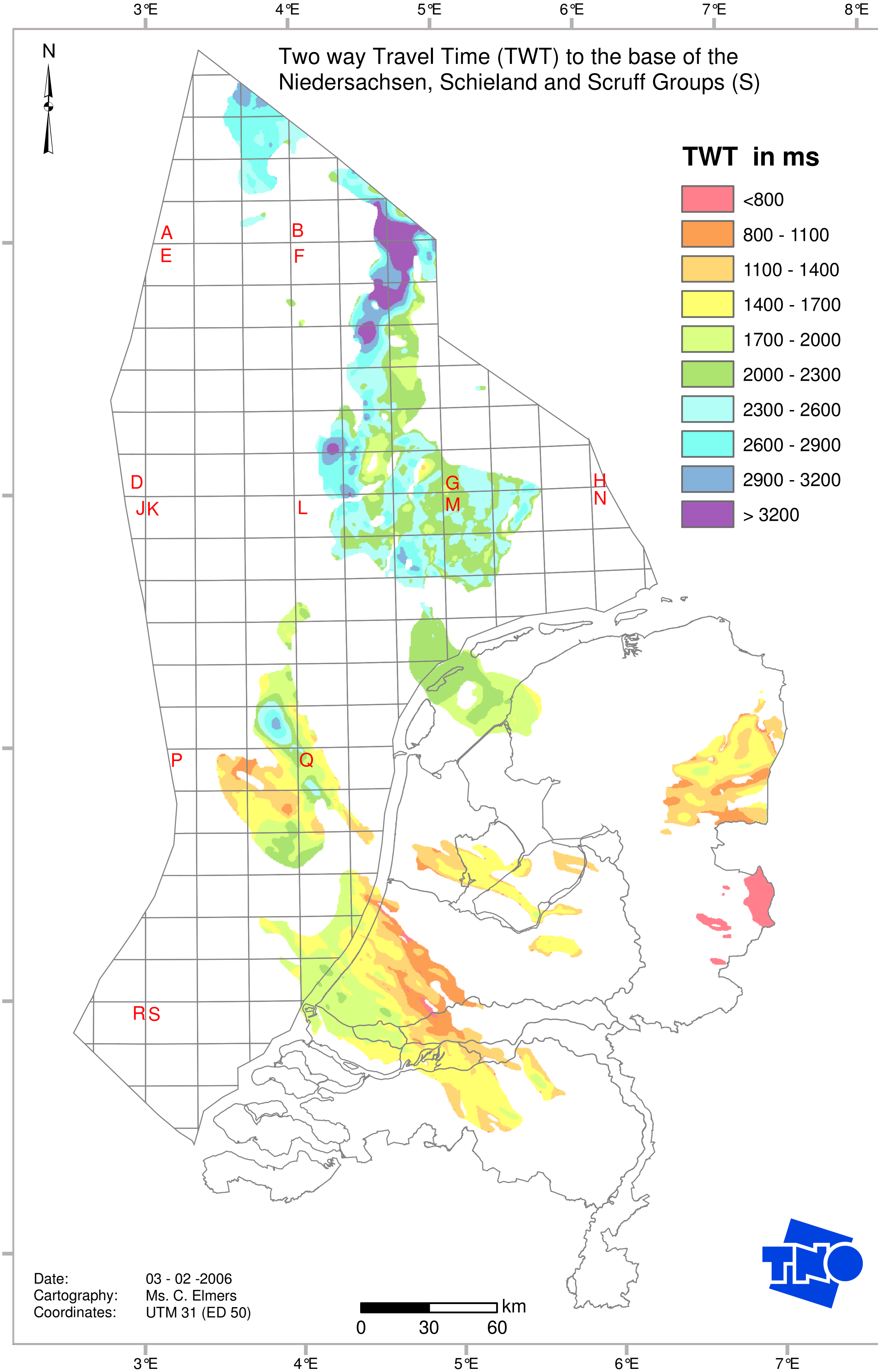

Date: 03 - 02 -2006
Cartography: Ms. C. Elmers
Coordinates: UTM 31 (ED 50)

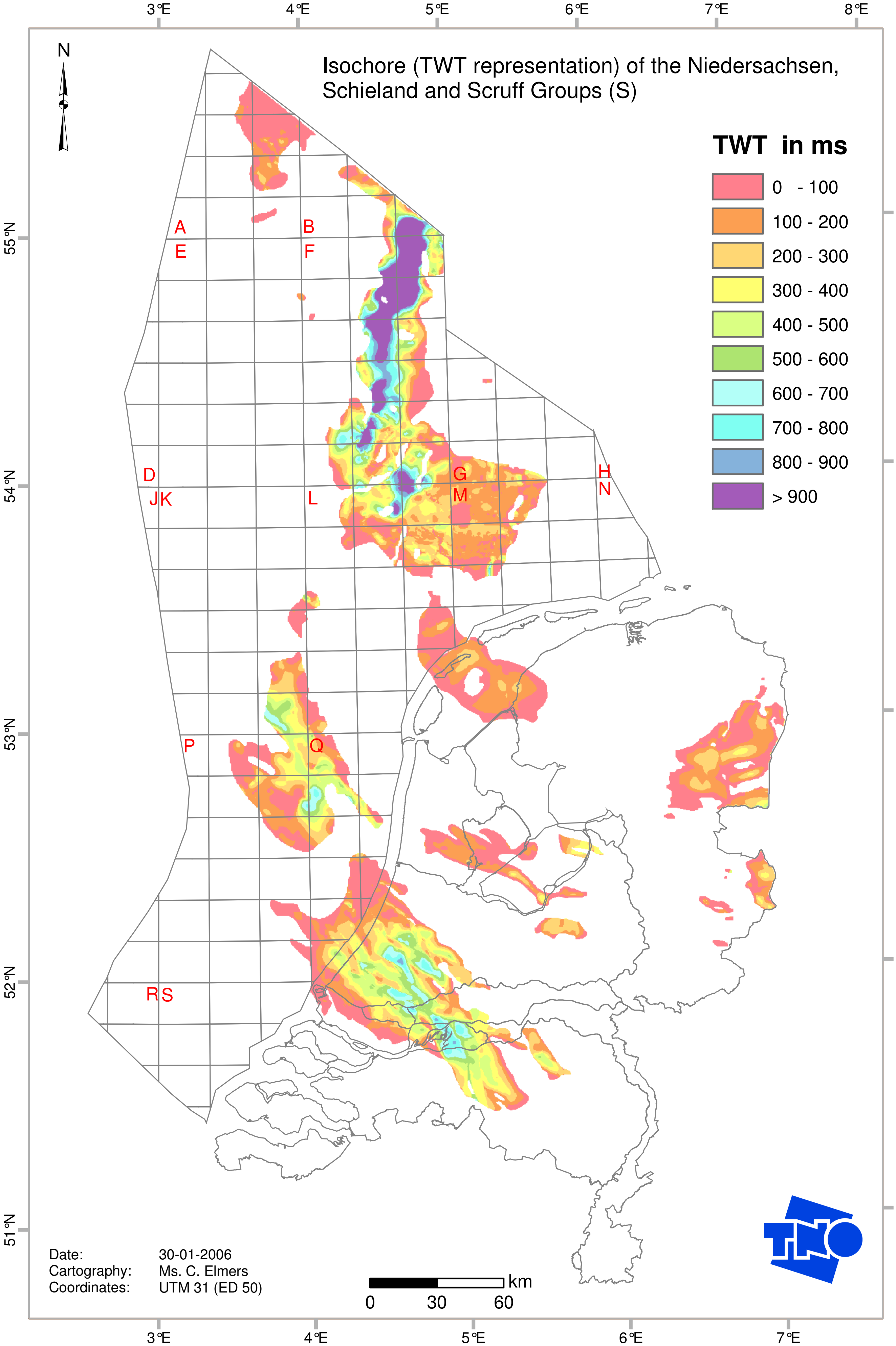
Isochore (TWT representation) of the Niedersachsen, Schieland and Scruff Groups (S)
TWT in ms
0 - 100
100 - 200
200 - 300
300 - 400
400 - 500
500 - 600
600 - 700
700 - 800
800 - 900
> 900
N
A
B
E
F
D
JK
L
G
M
H
N
P
Q
RS
3°E
4°E
5°E
6°E
7°E
8°E
51°N
52°N
53°N
54°N
55°N
Date: 30-01-2006
Cartography: Ms. C. Elmers
Coordinates: UTM 31 (ED 50)
0 30 60 km
TNO

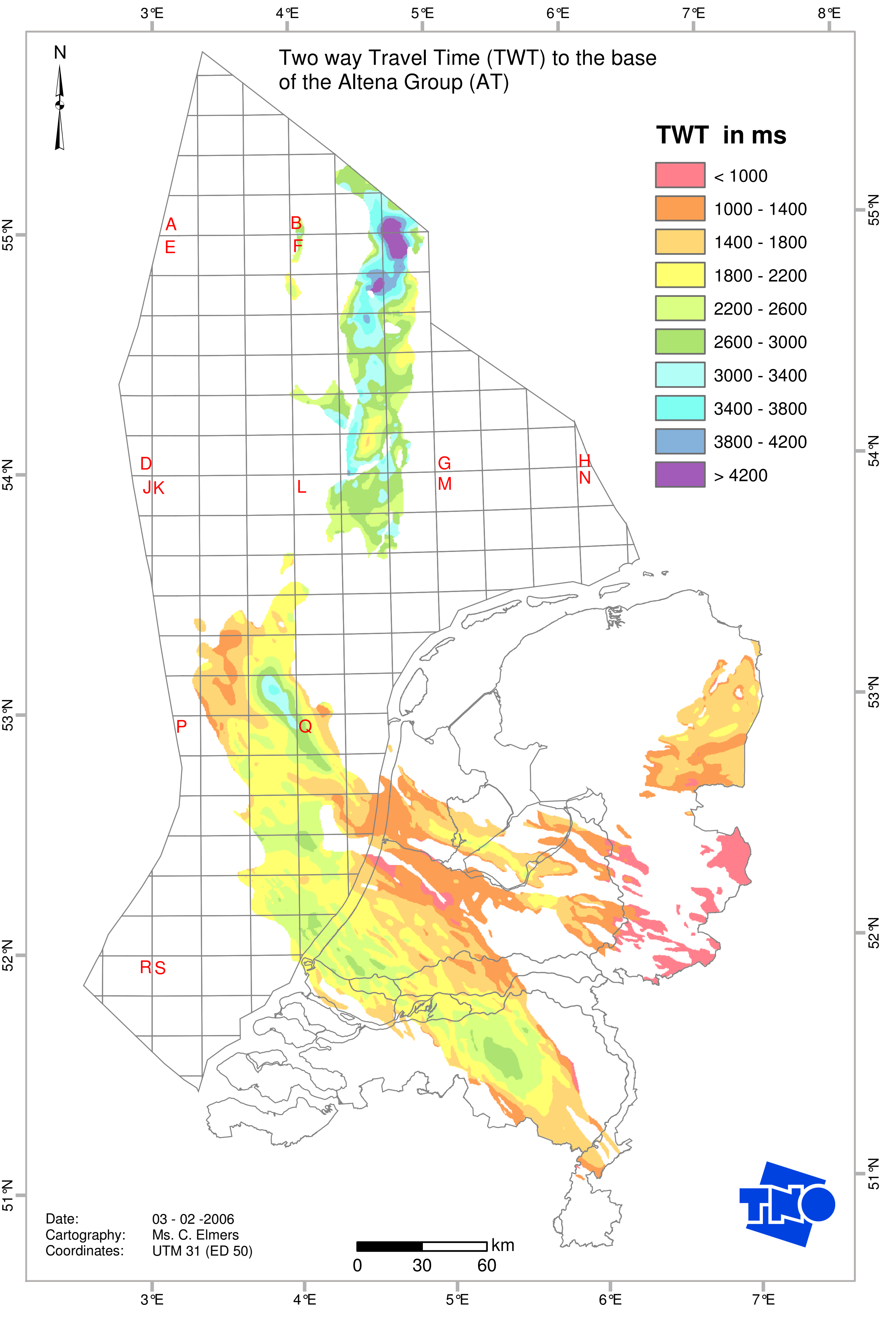

Two way Travel Time (TWT) to the base
of the Altena Group (AT)
TWT in ms
< 1000
1000 - 1400
1400 - 1800
1800 - 2200
2200 - 2600
2600 - 3000
3000 - 3400
3400 - 3800
3800 - 4200
> 4200
N
3°E
4°E
5°E
6°E
7°E
8°E
51°N
52°N
53°N
54°N
55°N
A
B
D
E
F
G
H
JK
L
M
N
P
Q
RS
Date: 03 - 02 -2006
Cartography: Ms. C. Elmers
Coordinates: UTM 31 (ED 50)
km
0
30
60
TNO

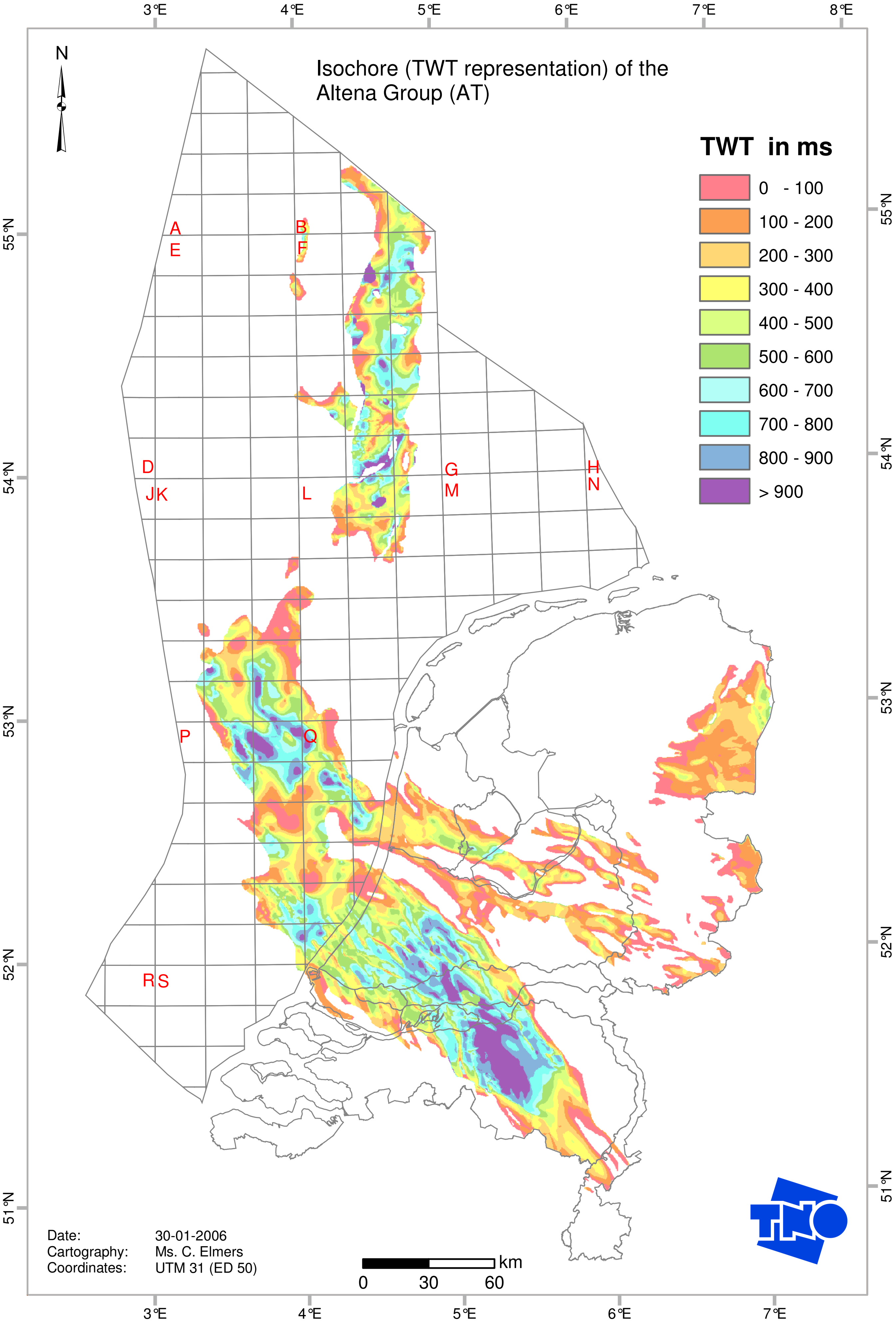

Date: 30-01-2006
Cartography: Ms. C. Elmers
Coordinates: UTM 31 (ED 50)

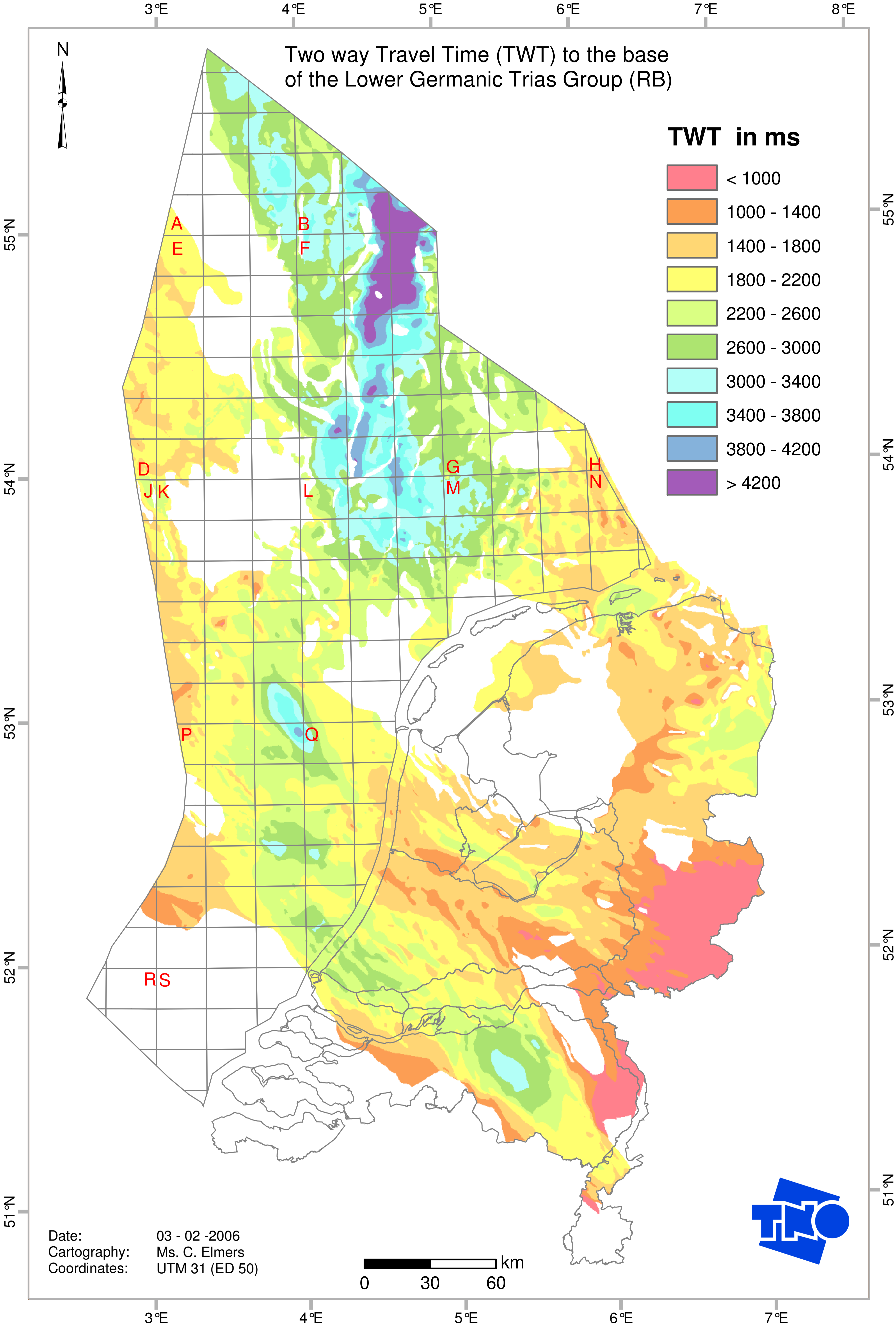

Two way Travel Time (TWT) to the base
of the Lower Germanic Trias Group (RB)
TWT in ms
< 1000
1000 - 1400
1400 - 1800
1800 - 2200
2200 - 2600
2600 - 3000
3000 - 3400
3400 - 3800
3800 - 4200
> 4200
N
3°E
4°E
5°E
6°E
7°E
8°E
55°N
54°N
53°N
52°N
51°N
A
E
B
F
D
J K
L
G
M
H
N
P
Q
R S
Date: 03 - 02 -2006
Cartography: Ms. C. Elmers
Coordinates: UTM 31 (ED 50)
0 30 60 km
TNO

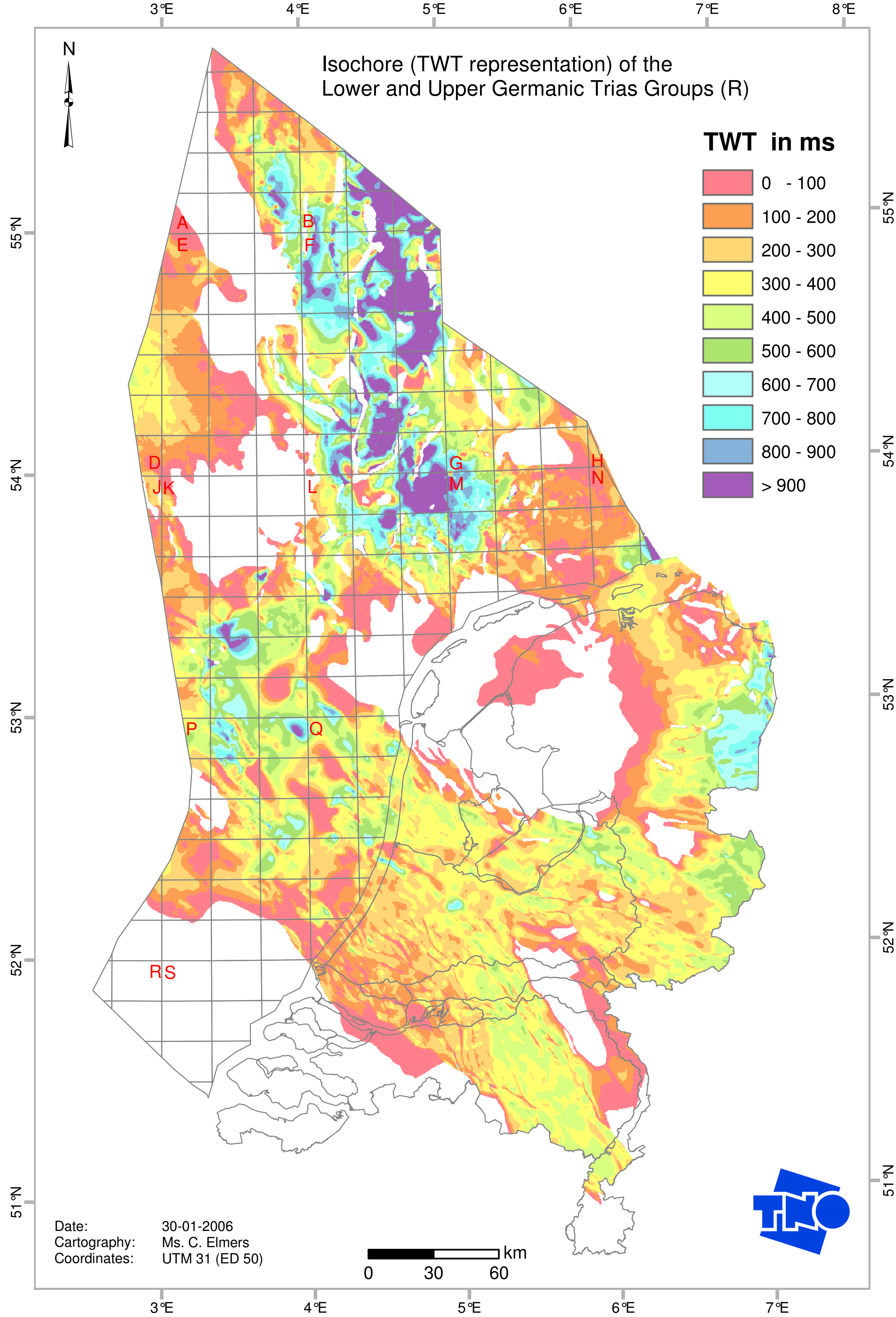

Isochore (TWT representation) of the
Lower and Upper Germanic Trias Groups (R)
TWT in ms
0 - 100
100 - 200
200 - 300
300 - 400
400 - 500
500 - 600
600 - 700
700 - 800
800 - 900
> 900
N
3°E
4°E
5°E
6°E
7°E
8°E
51°N
52°N
53°N
54°N
55°N
A
E
B
F
D
JK
L
G
M
H
N
P
Q
RS
Date: 30-01-2006
Cartography: Ms. C. Elmers
Coordinates: UTM 31 (ED 50)
km
0
30
60

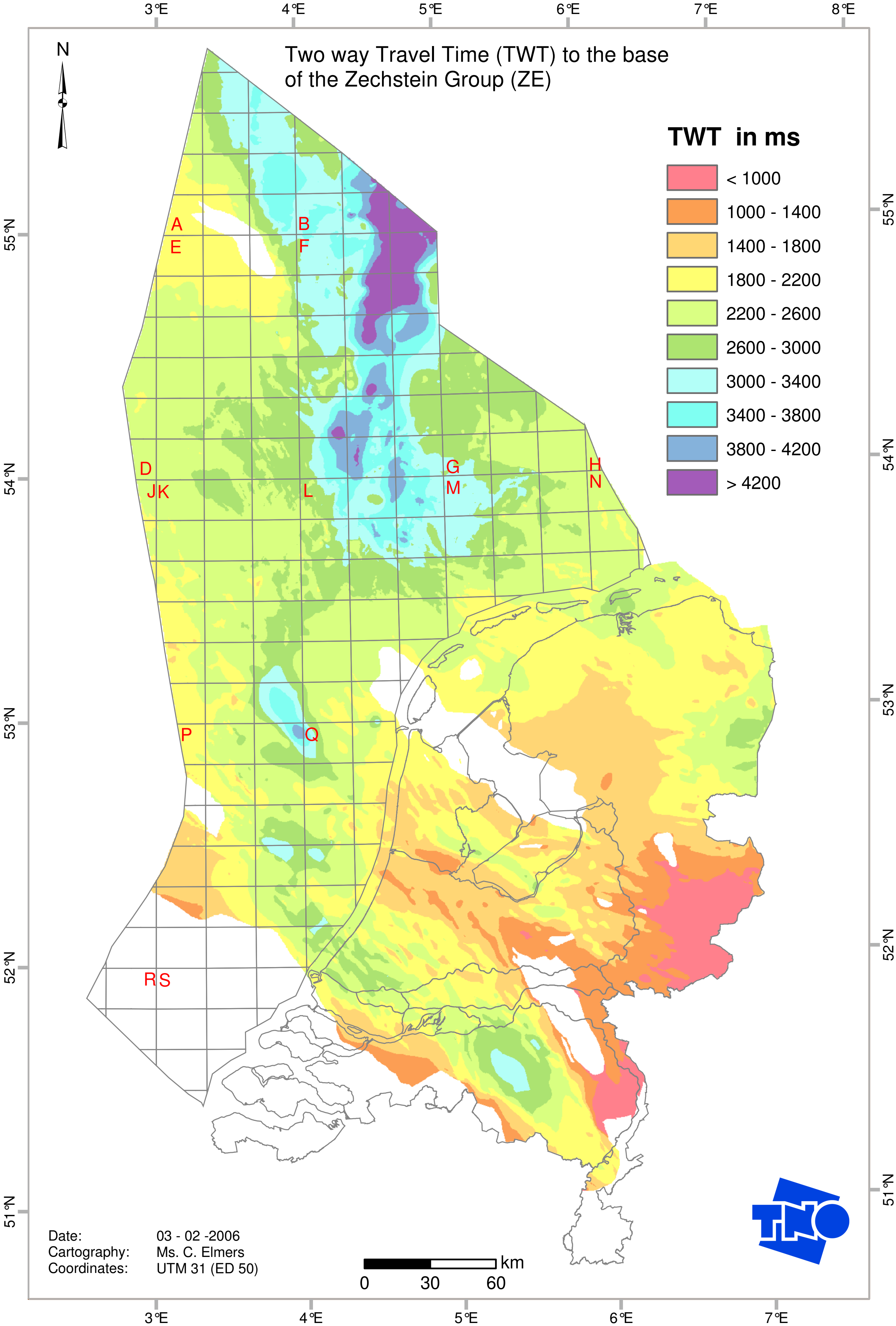
Two way Travel Time (TWT) to the base
of the Zechstein Group (ZE)
N
TWT in ms
< 1000
1000 - 1400
1400 - 1800
1800 - 2200
2200 - 2600
2600 - 3000
3000 - 3400
3400 - 3800
3800 - 4200
> 4200
3°E
4°E
5°E
6°E
7°E
8°E
55°N
54°N
53°N
52°N
51°N
A
E
B
F
D
JK
L
G
M
H
N
P
Q
RS
Date: 03 - 02 -2006
Cartography: Ms. C. Elmers
Coordinates: UTM 31 (ED 50)
km
0
30
60
TNO

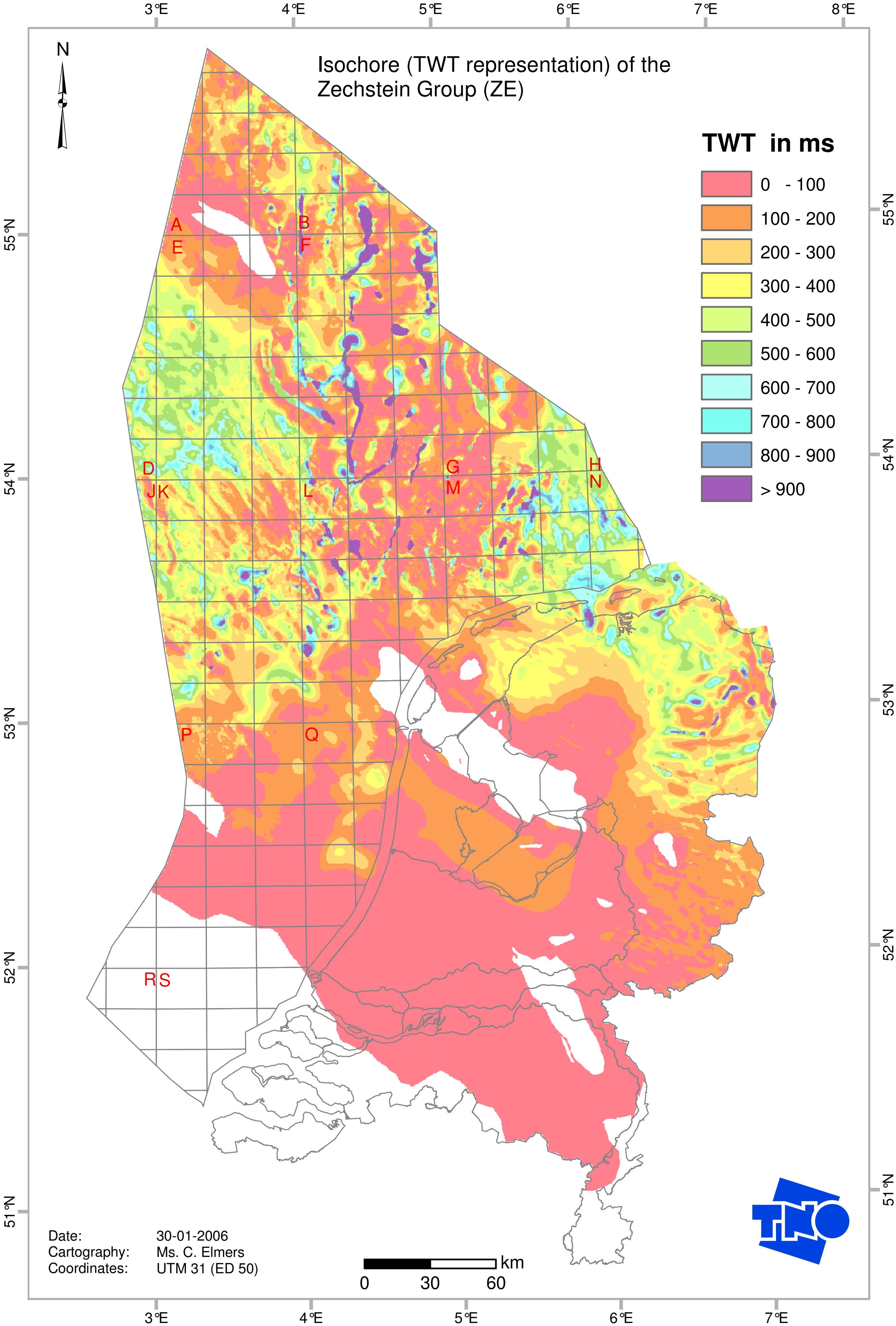
Isochore (TWT representation) of the
Zechstein Group (ZE)
TWT in ms
0 - 100
100 - 200
200 - 300
300 - 400
400 - 500
500 - 600
600 - 700
700 - 800
800 - 900
> 900
N
3°E
4°E
5°E
6°E
7°E
8°E
51°N
52°N
53°N
54°N
55°N
A
E
B
F
D
JK
L
G
M
H
N
P
Q
RS
Date: 30-01-2006
Cartography: Ms. C. Elmers
Coordinates: UTM 31 (ED 50)
km
0
30
60